

**STAGE ACOUSTICS FOR MUSICIANS:
A MULTIDIMENSIONAL APPROACH USING 3D
AMBISONIC TECHNOLOGY**

By

Anne Guthrie

A Dissertation Submitted to the Graduate
Faculty of Rensselaer Polytechnic Institute

in Partial Fulfillment of the
Requirements for the Degree of
DOCTOR OF PHILOSOPHY

Major Subject: ARCHITECTURAL SCIENCES (CONCENTRATION IN
ARCHITECTURAL ACOUSTICS)

Examining Committee:

Jonas Braasch, Dissertation Adviser

Michael Kalsher, Member

Ted Krueger, Member

Pauline Oliveros, Member

Henry Scarton, Member

Ning Xiang, Member

Rensselaer Polytechnic Institute
Troy, New York

April 2014
(For Graduation May 2014)

© Copyright 2014
by
Anne Guthrie
All Rights Reserved

CONTENTS

LIST OF TABLES	vi
LIST OF FIGURES	vii
ACKNOWLEDGMENT	xiii
ABSTRACT	xv
1. INTRODUCTION	1
2. DEVELOPMENT OF THE SPHERICAL MICROPHONE	5
2.1 Introduction	5
2.2 Theory	8
2.2.1 Spherical Wave Theory	8
2.2.2 Spherical Harmonic Decomposition	16
2.2.3 Tikhonov Regularization	18
2.2.4 Spatial Aliasing	19
2.2.5 Spherical Sampling	19
2.2.6 Beamforming	22
2.3 Methodology	26
2.3.1 Spherical Microphone Array Design	26
2.3.2 Spherical Microphone Array Calibration	29
2.4 Results	33
2.4.1 Spherical Microphone Array Testing	33
2.5 Discussion and Future Work	39
2.6 Conclusions	40
3. ROOM ACOUSTIC ANALYSIS USING THE SPHERICAL MICROPHONE	42
3.1 Introduction	42
3.2 Precedents	43
3.2.1 Stage Acoustics	43
3.2.1.1 Foundations	43
3.2.1.2 The Stage Support Parameters	44
3.2.1.3 Beyond Stage Support	51
3.2.1.4 Stage Enclosure Diffusion	55

3.2.2	Spatial Display and Analysis for Audience	57
3.3	Methodology	61
3.3.1	Concert Hall Stage Measurements	61
3.3.2	Free Field Measurements	66
3.4	Results	67
3.5	Discussion and Future Work	77
3.6	Conclusions	79
4.	AMBISONICS AND REAL-TIME AURALIZATION	80
4.1	Introduction	80
4.2	Theory	80
4.2.1	Encoding Conventions	80
4.2.2	Nearfield Compensation	81
4.2.3	Ambisonic Decoding	83
4.3	Methodology	89
4.3.1	Listener Auralization	90
4.3.2	Real-Time Performer Auralization	92
4.3.2.1	RTA Signal Capture	93
4.3.2.2	RTA Latency	93
4.3.2.3	Arup RTA Research	95
4.3.2.4	RTA Power Spectrum Corrections	102
4.3.2.5	Listening Room Setup	104
4.3.2.6	Listening Room Acoustics	106
4.3.3	Physical Test Setup	110
4.4	Results	113
4.4.1	Objective Characterization of RTA System	113
4.5	Discussion and Future Work	121
4.6	Conclusions	123
5.	SUBJECTIVE TESTS	124
5.1	Introduction	124
5.2	Precedents	125
5.3	Theory	127
5.4	Methodology	130
5.5	Results	136

5.5.1	Subjective Preference Mapping	136
5.5.2	Objective Parameter Mapping	153
5.5.2.1	Solo Parameters	154
5.5.2.2	Ensemble Parameters	163
5.6	Discussion and Future Work	172
5.7	Conclusions	175
6.	ARCHITECTURAL INVESTIGATIONS	177
6.1	Introduction	177
6.2	Methodology	179
6.3	Results	181
6.4	Discussion and Future Work	207
6.5	Conclusions	208
7.	CONCLUSIONS	210
	REFERENCES	213
	APPENDICES	
A.	SOLO PARAMETERS	222
B.	ENSEMBLE PARAMETERS	228
C.	IMAGES	237
C.1	Measurement	237
C.2	Spatial Analysis	243
C.3	Subjective Testing	245

LIST OF TABLES

2.1	Ambisonic Signal Names for Spherical Harmonic Components	15
2.2	Sensor Points and Quadrature Coefficients	21
3.1	Range of Parameter Values For Three Measured Halls, A.C. Gade	46
3.2	Summary of A.C. Gade Findings	48
3.3	Omnidirectional Parameters for Measured Hall Stages	66
3.4	Directional Sectors Used in Calculation of Spatial Parameters	76
3.5	Spatial Parameters	77
4.1	Encoding Conventions for Order $N=2$	81
4.2	Decoding Gains g_n for $N=2$	89
4.3	Initial RTA System Hardware/Software Chain	95
4.4	Instrument Power Spectrum Corrections in dB	104
4.5	Subjective Test Settings Implemented in the Arup 77W NY SoundLab .	104
5.1	Absolute Percentage of Variance Explained by Each MDS Dimension . .	138
5.2	Correlation of MDPREF First and Second Score Matrices	152
5.3	Clusters of Solo Parameters	158
5.4	Clusters of Ensemble Parameters	165
5.5	Summary of Perceptual Dimensions, Soloist Condition	175
5.6	Summary of Perceptual Dimensions, Ensemble Condition	176
6.1	Subjective Test Results: Perceptual Factors	177
7.1	Soloist Perceptual Dimensions	211
7.2	Ensemble Perceptual Dimensions	212

LIST OF FIGURES

2.1	Spherical Bessel Functions $j_n(kr)$	10
2.2	Spherical Bessel Functions $y_n(kr)$	11
2.3	Complex Spherical Harmonic Directivity Patterns for Order $N=2$. . .	13
2.4	Real Spherical Harmonic Directivity Patterns for Order $N=2$	16
2.5	Ideal Beam Patterns for a Single Plane Wave Decomposition for Values of N up to Order $N=2$	24
2.6	3D Computer Model of Spherical Microphone Array Showing Capsule Locations	27
2.7	Photos of Constructed Spherical Microphone Array	28
2.8	Functional Diagram of Spherical Microphone Array Measurement System	29
2.9	Unfiltered Log Magnitude Frequency Response of 16 Individual Cap- sules and Reference Mic	30
2.10	Mean Gain Deviations Between 100 Hz and 3 kHz for 16 Individual Capsules and B&K Reference Microphone	31
2.11	Log Magnitude Frequency Response of 16 Minimum Phase FIR Filters for Individual Capsule Calibration	32
2.12	Filtered Log Magnitude Frequency Response of 16 Individual Capsules .	33
2.13	Comparison of Beamformer with Real and Theoretical Far Field Signal, 2 kHz Octave Band	35
2.14	Beamformer with Measured Far Field Signals at 90° Increments, 2 kHz Octave Band	36
2.15	Beamformer with Measured Far Field Signals at 15° Increments, 2 kHz Octave Band	37
2.16	Beamformer with Theoretical Plane Wave Signals at 90° Increments, 2 kHz Octave Band	38
2.17	Beamformer with Theoretical Plane Wave Signals at 15° Increments, 2 kHz Octave Band	39
3.1	3D “Hedgehog” Plots of Impulse Responses from Two Concert Halls . .	59

3.2	Measured Concert Halls and Theatres	64
3.3	Measured Stage Dimensions: Plan View	65
3.4	Measured Stage Dimensions: Section View	65
3.5	St. Rose 3D Model vs. Measured Spatial Energy, Rear Reflection	69
3.6	St. Rose 3D Model vs. Measured Spatial Energy, Ceiling Reflection . .	70
3.7	Skidmore with and without Orchestra Shell, 3 ms	71
3.8	Skidmore with and without Orchestra Shell, 16 ms	72
3.9	Skidmore with and without Orchestra Shell, 32 ms	73
3.10	Skidmore with and without Orchestra Shell, 40 ms	74
3.11	Spatial Distribution of Cross-Stage LQ_{740} , 15° Resolution	75
4.1	Near Field Compensation Filters Applied to Each Order up to $N=2$. .	83
4.2	Localization Resolution of Three Decoding Types for a Single Plane Wave On Axis	88
4.3	RTA System Latency Components	94
4.4	Schematic Diagram of RTA System Latency Measurement Setup	97
4.5	Revised RTA System Latency Components	99
4.6	Measured Stage Enclosure Plans Comparison with RTA System Setup .	100
4.7	Measured Stage Enclosure Sections Comparison with RTA System Setup	101
4.8	Schematic Diagram: RTA System	101
4.9	Spherical Distribution of Area Weightings for Power Spectrum Calculations	103
4.10	Speaker Layout for Subjective Tests	105
4.11	G with and without Temporary Foam Panels	107
4.12	Arup SoundLab NY with and without Temporary Foam Panels	108
4.13	Schematic Diagram of Impulse Response Separation	109
4.14	IRs Before and After Denoising	112
4.15	Ensemble Playing Test Setup	113

4.16	1-meter IR from Arup SoundLab NY and Kodak Hall, Eastman, W Channel	114
4.17	1-meter IR from Arup SoundLab NY and Kodak Hall, Eastman, X Channel	115
4.18	1-meter IR from Arup SoundLab NY and Kodak Hall, Eastman, Y Channel	116
4.19	1-meter IR from Arup SoundLab NY and Kodak Hall, Eastman, Z Channel	117
4.20	Measured IR of Skidmore Hall Compared to Auralized IR of Skidmore Hall	118
4.21	Measured IR of Vassar Hall Compared to Auralized IR of Vassar Hall .	119
4.22	Smoothed IR Comparisons for Skidmore Hall, W Channel	120
4.23	Smoothed IR Comparisons for Skidmore Hall, R Channel	121
5.1	iPad Interface for Test 1: Listening Tests	133
5.2	iPad Interface for Test 2: Solo Playing Test	135
5.3	Scree Test for Dimensionality (Normalized Variance Explained by Each MDS Dimension)	137
5.4	Diagram of Sample MDPREF Mapping	139
5.5	Listening Test MDPREF Results, Set 1	140
5.6	Listening Test MDPREF Results, Set 2	141
5.7	Listening Test MDPREF Results, Set 3	142
5.8	Listening Test MDPREF Results, Set 4	143
5.9	Solo Playing Test MDPREF Results, 3D View	144
5.10	Solo Playing Test MDPREF Results, D1-D2	145
5.11	Solo Playing Test MDPREF Results, D2-D3	146
5.12	Solo Playing Test MDPREF Results, D1-D3	147
5.13	Ensemble Playing Test MDPREF Results, 3D View	148
5.14	Ensemble Playing Test MDPREF Results, D1-D2	149
5.15	Ensemble Playing Test MDPREF Results, D2-D3	150

5.16	Ensemble Playing Test MDPREF Results, D1-D3	151
5.17	Dendrogram From Hierarchical Cluster Analysis: Solo Parameters . . .	155
5.18	Dendrogram From Hierarchical Cluster Analysis: Dimensions 1 and 2 .	156
5.19	Dendrogram From Hierarchical Cluster Analysis: Dimension 3	157
5.20	Solo Playing Test Parameter Cluster Mapping, 3D View	159
5.21	Solo Playing Test Parameter Cluster Mapping, D1-D2	160
5.22	Solo Playing Test Parameter Cluster Mapping, D2-D3	161
5.23	Solo Playing Test Parameter Cluster Mapping, D1-D3	162
5.24	Ensemble Playing Test Parameter Cluster Mapping, 3D View	166
5.25	Ensemble Playing Test Parameter Cluster Mapping, D1-D2	167
5.26	Ensemble Playing Test Parameter Cluster Mapping, D2-D3	168
5.27	Ensemble Playing Test Parameter Cluster Mapping, D1-D3	169
5.28	Dendrogram From Hierarchical Cluster Analysis: Ensemble Parameters	170
6.1	Kodak Hall, Eastman: CATT-Acoustic Model	180
6.2	Kodak Hall, Eastman: Variations on Stage Enclosures Modeled in CATT-Acoustic	181
6.3	Eastman Model: Solo Parameters (Modeled Onstage T_{30})	182
6.4	Eastman Model: Solo Parameters (Modeled ST1 Top/Sides)	183
6.5	Eastman Model: Solo Parameters (Modeled ST1)	184
6.6	Eastman Model: Solo Parameters (Modeled $G_{40-\infty}$)	185
6.7	Bard House Ceiling: Curved Panels	187
6.8	Eastman Model: Ensemble Parameters (Modeled Cross-Stage DD_{0-30}) .	188
6.9	Eastman Existing Model: Image Sources	189
6.10	Eastman Wide Model: Image Sources	190
6.11	Eastman Small Model: Image Sources	191
6.12	Eastman Curved Model: Image Sources	192
6.13	Eastman Angled Model: Image Sources	193

6.14	Eastman Deep Model: Image Sources	194
6.15	Eastman High Model: Image Sources	195
6.16	Eastman Flat Model: Image Sources	196
6.17	Bard, St. Rose, and Skidmore Models: Image Sources	197
6.18	Eastman Measurements: Ensemble Parameters (Measured G)	199
6.19	Eastman Model: Ensemble Parameters (Modeled Early G)	200
6.20	Eastman Model: Ensemble Parameters (Modeled Late G)	201
6.21	Eastman Model: Ensemble Parameters (Modeled Cross-Stage LQ_{740} Top/Sides)	202
6.22	Eastman Model: Ensemble Parameters (Modeled Cross-Stage MTF) . .	204
6.23	Eastman Measurements: Ensemble Parameters (Measured Running Re- verberance)	206
6.24	Eastman Model: Ensemble Parameters (Modeled Running Reverberance)	207
C.1	Sound Source and Spherical Microphone Array	237
C.2	Spherical Array Interface and Processor with MaxSens Software	238
C.3	Individual Capsule Calibration at NYSTAR	239
C.4	Test Setup for Spherical Microphone Array	240
C.5	Free Field Measurements at EMPAC, Studio 2	241
C.6	Concert Hall Measurement Setup	242
C.7	Skidmore 3D Model and References	243
C.8	St. Rose 3D Model and References	244
C.9	Solo Violin Recording in an Anechoic Chamber	245
C.10	Arup SoundLab NY: IR Measurements	246
C.11	Arup SoundLab NY: RTA IR Measurements	247
C.12	Arup SoundLab LA: RTA System Testing (with Temporary MDF Plat- form)	248
C.13	Musician Platform in NY SoundLab	249
C.14	Musician Platform in NY SoundLab with Surrounding “Stage Floor” . .	250

C.15	Max/MSP Patch for Test 1 (Listening)	251
C.16	Max/MSP Patch for Test 2 (Solo Playing)	251
C.17	iPad Interface for Test 3 (Ensemble Playing)	252
C.18	Max/MSP Patch for Test 3 (Ensemble Playing)	252
C.19	Projected Hall Drawings Used in Subjective Tests	253

ACKNOWLEDGMENT

I would like to thank everyone who had a part in making this research a reality:

My Ph.D adviser, Jonas Braasch, who provided crucial support and feedback along the way, and gave me the necessary insight, techniques and tools to create and follow through with a coherent study. Ning Xiang, for providing me with advice, tools and equipment to build the spherical microphone array and perform the measurements. Henry Scarton, for providing anechoic facilities to test the microphone array and research guidance. The rest of my Ph.D committee: Pauline Oliveros, Ted Krueger, and Michael Kalsher, for guiding me through the process and providing key feedback at various stages of this study. Paul Calamia, who provided important resources for the ambisonic encoding process. My fellow Ph.D colleagues: Philip Robinson and Daniel Valente, for providing resources, feedback and contributing to the development of this research. Jon Botts and Samuel Clapp for assisting in the design and construction of the spherical microphone array as well as the measurement survey and the subsequent processing of the measurements.

My colleague and industry adviser, Terence Caulkins, who contributed significantly to this research, in particular the development of the real-time auralization system, and also provided feedback at various stages of this research. Arup colleagues Kathleen Stetson, Shane Myrbeck and Joseph Digerness for their contributions to the development of the real-time auralization system. My other Arup colleagues, who provided facilities, time, and support, including Todd Brooks, Alban Bassuet and Raj Patel. The Invest in Arup program, for providing funding for the subjective tests and the development of the real-time auralization system.

The staff at the 10 universities who provided me with access and support for the measurement survey in New York State: SUNY Albany, SUNY Buffalo, Bard College in Annandale-on-Hudson, Eastman Conservatory in Rochester, Skidmore College in Saratoga Springs, St. Rose College in Albany, Vassar College in Poughkeepsie and RPI's own EMPAC facilities. The musicians (who shall remain anonymous to maintain the objectivity of the study) who gave their time and en-

thusiasm to participating in these tests. My husband, Billy Gomberg, for all his support, insight and encouragement over the last seven years of this work.

This research was funded in part by the Rensselaer HASS Fellowship and the Invest in Arup program.

ABSTRACT

In this research, a method was outlined and tested for the use of 3D Ambisonic technology to inform stage acoustics research and design. Stage acoustics for musicians as a field has yet to benefit from recent advancements in auralization and spatial acoustic analysis. This research attempts to address common issues in stage acoustics - subjective requirements for performers in relation to feelings of support, quality of sound, and ease of ensemble playing in relation to measurable, objective characteristics that can be used to design better stage enclosures. While these issues have been addressed in previous work, this research attempts to use technological advancements to improve the resolution and realism of the testing and analysis procedures. Advancements include measurement of spatial impulse responses using a spherical microphone array, higher-order ambisonic encoding and playback for real-time performer auralization, high-resolution spatial beamforming for analysis of onstage impulse responses, and multidimensional scaling procedures to determine subjective musician preferences. The methodology for implementing these technologies into stage acoustics research is outlined in this document and initial observations regarding implications for stage enclosure design are proposed. This research provides a robust method for measuring and analyzing performer experiences on multiple stages without the costly and time-intensive process of physically surveying orchestras on different stages, with increased repeatability while maintaining a high level of immersive realism and spatial resolution. Along with implications for physical design, this method provides possibilities for virtual teaching and rehearsal, parametric modeling and co-located performance.

CHAPTER 1

INTRODUCTION

Room acoustics research has historically focused on acoustics for audience. As a result, much of the technology for measuring, analyzing and virtually reproducing concert hall acoustics has focused on the passive listening experience for audience members. In the world of research, this drives a great deal of development and testing. In the design world, however, many consultants work directly with orchestras and individual musicians to obtain feedback about their spaces. When consultants are called back to follow up on previous designs, the call often comes from the orchestra manager with questions regarding support and ensemble playing onstage. The seminal survey of concert halls and opera houses, by Leo Beranek, obtains its subjective ratings from conductors [8].

Musicians often have the best position to judge the acoustics of rooms. They can intuitively understand the acoustics of a room through experience, often play the same repertoire in several halls, and have intimate knowledge of their own signal in order to subjectively separate it from the room response. On the other hand, there are several compounding variables that the audience member does not experience: musicians have to contend with a high cognitive load, the unique directivity and frequency characteristics of their own instrument, and their specific position onstage and within the ensemble. They may have strong opinions about different repertoire (classical versus contemporary classical, for example) and are often used to adapting their playing to the existing acoustics of a space rather than judging objectively its quality (research in cognitive modeling has attempted to understand this phenomenon) [103]. Additionally, while placing a passive listener in a laboratory situation is reasonably straightforward, bringing the musician to a lab requires another level of computational power. The direct sound of the instrument, the vibrations and bone-conducted sound, and the physical conditions of an occupied stage are all things that cannot be recreated virtually using available technologies. However, there are several recent advancements that can be adapted in order to

provide an adequate testing environment for improved stage acoustics research.

Previous research in stage acoustics has taken two main approaches: the in-situ survey, and the laboratory test. In-situ, the test environment is as realistic and natural as it can be: the physical orchestra is present in the space and all musicians are playing in real-time on stage in full 3D. However, this type of test often relies on descriptive language, impressions given after the fact, and long periods of time or even different orchestras between different halls. It would be difficult to determine any standardized stage acoustics parameters this way, although it is still the best way for adjusting variable acoustics in a space such as reflector height and orchestra shell configurations.

The laboratory test, on the other hand, is the best environment for controlled, A-B comparisons of several spaces. Previous work by Gade, Ueno et al. and others have examined individual elements of stage acoustics such as delay and direction of initial reflections, frequency response, and reverberant energy levels in an abstract and controlled way [34], [102], [100]. This work led to the development of standard stage acoustics parameters including Stage Support [35].

When measured IRs were used in real-time laboratory auralizations, they were omnidirectional or binaural in form. Up until recently, computational power and measurement techniques prevented anything with higher resolution from being used. More recently, it has become possible to convolve multi-channel audio in real time with very low latencies, allowing the real-time performer auralization to be upgraded to higher-order ambisonics. Additionally, research by Daniel, Moreau et al. and others into higher-order ambisonics has led to the development of spherical microphone arrays for efficient measurement of spatial impulse responses [28], [73]. While these arrays have previously only been tested in audience conditions, the development of near-field corrections allows onstage impulse responses to be measured using this method. This research attempts to show that these technologies can be used to improve the realism of the laboratory setting for performers while maintaining the level of control and repeatability not possible with in-situ surveys.

This document is divided into an Introduction, five main Chapters, and overall Conclusions. Chapter 2: Development of the Spherical Microphone details the

theoretical foundations of the design and construction of the spherical microphone array used for the recording of spatial impulse responses, as well as the process of building and testing the microphone used in this research. The Theory section details the derivation of microphone design from its basis in spherical wave acoustics. It also looks at the use of spherical harmonic theory for beamforming analysis. The Methodology section details the construction, calibration and testing of the spherical microphone array. The performance and spatial resolution of the array is described in the Results section. The Discussions and Conclusions sections describe the uses of the microphone and the potential improvements that could be made to future designs.

Chapter 3: Room Acoustic Analysis using the Spherical Microphone describes the first main component of this research: spatial analysis of onstage 3-dimensional impulse responses. The Precedents section details the history of stage acoustics research, including previous work by the author. It addresses previous work in the use of spatial information in room acoustics. The Methodology section describes the concert hall measurement survey, and the process of spatial analysis from the concert hall measurements. Results contains the results of the beam-forming analysis from the concert hall measurements and subsequent development of tested spatial parameters. Discussion and Conclusions describe the potential applications and also the future work necessary to refine the parameter analysis process.

Chapter 4: Ambisonics and Real-Time Auralization describes the second main component of this research: the reproduction of the spatial impulse response over a higher-order ambisonic system for use in real-time performer auralization. The Theory section describes the theoretical foundations of higher-order ambisonics. It details the various shortcomings of ambisonic theory and the methods developed by others for compensating or correcting these shortcomings. The Methodology section describes the development of the real-time auralization system, based on previous work and developed through internal research funding at Arup. It describes the testing facility, the Arup SoundLab, and the modifications made to the facility for real-time performer auralization. The performance specifications of the utilized system are detailed in the Results section. Discussion and Conclusions describe the

possible uses of such a system and also potential improvements.

Chapter 5: Subjective Tests describes the utilization of the system described in Chapter 4 for subjective preference experiments. These experiments are structured around an exploratory statistical method known as multidimensional scaling, and its previous use in acoustics research is detailed in the Precedents section. Theory provides a basic outline of the multi-dimensional scaling method. Methodology describes the preparation of the signals and the design of the subjective tests. In the Results section, the preference data from the subjective tests are examined. In the Discussion section, the subjective data is compared to the predefined objective parameters. Conclusions regarding the influence of objective acoustic parameters on subjective preference are proposed.

In Chapter 6: Architectural Investigations, initial assays are made into the application of this study to architectural design criteria for stage enclosures. A preliminary modeling study is performed on one of the measured halls using CATT-Acoustics. Based on comparisons with this study and the subjective testing results, some basic observations regarding stage enclosure design are outlined, many of which parallel previous observations by Dammerud, Barron and others [27], [26]. Possible extensions and refinements of this research are outlined, providing direction for future improvement and application of this work.

CHAPTER 2

DEVELOPMENT OF THE SPHERICAL MICROPHONE

2.1 Introduction

Several methods exist for the recording and reproduction of spatial audio. The most prevalent method uses binaural techniques, which allow spatial sound-fields to be recorded using in-ear microphones or dummy-head microphone systems that can be reconstructed over headphones using generic or individualized head-related transfer functions (HRTFs) to provide localization cues. While the HRTFs provide good left-right localization, a disadvantage of this technique is that listeners often use motion cues to resolve distance and front-back confusion, which cannot be accomplished with headphones (the signal will travel along with the head movement). Head-tracking devices can be used in this case, which filter the signal based on head motions. Another disadvantage is that, for performers, the direct sound caused by the performer’s instrument is attenuated by the headphones and the bone-conduction paths from the sound source to the ear (mouth for singers and wind players, chin for string players, hand for percussionists and pianists) are damped, reducing feelings of realism [12].

In previous research by the author, a rudimentary real-time auralization system was used to compare variations to an acoustic model, convolving close microphoned signal from each instrument with binaural impulse responses (calculated with specific instrument directivities) and playing back the room response for both players over open-back headphones. The players were physically separated to control the acoustic environment but connected visually using a simple camera feed. Although musicians could detect differences during passive listening scenarios (only listening to the “other” performer), there were no significant preferences, and differences could not be detected during the playing scenarios. One main limitation was the use of headphones in the auralization, which the musicians claimed detracted from the feelings of realism in the study. Additionally, the lack of head-tracking prevented the player from determining spatial information via head movements.

Therefore, the research in this dissertation focuses on spatial impulse responses reproduced over loudspeakers rather than headphones.

Spatial reproduction over loudspeakers has been developed in a number of ways, including ViMiC, Wavefield Synthesis, Ambisonics (B-Format), and Higher-Order Ambisonics.

Virtual Microphone Control (ViMiC) is a method for virtual spatialization using a mono signal [84]. In real-time auralization, this signal is the close microphone recording from the instrument. Using level and time differences between an array of virtual microphones, the soundfield can be synthesized for any virtual source location. Room information is determined using mirror-image techniques and statistical reverberation is applied to all signals. ViMiC can be used with any loudspeaker layout and works well in situations where computation power is limited and low latency is important, such as telepresence. Previous research by the author utilized a synthesized sound field created by ViMiC to create various acoustic scenarios for subjective preference comparisons [48], [15]. The simplicity of the sound field allowed parameters to be varied with a great deal of control. However, the system cannot be used to simulate more complex auditory scenes like those experienced outside the laboratory setting, using measured impulse responses or impulse responses generated with ray-tracing algorithms. Additionally, the spatial reproduction of the sound field was restricted to a single azimuthal plane at ear level, and in real rooms the periphonic or vertical information may influence subjective perception.

Wavefield Synthesis (WFS) is based on the Huygens principle, which states that any wavefront can be represented as a continuous distribution of smaller sources at the edge of the wavefront [30]. Using the Kirchhoff-Helmholtz integral, wave behavior inside a closed volume can be fully described based on the acoustic pressure and velocity along the enclosing surface, spatially sampled by a continuous line of loudspeakers around the listening area [51], [54]. This method provides two main advantages: the spatial resolution is extremely high, and there is no “sweet spot,” as the reproduced soundfield at any position inside the boundary defined by the loudspeakers will be spatially resolved. However, there are several disadvantages to this method. First, the sound field can only be reproduced in two dimensions.

This means there can be no elevation information produced. Some techniques have been developed to adapt binaural elevation cues for WFS, but any impressions of elevated sound sources or reflections will disappear when the listener moves his or her head. This makes stage acoustics auralizations difficult, especially since the ceiling reflection is one of the most important early reflections for hearing other musicians onstage. Additionally, spatial aliasing (caused by diffraction effects) is problematic in WFS, typically requiring a prohibitively large number of speakers to reproduce any kind of complex soundfield. Finally, recording impulse responses for a WFS system requires a large number of measurement positions, which can take several hours to capture [54].

B-Format or first-order ambisonic reproduction was first developed by Gerzon in the early 1970s to provide easily portable and transmissible spatial audio [38], [39]. The format encodes signals into spherical harmonic channels that can be decoded into any loudspeaker configuration. Spherical harmonics are the result of decomposition of the continuous soundfield using the spherical Fourier Transform, the spatial equivalent of the Fourier series. The discrete harmonics, when summed in an infinite series, recreate the complete soundfield. The theory of ambisonics relies on the fact that a small sum of lower harmonics can accurately reproduce the soundfield and an infinite sum is not necessary. Harmonics are divided into orders, with $(N + 1)^2$ harmonics for N orders. Order $N = 0$ has 1 harmonic, the mono or omnidirectional signal. The $N = 1$ or first order harmonics are set of orthogonal dipoles, originally called B-Format signals. The recording device (now commercially available from multiple manufacturers, including SoundField) consists of a tetrahedral configuration of 4 coincident cardioid-microphone capsules. The recorded signals were known as A-Format, and due to the low level of complexity, the transformation from A-Format to B-Format is a simple set of sums and differences.

In the last decade, the development of higher-order ambisonics (orders $N \geq 2$) has offered increased spatial resolution over B-Format [11]. Although this method requires a larger microphone array, more complex encoding transformations, and a higher number of loudspeakers for accurate reproduction, higher-order ambisonics were used for this study because they provide an optimal balance between tech-

nological requirements, spatial resolution and impressions of acoustic realism. The theoretical foundations for higher-order ambisonics (HOA) will be described in more detail in Section 2.2.1.

2.2 Theory

2.2.1 Spherical Wave Theory

Spherical harmonics, as described in the previous section, are used to recreate the 3-dimensional soundfield in ambisonic encoding and decoding. Spherical harmonics appear in the general solution to the wave equation in spherical coordinates [62]. A hyperbolic partial-differential equation, the spherical wave equation is useful when examining the sound field in the near-field or in the case of a point source [75], [106]. The equation is shown below:

$$\frac{1}{r^2} \frac{\partial}{\partial r} \left(r^2 \frac{\partial p}{\partial r} \right) + \frac{1}{r^2 \sin \phi} \frac{\partial}{\partial \phi} \left(\sin \phi \frac{\partial p}{\partial \phi} \right) + \frac{1}{r^2 \sin^2 \phi} \frac{\partial^2 p}{\partial \theta^2} - \frac{1}{c^2} \frac{\partial^2 p}{\partial t^2} = 0 \quad (2.1)$$

The spherical wave equation can be solved using separation of variables:

$$p(r, \theta, \phi, \omega) = R(r) \Theta(\theta) \Phi(\phi) T(\omega) \quad (2.2)$$

Through this method, we obtain a system of ordinary differential equations that can be solved individually and inserted into the solution shown above.

$$\begin{aligned} \frac{d^2 \Theta}{d\theta^2} + m^2 \Theta &= 0 \\ \frac{1}{\sin \Phi} \frac{d}{d\phi} \left(\sin \phi \frac{d\Phi}{d\phi} \right) + \left(n(n+1) - \frac{m^2}{\sin^2 \phi} \right) \Phi &= 0 \\ \frac{1}{r^2} \frac{d}{dr} \left(r^2 \frac{dR}{dr} \right) + k^2 R - \frac{n(n+1)}{r^2} R &= 0 \\ \frac{1}{c^2} \frac{d^2 T}{dt^2} + k^2 T &= 0 \end{aligned} \quad (2.3)$$

The solution to the azimuth and time equations can be found using the method of characteristic equations:

$$\Theta(\theta) = \Theta_1 e^{im\theta} + \Theta_2 e^{-im\theta} \quad (2.4)$$

and

$$T(\omega) = T_1 e^{i\omega t} + T_2 e^{-i\omega t} \quad (2.5)$$

The solution to the elevation equation is given by Legendre functions, P_n^m :

$$\Phi(\phi) = \Phi_1 P_n^m(\cos\phi) \quad (2.6)$$

where

$$P_n^m(x) = (-1)^m (1-x^2)^{\frac{m}{2}} \frac{d^m}{dx^m} \left(\frac{1}{2^n n!} \frac{d^n}{dx^n} (x^2-1)^n \right) \quad (2.7)$$

Spherical harmonics are defined from a combination of the azimuth and elevation solutions.

$$Y_n^m(\theta, \phi) = \sqrt{\frac{2n+1}{4\pi} \frac{(n-m)!}{(n+m)!}} P_n^m(\cos\phi) e^{im\theta} \quad (2.8)$$

where $m = -n..n$ and n is the order of the harmonic. Spherical harmonics are orthonormal, which means they can be used to expand any arbitrary function on a sphere. The orthonormality relation is shown below:

$$\int_0^{2\pi} d\phi \int_0^\pi Y_n^m(\theta, \phi) Y_{n'}^{m'}(\theta, \phi)^* \sin\theta d\theta = \delta_{nn'} \delta_{mm'} \quad (2.9)$$

The radial equation can be rewritten as a form of Bessel's equation:

$$\left[\frac{d^2}{dr^2} + \frac{1}{r} \frac{d}{dr} + k^2 - \frac{(n+1/2)^2}{r^2} \right] u_n(r) = 0 \quad (2.10)$$

where

$$R_n(r) = \frac{1}{r^{1/2}} u_n(r) \quad (2.11)$$

The solution is then given in terms of Bessel functions of the first and second kind: $J_{n+1/2}(kr)$ and $Y_{n+1/2}(kr)$:

$$R_n(r) = \frac{A_n}{r^{1/2}} J_{n+1/2}(kr) + \frac{B_n}{r^{1/2}} Y_{n+1/2}(kr) \quad (2.12)$$

where $k = \frac{\omega}{c}$. This solution allows us to define spherical Bessel functions of the first and second kind ($j_n(kr)$ and $y_n(kr)$) and spherical Hankel functions of the first and second kind ($h_n^{(1)}$ and $h_n^{(2)}$), which are defined in terms of the regular Bessel

functions as shown below:

$$\begin{aligned}
 j_n(kr) &= \left(\frac{\pi}{2kr}\right)^{\frac{1}{2}} J_{n+\frac{1}{2}}(kr) \\
 y_n(kr) &= \left(\frac{\pi}{2kr}\right)^{\frac{1}{2}} Y_{n+\frac{1}{2}}(kr) \\
 h_n^{(1)}(kr) &= \left(\frac{\pi}{2kr}\right)^{\frac{1}{2}} [J_{n+\frac{1}{2}}(kr) + iY_{n+\frac{1}{2}}(kr)] \\
 h_n^{(2)}(kr) &= \left(\frac{\pi}{2kr}\right)^{\frac{1}{2}} [J_{n+\frac{1}{2}}(kr) - iY_{n+\frac{1}{2}}(kr)]
 \end{aligned} \tag{2.13}$$

The actual functions depend on the value of n . Spherical Bessel functions are shown for a range of n in Figures 2.1 and 2.2.

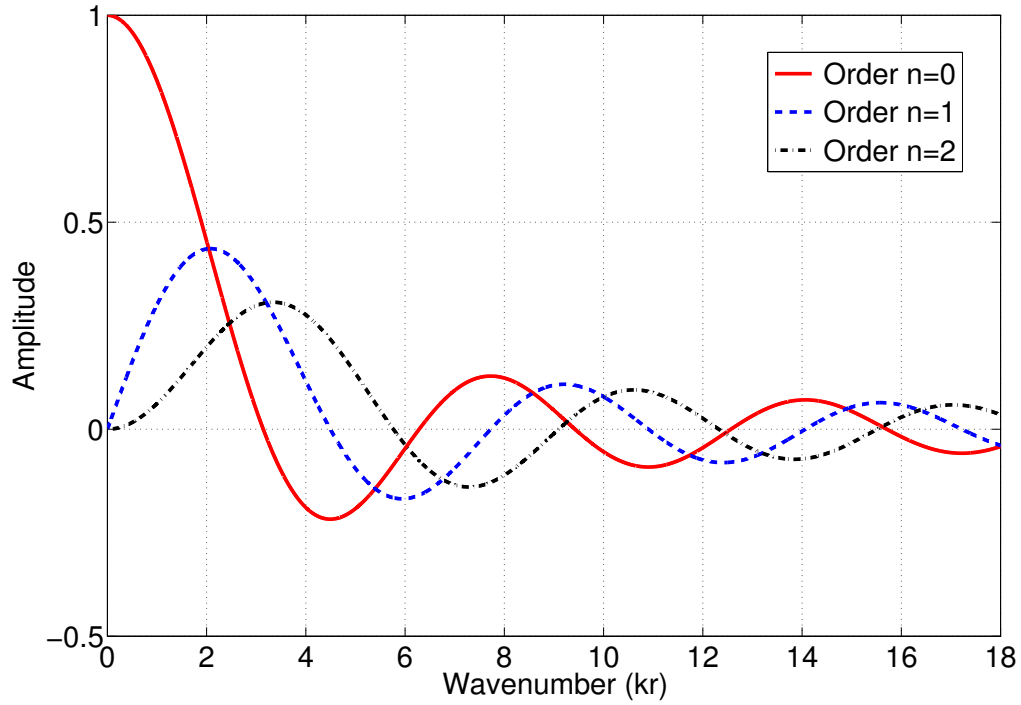


Figure 2.1: Spherical Bessel Functions $j_n(kr)$ for Orders $n=0$, $n=1$, and $n=2$

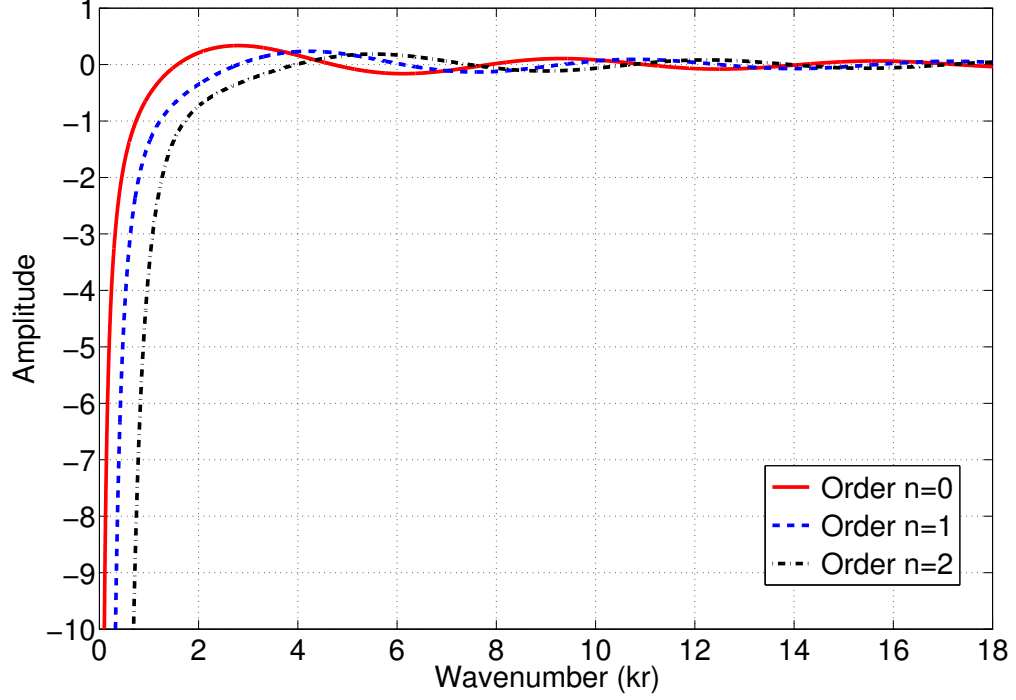


Figure 2.2: Spherical Bessel Functions $y_n(kr)$ for Orders $n=0$, $n=1$, and $n=2$

Using the expressions defined above, we can define the complete general solution for standing waves ($e^{-i\omega t}$ implicit):

$$p(r, \theta, \phi, \omega) = \sum_{n=0}^{\infty} \sum_{m=-n}^n (A_{mn} j_n(kr) + B_{mn} y_n(kr)) Y_n^m(\theta, \phi) \quad (2.14)$$

and for traveling waves ($e^{-i\omega t}$ implicit):

$$p(r, \theta, \phi, \omega) = \sum_{n=0}^{\infty} \sum_{m=-n}^n (C_{mn} h_n^{(1)}(kr) + D_{mn} h_n^{(2)}(kr)) Y_n^m(\theta, \phi) \quad (2.15)$$

In the case of a spherical microphone array, the waves incident on the sphere are assumed to be planar in relation to the size of the spherical array. This is considered an interior problem. The radial function that describes the pressure incident on the sphere for amplitude P_0 is simply the positive portion of the standing wave solution, assuming that the incident field is finite at the origin, which eliminates the y_n

portion:

$$p_i(r, \theta, \phi, \omega) = P_0 \sum_{n=0}^{\infty} \sum_{m=-n}^n A_{mn} j_n(kr) Y_n^m(\theta, \phi) \quad (2.16)$$

Solving for A_{mn} we can determine the incident pressure for all directions (θ_i, ϕ_i) :

$$p_i(r, \theta, \phi, \omega) = P_0 4\pi \sum_{n=0}^{\infty} i^n j_n(kr) \sum_{m=-n}^n Y_n^m(\theta, \phi) \quad (2.17)$$

The total pressure at the surface of the sphere includes both the incident pressure, defined above, and the scattered pressure from the surface, which is considered an exterior problem. The radial function that describes the pressure scattered from a sphere is simply the outgoing portion of the traveling wave solution:

$$p_s(r, \theta, \phi, \omega) = \sum_{n=0}^{\infty} \sum_{m=-n}^n C_{mn} h_n^{(1)}(kr) Y_n^m(\theta, \phi) \quad (2.18)$$

At the surface of a rigid sphere, the radial velocity is zero at $r = a$ if a is the radius of the sphere. This means that the derivative of the total pressure (incident and scattered pressure) is equal to zero when $r = a$, which allows us to solve for C_{mn} .

As a result, the final equation to describe the soundfield scattered from the surface of a rigid sphere of radius a for a plane wave incident from any direction (θ_i, ϕ_i) is given below:

$$p_t(r, \theta, \phi, \omega) = P_0 4\pi \sum_{n=0}^{\infty} i^n \left(j_n(kr) - \frac{j'_n(ka)}{h'_n(ka)} h_n^{(1)}(kr) \right) \sum_{m=-n}^n Y_n^m(\theta, \phi) Y_n^m(\theta_i, \phi_i)^* \quad (2.19)$$

In reality, a finite number of spherical harmonics are used for decomposition, and the equation is restricted to order N :

$$p_t(r, \theta, \phi, \omega) = P_0 4\pi \sum_{n=0}^N i^n \left(j_n(kr) - \frac{j'_n(ka)}{h'_n(ka)} h_n(kr) \right) \sum_{m=-n}^n Y_n^m(\theta, \phi) Y_n^m(\theta_i, \phi_i)^* \quad (2.20)$$

In spherical harmonic decomposition, 0th order consists of a monopole, 1st order consists of a monopole and 3 dipoles, and 2nd order consists of a monopole, 3 dipoles, and 4 quadrupoles. For example, spherical harmonics for order $N = 2$ also

include those for $N = 0$ and $N = 1$. The complex spherical harmonics for order $N = 2$ are shown below:

$$\begin{aligned}
 Y_0^0 &= \frac{1}{\sqrt{4\pi}} & Y_2^{-2} &= 3e^{-2i\theta} \sqrt{\frac{5}{96\pi}} \sin^2 \phi \\
 Y_1^{-1} &= e^{-i\theta} \sqrt{\frac{3}{8\pi}} \sin \phi & Y_2^{-1} &= \frac{3}{2} e^{-i\theta} \sqrt{\frac{5}{24\pi}} \sin 2\phi \\
 Y_1^0 &= \sqrt{\frac{3}{4\pi}} \cos \phi & Y_2^0 &= \sqrt{\frac{5}{16\pi}} (-1 + 3 \cos^2 \phi) \\
 Y_1^1 &= -e^{i\theta} \sqrt{\frac{3}{8\pi}} \sin \phi & Y_2^1 &= -\frac{3}{2} e^{i\theta} \sqrt{\frac{5}{24\pi}} \sin 2\phi \\
 & & Y_2^2 &= 3e^{2i\theta} \sqrt{\frac{5}{96\pi}} \sin^2 \phi
 \end{aligned} \tag{2.21}$$

Figure 2.3 shows directivity patterns for these harmonics [85], [106].

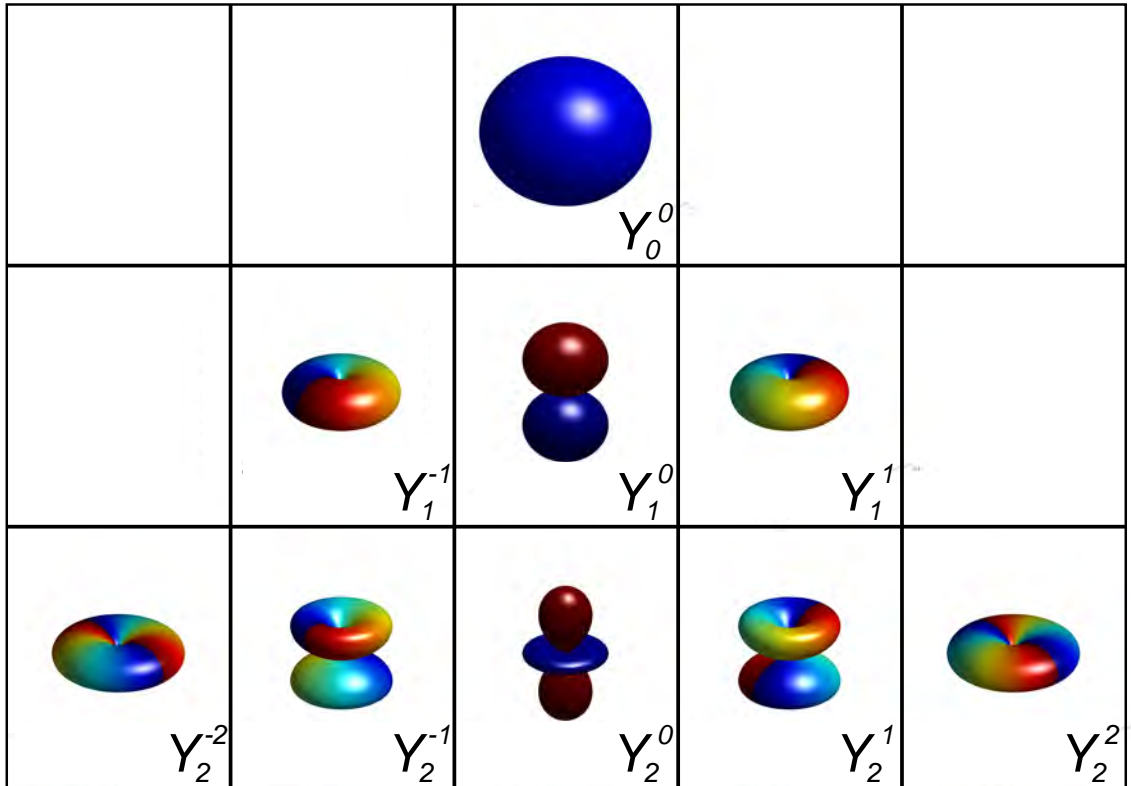


Figure 2.3: Complex Spherical Harmonic Directivity Patterns for Order $N=2$ (Harmonics by Increasing Degree, Color by Phase)

In the case of a recorded audio signal, only the real part of the time-domain signal is present. Therefore, only real spherical harmonics are used. These are related to the complex harmonics described above as follows:

$$\begin{aligned}
Re\{Y_n^m\} &= \frac{1}{\sqrt{2}}(Y_n^m + (-1)^m Y_n^{-m}) && \text{when } m > 0 \\
&= \sqrt{\frac{2n+1}{2\pi} \frac{(n-m)!}{(n+m)!}} P_n^m(\cos \theta) \cos m\phi \\
Re\{Y_n^m\} &= Y_n^m && \text{when } m = 0 \\
Re\{Y_n^m\} &= \frac{1}{i\sqrt{2}}(Y_n^m - (-1)^m Y_n^{-m}) && \text{when } m < 0 \\
&= \sqrt{\frac{2n+1}{2\pi} \frac{(n-m)!}{(n+m)!}} P_n^m(\cos \theta) \sin |m|\phi
\end{aligned} \tag{2.22}$$

From this point forward, Y_n^m will refer to real spherical harmonics. For reference, the real spherical harmonics for order $N = 2$ used in this work are shown below:

$$\begin{aligned}
Y_0^0 &= \sigma_{nm} 1 & Y_2^{-2} &= \sigma_{nm} \sin(2\theta) \sin^2 \phi \\
Y_1^{-1} &= \sigma_{nm} \sin \theta \sin \phi & Y_2^{-1} &= \sigma_{nm} \sin \theta \cos \phi \sin \phi \\
Y_1^0 &= \sigma_{nm} \cos \phi & Y_2^0 &= \sigma_{nm} 3 \cos^2 \phi - 1 \\
Y_1^1 &= \sigma_{nm} \cos \theta \sin \phi & Y_2^1 &= \sigma_{nm} \cos \theta \cos \phi \sin \phi \\
& & Y_2^2 &= \sigma_{nm} \cos(2\theta) \sin^2 \phi
\end{aligned} \tag{2.23}$$

where σ_{nm} refers to the encoding convention used. In Ambisonics, these signals are assigned the letters R-Z as shown in Table 2.1.

Table 2.1: Ambisonic Signal Names for Spherical Harmonic Components by Increasing Degree, Order $N=2$

Harmonic	Name
Y_0^0	W
Y_1^{-1}	Y
Y_1^0	Z
Y_1^1	X
Y_2^{-2}	V
Y_2^{-1}	T
Y_2^0	R
Y_2^1	S
Y_2^2	U

An image of the real harmonics is shown in Figure 2.4.

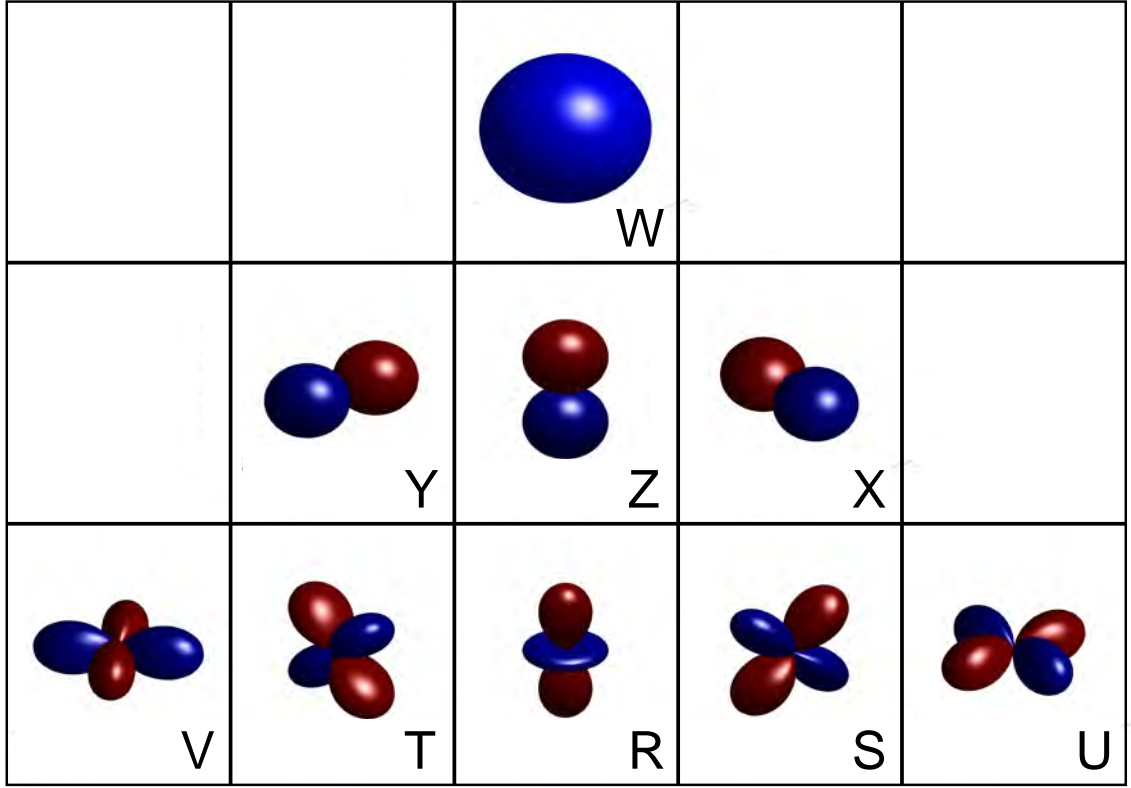


Figure 2.4: Real Spherical Harmonic Directivity Patterns for Order $N=2$ (Harmonics by Increasing Degree)

2.2.2 Spherical Harmonic Decomposition

In the case of a recorded signal in a real soundfield, multiple plane waves are incident from several directions and several points in time, and so the term representing the spherical harmonic decomposition of a single plane wave $Y_n^m(\theta_i, \phi_i)^*$ is generalized into a term representing the spherical harmonic decomposition of the general incident sound field, B_n^m . Additionally, we are now only concerned about the pressure at the surface of the sphere, where $r = a$, so for ease of writing, we use r to refer to the radius of the sphere and group the radial components of the sound field into a single term describing “modal amplitude,” $b_n(kr)$:

$$b_n(kr) = j_n(kr) - \frac{j'_n(kr)}{h'_n(kr)} h_n(kr) \quad (2.24)$$

so that the equation for pressure on the surface of the rigid sphere is given as:

$$p(\theta, \phi) = P_0 4\pi \sum_{n=0}^N i^n b_n(kr) \sum_{m=-n}^n Y_n^m(\theta, \phi) B_n^m \quad (2.25)$$

In order to solve for B_n^m or “encode” the recorded signal $p(\theta, \phi)$ into its spherical harmonic components, a spatial Fourier transform is necessary:

$$B_n^m = \frac{1}{4\pi i^n b_n(kr)} \int_0^{2\pi} \int_0^\pi p(\theta, \phi) Y_n^m(\theta, \phi)^* \sin \theta d\theta d\phi \quad (2.26)$$

In the case of a recorded signal, it is not possible to record a spatially-continuous signal over all points of the sphere. Therefore, a discrete number of signals S are recorded using q sensors distributed evenly over the surface of the sphere [2]. These signals spatially sample the pressure on the sphere, replacing the spatially-continuous signal $p(\theta, \phi)$ as shown:

$$S_q = P_0 4\pi \sum_{n=0}^N i^n b_n(kr) \sum_{m=-n}^n Y_n^m(\theta_q, \phi_q) B_n^m \quad (2.27)$$

In order to solve for B_n^m , the spatial Fourier transform becomes a system of linear equations that must be solved using matrix operations [73]. The system is shown below:

$$\mathbf{T} \cdot \mathbf{b} = \mathbf{s} \quad (2.28)$$

where \mathbf{T} is the $Q \times (N+1)^2$ matrix of spatial Fourier transforms, \mathbf{b} is the vector of spherical harmonic components (length $(N+1)^2$) of the incident sound field B_n^m , and \mathbf{s} is the vector of recorded signals S_q for $1 \leq q \leq Q$.

This system is shown below:

$$\left(\begin{bmatrix} Y_0^0(\theta_1, \phi_1) & \cdots & Y_2^2(\theta_1, \phi_1) \\ \vdots & \vdots & \vdots \\ Y_0^0(\theta_q, \phi_q) & \cdots & Y_2^2(\theta_q, \phi_q) \end{bmatrix} \cdot \text{diag}[4\pi P_0 i^n b_n(kr)] \right) \cdot \begin{bmatrix} B_0^0 \\ \vdots \\ B_n^m \end{bmatrix} = \begin{bmatrix} S_1 \\ \vdots \\ S_q \end{bmatrix} \quad (2.29)$$

Because there are more sensors than harmonic components, the system is overde-

terminated and a “naive” least-squares solution may be found, \mathbf{b}_{LS} . Multiplying both sides of the system by the conjugate transpose of \mathbf{T} generates the invertible matrix $\mathbf{T}^*\mathbf{T}$:

$$\mathbf{b}_{\text{LS}} = (\mathbf{T}^* \mathbf{T})^{-1} \mathbf{T}^* \mathbf{s} \quad (2.30)$$

Replacing \mathbf{T} with $\mathbf{Y} \cdot \text{diag}[4\pi P_0 i^n b_n(kr)]$ where \mathbf{Y} is the matrix of spherical harmonics, the equation becomes:

$$\mathbf{b}_{\text{LS}} = \text{diag} \left[\frac{1}{4\pi P_0 i^n b_n(kr)} \right] \mathbf{E} \mathbf{s} \quad (2.31)$$

where \mathbf{E} is the Moore-Penrose inverse of \mathbf{Y} :

$$\mathbf{E} = (\mathbf{Y}^t \mathbf{Y})^{-1} \mathbf{Y}^t \quad (2.32)$$

and \mathbf{b}_{LS} is the set of “encoded” HOA signals, available for reproduction over the loudspeaker array.

2.2.3 Tikhonov Regularization

The solution described above degrades when $\text{diag}[4\pi P_0 i^n b_n(kr)]$ is very small, which occurs for higher orders at low frequencies, creating noise in these components. Using the Tikhonov method, a set of filters can be applied to regularize the solution and reduce the levels of noise these components while still retaining the relevant data [73]. The filters are applied to the least-squares solution to replace \mathbf{b}_{LS} with \mathbf{b}_{reg} as follows:

$$\mathbf{b}_{\text{reg}} = \text{diag} \left[F_n(kr) \cdot \frac{1}{4\pi P_0 i^n b_n(kr)} \right] \mathbf{E} \mathbf{s} \quad (2.33)$$

where

$$F_n(kr) = \frac{|4\pi P_0 i^n b_n(kr)|^2}{|4\pi P_0 i^n b_n(kr)|^2 + \lambda^2} \quad (2.34)$$

λ is the regularization parameter, and its exact value should be optimized for individual sampling schemes using trial and error in order to maximize the rejection of

noise from the signal. An iterative optimization method was used for determining λ in this research, determining that a value of $\lambda = 0.127$ provided the best rejection of noise.

2.2.4 Spatial Aliasing

Due to the discrete nature of the spatially-sampled soundfield, the reconstruction of the actual signal has the potential for degradation, known as spatial aliasing [88]. This occurs in two situations. At high frequencies, when the distance between the sensors on the sphere is too large compared with the wavelength (similar to the Nyquist frequency in time-domain sampling). The frequency above which aliasing occurs for a given sampling scheme is defined as:

$$f_{al} = \frac{c}{2r\gamma} \quad (2.35)$$

for speed of sound c , radius r and angle between sensors γ .

Additionally, spatial aliasing can occur at higher orders, if the number of spherical harmonic components is higher than the number of sensors or the sampling scheme is irregular. This results in undersampling of the higher order components, which can create both orthonormality error noise within the higher components and aliasing noise folding down into lower orders components. Therefore, both the size of the size of the sphere and the chosen sampling scheme (number of sensors and sensor locations) influence the accuracy of the sound field reconstruction.

2.2.5 Spherical Sampling

The number of sensors q and sensor locations (θ_q, ϕ_q) on the sphere are chosen to minimize orthonormality errors (which can prevent an accurate reconstruction of the sound field). The number of sensors should be greater than the number of spherical harmonic components $(N + 1)^2$ for a given order N , and the optimal number of sensors is determined by the sampling scheme [86].

Possible modes of sampling include equiangular, Gaussian, regular polyhedral and semi-regular polyhedral schemes. Equiangular sampling requires uniform sampling along both azimuth and elevation, which generates an uneven distribu-

tion of points with increased density at the poles of the sphere. In addition, this scheme requires a large number of points to accurately reconstruct the sound field, $4(N + 1)^2$. Gaussian sampling uses the Legendre polynomials to sample the sphere at unequally-spaced angles. In this scheme, the number of points required is still high at $2(N + 1)^2$.

Regular polyhedral sampling is only possible if the number of required points matches one of the five Platonic polyhedra. Unfortunately, the orthonormality error for most of these schemes is significant for higher orders. Only the dodecahedron (12 points) and icosahedron (20) would provide accurate reconstruction up to order $N = 2$. However, these numbers are not always convenient for signal processing purposes.

Due to the availability of multi-channel recording equipment, a 16-sensor scheme was chosen for this research. Because this scheme does not match one of the acceptable Platonic polyhedra, a semi-regular polyhedral scheme was chosen. Although multiple methods of semi-regular sampling exist, the one of interest for this study uses a stochastic dispersion and interpolation method to determine the coordinates and the weights for integration. The goal of the stochastic dispersion is to minimize the largest difference between 2 distances, E , for all points [33]:

$$E(x_1 \dots x_N) = \sum_{i=1}^N \sum_{j=1+i}^N \frac{1}{\|x_i - x_j\|} \quad (2.36)$$

The multivariate interpolation theory used to find the quadrature coefficients α_j (weights assigned to each point to allow even integration over the sphere) uses a cubature formula with Lagrange polynomials:

$$\alpha_j = \sum_{k=1}^N \left(\int_S l_j(x) l_k(x) dx \right) \quad (2.37)$$

where Lagrange polynomials are found with the following equation:

$$l_j(x) = \prod_{i=0, i \neq j}^k \frac{x - x_i}{x_j - x_i} \quad (2.38)$$

The sampling scheme determined using this method for 16 points is shown in Table 2.2 along with the quadrature coefficients α_q for q sensors.

Table 2.2: Sensor Points and Quadrature Coefficients for 16-Point Semi-Regular Polyhedral Sampling

Sensor	θ (rad)	ϕ (rad)	α_q
1	0.00	0.00	0.76
2	0.00	0.85	0.76
3	-1.42	0.95	0.87
4	-2.80	0.92	0.76
5	2.30	0.92	0.76
6	1.16	1.08	0.87
7	1.12	2.03	0.76
8	0.27	1.74	0.76
9	-0.64	1.57	0.76
10	-1.38	2.03	0.76
11	-2.20	1.57	0.76
12	3.01	1.76	0.87
13	2.04	1.74	0.76
14	-0.25	2.61	0.87
15	-2.47	2.46	0.76
16	2.15	2.65	0.76

In semi-regular schemes, some orthonormality error exists for all orders. This error can be audible as noise in the signal. However, if the orthonormality error is below the noise floor of the signal, it will not interfere with the perceptual accuracy of the reconstruction. The sampling scheme used in this research generates orthonormality error that is 100 dB below the signal level up to order $N = 1$ and 40 dB below the signal level up to order $N = 2$. For orders $N = 3$ and higher, the orthonormality error begins to interfere with the signal level and prevents perceptually accurate reconstruction. Therefore, this research is limited to spherical

harmonic decompositions of order $N = 2$ [21].

2.2.6 Beamforming

In addition to ambisonic encoding, signals recorded by the spherical array must also be analyzed in order to examine the spatial resolution of the sound field. The ideal way to do this is using a method called beamforming, described below [72].

Due to the orthonormality properties of spherical harmonics, the inner product of two spherical harmonics will be zero except where they are the same, when they will be equal to one:

$$\int_0^{2\pi} \int_0^\pi Y_{n'}^{m'}(\theta, \phi)^* Y_n^m(\theta, \phi) \sin\theta d\theta d\phi = \delta_{nn'} \delta_{mm'} \quad (2.39)$$

This means that a signal can be weighted by an infinite sum of spherical harmonics, which will function as a “beam” that can be pointed in different “look directions” and reject all other information on the sphere. This allows the spatial sound field to be mapped over multiple look directions, or spatially filtered to auralize only a narrow segment of the sound field. Beamforming uses the same spherical harmonic decomposition as ambisonics, but then weights the components by look direction and uses the linear sum of these weighted components to create a beam pattern for that look direction.

As shown in [64], returning to the equation for pressure at the surface of the rigid sphere due to a plane wave incident from (θ_i, ϕ_i) :

$$p(\theta, \phi, kr) = P_0 4\pi \sum_{n=0}^{\infty} i^n \left(j_n(kr) - \frac{j'_n(kr)}{h'_n(kr)} h_n(kr) \right) \sum_{m=-n}^n Y_n^m(\theta, \phi) Y_n^m(\theta_i, \phi_i)^* \quad (2.40)$$

and applying a weighting function to each point on the sphere:

$$W_{n'}^{m'}(\theta, \phi, kr) = \frac{Y_{n'}^{m'}(\theta, \phi)^*}{4\pi i^{n'} b_{n'}(kr)} \quad (2.41)$$

provides the following relationship, due to the orthonormality of the spherical harmonics as defined above:

$$\int_0^{2\pi} \int_0^\pi W_{n'}^{m'}(\theta, \phi, kr) p(\theta, \phi, kr) \sin\theta d\theta d\phi = Y_{n'}^{m'}(\theta_i, \phi_i)^* \quad (2.42)$$

This once again proves that spherical harmonic decomposition of a plane wave can be performed on the surface of a rigid sphere, and that any function on the surface of that sphere can be expressed in terms of these components. In this case, the function to be expressed is a delta function or “beam” pointed in the look direction (θ_0, ϕ_0) :

$$F(\theta, \phi, \theta_0, \phi_0) = \delta(\theta - \theta_0) \delta(\phi - \phi_0) \quad (2.43)$$

This ideal beam, when expressed in terms of spherical harmonic components, becomes:

$$F(\theta, \phi, \theta_0, \phi_0) = 2\pi \sum_{n=0}^{\infty} \sum_{m=-n}^n Y_n^m(\theta_0, \phi_0)^* Y_n^m(\theta, \phi) \quad (2.44)$$

As described above, a weighting function applied to each point (θ_s, ϕ_s) on the surface of the sphere can be found that will generate any beam pattern. The function that will generate $F(\theta, \phi, \theta_0, \phi_0)$ is shown below:

$$w(\theta_0, \phi_0, \theta_s, \phi_s, kr) = \sum_{n=0}^{\infty} \frac{1}{2i^n b_n(kr)} \sum_{m=-n}^n Y_n^m(\theta_0, \phi_0)^* Y_n^m(\theta_s, \phi_s) \quad (2.45)$$

In the case of an array of microphones distributed on a rigid sphere, the signal p is of course discretely sampled at q points, and the orthonormality relationship must be approximated for a discrete sampling:

$$\frac{4\pi}{Q} \sum_{q=1}^Q Y_n^{m*}(\theta_q, \phi_q) Y_{n'}^{m'}(\theta_q, \phi_q) C_{n'}^{m'} = \delta_{nn'} \delta_{mm'} \quad (2.46)$$

where C_n^m are the quadrature coefficients for the specific sampling scheme, defined in Section 2.2.5. Additionally, the sum of spherical harmonic components is limited to order N . Truncated beamformer equations are shown below:

$$F_N(\theta, \phi, \theta_0, \phi_0) = 2\pi \sum_{n=0}^N \sum_{m=-n}^n Y_n^m(\theta_0, \phi_0)^* Y_n^m(\theta, \phi) \quad (2.47)$$

$$w_N(\theta_0, \phi_0, \theta_q, \phi_q, kr) = \sum_{n=0}^N \frac{1}{2i^n b_n(kr)} \sum_{m=-n}^n Y_n^m(\theta_0, \phi_0)^* Y_n^m(\theta_q, \phi_q) C_n^m(\theta_q, \phi_q)$$

Because the beam orders are truncated, they will not converge to a perfect delta. The width of the beam in the look direction will be determined by the order N and side and rear lobes will form. Images of beams for orders up to $N = 2$ are shown in Figure 2.5.

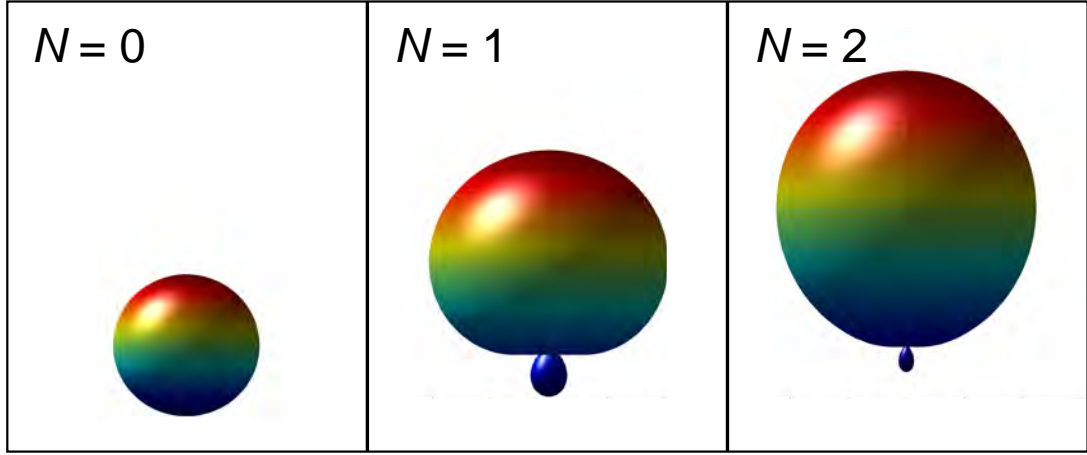


Figure 2.5: Ideal Beam Patterns for a Single Plane Wave Decomposition for Values of N up to Order $N=2$

As with the ambisonic encoding process, beamforming with a discrete sampling scheme takes the form of a linear system of equations:

$$\begin{aligned} \mathbf{A}\mathbf{W} &= c_N \mathbf{B}_N \\ \mathbf{d}^T \mathbf{W} &= 1 \end{aligned} \quad (2.48)$$

where \mathbf{A} is the matrix of spherical harmonic components of the soundfield at each microphone:

$$\mathbf{A} = 4\pi \begin{bmatrix} i^0 b_0(kr) Y_0^{0*}(\theta_1, \phi_1) & \cdots & Y_0^{0*}(\theta_q, \phi_q) \\ \vdots & \vdots & \vdots \\ i^N b_N(kr) Y_N^{N*}(\theta_1, \phi_1) & \cdots & Y_N^{N*}(\theta_q, \phi_q) \end{bmatrix} \quad (2.49)$$

\mathbf{B}_N is the vector of spherical harmonic components of the beam pointed in look direction (θ_0, ϕ_0) :

$$\mathbf{B}_N = 2\pi \begin{bmatrix} Y_0^{0*}(\theta_0, \phi_0) \\ \vdots \\ Y_N^{N*}(\theta_0, \phi_0) \end{bmatrix} \quad (2.50)$$

\mathbf{d} is the vector of pressure produced at q sensors by a unit plane wave from the look direction (θ_0, ϕ_0) and c_N is a normalizing coefficient which can be approximated to:

$$c_N \approx \frac{2}{(N+1)^2} \quad (2.51)$$

\mathbf{W} is the vector of weights applied to each sensor. It can be determined by finding the least-squares solution to the system:

$$\mathbf{W} = [(\mathbf{A}^H \mathbf{A})^{-1}] c_N \mathbf{B}_N \quad (2.52)$$

The robustness of the beam can be determined by the white noise gain (WNG), based on the equality defined above for \mathbf{W} :

$$\text{WNG}(\theta_0, \phi_0, \theta_q, \phi_q, kr) = 10 \log_{10} \left(\frac{|\mathbf{d}^T \mathbf{W}|^2}{\mathbf{W}^H \mathbf{W}} \right) \quad (2.53)$$

Once \mathbf{W} is found, it can be applied to the vector of pressures recorded at each sensor and summed over all sensors to provide the complex frequency response of the spherical harmonic decomposition of the beam pattern, as defined above:

$$F(\theta_0, \phi_0, kr) = \sum_{q=1}^Q W(\theta_q, \phi_q, kr) p(\theta_q, \phi_q, kr) \quad (2.54)$$

This can then be returned to the time domain using the inverse Fourier transform to provide the spatially-filtered signal. The spatial energy distribution over

a single measurement or time window can be determined by summing the energy in the signal for each look direction over a number of look directions. The spatial resolution of the map is dictated by the overlapping and lobing created by each beam.

2.3 Methodology

2.3.1 Spherical Microphone Array Design

The microphone array used in this research was designed based on principles described in Section 2.2.5. The microphone has 16 capsules distributed in a semi-regular arrangement over the surface of a sphere, with Capsule #1 at the “top” of the sphere. The coordinates of the microphones (at the center of each capsule) and the quadrature coefficients for each signal were given in Table 2.2. The sphere itself is hollow plastic, printed on a rapid prototyping machine at the Rensselaer Polytechnic Institute Materials Laboratory. The sphere was designed to have a radius of 2.5 centimeters, based on an upper limit design frequency for spatial aliasing of 8 kHz. For reference, the equation is given below:

$$f_{al} = \frac{c}{2r\gamma} \quad (2.55)$$

for speed of sound c , radius r and angle between sensors γ , which is $\frac{5\pi}{18}$ radians (50°) on average.

In reality, the array is also limited by the order of spherical harmonics, which as described in Section 2.2.2, is limited to $N = 2$ for the microphone because the redundancy necessary to achieve an over-determined system for higher orders (for example, there are exactly 16 harmonics in order $N = 3$) is not possible with only 16 capsules. The spatial aliasing frequency for this limitation is determined by [88]:

$$f_{al} = \frac{cN}{2\pi r} \quad (2.56)$$

which is just over 4 kHz for this sphere. In practice, it was found that for auralization, localization and realistic spatialization were achieved up to 8 kHz, whereas for beamforming, signals needed to be band-limited at an upper frequency limit of

4 kHz.

The sphere was designed to house the cabling necessary to connect the capsules to a preamplifier/soundcard. Therefore, the walls of the sphere are 5 mm thick, and the sphere is formed in two pieces that lock together with screws. After the rapid prototyping, the sphere was sanded to eliminate any large irregularities on the surface. A 6 mm threaded rod is connected to the bottom of the sphere in order to mount it on the standard boom of a microphone stand. It is likely that some diffraction artifacts at high frequencies were generated by this rod, which would fall in the 6 kHz range. The design of the sphere is shown in Figure 2.6.

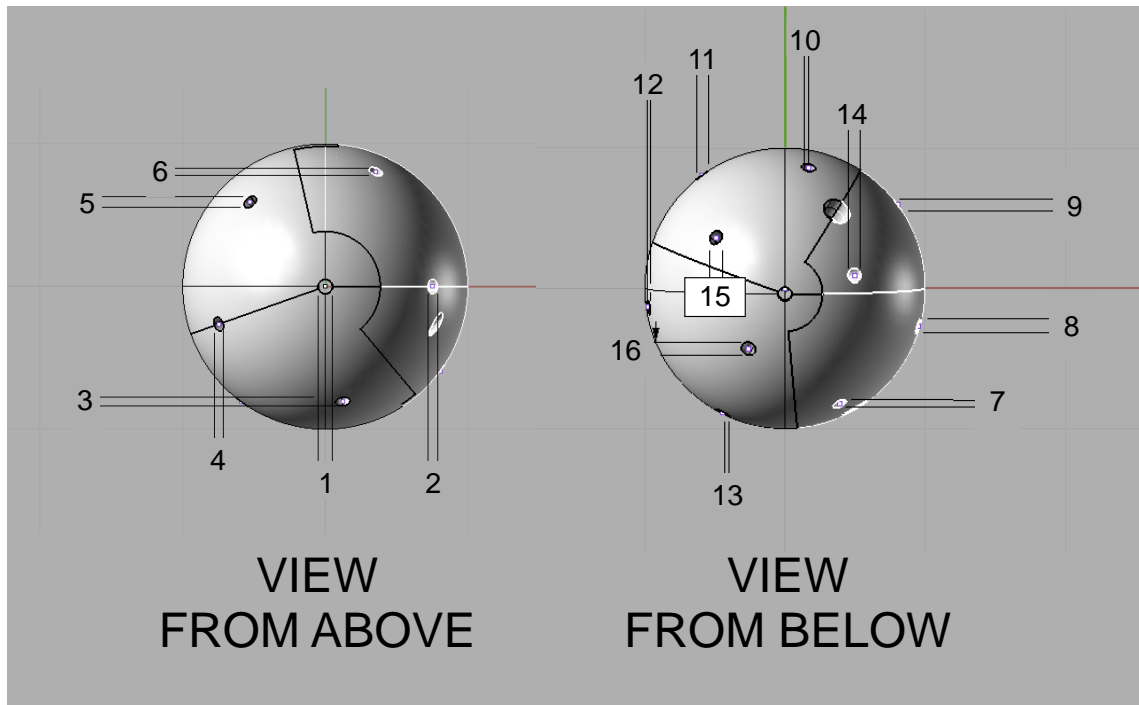


Figure 2.6: 3D Computer Model of Spherical Microphone Array Showing Capsule Locations

The capsules themselves are electret condenser microphone capsules produced by CUI, Inc. They are omnidirectional capsules with a 60 dB signal-to-noise ratio from 100 Hz - 20 kHz. They have a diameter of 6 mm. An image of the microphone array is shown in Figure 2.7.



Figure 2.7: Photos of Constructed Spherical Microphone Array

The capsules were soldered to a multi-conductor cable with 28 AWG solid copper wire. The cable was terminated in 16 RCA connectors in order to connect to a proprietary 16-channel interface built by the RPI Acoustics Department. The interface provides the low-voltage phantom power, A/D conversion and amplification necessary to transmit the signal over a National Instruments (68-pin SCSI) cable into the computer processor. Proprietary acoustic measurement software built by Dr. Ning Xiang (MaxSens) records and processes the 16-channel signal. The software was used in this research to generate impulse responses applying the deconvolution method to exponential sine sweeps.

The interface has an XLR output connection for sending an excitation signal to a sound source, which in the case of these measurements consisted of a two-dodecahedron set (mid and high-frequency sources, also proprietary to RPI) and a subwoofer with crossovers between each device. The signal is captured by the 16 capsules on the sphere and recorded by MaxSens. In this case, a 10-second exponential sweep was used. The system sends out and records multiple sweeps (10 sweeps were used in this research) and takes an average in order to maximize the signal-to-noise ratio of the measurement. The recorded signal is deconvolved using the reference signal (internally captured by the software) in order to provide the impulse response of each capsule. Due to the requirements of the National Instruments card in the computer processor, the sampling rate of the signal is 62.5

kHz. The multi-channel impulse response is then saved as a “.tid” file, which can be processed using MatLab. A diagram of the system is shown in Figure 2.8.

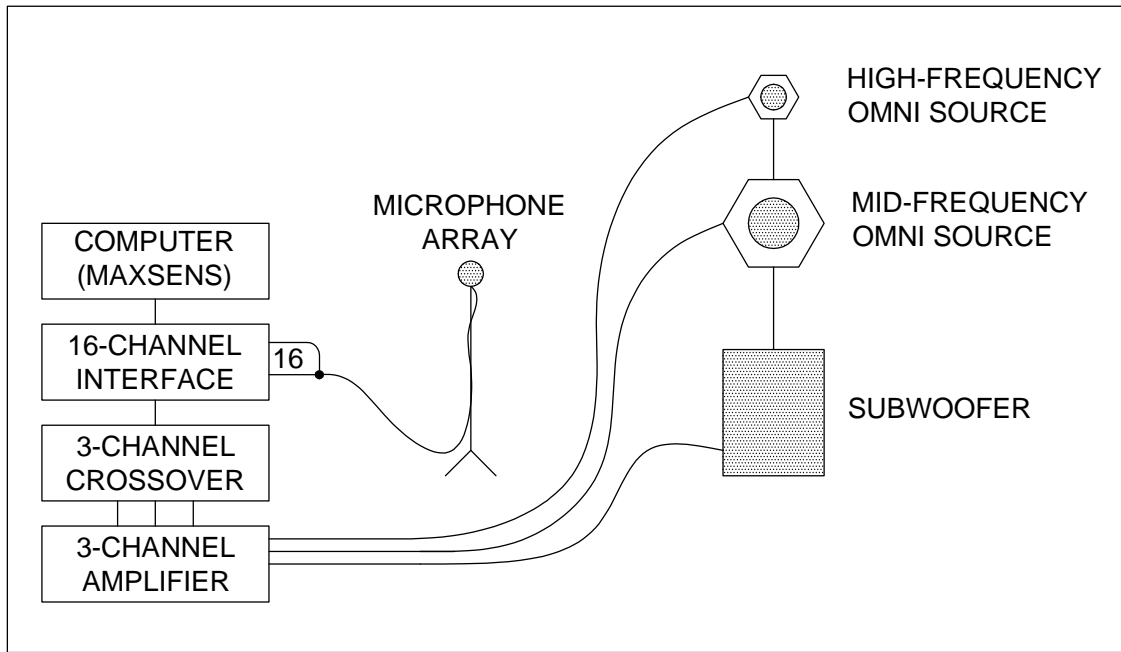


Figure 2.8: Functional Diagram of Spherical Microphone Array Measurement System

Images of the system are shown in Appendix C.1.

2.3.2 Spherical Microphone Array Calibration

Calibration filters should be applied to the recorded signal for two reasons. First, the frequency response of the individual capsules contain slight variations due to the fact that the capsules were not matched in the factory. Second, the irregularities in the sphere (surface texture generated by the rapid prototyping process and mic positioning errors, as well as diffraction artifacts generated by the rod, cable and mic stand) cause variations in the frequency response of each channel when the capsules are mounted in the sphere. It was determined that the best method for capturing all frequency and level variations was to measure the response of each capsule in situ. The calibration measurements were conducted in the NYS-TAR Acoustics and Telepresence Lab in the Gurley Building at RPI. Images of the

calibration process are shown in Appendix C.1.

The sound source was positioned in a fixed location. Using a laser range finder, the microphone was positioned so that the capsule under test was located 1 meter from the source on axis. The impulse response of the capsule under test was captured using the method described in Section 2.3.1. The NYSTAR Lab was used for calibration because the reverberation was relatively short (although it was not anechoic) and the background noise levels were low compared to other available spaces. The signals were recorded for each capsule in the same location, and then the signals were truncated to isolate the direct sound (eliminating the room response of the NYSTAR Lab as much as possible). A reference signal was recorded using a Bruel & Kjaer omnidirectional capsule (calibrated for acoustic measurements) mounted in the same location as the capsules under test in the absence of the sphere. The recorded frequency response of the capsules (with the B&K signal shown for reference) is shown in Figure 2.9.

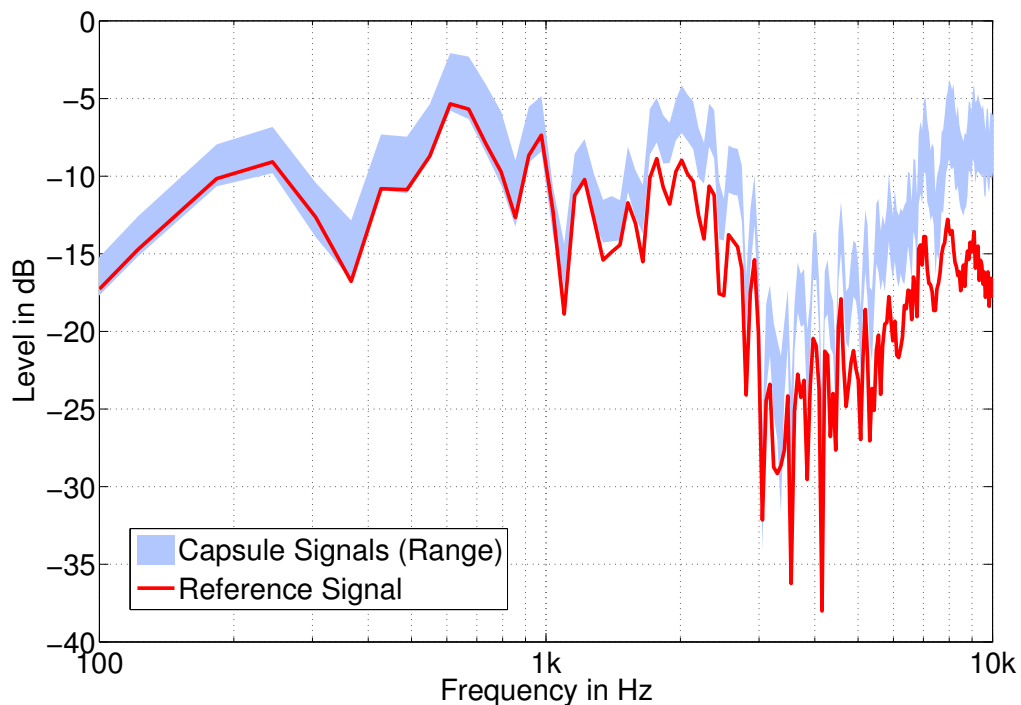


Figure 2.9: Unfiltered Log Magnitude Frequency Response of 16 Individual Capsules (Shaded Area) and Reference Mic (Solid Line)

The overall gain deviation between the capsules and the reference microphone is shown in Figure 2.10.

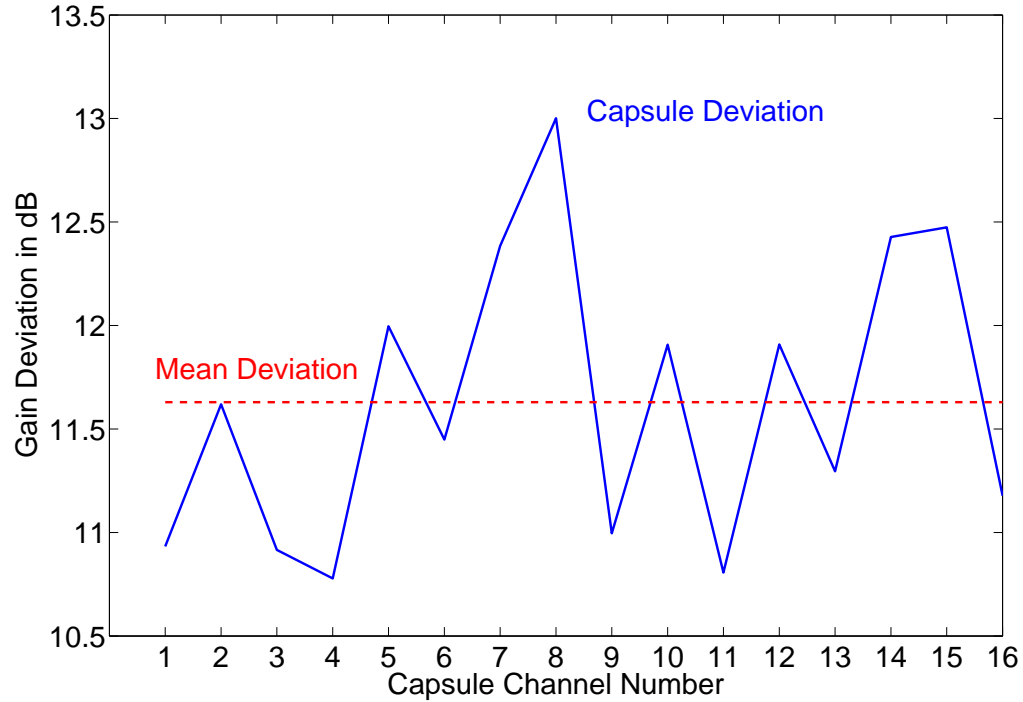


Figure 2.10: Mean Gain Deviations Between 100 Hz and 3 kHz for 16 Individual Capsules and B&K Reference Microphone

Using the transfer function of each capsule deconvolved with the reference signal, minimum phase FIR filters were generated to equalize the channels. These filters are shown in Figure 2.11.

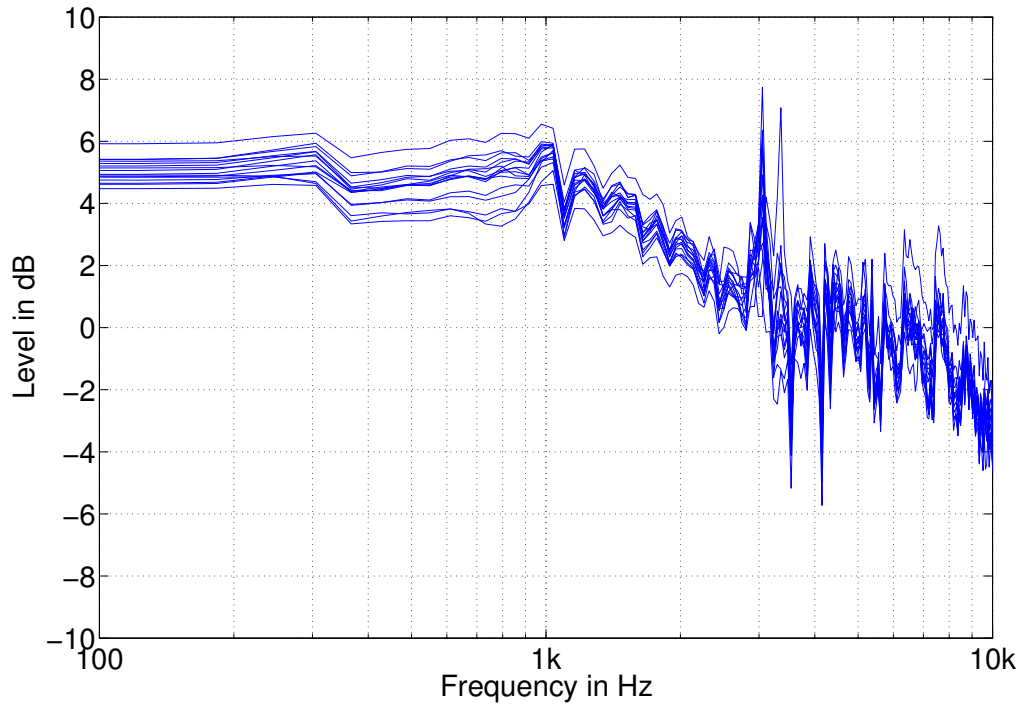


Figure 2.11: Log Magnitude Frequency Response of 16 Minimum Phase FIR Filters for Individual Capsule Calibration

The FIR filters were then applied to the individual capsules before any spherical harmonic decomposition is performed. The equalized calibration signals are shown in Figure 2.12. There is a marked improvement, especially in the mid and high frequencies, where localization is most affected.

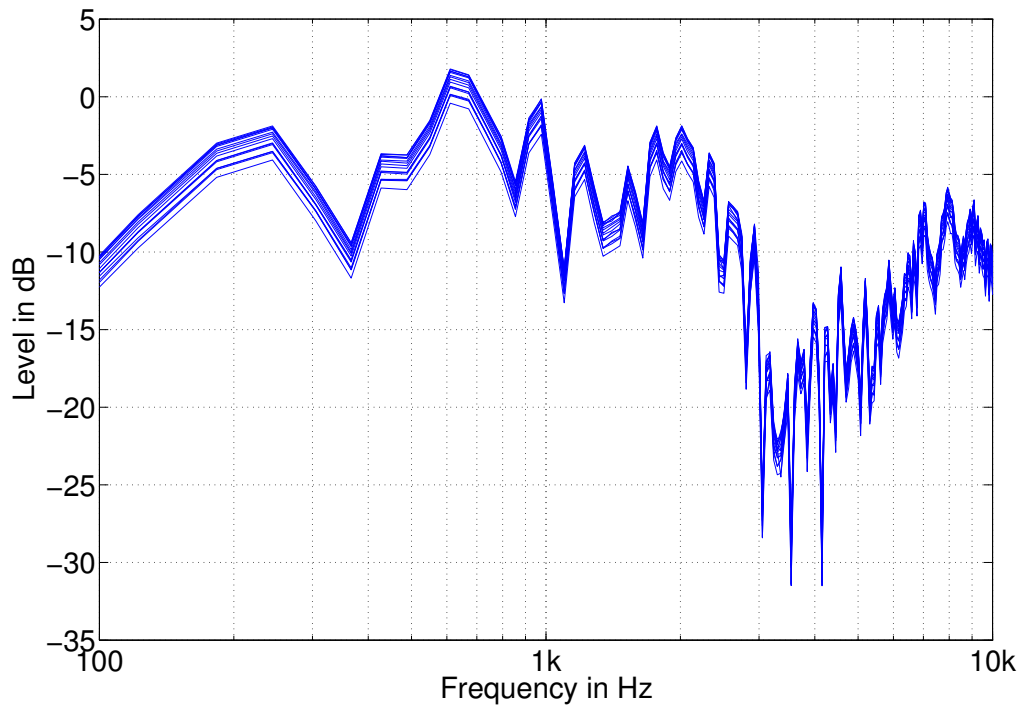


Figure 2.12: Filtered Log Magnitude Frequency Response of 16 Individual Capsules

2.4 Results

2.4.1 Spherical Microphone Array Testing

Once the capsules were calibrated, it was necessary to determine the performance of the array. The first testing scenario was conducted in Room 101 of the Greene Building at RPI. The room was chosen because it was large enough that the distance between the microphone array and the sound source could be considered “far field.” For the frequency range under test, this distance was set at 2 meters. Additionally, the microphone was positioned approximately 2 meters from the nearest surface (including the floor). The room was reverberant, and so the recorded signals had to be time-windowed, but the first reflection from the nearest surface would arrive 7 ms after the direct sound, corresponding to a wavelength of 140 Hz. For localization testing, this frequency limit was sufficient. A directional loudspeaker was used to reduce unwanted reflections. Images of the test setup are

shown in Appendix C.1.

The microphone was positioned with Capsule #1 facing directly up and rotated horizontally in 15° increments. Impulse responses from the loudspeaker were recorded in each position for all capsules. Then the microphone was rotated in 45° increments in elevation and impulse responses were recorded. Using beamforming techniques described in Section 2.2.6, the 2nd-order spherical harmonic directivity of the time-windowed impulse responses were calculated [64]. For comparison, the pressure was calculated at each capsule location for a theoretical plane wave from the same directions as those measured, and 2nd-order theoretical beams were generated using the same methods. For comparison, beams generated from a measured excitation signal and a theoretical plane wave from the same direction are shown in Figure 2.13. The beams have been normalized to account for errors in physical placement when turning the microphone. The beam is band-limited at the 2kHz octave band and displayed in dB. As shown, the beam size and shape for the measured and theoretical beam are almost identical for this direction.

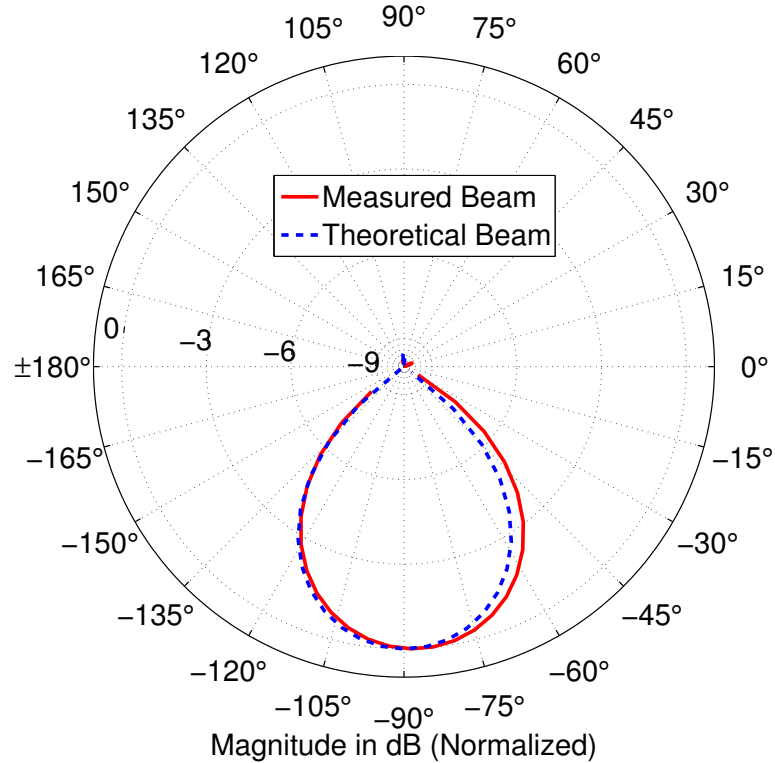


Figure 2.13: Comparison of Beamformer with Real and Theoretical Far Field Signal, 2 kHz Octave Band (Measured = Solid Line, Theoretical = Dashed Line)

However, not all beams are identical for the real measurements. This is likely due to the limitations of the test setup. Positioning errors (angle and distance) and change in orientation of surface reflections due to microphone rotation may contribute to the shape and magnitude of the beams. Additionally, some irregularities in the spherical array that are not accounted for by the capsule filters, such as small discrepancies in capsule placement from the theoretical coordinates, can affect the beam shapes. However, the uniformity of beam width and direction of maximum magnitude show that the microphone array is usable for auralization and beam-forming analysis. Measured beams from 4 azimuthal directions (90° increments) are shown in Figure 2.14. Measured beams from all measured azimuthal directions (15° increments) are shown in Figure 2.15. The same directions for the theoretical beams are shown in Figure 2.16 and Figure 2.17.

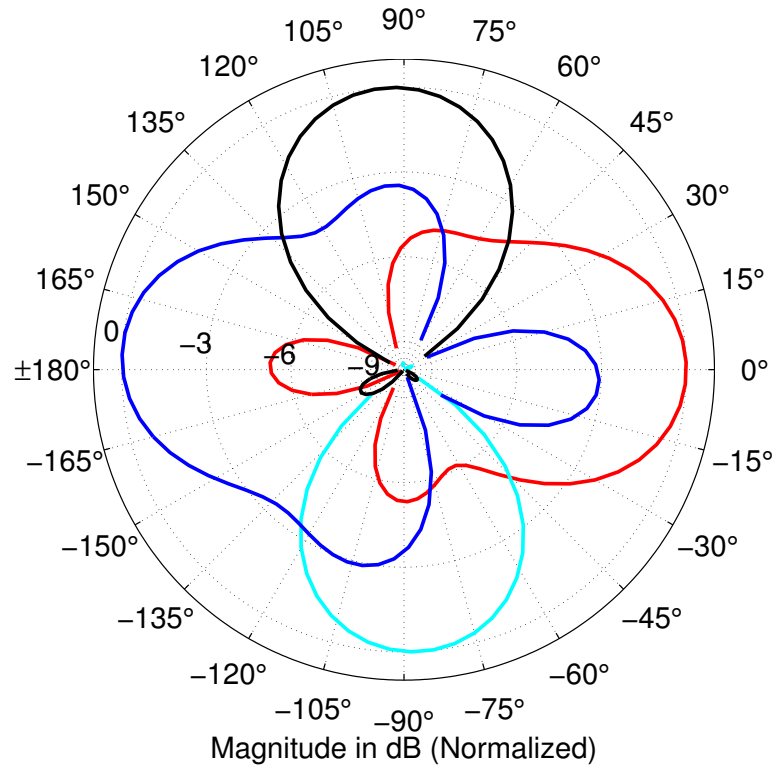


Figure 2.14: Beamformer with Measured Far Field Signals at 90° Increments, 2 kHz Octave Band

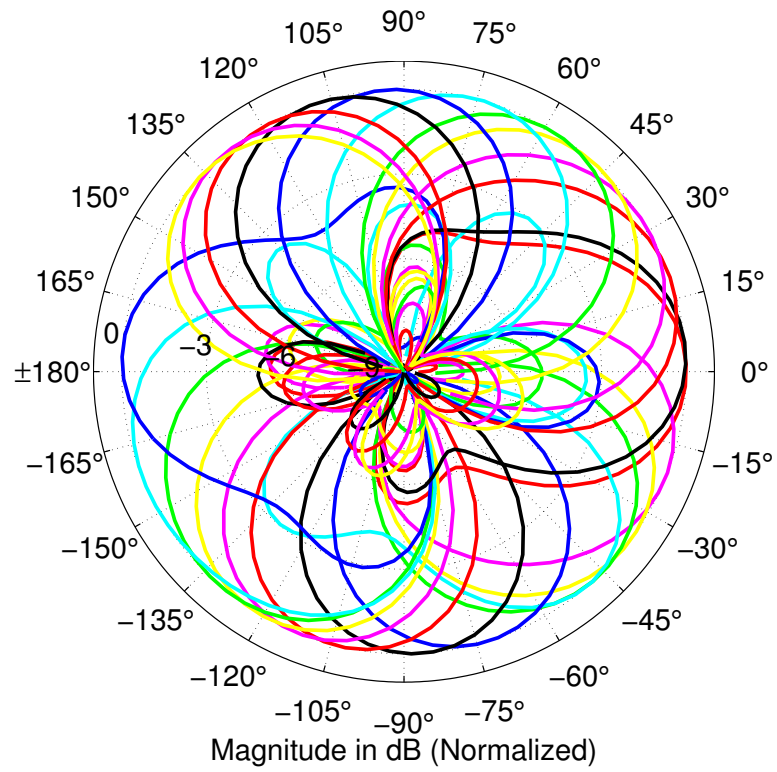


Figure 2.15: Beamformer with Measured Far Field Signals at 15° Increments, 2 kHz Octave Band

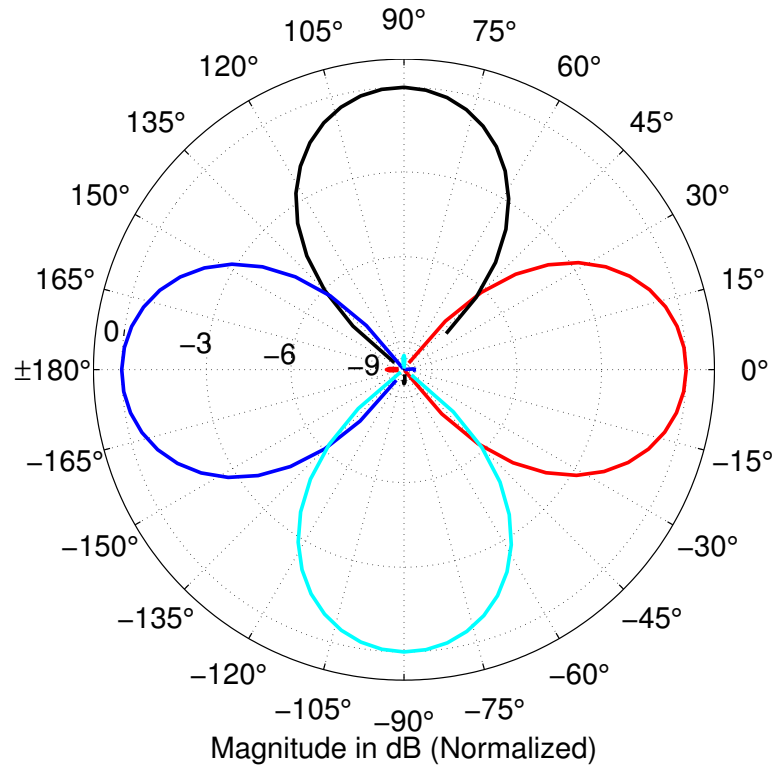


Figure 2.16: Beamformer with Theoretical Plane Wave Signals at 90° Increments, 2 kHz Octave Band

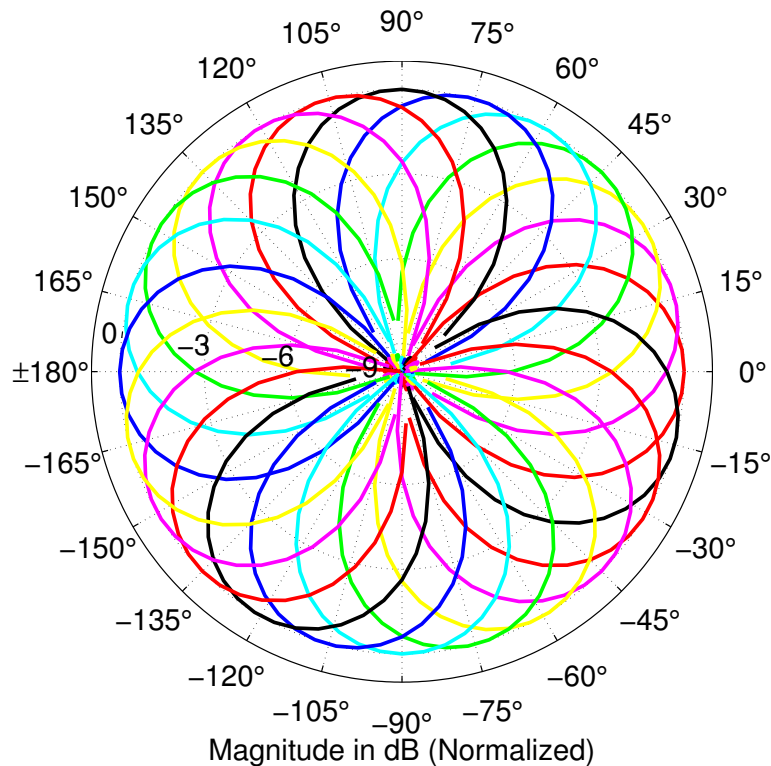


Figure 2.17: Beamformer with Theoretical Plane Wave Signals at 15° Increments, 2 kHz Octave Band

The beams produced by both real and theoretical excitation show that the average beam width (half-power or -3dB width) of the spherical microphone array using 2nd-order spherical harmonic decomposition is 70°. The same array processed using 1st-order spherical harmonics only produces beamwidths of 100°. Additionally, the measured signals were auralized using 2nd-order ambisonic reproduction in the Arup SoundLab (refer to Section 4.3.2.5 for physical setup) and the relative shift in localization between each 15° increment was clearly audible.

2.5 Discussion and Future Work

The microphone array described in this chapter has many potential applications, although it is most directly applicable to the capture of impulse responses. While this research focuses on onstage measurements, the array has already been used for audience measurements in real halls, as well as tests in a scale-model chamber constructed to simulate coupled spaces [107]. It could be used for in-situ ab-

sorption measurements, as tested using a higher-order spherical array by Rathsam & Rafaely [89]. In beam-forming research, the use of Bayesian analysis is under investigation for possible improvements to side and rear-lobe rejection and the use of irregular arrays [22].

Many refinements remain to this method. The most evident avenue for refinement is of course to increase the order of spherical harmonic decomposition. In order to do this, a higher number of capsules is required along with a higher number of channels in the recording interface. Higher-order arrays have been built by Moreau et al., Meyer et al., and Li & Duraiswami [73], [72], [64]. Some of these arrays are commercially available, with microphone processing elements incorporated into the sphere, as well as additional elements such as averaging over multiple elements to reduce the effect of sensor distance on spatial aliasing, or video cameras for real-time visual acoustic mapping [72], [64]. For the purposes of this study, the number of required spherical harmonics was limited by the available loudspeaker setup and the computation power required for real-time convolution, so a higher-order array was not necessary. As the reproduction capabilities improve, a higher-order array could be valuable. Regardless of array size, improvements to the recording setup and the quality of both the sphere construction and the capsule quality could also be made to allow the array to be used for direct recording rather than impulse response capture. The measurement kit itself could also be made more portable to reduce measurement time and allow greater distances between the source and receiver.

2.6 Conclusions

The ultimate goal of this research is to attempt to provide both a more realistic testing experience in a laboratory setting as well as a more refined analysis of the acoustics on the stage platform. In order to do this, several measurement and reproduction techniques were considered, as described above. The technique that best combines a quality of measurement for analysis with the flexibility and practicality necessary for auralization is higher-order ambisonics using spherical harmonic decomposition of spatially-sampled recordings on a rigid sphere. Impulse responses captured using this method can be used for both beamforming analy-

sis and ambisonic auralization. This chapter outlined the development and testing of a spherical microphone array for recording and processing such spatial impulse responses. Based on beamforming tests, the microphone is shown to provide the expected spatial resolution and to be applicable for the measurement of 2nd-order impulse responses.

CHAPTER 3

ROOM ACOUSTIC ANALYSIS USING THE SPHERICAL MICROPHONE

3.1 Introduction

Throughout the history of room acoustics research, understanding the characteristics of a venue that contribute to the quality listening experience of a musical performance has been a priority, with good reason. Ticket sales and concert hall reputations rely on a positive audience reaction. A comprehensive set of parameters has been developed and standardized in ISO 3382 (and described in more detail in work by Beranek) that can be derived from the impulse response measurements at multiple audience positions in a concert hall. These parameters go a long way to describing and predicting the audience impression of a venue for classical, orchestral performance [55], [8].

In order for the audience to have a quality experience, however, the performance itself must be of high quality. The entire venue, including the stage enclosure, must assist the individual performers and the entire ensemble in their musical goals. Musicians rely on the response of their own instrument in the hall as well as the relationship of their sound to that of the ensemble in order to synchronize and communicate onstage. If the hall stage acoustics are not ideal, resident ensembles may still be able to adapt and play with technical competence after several rehearsals and performances in the hall, but they will struggle to create a unified ensemble sound. If touring musicians are performing for the first time in venues with poor stage acoustics, even a technically competent performance may be a challenge as signal transmission between musicians is degraded or interrupted. For soloists, playing alone or with an orchestra, lack of quality response from the hall and balance with the group may prevent them from developing their interpretation of the music and result in a dull, flat performance. Intonation often suffers in the absence of room response, as proven by the experiences of musicians in anechoic chambers. This in turn affects the quality of the audience experience.

While some parameters have been developed to address these issues, the majority of acoustic parameters developed to describe both audience and performer experiences are mainly determined from an omnidirectional measurement and rely only on the time and frequency characteristics of the impulse response, with no influence from spatial information. Two parameters have been added to the ISO 3382 that describe basic spatial relationships in the room, Lateral Fraction (measures the proportion of energy from the sides of the hall using a dipole measurement, a parameter thought to contribute to feelings of envelopment) and Inter-Aural Cross-correlation Coefficient (measures the difference between left and right signals in a binaural measurement, thought to contribute to feelings of spaciousness). Up until recently, the inclusion of more spatial parameters has been limited by the technology available for spatial recording [55], [8].

With the increase in availability of 3-dimensional measurement techniques and equipment, many researchers have begun to examine the importance of spatial distribution in the impulse response for audience impressions, although no additional parameters have been robustly tested and standardized at this point. This chapter describes the use of a higher-order ambisonic spherical microphone array for the measurement and analysis of stage acoustics, with the goal of determining spatial parameters for comparison in subjective tests.

3.2 Precedents

3.2.1 Stage Acoustics

3.2.1.1 Foundations

In the past 50 years, stage acoustics have taken a more prominent position in acoustic design. Initially, Beranek et al. suggested in 1962 that reverberation was important to a musician's impression of his or her own sound in a hall [9]. Subsequently, Marshall et al., among others, began to research the importance of early reflections to these soloistic impressions [36]. As for ensemble impressions, early reflections were credited as early as 1968, when Jordan suggested an objective stage acoustics parameter called the “Inversion Index” [56]. This parameter is simply the ratio of Early Decay Time (EDT, or the decay curve from 0 dB to -10 dB

extrapolated to -60 dB) in the audience to the EDT onstage, based on the idea that if this ratio is larger than 1, then the early energy will build up faster onstage than in the audience, and therefore have a strong effect on support. Thomasson in 1974 also suggested another parameter, EDT5 (EDT extrapolated from a -5 dB decay curve), to address the importance of early reflections [99].

In 1978, Marshall determined that early reflections are important from 17-35 ms after the direct sound (path length of reflected sound 5.8-12 m longer than direct sound path length), and also demonstrated some frequency dependence of these reflections (high-frequency reflections are more important than those below 500 Hz) [69]. This corresponds to Meyer’s hypothesis that higher frequencies (the frequencies created by transients, or attacks) are more important for rhythmic precision [70]. However, as confirmed by Meyer in 1978, due to the masking of overtones in most instruments, the masking threshold of other instruments in the presence of self-produced sound is lower at low frequencies (the specific frequency range is of course related to the range of the instrument played, and additionally, the emphasis on harmonics becomes stronger in relation to the fundamental with an increase in self-produced volume). Of course, due to instrument directivity (which narrows significantly at higher frequencies), the masking threshold of other instruments is highly dependent on the angle of incidence. For example, Meyer & de Serra show that for a violinist, at 1 kHz, the masking threshold is 10 dB lower at lateral and elevated positions than elsewhere, and at 2 kHz the threshold is lowest for frontal and elevated positions [71].

3.2.1.2 The Stage Support Parameters

In the 1980s, Gade conducted extensive subjective experiments and determined a set of stage acoustics parameters that are still widely used [37]. The Stage Support parameters were created to address soloist concerns, or the musician’s impression of their own sound in the hall and how this relates to the aesthetics of their performance. These parameters are divided by time windows for the arrival of early energy: ST1 or ST_{early} (20-100 ms), ST2 or ST_{late} (100-1000 ms), and ST3 or ST_{total}

(20-1000 ms) [34]. The parameters are shown below:

$$\text{ST1} = 10 \log_{10} \left(\frac{\int_{20}^{100} p^2(t) dt}{\int_0^{10} p^2(t) dt} \right) \quad (3.1)$$

$$\text{ST2} = 10 \log_{10} \left(\frac{\int_{100}^{1000} p^2(t) dt}{\int_0^{10} p^2(t) dt} \right) \quad (3.2)$$

$$\text{ST3} = 10 \log_{10} \left(\frac{\int_{20}^{1000} p^2(t) dt}{\int_0^{10} p^2(t) dt} \right) \quad (3.3)$$

where $p(t)$ is the sound pressure of the impulse response.

The impulse response is measured with a microphone 1 meter away from the source (based on the assumption that the direct-sound path-length from instrument to ear is approximately 1 m). The 100-ms cutoff time for the ST1 parameter was chosen because it corresponds to the duration of a short tone in music and also to the integration time of the ear. This parameter has been incorporated into ISO 3382 as well as the output of some acoustic modeling software and is typically included in most measurement surveys. Recent work by Kim et al. and others has cast doubt on the usefulness of this parameter, although it has been suggested that the value of this parameter is improved when the direct sound is excluded from the ratio [61].

An additional parameter, which Gade proposed to address ensemble concerns, or musicians impressions of the relationship between their sound and the sound from the rest of the ensemble (also referred to as “functional” concerns), is called Early Ensemble Level (EEL). Although Dammerud and even Gade himself have later questioned the applicability and reliability of this parameter, the experiments leading to the choice of this parameter and its definition will be described in detail below [26], [35].

In 1981, Gade conducted subjective evaluations with professional classical musicians of all instrumentations, including pianists, singers, orchestral performers, and conductors. Based on the survey and the instrument-dependence of the results, Gade ranked the chosen parameters in order of importance and designated them based on importance for “ensemble” (functional) or “soloist” (aesthetic) playing [36]. In 1982, Gade built on this survey by testing subjective preference for specific objective

parameters and using multidimensional scaling to determine the objective parameters most directly related to the aforementioned subjective list. His initial matching of subjective and objective parameters is listed below [37]:

1. Reverberation (soloist concern): T_{20} , C_{80}
2. Support (soloist concern): ST1, ST3
3. Timbre (soloist concern): Frequency-dependence of T_{20} , C_{80} , ST1, ST3
4. Dynamics (soloist concern): Assumed to be related to “Support”
5. Hearing Each Other (ensemble concern): EDT, EDT5 , C_{80} , ST1, ST3, Frequency dependence of all parameters listed
6. Time Delay (ensemble concern): Delay of direct sound (calculated based on source-receiver distance assuming that sound travels 1 m every 2.8 ms)

These parameters were measured by Gade using the impulse-response method, with a source and receiver onstage in different orchestral positions in three concert halls. The soloist positions were based on the measurement techniques defined by the Stage Support parameter, and the ensemble positions were based on the distances between orchestral instrument groups (6-8 m). Based on these measurements, the halls offered the ranges of parameter values shown in Table 3.1.

Table 3.1: Range of Parameter Values For Three Measured Halls, A.C. Gade [37]

Parameter	Soloist Values	Ensemble Values
T_{20} (s)	1.2 - 1.8	1.7 - 2.2
EDT (s)	n/a	1.2 - 1.8
EDT5 (s)	n/a	0.9 - 1.8
C_{80} (dB)	10.4 - 12.3	-1.6 - 4.6
ST1 (dB)	-12.5 - -5.5	2.5 - 9.1
ST3 (dB)	-9.9 - -4.6	6.6 - 10.5

These values were then used to determine the test conditions for Gade’s experiments. Experiments were also conducted to determine thresholds of audibility for a single reflection and a cluster of six reflections. The mean threshold of single reflections was -9 dB for strings and -15 dB for flutes, indicating the high level of variance between instrument groups (possibly due to masking based on instrument directivity patterns and the geography of the instrument’s acoustic center in relation to the ears). A comparison of the ST1 parameter measured in the three halls shows a correlation between this audibility threshold and subjective impressions of the halls: halls with ST1 values below this threshold resulted in impressions of “lacking support.”

An impulse response was simulated using a delay unit, reverberation chamber and mixer to allow more control over the individual parameters. All values for direct sound, discrete early reflections, and statistical reverberant tail were based on the expected attenuation due to spherical spreading in a hall. Then these values were changed in relation to this control value. Gade’s findings from this study regarding the relationships between subjective and objective parameters are summarized in Table 3.2.

Table 3.2: Summary of A.C. Gade Findings [37]

Subjective Parameters	Objective Parameters	Preferred Values
Reverberation (soloist)	T_{20} , TA , C_{80}	Higher values preferred
Support (soloist)	ST1	Higher values (above -10 dB) preferred
Timbre (soloist)	Early Reflection Spectra	High frequencies preferred by violins, Low frequencies preferred by cellists and flutists
Hearing Each Other (ensemble)	EEL, EDT, C_{80}	High values of high-frequency early energy preferred, low values of reverberation preferred
Time Delay (ensemble)	Direct sound delay	Delays of less than 20 ms preferred

A strong correlation was found between “Hearing Each Other” and the ratio of sound received to sound emitted, but only low correlations were found with most existing energy ratio parameters. Because of this, the parameter “EEL” or Early Ensemble Level was proposed that compared sound at two positions, one close to the source and one at a reasonable distance for a receiver elsewhere in the orchestra. The “emitted sound” receiver p_e is 1 m from the source and the “received sound” receiver p_r is 8.5 m from the source. Because higher levels of reverberation were correlated slightly with lower impressions of “hearing each other,” this parameter was recommended in conjunction with C_{80} and EDT measurements. The equation for EEL is shown below:

$$\text{EEL} = 10 \log_{10} \left(\frac{\int_0^{80} p_r^2(t) dt}{\int_0^{10} p_e^2(t) dt} \right) \quad (3.4)$$

Unfortunately, direct comparisons between rooms using this parameter would require measurements from each room at an 8.5 m source-receiver distance, which

is not always possible given the stage size (for this research, the smallest measured stage was only 6.4 m wide). Therefore, EEL was not examined in this research.

Ueno et al. conducted similar experiments using a version of the Gade large ensemble setup in 2005 using real-time convolution with impulse responses from seven concert halls [100]. From these experiments, it was found that while string players preferred an early-reflected-energy level that is neither too weak nor too strong, wind players occasionally preferred stronger early reflections (absolute levels, not equalized to 0 dB for attenuation due to spherical spreading, ranged from -23.5 dB to -16.5 dB below the direct sound). They also found that, although the effects of reverberation time were small, an increase was generally preferred (times tested varied from 1.36 s to 2.22 s). With reverberant energy levels, a condition that was neither too weak nor too strong was preferred (conditions ranging from -23.4 to -14.8 dB below the direct sound) by strings and a stronger reverberation was preferred by winds.

The works described above are crucial to this research because they have defined what subjective and objective parameters are important to classical music and both symphonic and chamber ensemble instrumentation. The solo and ensemble comparisons are especially important because in musical performance (both classical and contemporary) there is often a tenuous balance between soloist and ensemble playing that is shifted depending on the clarity of communication between musicians. A logical progression to contemporary relevance would involve the testing of the aforementioned parameters with different musical material (comparing contemporary and classical), testing methodology (passive listener, active performer), and reproductive methods (ambisonics, binaural reproduction). This is one of the goals of this research. However, the introduction of new performance venues and the emphasis on different psychoacoustic principles require additional parameters to be tested beyond those listed here.

Additionally, in previous research by the author, similar tests were conducted using ViMiC (described in Section 2.1), focusing on contemporary improvised music. The tests varied similar acoustic parameters but did not show significant trends in rated preference for this type of music. However, a musical content analysis of

musician performances in conditions with varying early reflected energy and reverberant energy showed that some trends were visible in the performed content, such as variations in pitch register, self-produced volume, musical contrast, counterpoint, melodic development, and stylistic homogeneity. In indeterminate or improvised music, the range of possible adjustment by performers is extreme. Work by Ueno et al. and Kato et al. has shown that even in notated music where the possible adjustments are more restricted to small changes in tempo, dynamics and coloration, adjustments can be measured to determine the influence of certain acoustic parameters [101], [59], [60]. In the studies by Ueno et al. and Kato et al., differences between each performance were measured using the auto-correlation function (ACF). Due to the added complexity of musical analysis, these methods were not utilized in the research for this dissertation.

As mentioned above, directivity of individual instruments influences the stage acoustics in complex ways. Meyer has shown how multiple directivity patterns can interfere with each other in different orchestral seating arrangements and within individual instrument groups [70]. In groups with particularly varied directivities, such as the woodwinds (flutes, bassoons, oboes, clarinets), the balance of this section changes drastically depending on the position of an audience member or a musician from another section of the orchestra. Kirkwood has conducted listening experiments to determine the audibility and importance of directivity patterns (vs. an omnidirectional average) and proposed that loudness, reverberance, and clarity judgments were all effected by the changes in directivity patterns and that the specific directivities were preferred by the listeners to simulated omnidirectional averages [80].

Additionally, Gade addressed the issue of comb-filtering of direct and reflected sound propagating in the orchestra by using a spectral correction curve in his experiments to simulate the direct sound attenuation. This curve was determined by Krokstad in experiments with rows of seating between source and receiver positions [37]. Additional examinations of comb-filtering in stage enclosures were completed by Halmrast in 2000 [37].

In a different arena, Ternström et al. have recently utilized the in-situ mea-

surement technique to address stage acoustic conditions in an opera chorus and a chamber choir [97], [98]. Their focus in this research was on the Self-to-Others Ratio (SOR), or the difference in SPL between the self-produced sound reaching the ear and the direct sound from other performers. Of course, because of the additional bone-conduction path created by singing, this SOR may be significantly higher for singers than for instrumentalists, even in the presence of a full chorus. Ternström found SORs among opera singers ranging from +15 dB (sopranos) to +10 dB (tenors) and in chamber choirs ranging from 0 dB to +8 dB. Looking back at the Gade data, however, it becomes clear that due to the great distances between members of the orchestra, it is possible to have even higher SORs between individual musicians (+19 to +23 dB ratios were used in Gade’s large ensemble experiments [37]), which may have important relevance for contemporary works for small ensembles that include spatial instructions (*Atlas Eclipticalis* by John Cage, for example, requires musicians to be spread throughout the hall, creating wide separations between individuals) [79]. Inferring from Gade’s construction of the EEL parameter, it can be said that SOR also is a possible contributor to subjective feelings of “Hearing Each Other” in an ensemble.

3.2.1.3 Beyond Stage Support

More recently, doctoral research by Dammerud at University of Bath has examined the effect of ensembles onstage and surveyed large orchestras with regards to acoustic preferences [26]. Although this work concentrates mainly on large, traditional ensembles, it proposes several new parameters for measuring stage acoustics. Dammerud examined several parameters, including those traditionally used for audience impressions along with the standard stage support parameters. He examined a parameter called RR_{160} developed by Kahle & Jullien based on proposals by Griesinger for “running reverberance” or the perception of reverberance during performance [58], [44], [46], [45]. Traditionally used for audience, this could also theoretically apply to musician perception of reverberance. The parameter is described below:

$$RR_{160} = 10 \log_{10} \left(\frac{\int_{160}^{320} p^2(t) dt}{\int_0^{160} p^2(t) dt} \right) \quad (3.5)$$

Dammerud examined variations on the strength parameter G outlined in the ISO 3382 and developed to measure audience perception of loudness. G is measured by a ratio of energy measured in the hall to a 10-meter free-field (anechoic) measurement using the same source/receiver pair.

$$G = 10 \log_{10} \left(\frac{\int_0^\infty p^2(t) dt}{\int_0^\infty p_{ref}^2(t) dt} \right) \quad (3.6)$$

Dammerud in particular focused on G_{early} and G_{late} , which he estimated using previous equations developed by Barron & Lee and verified by Chiles & Barron, using a 1-meter reference measurement for the free-field signal [4], [20]:

$$G_{early} = 10 \log_{10} \left(\frac{10^{C_{80}/10} * 10^{G/10}}{1 + 10^{C_{80}/10}} \right) \quad (3.7)$$

$$G_{late} = 10 \log_{10} \left(\frac{10^{G/10}}{1 + 10^{C_{80}/10}} \right) \quad (3.8)$$

For comparison, work by Jurkiewicz defines these parameters slightly differently, using a 100 ms cutoff time rather than 80 ms, and calculating the energy ratios directly from the impulse response compared to a 10-meter reference measurement [57].

$$G_{early} = 10 \log_{10} \left(\frac{\int_{10}^{100} p^2(t) dt}{\int_0^\infty p_{ref}^2(t) dt} \right) \quad (3.9)$$

$$G_{late} = 10 \log_{10} \left(\frac{\int_{100}^\infty p^2(t) dt}{\int_0^\infty p_{ref}^2(t) dt} \right) \quad (3.10)$$

For this research, the 80-ms cutoff time is used for G_{early} and G_{late} . Another variation on strength used by Dammerud uses the same cutoff time as ST1, called $G_{support}$:

$$G_{support} = 10 \log_{10} \left(\frac{\int_{20}^{100} p^2(t) dt}{\int_0^\infty p_{ref}^2(t) dt} \right) \quad (3.11)$$

Dammerud also utilized a parameter developed by van den Braak & van Lux-

emburg based on conductor preferences and reflection times for onstage reflections, LQ_{740} [105]:

$$LQ_{740} = 10 \log_{10} \left(\frac{\int_7^{40} p^2(t) dt}{\int_{40}^{\infty} p^2(t) dt} \right) \quad (3.12)$$

Dammerud's work showed that, in the presence of the orchestra, the early part of the impulse response (10-50 ms) as well as certain frequency components of the direct-sound (2 kHz) are significantly attenuated (the effect is stronger in non-diffuse stage enclosures). According to this research, parameters that most closely indicate this effect are G_{late} and ST2. Similar studies were done with empty chairs onstage and showed that chairs were not a good substitute for full orchestra.

Dammerud used questionnaires to determine subjective impressions of stages. The musicians based their judgements on past performance experiences of various stages. Comparisons of the measured parameters with subjective impressions of these stages showed that early stage support and strength had no significant correlation with subjective preference when accounting for the effects of a full onstage orchestra (Gade's decay curves did not include onstage musicians), although later energy in the hall (indicated by G_{late}) improved the overall impression of sound quality. Instead, architectural measures had a stronger correlation with subjective impressions of hearing the self and others onstage (important for communication). For example, the ratio $\frac{H_{rb}}{W_{rs}}$ (H_{rb} = height to reflecting ceiling surfaces in the brass section, W_{rs} = width to reflecting side surfaces in the string section) showed a strong correlation with overall acoustic impression. This shows that while parameters such as stage support indicate the importance of early reflections, they do not emphasize the direction of arrival of these reflections, which can be useful or detrimental depending on the spatial pattern [26].

In particular, for halls with the same ratio of early energy, stage enclosures with narrow side walls and high ceilings (13 m or higher) proved most beneficial to communication. In addition, moderate depth and a lack of proscenium (exposing the stage directly to the hall) contribute to improved communication. These findings are in accordance with suggested geometries by Griesinger and Meyer. In particular, these findings show the importance of directional information to stage

acoustics. The goal of this research is to obtain spatial information about halls from impulse responses directly (rather than comparing reflection time delays found in omnidirectional recordings to architectural drawings to determine direction of arrival) and examine direct effects of enclosure shape on acoustic impression and communication.

Jurkiewicz examined several of the aforementioned parameters with respect to two halls with variable geometries [57]. One hall was measured with multiple orchestra shell configurations, and the other with multiple stage-ceiling heights. Subjective impressions were determined by questionnaire. Jurkiewicz also included two additional parameters in his study. The first is EDTR or the ratio of EDT values measured onstage and in the audience. The second parameter is SMTI, modified from the Modulation Transfer Function MTF first used by Houtgast & Steeneken to determine speech intelligibility in rooms [53], [92]. Houtgast & Steeneken used the MTF to calculate the STI or Speech Transmission Index, which takes into account the decay time and the signal-to-noise ratio (SNR) of a room. The STI is calculated from the low frequency ($f = 0.4\text{--}20$ Hz) 1/3-octave band values of the MTF , which can be determined from the impulse response as follows [95]:

$$MTF(f) = \frac{|\int_0^\infty e^{-j2\pi ft} p^2(t) dt|}{\int_0^\infty p^2(t) dt} (1 + 10^{-SNR/10})^{-1} \quad (3.13)$$

This is essentially the product of the normalized Fourier transform of the squared impulse response and the modulation reduction factor created by additional interference or background noise in the space. It describes the amount of signal degradation generated by its transmission through the room from source to receiver.

Naylor (and later Naylor & Craik) attempted to show the value of MTF for ensemble cross-stage communication [77], [78]. In this work, Naylor assumed that the SNR is not only a ratio of source signal energy and background noise, but also a ratio of the ensemble energy (L_{others}) and interfering energy generated by one's own instrument (L_{self}). Naylor tested the parameter in a laboratory setting having test subjects play along with a pre-recorded musician in a synthesized sound field. Naylor varied the levels of pre-recorded musicians and the level of room response from the test subject as well as varying the timing and level of the reflections and

reverberance. Based on these experiments, a variation on MTF was determined to have a logarithmic correlation with the subjective perception of “hearing-of-others” during the tests. The logarithmic relationship implies that increases in MTF are more perceptible when the overall MTF is low, and that above a certain threshold the increase in signal preservation is less relevant to ensemble communication. The exact preferred values of MTF were dependent on the type of music, which led to the inclusion of a correction factor K , where lower values of K were used for decreased ensemble complexity (i.e. unison playing). Initial estimates of K were determined in dB based on the difference (resulting in a relative release from masking) between simultaneous sound levels created by the self and by the other. In other words, if the self were playing in unison with the other, the level difference would be close to 0 dB, whereas if the self and other were playing in counterpoint, the level difference between the self and other at any moment would be large. After this initial estimate, the exact values of K were determined iteratively to minimize the summed squared error between the MTF and the subjective ratings. The modified version of MTF , or M_{tot} , is shown below:

$$MTF(f) = \frac{|\int_0^\infty e^{-j2\pi ft} p^2(t) dt|}{\int_0^\infty p^2(t) dt} (1 + 10^{-(L_{others} - L_{self} + K)/10} + 10^{-SNR/10})^{-1} \quad (3.14)$$

Jurkiewicz used the modifications proposed by Naylor & Craik in SMTI. Outside the laboratory setting, where determining L_{self} and L_{others} is more difficult, he has proposed using G_{cross} and G_{1m} instead, which refer to values of G measured at the same cross-stage distance used for the impulse response and at 1 meter from the source. Exact values for K are determined again specifically by the subjective response. In this research, MTF will be used to refer to the parameter developed by Jurkiewicz as a variation on SMTI.

3.2.1.4 Stage Enclosure Diffusion

Although no parameter currently exists to quantify distribution and level of diffusing surfaces directly from impulse response analysis, design of contemporary stage enclosures often includes scattering elements to increase the amount of dif-

fusion on the stage. One hypothesized effect of diffusion in the stage enclosure includes the influence of spatial unmasking (generated by decreased diffusion) on a poor self-to-others ratio in the case of distant or occluded players, based on studies of the “cocktail-party effect” often observed in speech scenarios [16], [90]. On the other hand, spatial and amplitude dispersion caused by increased diffusion could also provide early reflections to other musicians of instrumentalists from distant parts of the stage, allowing all musicians to hear each other equally well regardless of stage position. Additionally, studies by Krokstad show that comb filtering on stages in the presence of large ensembles can cause serious problems for musical communication (especially in the case of frequency-dependent cues), which could be alleviated by the presence of diffusion [37].

Cox & D’Antonio conducted surveys with musicians examining the effect of diffusion on stage acoustics. They found that ceiling reflections, while important to ensemble communication (source of strong early reflections), can cause coloration of the sound and masking of self-produced signals. The presence of diffusion on the ceiling reflector can alleviate these problems and also redirect some reflections to the side and rear walls, improving the overall acoustics of the stage area. Subjective tests were conducted with a modular performance shell, and while the results were highly instrument-dependent, the overall consensus was that increased diffusion on portions of all surfaces improved the musical communication onstage. Strings and brass preferred vertical diffusion on the lower portion of the shell and horizontal diffusion on the upper portion. Other musicians preferred more flat surfaces interspersed with diffusion, and some instrumentalists preferred flat surfaces on the lower portion for bass coupling [23].

In previous research by the author, an acoustic model from CATT-Acoustic was created to examine the preferred amount of diffusion in the stage enclosure using real-time auralization over headphones. As previously mentioned, the results of this study were not significant. One main limitation of this study was the fact that the computer model uses the Lambertian Model for scattering [25]. This approximation does not account for wavelength or incident angle, two very important elements in determining the local effects of diffuse surfaces onstage. Therefore, the research in

this dissertation uses measured impulse responses rather than a computer model to provide the highest level of realism possible in a laboratory setting.

3.2.2 Spatial Display and Analysis for Audience

The parameters described in the previous section (Section 3.2.1) describe the behavior of sound in a room along the dimensions of time, magnitude and frequency. As shown in countless subjective evaluations by passive listeners, certain subjective criteria for audience members cannot be described by these dimensions alone, but include the distribution of these dimensions in space. Traditional subjective criteria for audience that indicate the relevance of spatial information include Spaciousness, Listener Envelopment (LE), and Apparent Source Width (ASW), although many other spatial characteristics have yet to be named or measured [8], [47]. Recent work by Lokki et al. utilizes Individual Vocabulary Profiling (IVP) to determine additional subjective criteria without the traditional bias of interpreting a common vocabulary (each individual creates their own attribute names, which are collated into groups using statistical clustering analysis) [65]. Some of the terminology from this study can be interpreted as being spatially-driven, such as “size/sense of space,” “width/wideness/spread of sound,” “3-dimensional,” “focused/localizability,” and “symmetry.”

Two objective spatial parameters are included in the ISO 3382 standard, Lateral Fraction (LF) and Inter-Aural Cross-correlation Coefficient (IACC) [55]. These parameters utilize standard available recording equipment (omnidirectional microphone, figure-of-8 or dipole microphone, and in-ear or dummy head binaural microphones) and a standard omnidirectional source. LF and IACC have been shown to correlate with overall feelings of spaciousness. Additionally, values of these parameters for early and late portions of the impulse response have been shown to correlate with feelings of (ASW) and (LE), respectively. These measures divide the sound field into rudimentary segments, LF separating the lateral field from the omnidirectional field, IACC separating the left hemisphere from the right hemisphere using psychoacoustic segmentation of the 3-dimensional sound field.

As the availability of technology for spatial recording has increased, higher res-

olution of the 3D sound field in analyzing an impulse response is possible. Whereas divisions of the field into two spatial segments is quite simple to condense into a single-value parameter or ratio, higher resolution makes it difficult to determine salient parameters that can be correlated with subjective judgements. Some researchers have chosen to use visual display rather than single numeric values to describe the spatial behavior of sound in rooms. Bassuet recorded impulse responses using an omnidirectional source and a SoundField microphone with four coincident capsules and B-Format encoding methods described in Section 2.1 [5]. The magnitude of energy and 3D directionality in each millisecond time window are determined from the instantaneous acoustic intensity of the impulse response. The vectors are color coded by time frame (0-15 ms = red, 15-40 ms = blue, 40-100 ms = cyan, 100-200 ms = yellow) and plotted in spherical coordinates to create a “hedgehog” shape, shown in Figure 3.1.

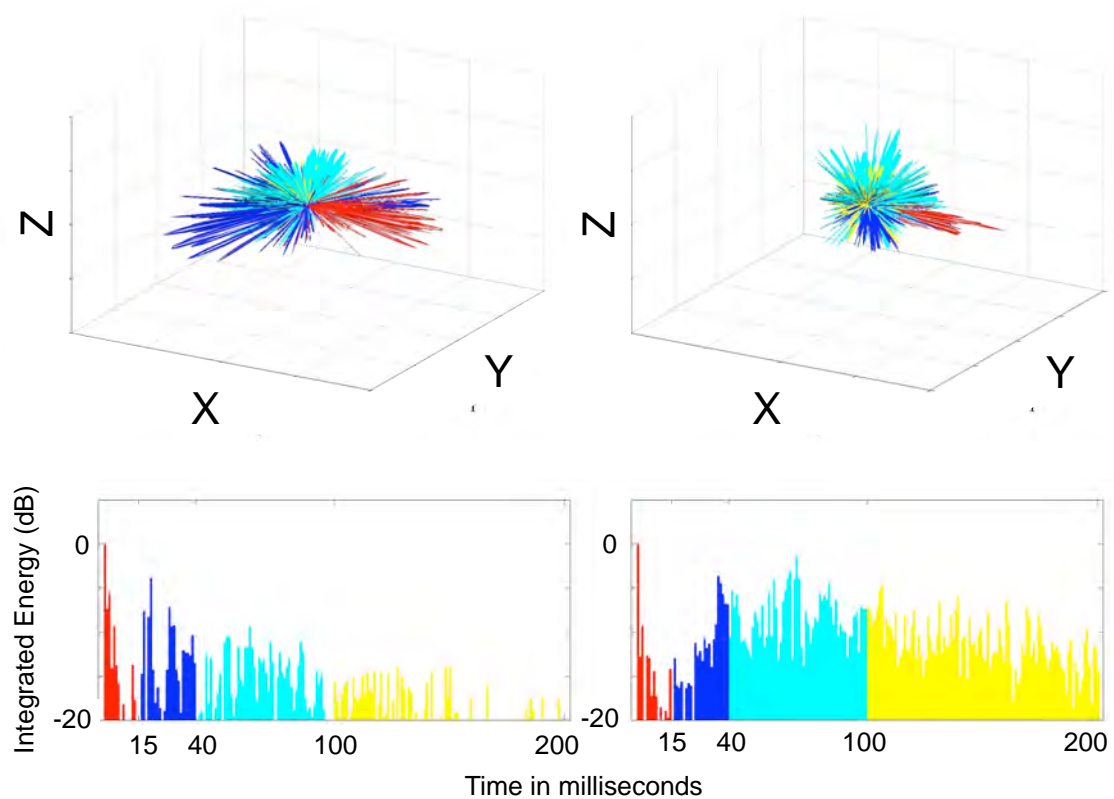


Figure 3.1: 3D “Hedgehog” Plots of Impulse Responses from Two Concert Halls [5]

Bassuet also utilized these impulse responses to divide the sound field into six azimuthal segments and five vertical segments. Two ratios were developed from these segments, LH or the ratio of low lateral to high lateral energy and FR or the ratio of front lateral to rear lateral energy [5]. Both ratios are limited to the energy in the first 150 ms of the impulse response.

Patynen et al. have recently utilized a six-channel intensity probe to measure spatial impulse responses [83]. In addition to measuring the spatial distribution of sound at the receiver position, the study also addresses the spatial distribution of the sound source itself. Standard impulse response measurements are made using equipment that approximates a single point source. Therefore, the excitation of the room by the standard source best represents a single instrument or voice onstage and individual instrument directivities are not considered. Using a cali-

brated “loudspeaker orchestra” with 34 loudspeakers corresponding to orchestral instrument positions and instrument-based directivities for each position, the study measures individual source-receiver impulse responses for each instrument onstage which can then be convolved and played simultaneously for orchestra auralizations or summed for spatial analysis.

The spatial display in this study is generated using the directional analysis method (DIR), which calculates the least-squares solution of time-difference-of-arrival estimates to determine the direction of incidence of sound energy for each audio sample. The information is displayed in 2-dimensional polar projections overlaid with the plan and section of the room. Contours are shown simultaneously for the cumulative energy measured every 10 ms, indicating the change in spatial distribution over time.

Spherical microphone arrays of various complexity have also been used to analyze the spatial soundfield in rooms. These arrays capture impulse responses at each capsule on the sphere and use spherical harmonic decomposition and beamforming analysis (described in Section 2.2.2 and Section 2.2.6) to examine the direction of incident energy over time. Rafaely & Avni have utilized a 32-capsule spherical array to calculate IACC. This allows multiple spatial parameters to be measured with a single microphone, rather than obtaining a dummy head with binaural microphones and capturing separate binaural impulse responses, which can be impractical [87]. Li & Duraiswami have coupled a 64-capsule array with a multi-directional video-camera to superimpose visual displays of acoustic energy onto 3-dimensional video projections of rooms [64].

Gover et al. have utilized a 32-capsule spherical array to measure the spatial sound field in multiple rooms [40], [41], [42]. Based on an analysis of several different types of spaces, the study proposes a new parameter for describing the spatial homogeneity or isotropy of the soundfield over time. The parameter, Directional Diffusion (DD) is defined below:

$$DD = \left(1 - \frac{\mu}{\mu_0}\right) * 100\% \quad (3.15)$$

where

$$\mu = \frac{1}{e_{avg}} \sum_{i=1}^n |e_i - e_{avg}| \quad (3.16)$$

n is the number of beam directions and e_{avg} is the incident energy averaged over n directions:

$$e_{avg} = \frac{1}{n} \sum_{i=1}^n e_i \quad (3.17)$$

and μ_0 is the value of μ calculated for the anechoic impulse response of a single plane wave using the same array. A room that is completely anechoic will provide a value of 0% whereas a room that is completely isotropic will provide a value of 100%. This parameter was also derived over varying time frames to show the change in isotropy over time.

All the spatial parameters and display methods described above have been developed for audience receiver positions. Onstage receivers can also be utilized to determine the value of spatial information for performers onstage, a method that has been explored in depth for this dissertation.

3.3 Methodology

3.3.1 Concert Hall Stage Measurements

In May 2010, impulse response measurements were captured in 10 different concert halls and theatres around the Upstate New York region. Hall sizes varied from 242 seats to 2,300 seats, with stage sizes from 50m² to 550m². Measurements were captured using the system described in Section 2.3. For comparison, omnidirectional and binaural recordings were captured for the same receiver locations in some of the halls using an Earthworks omnidirectional microphone and a HEAD-Acoustics dummy head with in-ear microphones. Images of the survey setup are shown in Appendix C.1.

Multiple source-receiver locations were measured, exact locations and distances determined by the size and shape of each stage. Audience receiver positions were also captured. The onstage positions common to all 10 halls were:

1. Soloist Position S-R pair (“Self” source): Stage Front (1-meter distance)
2. UpDown-Stage S-R pair (“Others” source): Back-Front (distance varies)
3. Cross-Stage S-R pair (“Others” source): Left-Right (distance varies)

Images of the 10 measured halls are shown in Figure 3.2.



Recital Hall, SUNY Albany
(242 Seats)



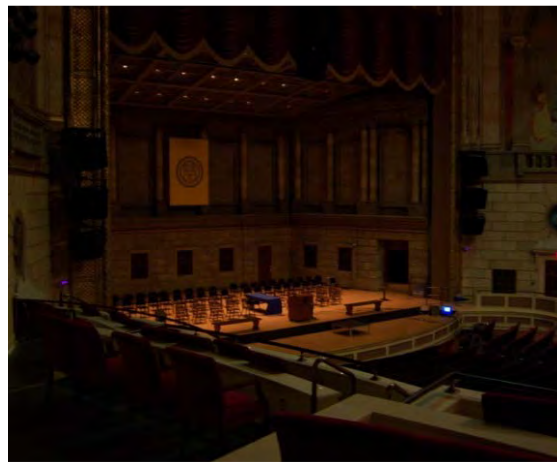
Theater, SUNY Albany
(500 Seats)



Fisher Center, Bard College
(900 Seats)



Lippes Hall, SUNY Buffalo
(670 Seats)



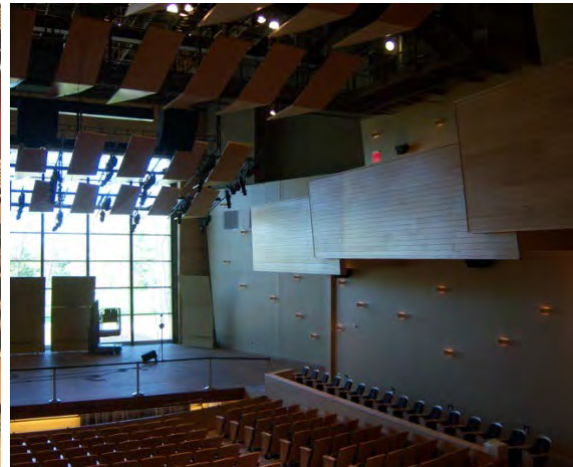
Kodak Hall, Eastman
(2300 Seats)



EMPAC Concert Hall, RPI
(1200 Seats)



EMPAC Theater, RPI
(400 Seats)



Zankel Music Center, Skidmore
College (600 Seats)



Picotte Recital Hall, College of
St. Rose (400 Seats)



Belle Skinner Hall, Vassar College
(325 Seats)

Figure 3.2: Measured Concert Halls and Theatres

Basic stage dimensions with example cross-stage source-receiver locations (Back-Front pair) are shown in plan view in Figure 3.3 and section view (3 halls are not shown in section because stage heights were not measured for these halls) in Figure 3.4.

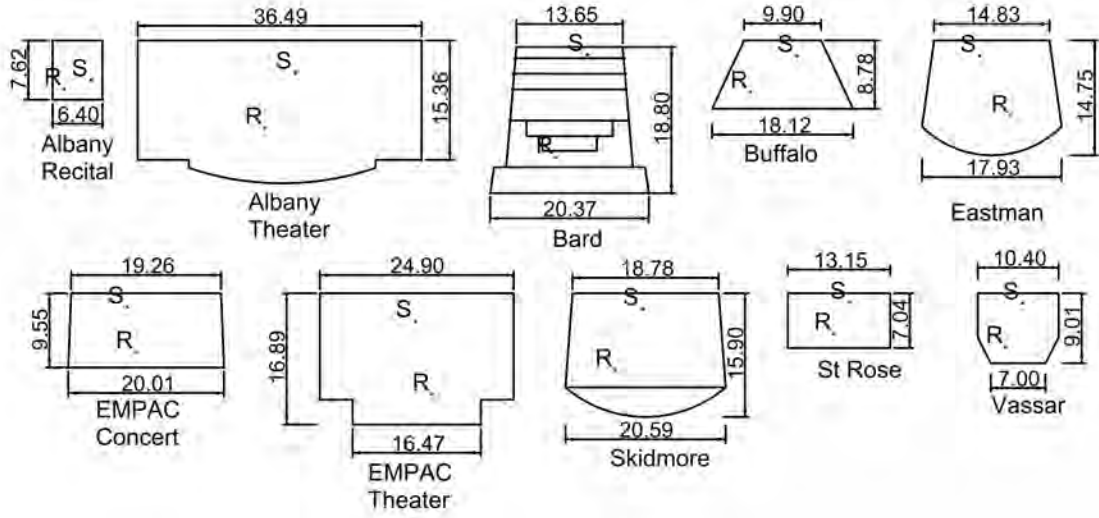


Figure 3.3: Measured Stage Dimensions: Plan View

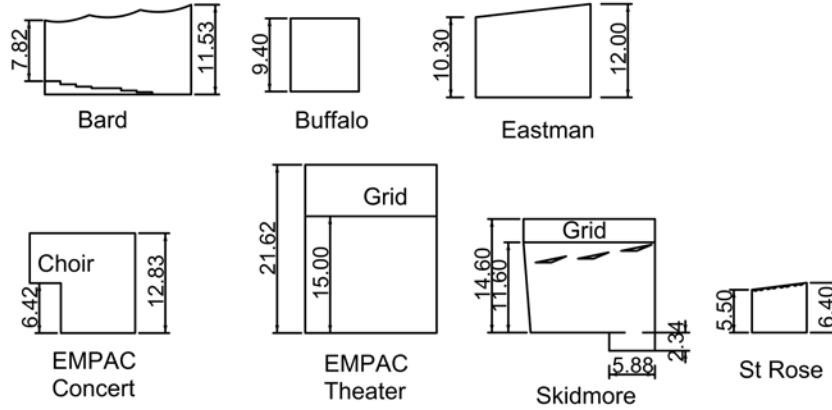


Figure 3.4: Measured Stage Dimensions: Section View

Standard omnidirectional parameters have been calculated for each hall using $N = 0$ or W component of the spherical harmonic array [55]. Back-Front source-receiver pairs were used (except in the case of Stage Support, where the soloist position was used). Parameters are averaged over 500 Hz, 1 kHz and 2 kHz octave bands, except for Bass Ratio (BR), which is a ratio of T_{30} at 250 Hz & 500 Hz over 1 kHz & 2 kHz. These parameters are shown in Table 3.3.

Table 3.3: Omnidirectional Parameters for Measured Hall Stages

Hall	T_{30} (s)	EDT (s)	C_{80} (dB)	D_{50} (%)
Albany Recital	0.97	0.90	3.2	53.7
Albany Theatre	1.53	1.49	0.4	39.7
Bard	1.78	1.47	1.9	48.7
Buffalo	2.05	1.96	1.3	47.7
Eastman	2.01	1.71	1.4	42.3
EMPAC Concert	2.25	2.15	4.6	68.7
EMPAC Theatre	1.07	1.11	2.4	50.0
Skidmore	2.18	2.24	2.7	53.3
St. Rose	1.64	1.60	2.1	52.0
Vassar	1.56	1.52	1.3	49.0

Hall	T_c (ms)	G_{total} (dB)	BR	ST1 (dB)
Albany Recital	63.7	17.7	1.31	-14.3
Albany Theatre	101.7	9.2	1.18	-18.7
Bard	95.7	11.6	0.91	-17.7
Buffalo	100.0	17.0	0.98	-13.0
Eastman	102.0	16.9	1.15	-12.7
EMPAC Concert	60.7	14.2	1.19	-16.3
EMPAC Theatre	67.0	12.6	1.39	-14.3
Skidmore	85.7	9.3	1.03	-15.0
St. Rose	82.3	17.8	1.22	-10.7
Vassar	85.7	18.9	0.93	-10.3

3.3.2 Free Field Measurements

In order to calculate many of the variations on the G or strength parameters described in Section 3.2.1.3, it was necessary to determine the free-field response

of the microphone array. Typically, this is recorded in an anechoic chamber with a 10-meter source-receiver distance. In the absence of such an available space, shorter distances often occasionally recorded in smaller anechoic chambers and then the signal is attenuated to account for spherical spreading using the inverse square law. However, in the case of the spherical microphone array, such a change in distance would also affect the spatial distribution of the sound at each capsule, and so simple attenuation correction would not be sufficient. In order to obtain a 10-meter distance, the black-box studio space at EMPAC (Studio 2) at RPI was used. Although the space is not anechoic, the surfaces are distant, and banners can be deployed to cover all the wall surfaces and produce a low reverberation time (0.6 seconds at mid frequencies). The microphone array and a directional loudspeaker were mounted equidistant from nearby surfaces (including the floor). In order to provide additional attenuation to the floor reflection, fabric was applied to the floor between the source and receiver. An image of the measurement setup is shown in Appendix C.1.

3.4 Results

In order to obtain a set of spatial parameters describing the measured stages, including those described in Section 3.2.2, beamforming analysis was performed on the impulse responses from the measured halls. In order to determine salient differences between the spatial distribution of stage reflections in each hall, the impulse responses were divided into time windows using overlapping Hanning windows. Spatial maps for specific time windows were generated as grids of resolution $j \times k$ by determining the energy contained within each beam pointed in (θ_j, ϕ_k) look directions. For a more complete picture, the spherical map was flattened such that azimuth is plotted along the abscissa and elevation along the ordinate axis. Although this distorts the proportions of the map such that the poles are overly represented, it allows the viewer to see all sides of the sphere at once.

Initially, the time windows were set to 1 millisecond and each map (resolution 36×18 or 10° beam increments) was treated as a frame in an animation. This display method allows simultaneous display of 2D and 3D information and comparison of

multiple rooms. It is an exploratory method, as the level of data resolution is still too high to extract any salient parameters. However, it could be used as a design tool when optimizing a stage enclosure design to create specific reflections. For example, 3D models of the stage enclosures for two halls (Skidmore and St. Rose) were created in CATT-Acoustic and were analyzed using basic image-source-modeling techniques. Images of the Skidmore and St Rose 3D models (and architectural references) are shown in Appendix C.2.

When the animated spatial maps of the measurements are viewed simultaneously with the image source analysis of the 3D model, similarities (specular reflections from the stage enclosure) and differences (potential scattered energy and reflections from the hall) can be viewed. Specific reflections are shown for the St. Rose model in Figure 3.5 and Figure 3.6. The CATT model shows a specular reflection from the rear left at approximately 8 milliseconds, which corresponds to a high concentration of energy (red) from -120° for the same time window in the animation (smaller energy concentrations shown in yellow from front and sides represent the rear and side lobes of the beamformer, which are not fully attenuated). This reflection is shown in Figure 3.5. For comparison, a specular reflection is shown from one of the rear curved ceiling reflectors at approximately 22 milliseconds, which corresponds to a high concentration of energy from above and from the upper rear left in the animation, as shown in Figure 3.6.

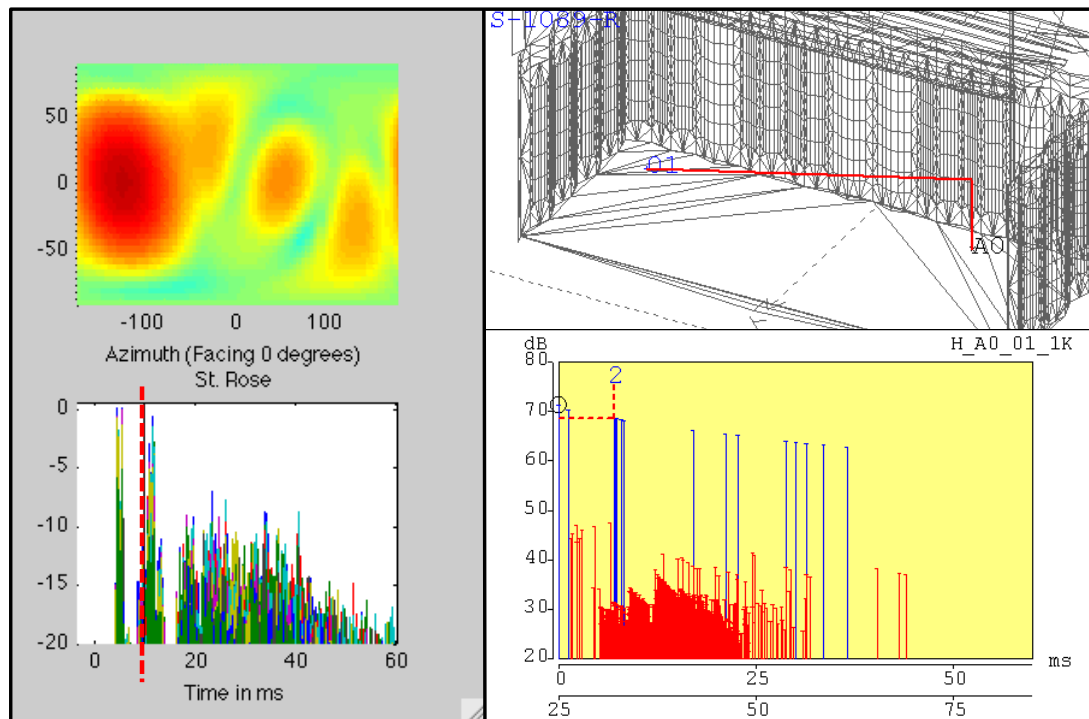


Figure 3.5: St. Rose 3D Model vs. Measured Spatial Energy, Rear Reflection

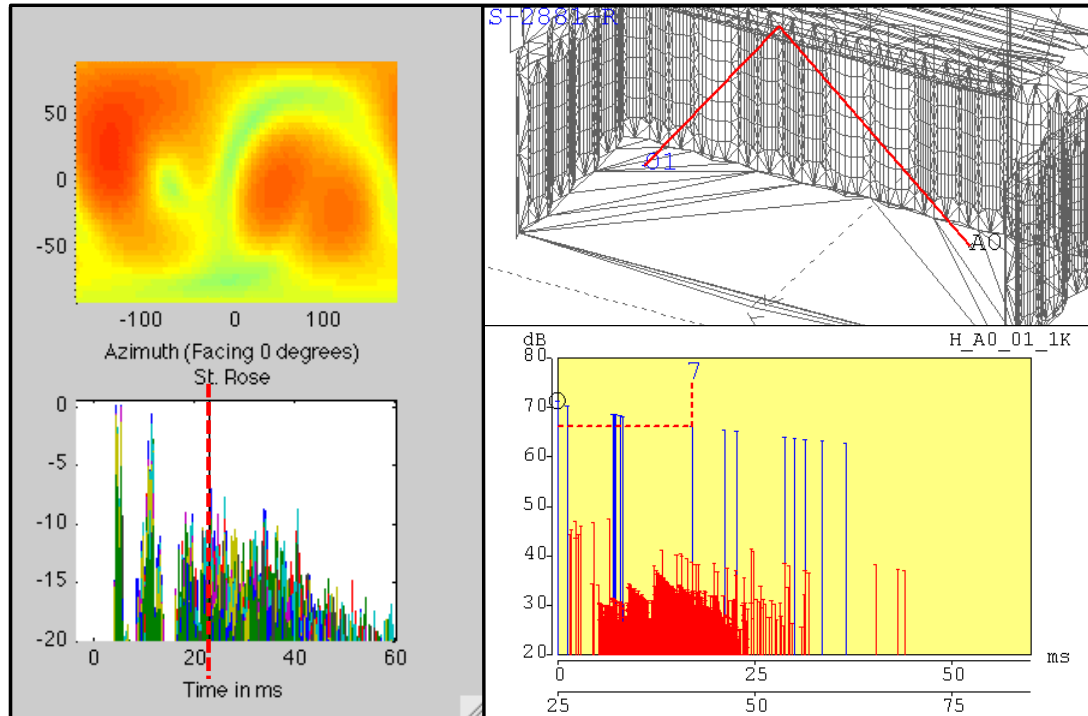


Figure 3.6: St. Rose 3D Model vs. Measured Spatial Energy, Ceiling Reflection

This shows that the spatial maps are useful for confirming the presence of specular reflections predicted by the 3D model. Additionally, it is clear from the 2D display of the measured impulse (in the lower left corner of Figure 3.6) that there is great deal of reflected energy between 20-40 ms that is not shown in the CATT-Acoustic model. This is likely energy scattered from the curved reflectors on the walls and ceiling that cannot be shown by the CATT model because it uses a statistic method to determine scattering. When examining the 3D display in that time range, it is possible to separate the specular reflections (those matching the CATT model) from the scattered reflections. Therefore, such comparisons are useful for determining the performance of scattering elements in a room, which could not be determined from the 2D comparison alone.

Additionally, in the case of Skidmore, a set of portable Wenger orchestra reflectors were present onstage (flush with the back wall) during the measurements. The reflector elements were deployed into a shell configuration for some measure-

ments, and the animations of these measurements can be compared to determine the impact of the shell on the spatial distribution of sound onstage. For example, the direct sound from the source in the rear is nearly identical in both conditions (the receiver is at the front of the stage), as shown in Figure 3.7.

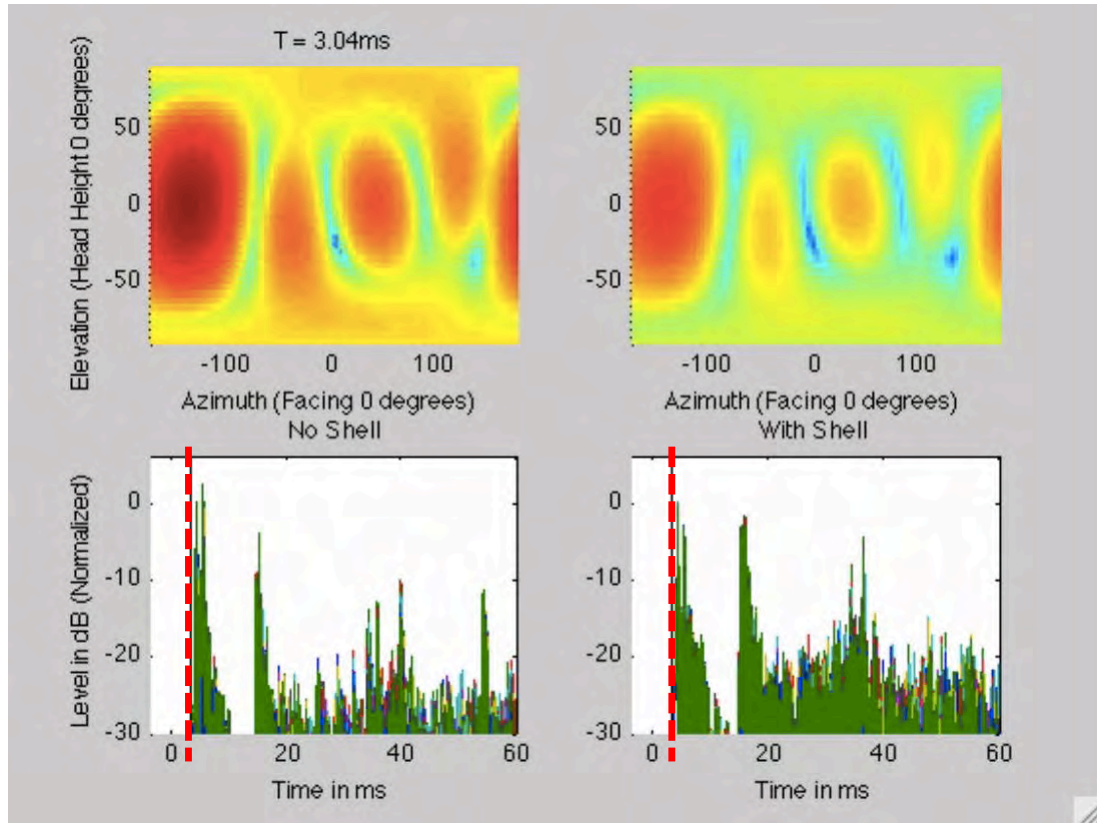


Figure 3.7: Skidmore with and without Orchestra Shell, 3 ms

The energy is highest from the rear at 16 ms in both conditions, but the overall increase in energy from all directions in the shell configuration suggests some focusing from the concave shape of the shell, as shown in Figure 3.8.

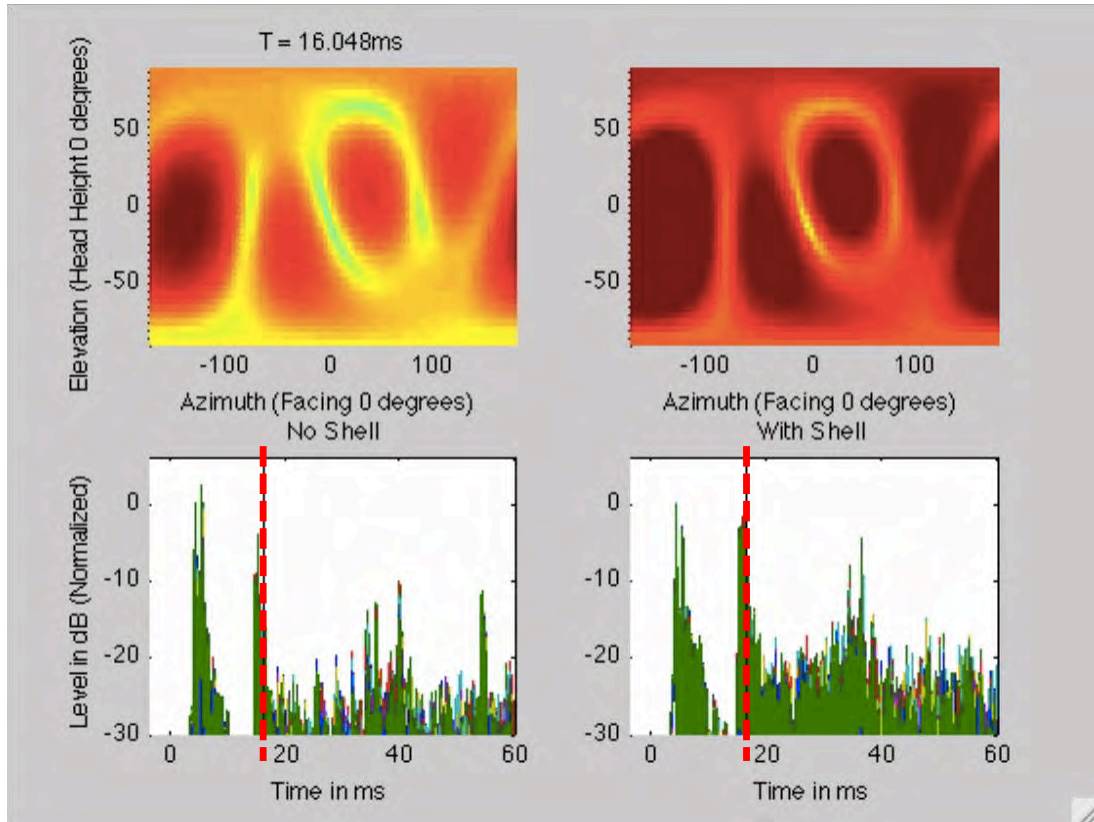


Figure 3.8: Skidmore with and without Orchestra Shell, 16 ms

At 32 ms, energy arriving from the upper rear in the shell configuration is absent in the no-shell condition, suggesting that the angled upper portion of the reflectors is sending more early reflections down onto the stage, as shown in Figure 3.9.

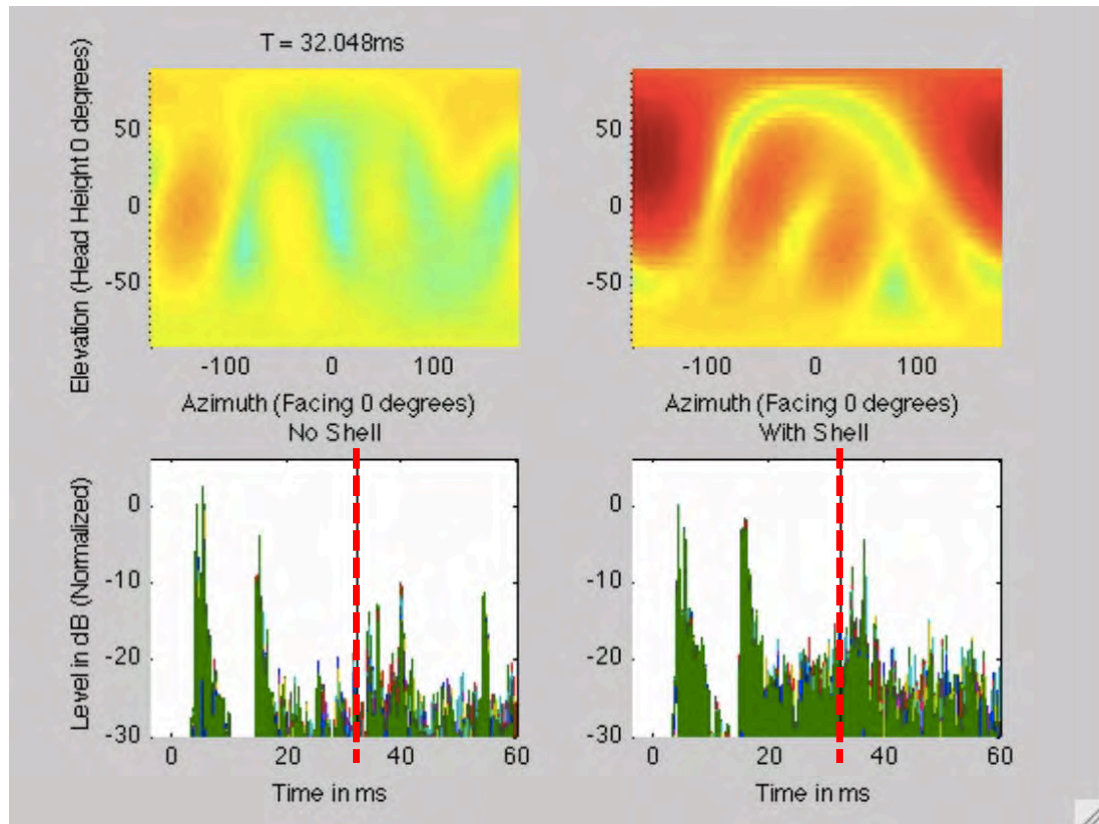


Figure 3.9: Skidmore with and without Orchestra Shell, 32 ms

At 40 ms, the energy arriving from the rear right corner in the no-shell condition only suggests that the lateral energy (normally reflected off the side wall) is reflected much earlier (16 ms) when the shell is deployed, as shown in Figure 3.10.

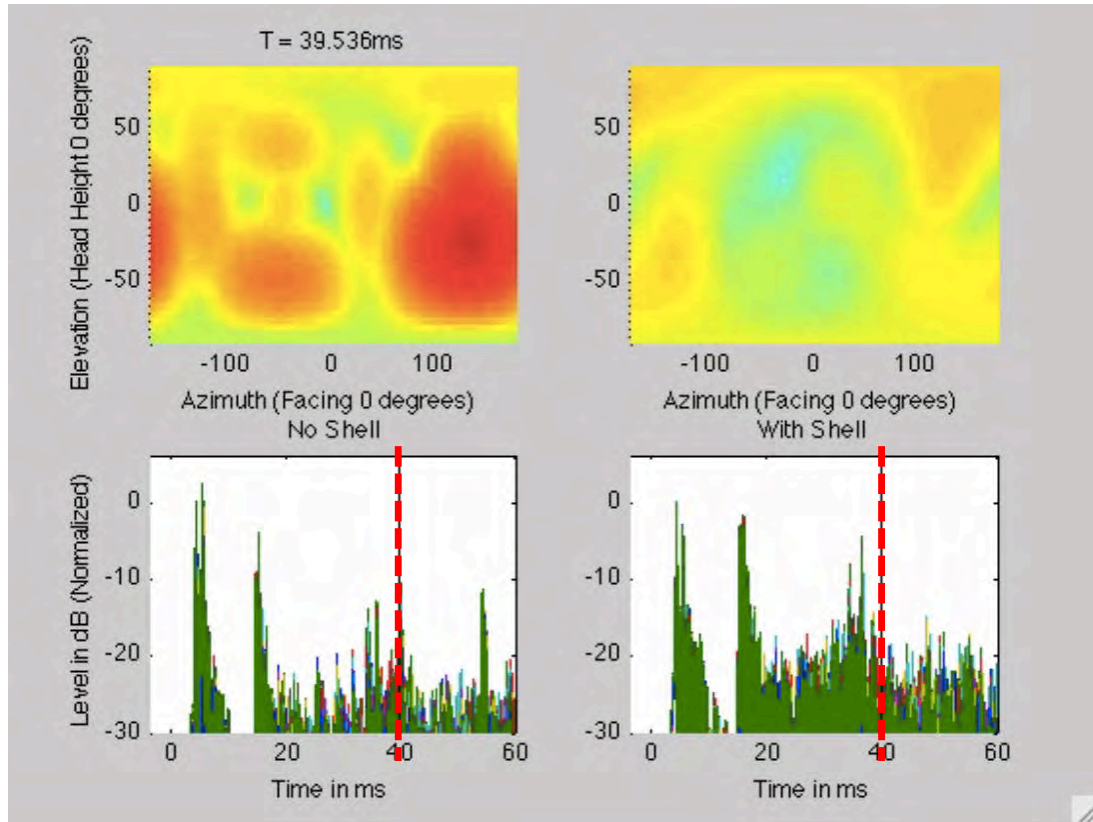


Figure 3.10: Skidmore with and without Orchestra Shell, 40 ms

These spatial display techniques are useful design tools. However, they cannot show which characteristics of the spatial energy are relevant to performers. Previous research into stage acoustics and spatial room-acoustic analysis (see Section 3.2.1 and Section 3.2.2) has generated several parameters that can be used to reduce the dimensionality of the measured data into manageable pieces. The frequency range used in calculating these parameters is band-limited to the 1 kHz octave band because spatial resolution is highest in this frequency range. The chosen parameters already eliminate any time-based information by integrating over designated time windows, so the only remaining dimension with multiple data points is the spatial domain. Decreasing or averaging the spatial information is a necessity for this study, but a level of detail will be lost in this process that can also be useful as a design tool. For example Figure 3.11 shows the spatial deviation of cross-stage LQ_{740} with a $j = 24$ or 15° resolution for four of the measured halls.

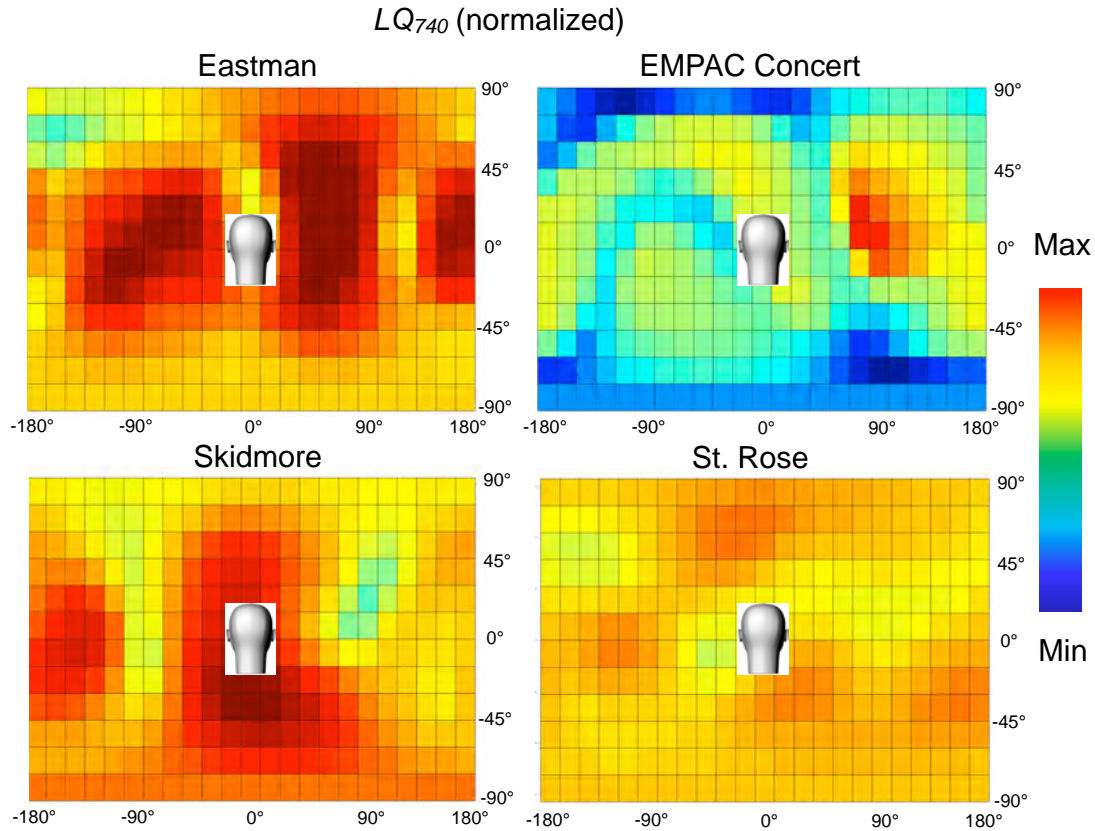


Figure 3.11: Spatial Distribution of Cross-Stage LQ_{740} , 15° Resolution

It is clear that any further spatial averaging may cause some of the nuanced differences between halls to disappear. However, it is likely that not all the information shown is relevant or even audible for musicians onstage during a performance. First, the number of look directions can be reduced to only overlap near half-power points, based on the 2nd-order beamwidth of the microphone array (70°). Then, look directions can be grouped (and the subsequent parameter values averaged) based on hall geometry and assumptions about traditional performance practice. Additionally, the spatial localization blur of the human auditory system should be considered. Based on these criteria, directional regions were determined, shown in Table 3.4.

Table 3.4: Directional Sectors Used in Calculation of Spatial Parameters

Sector	Beam Look Directions θ, ϕ where ϕ = inclination from vertical			
Top	(0°, 45°)	(90°, 45°)	(-90°, 45°)	(180°, 45°)
Bottom	(0°, 135°)	(90°, 135°)	(-90°, 135°)	(180°, 135°)
Front	(0°, 45°)	(0°, 135°)	(45°, 90°)	(-45°, 90°)
Rear	(180°, 45°)	(180°, 135°)	(135°, 90°)	(-135°, 90°)
Left	(-90°, 45°)	(-90°, 135°)	(-45°, 90°)	(-135°, 90°)
Right	(90°, 45°)	(90°, 135°)	(45°, 90°)	(135°, 90°)
Audience	(0°, 60°)	(30°, 105°)	(-30°, 105°)	
Side Walls Left	(-90°, 60°)	(-60°, 105°)	(-120°, 105°)	
Side Walls Right	(90°, 60°)	(60°, 105°)	(120°, 105°)	

In addition to averaged values for each sector, spatially-normalized parameters were also calculated for all sectors by taking the ratio of each sector over the total energy from all directions. Ratios of specific sectors were also calculated, including $\frac{\text{Top}}{\text{Bottom}}$, $\frac{\text{Front}}{\text{Rear}}$, $\frac{\text{Left}}{\text{Right}}$, $\frac{\text{Audience}}{\text{Side Walls}}$, $\frac{\text{Top}}{\text{Side Walls}}$, $\frac{\text{Top}}{\text{Rear}}$, and $\frac{\text{Top+Front}}{\text{Bottom+Rear}}$.

Spatial parameters used in this study are listed in Table 3.5. For each parameter listed with the exception of Directional Diffusion DD , values for each directional sector (normalized and un-normalized) and the listed sector ratios were calculated for soloist (1-meter) and ensemble (cross-stage) measurement positions. Standard omnidirectional parameters as well as omnidirectional values of all spatial parameters were also determined for comparison using the $N = 0$ or W spherical harmonic component. Full tables of all parameters with values for each measured hall are in Appendix A (Solo) and Appendix B (Ensemble).

Table 3.5: Spatial Parameters

Parameter	Stage Condition
Tc	(Soloist + Ensemble)
G_{early}	(Soloist + Ensemble)
G_{late}	(Soloist + Ensemble)
$G_{support}$	(Soloist + Ensemble)
G_{7-40}	(Soloist + Ensemble)
$G_{40-\infty}$	(Soloist + Ensemble)
LQ_{740}	(Soloist + Ensemble)
RR_{160}	(Soloist + Ensemble)
DD	(Soloist + Ensemble)
ST1	(Soloist only)
ST2	(Soloist only)
ST3	(Soloist only)
MTF	(Ensemble only)
EDT	(Ensemble only)
EDTR	(Ensemble only)

3.5 Discussion and Future Work

As outlined in this chapter, the spherical microphone array described in Chapter 2 has been used for the measurement and analysis of the spatial distribution of sound onstage. The applications of this method are not limited to those single-number parameters defined above. Given the exponential increase in information provided for each measurement with a spherical array, single parameters can be quite reductive for the sake of convenience and subjective research. It is possible that the full visual display of spatial information, whether as an animation or a set of time-windowed maps, can be more valuable to describe this more ecologically-accurate acoustic experience. Currently, a hot topic in the field of acoustic design is that of optimization. Perhaps the information provided in such maps can be used

to directly connect measurement and auralization to design changes, bypassing the typical single target values provided as “acoustic design criteria.” Reverse engineering is another topic currently under investigation by several individuals in the field, and the use of such spatial maps, providing information about “ideal” or desired spatial distribution of energy, could be useful in this method as well [13].

Many future developments remain for the methods described above. As shown, many different methods are possible for the display of spatial information, none of which have been robustly field-tested for readability and usefulness in the understanding of acoustic experience. Additional parameters can be developed and tested. Capturing additional measurements in a wider variety of spaces with the goal of increasing the database of onstage measured IRs is crucial to improving the robustness of the analysis. In the process of increasing the measurement library, measurement methodology should be standardized for better stage comparisons. A wider set of measured halls with both greater variation and redundancy in hall volume and seat count (nothing measured was larger than 2,300 seats, and no measured halls were the same size) would improve the robustness of the tests.

In this study, time constraints and lack of forehand knowledge about the halls resulted in a wide variety of source-receiver arrangements. To reduce variability, measurements should be captured in a grid with standardized spacing, with as many source-receiver pairs as possible. Improvements in efficiency (such as reducing the weight of the kit, recording raw sweeps and processing IRs offline) could allow time for more measurements. Some other procedures which slowed the measurement time included the use of omnidirectional and binaural microphones, which were not relevant for this study. More thorough documentation of measurements including exact orientation of the microphone array and simultaneous measurement of dB(A) levels using a Type II meter, as well as better documentation of hall dimensions, would have been valuable as well.

Another issue with onstage measurements is standardization of onstage conditions. The presence of chairs and risers onstage can have strong effects on the tested parameters. These conditions should be reproduced as much as possible between measured halls. Previous work has shown that the presence of chairs and

even musicians onstage cannot be discounted when making onstage measurements [26]. While it is not usually possible to have a full orchestra onstage for 4 hours during a measurement survey, some approximation could be made with chairs and draped fabric.

3.6 Conclusions

In this chapter, a spherical microphone array was utilized to capture onstage spatial impulse responses in 10 different halls. The measurements were analyzed using beamforming techniques (described in Chapter 2) and visual spatial maps were generated for various time windows. These maps were compared to acoustic models to show the usefulness of such spatial display in understanding the spatial distribution of energy onstage. From the spatial analysis, a set of possible parameters was proposed to describe the acoustic experience onstage, based on previous work in the fields of stage acoustics and spatial audience acoustics. These parameters will be used in an attempt to categorize the onstage performer experience in subjective listening and playing experiments, which will be outlined in Chapters 4 and 5.

CHAPTER 4

AMBISONICS AND REAL-TIME AURALIZATION

4.1 Introduction

As described in Chapter 2, a spherical microphone was developed to record spatial impulse responses for ambisonic reproduction. In Chapter 3, the microphone array was used to measure spatial impulse responses onstage in 10 concert halls. These measurements included cross-stage measurements for a passive listening experience, requiring the auralization of pre-recorded anechoic material to produce the sound of other solo or ensemble musicians onstage at the listener position. Additionally, 1-meter measurements were captured to simulate the self-generated sound of the listener’s instrument in this same position. These measurements required the development of a system for the convolution of the sound generated by the performer in real-time in order to virtually recreate the onstage experience in the laboratory setting. Both methods, described in this chapter, will be used in subjective tests for performer preference, as outlined in Chapter 5.

4.2 Theory

The method for encoding the recorded signal was described in Section 2.2.2. While direct application of spherical harmonic decomposition is possible for the encoding of the recorded signal for the purpose of beamforming analysis as described in Section 2.2.6, some further modifications are necessary before the signal can be reproduced over loudspeakers in a realistic and natural-sounding way. Additionally, the signal must be decoded for reproduction over the given loudspeaker array. The theory behind these processes are described below.

4.2.1 Encoding Conventions

For auralization purposes, scaling factors σ_{nm} are typically applied to each component to optimize the dynamic range of each component. The typical convention is the Furse-Malham (FuMa) set, which are based on the original normalization

of B-Format signals by Gerzon [67]. While these normalizations are useful for auralization, they reduce the orthonormality of the harmonic components, which is not helpful for analysis. The un-normalized values of σ_{nm} in the orthonormal basis is referred to as N3D. Daniel has introduced another convention, SN3D, which is a normalization (related to N3D by factor of $\sqrt{2n+1}$ optimized to increase dynamic range while maintaining maximum orthonormality [28]. These three conventions are listed up to order $N = 2$ in Table 4.1.

Table 4.1: Encoding Conventions for Order $N=2$

Harmonic	N3D	SN3D	FuMa
W	1	1	$\frac{1}{\sqrt{2}}$
Y	$\sqrt{3}$	1	1
Z	$\sqrt{3}$	1	1
X	$\sqrt{3}$	1	1
V	$\frac{\sqrt{15}}{2}$	$\frac{\sqrt{3}}{2}$	1
T	$\frac{\sqrt{15}}{2}$	$\frac{\sqrt{3}}{2}$	1
R	$\frac{\sqrt{5}}{2}$	$\frac{1}{2}$	$\frac{1}{2}$
S	$\frac{\sqrt{15}}{2}$	$\frac{\sqrt{3}}{2}$	1
U	$\frac{\sqrt{15}}{2}$	$\frac{\sqrt{3}}{2}$	1

4.2.2 Nearfield Compensation

The theory described in Section 2.2.2 provides the basis for perceptually accurate spatial encoding of plane waves. This is a good approximation of far field sound sources. However, in a realistic sound environment, there are both far field and near field sources. In the near field case, the wavefronts are still spherical due to the proximity of the source. The curvature of the wavefront allows the listener to perceive the relative distances of each source [32], [29].

Recalling the spherical expression of pressure for traveling waves ($e^{-i\omega t}$ implicit):

$$p(r, \theta, \phi, \omega) = \sum_{n=0}^{\infty} \sum_{m=-n}^n (C_{mn} h_n^{(1)}(kr) + D_{mn} h_n^{(2)}(kr)) Y_n^m(\theta, \phi) \quad (4.1)$$

In the near field, the radiation from a sphere at a point ρ is expressed by the divergent portion:

$$p(\rho, \theta, \phi, \omega) = \sum_{n=0}^{\infty} \sum_{m=-n}^n D_{mn} h_n^{(2)}(k\rho) Y_n^m(\theta, \phi) \quad (4.2)$$

Solving for D_{mn} we obtain the following term for the near field effect at distance ρ_0 :

$$\Gamma_m(k\rho) = k\rho_0 h_m^{(2)}(k\rho) (-i)^{m+1} \quad (4.3)$$

Assuming that the on-axis effect is already modeled (in the plane wave case), the $m = 0$ case can be removed from this term, obtaining the general term for near field effect compensation:

$$F_m^{\rho/c}(\omega) = \frac{\Gamma_m(k\rho)}{\Gamma_0(k\rho)} = (-i)^{m+1} \frac{h_m^{(2)}(k\rho)}{h_0^{(2)}(k\rho)} = \sum_{n=0}^m \frac{(m+n)!}{(m-n)!n!} \left(\frac{-ic}{\omega\rho} \right)^n \quad (4.4)$$

In the spherical harmonic decomposition, this expression modifies the spherical harmonic components B_n^m :

$$B_n^{mNFC(\rho/c)} = F_m^{\rho/c}(\omega) B_n^m \quad (4.5)$$

This is very useful for distance coding of near field sources if the distance ρ for each source is known. In other words, it is ideal for encoding of virtual sources. Unfortunately, it cannot be easily applied to a real field of several sources with unknown distances. Therefore, for auralizations of recorded ambisonic signals, the relative distances of sources in the near field are not well resolved. However, the theory is still quite useful to eliminate another problem in ambisonic auralization, which occurs as part of the decoding process. Decoding theory will be described more detail in Section 4.2.3. In ambisonic auralization, the loudspeakers themselves

produce spherical wavefronts as they are in the near field of the listener. This can create proximity effects, audible as an increase in low frequencies with increasing order. Pre-compensating the signal (if the distance R of the loudspeakers is known) with order-specific, complex high-pass filters can alleviate this problem and allow for more accurate reconstruction of the sound field. In this case, the compensation is inversely proportional to the spherical components:

$$B_n^{m_{NFC(R/c)}} = \frac{1}{F_m^{R/c}(\omega)} B_n^m \quad (4.6)$$

The magnitudes of these filters are shown in Figure 4.1.

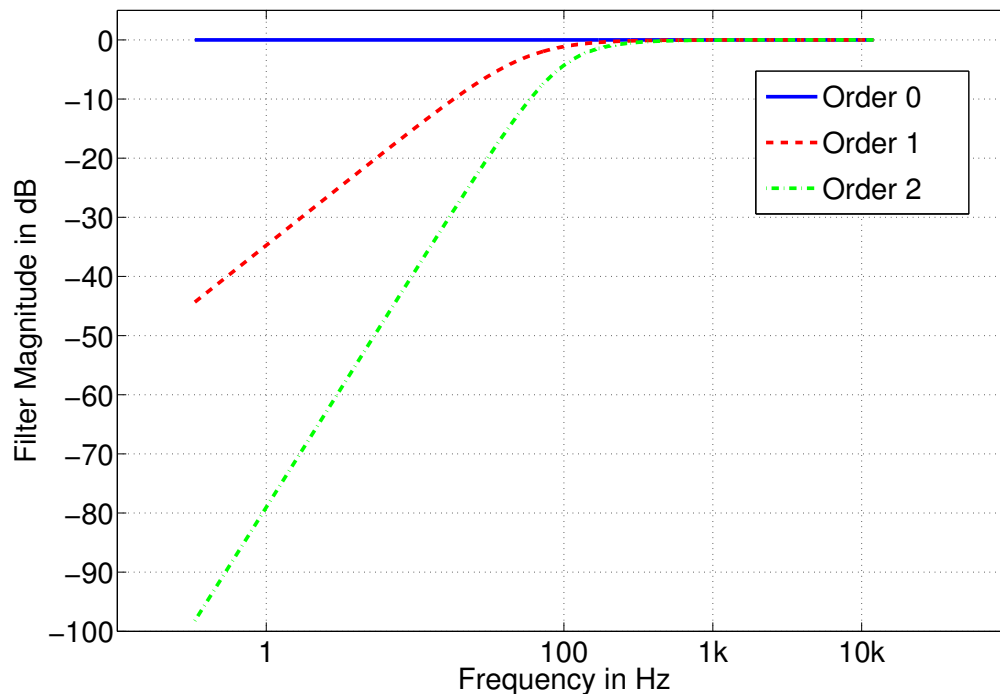


Figure 4.1: Near Field Compensation Filters Applied to Each Order up to $N=2$

4.2.3 Ambisonic Decoding

Once the signals recorded by the spherical microphone array have been encoded into spherical harmonic components, they are completely portable. Matrix operations can be applied, such as rotation, scaling, or flipping. Signal processing

operations such as convolution can be applied so long as they are equally applied to all channels. For auralization purposes, the ambisonic signals must then be “decoded” into L signals that can be reproduced over L loudspeakers. In theory, the loudspeaker arrangement is flexible. However, some restrictions apply in reality. The number of loudspeakers should be greater than the number of spherical harmonic components to prevent spatial aliasing. However, increasing the number of loudspeakers to an excessive number decreases the area of accurate reconstruction. The arrangement should be fairly regular, although small irregularities can be accommodated. Additionally, if the near field pre-compensation has been applied, the value for R should match the distance to the loudspeakers from the center of the arrangement (called the “sweet spot”) or a correction factor must be applied. As opposed to the recording and encoding processes, the decoding process is fairly standardized and there are several commercially-available decoders. These decoders allow the decoding to be performed in real time once the system is calibrated, and signals can remain in ambisonic format up until the moment of playback. This research uses a commercial decoder calibrated to a fixed loudspeaker arrangement, and therefore decoding theory will not be described here in great detail. A more detailed explanation of decoding can be found in [28].

Typically, decoding is performed using the method of mode matching. Recently, some other methods have been proposed, including energy-preserving and all-round ambisonic decoding, but these methods were not explored in this research [110], [109]. The general process of mode matching can be described as follows. Each loudspeaker can be modeled as a point source generating a spherical wavefront. The goal is to re-synthesize the sound field generated at the sweet spot with a finite sum of spherical wavefronts from L loudspeakers. For example, if the source is a plane wave incident from (θ_i, ϕ_i) , the incident pressure at the sweet spot should be:

$$e^{ikr} = 4\pi \sum_{n=0}^{\infty} i^n j_n(kr) \sum_{m=-n}^n Y_n^m(\theta, \phi) Y_n^m(\theta_i, \phi_i)^* \quad (4.7)$$

On the other hand, the pressure generated by each loudspeaker point source from distance R on the sweet spot is:

$$\frac{e^{ik|r-R|}}{4\pi|r-R|} = ik \sum_{n=0}^{\infty} i^n j_n(kr) h_n(kR) \sum_{m=-n}^n Y_n^m(\theta, \phi) Y_n^m(\theta_l, \phi_l)^* \quad (4.8)$$

The signal generated by a plane wave incident from (θ_i, ϕ_i) , re-synthesized by the sum of signals from L loudspeakers of distance R from the sweet spot is then:

$$\hat{p}(r, \theta, \phi, k) = ik \sum_{n=0}^{\infty} i^n j_n(kr) h_n(kR) \sum_{m=-n}^n Y_n^m(\theta, \phi) \sum_{l=1}^L w_l(\theta_i, \phi_i) Y_n^m(\theta_l, \phi_l)^* \quad (4.9)$$

Where $w_l(\theta_i, \phi_i)$ is the gain applied to each loudspeaker in the decoding process. In order to determine the values of $w_l(\theta_i, \phi_i)$ necessary to accurately reconstruct the sound field, the two previous equations must be set equal to each other, which simplifies to provide the following relationship:

$$\sum_{l=1}^L w_l(\theta_i, \phi_i) Y_n^m(\theta_l, \phi_l)^* = \frac{4\pi i^n}{ik h_n(kR)} Y_n^m(\theta_i, \phi_i)^* \quad (4.10)$$

This can be generalized for an arbitrary sound field that has been encoded into spherical harmonic components:

$$p(r, \theta, \phi, k) = \sum_{n=0}^{\infty} \sum_{m=-n}^n A_n^m(k) j_n(kr) Y_n^m(\theta, \phi) \quad (4.11)$$

providing the following relation:

$$\sum_{l=1}^L w_l(\theta, \phi) Y_n^m(\theta_l, \phi_l)^* = \frac{A_n^m(k)}{ik h_n(kR)} \quad (4.12)$$

In the discrete case, this relation can be redefined as a system of linear equations:

$$\mathbf{Y}_L \cdot \mathbf{W} = \mathbf{B} \quad (4.13)$$

where \mathbf{B} is the $(N+1)^2$ vector of previously encoded signals, \mathbf{Y}_L is the matrix of spherical harmonic components for L loudspeakers, and \mathbf{W} is the vector of decoded signals for each loudspeaker, as defined above. Least-squares resolution is used to solve for \mathbf{W} :

$$\mathbf{W} = \mathbf{Y}_L^H [\mathbf{Y}_L \mathbf{Y}_L^H]^{-1} \cdot \mathbf{B} \quad (4.14)$$

Given a fixed loudspeaker arrangement, the matrix inversion process can be pre-determined. This is known as the decoding matrix \mathbf{D} . Then the decoding process can be performed using a real-time matrix multiplication with any arbitrary signal pre-encoded into a set of spherical harmonic components:

$$\mathbf{W} = \mathbf{D} \cdot \mathbf{B} \quad (4.15)$$

This is known as the “basic” form of mode-matching decoding. Given an infinite order of spherical harmonics and infinite number of loudspeakers, it reproduces the exact sound field at the sweet spot. Of course, given a finite order of harmonics and a finite number of loudspeakers, this sound field is not exactly reproduced. Additionally, the sweet spot is small with relation to listener area. Because of these limitations, various weighting factors have been proposed that can be used to optimize the auralization for different conditions [73], [28]. The limitations on reconstruction are frequency-dependent, and some decoders use different weightings for high and low frequencies, called “dual-band” decoding. This concept is modeled after the binaural localization mechanisms inter-aural level and time differences, which dominate auditory localization in the high and low frequency ranges, respectively. However, at the time of this research, dual-band decoding had not fully been developed for the chosen decoder.

Two of the proposed corrections to basic decoding are “max r_E ” decoding and “in phase” decoding. In max- r_E decoding, the goal is to “concentrate” the energetic contributions in the expected direction by maximizing the magnitude r_E of the energy localization vector $\hat{\mathbf{r}}_E$ [7], [50]:

$$r_E \hat{\mathbf{r}}_{\mathbf{E}} = \frac{\sum_{l=1}^L (W_l W_l^*) \hat{\mathbf{u}}_l}{\sum_{l=1}^L (W_l W_l^*)} \quad (4.16)$$

$$\hat{\mathbf{u}}_l = \begin{pmatrix} \cos \theta_l \\ \sin \theta_l \end{pmatrix}$$

The values r_E for each order N of spherical harmonics can be maximized by changing the gains g_n applied to the harmonics in each order. For 3D loudspeaker arrangements using higher order ambisonics, the maximum value of r_E for each order is determined by the largest root of the Legendre polynomial for that order:

$$r_E = P_{N+1}^{-1}(0) \quad (4.17)$$

and the resulting weights per order $n = 1 : N$ for a 3D rig:

$$g_n = P_n(r_E) \quad (4.18)$$

For a source incident from a specific direction, max r_E decoding has the effect of reducing the amount of all off-axis energy in the re-synthesis, while in-phase decoding has the effect of increasing the energy from the sides while reducing the energy from the rear, which makes in-phase decoding ideal for large listening areas [68]. A comparison of the localization resolution for each of the decoding schemes is shown in Figure 4.2 by applying each set of decoding gains to the spherical harmonic decomposition of a single plane wave on axis:

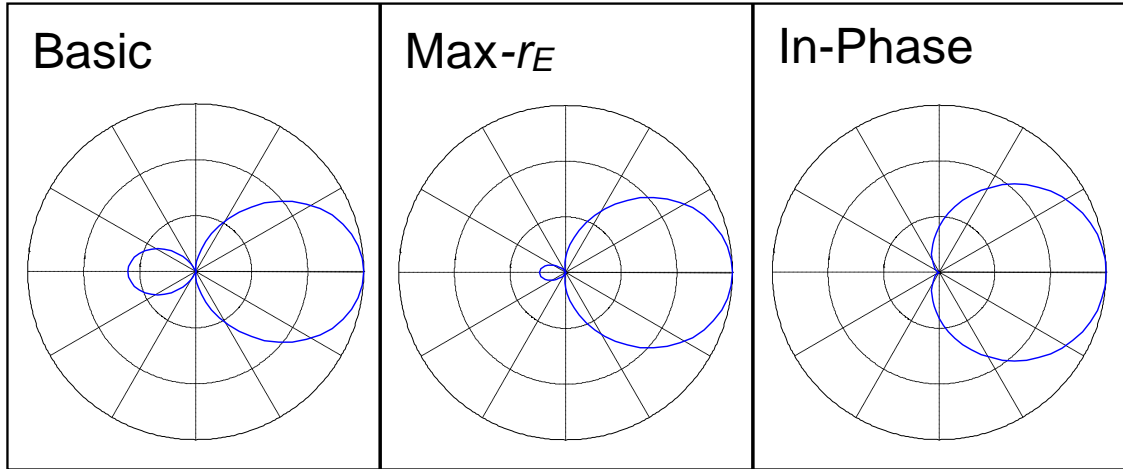


Figure 4.2: Localization Resolution of Three Decoding Types for a Single Plane Wave On Axis for Order $N=2$

With in-phase decoding, in order to minimize the phase differences over a large area, the higher-order harmonics receive lower weightings. The resulting weights for each order are given for a 3D rig [28]:

$$g_n = \frac{N!(N+1)!}{(N+n+1)!(N-n)!} \quad (4.19)$$

For $N = 2$, the gains for each ambisonic channel for basic, max- r_E and in-phase are listed in Table 4.2 [28]:

Table 4.2: Decoding Gains g_n for $N=2$

Harmonic	Basic	Max- r_E	In-Phase
W	1	1	1
Y	1	0.775	0.500
Z	1	0.775	0.500
X	1	0.775	0.500
V	1	0.400	0.100
T	1	0.400	0.100
R	1	0.400	0.100
S	1	0.400	0.100
U	1	0.400	0.100

4.3 Methodology

In order to determine the characteristics of the measured stages that are relevant to performer experience, a set of subjective laboratory tests were prepared that would cover a range of conditions for performers onstage. The tests involved three conditions: passive listening, soloist playing and ensemble playing. These tests will be described in more detail in Chapter 5. The tests were the main drivers in the choices and development of the auralization systems described in this chapter.

Passive listening is the most common test condition used in laboratory experiments. It has the lowest cognitive load and the highest repeatability between stimuli. Active playing scenarios involve increased cognitive load and high levels of variability in the self-generated stimuli (as it is played in real time and not pre-recorded). However, the level of realism and applicability to the kind of complex onstage communication and feedback necessary for live performance is much higher than in the passive listening scenario. Both methods were used in this research.

4.3.1 Listener Auralization

Portions of the laboratory tests involved subjects listening to pre-recorded audio and making comparisons between the measured halls. In one portion, subjects judged the pre-recorded stimuli in a passive, non-playing condition. This was intended to simulate a resting condition where the musician is not actively playing but must still be aware of cues from other musicians that would indicate the proximity of their next entrance. In this condition, it is possible through the convolution of the room impulse responses with music recorded in an anechoic chamber to remove the variability of musical interpretation and truly provide A-B comparisons of stage acoustic environments. Two impulse responses were used from each hall for the passive listening scenario: front-back and side-side cross-stage measurements as described in Section 3.3.1.

Some variability existed in the source-receiver distances due to stage size (ranging from 4.4 m source-receiver distance in Albany Recital to 13.5 m in Skidmore). However, after pilot tests were conducted, in which absolute level differences between impulse responses (created by these variations in distance) were applied, it was determined that such level changes would overwhelm all other acoustical factors when making comparisons and skew the judgements of the subjects towards overall direct-sound level preferences alone. Therefore, all impulse responses were normalized to the level of the average source-receiver distance in order to allow the subjects to focus on relative acoustic differences between the halls themselves.

For the convolution, anechoic audio samples were recorded of solo violin in the anechoic chamber at GE Global Research Labs in Niskayuna, New York. Excerpts of both baroque (*Prelude* by J.S. Bach) and contemporary (*Mikka* by Iannis Xenakis) music were recorded for comparison. Recordings were captured with 6 omnidirectional Audix microphones in a hemisphere around the soloist and summed in order to eliminate any attenuation or filtering of the signal due to instrument directivity. Ideally, the individual signals would be used to recreate the directivity in the convolution process, and this is currently possible using modeled impulse responses or impulse responses recorded using individually-controlled directional sources [6]. However, because the halls in this research were only measured using an omnidi-

rectional source, directivity information was not usable. An image of the recording setup is shown in Appendix C.3.

These recordings were then convolved with the impulse responses described above. The same mono anechoic file was convolved offline with each ambisonic channel from all 10 impulse responses. The pre-convolved audio was then played back in a laboratory setting over a sphere of loudspeakers surrounding the subject, using a real-time ambisonic decoder in Max/MSP. An iPad interface and computer playback system were generated in Max/MSP that allowed musicians to switch between all 10 halls in real-time while the musical excerpt played continuously. The system will be described in Section 4.3.3.

In another portion of the experiment, the subjects played in real-time along with a pre-convolved orchestral accompaniment. Due to the difficulty in recording a full orchestra in an anechoic chamber, audio excerpts recorded by researchers at the Helsinki University of Technology were used [82], [66]. These recordings were made of individual instruments performing separately in an anechoic chamber while listening to a piano arrangement played back over headphones for synchronization purposes. The recordings can be auralized separately if multiple source positions have been recorded [91]. For this research, since only one cross-stage source position was recorded for each receiver, the front-back cross-stage pair was used.

The subject, located at the downstage receiver position, was meant to simulate the traditional “soloist” position with the orchestra upstage. The individual instrument recordings were mixed into a single mono file (with a filter applied to attenuate the background noise, which increased due to the contribution of multiple recordings) and convolved with the upstage source position to simulate the orchestra as a point source behind the soloist. A 24-second musical excerpt consisting of 19 bars of *Symphony I, Movement IV* by Gustav Mahler (bars 67-86) was used, with a 4-beat click track inserted at the beginning for subject synchronization.

Exact dB(A) levels for the recorded Mahler excerpt were not available for calibration purposes. Average sound pressure levels onstage during an orchestral performance of a late romantic symphony (approximately 100 musicians) can range from 80 dB(A) to 115 dB(A) L_{eq} . OSHA standards limit the level for 2 hours of

exposure (the length of the tests) to 90 dB(A). These are the standards required for testing approval by the Institutional Review Board. Therefore, the playback level of the Mahler excerpt was calibrated so that it did not exceed 90 dB(A) L_{max} . Although it could be argued that this provided an unrealistic self-to-ensemble balance, the relative level differences between the halls were maintained and therefore the comparisons were still considered viable.

4.3.2 Real-Time Performer Auralization

The second and third portions of the laboratory tests involved subjects performing in real-time, whether improvised or notated music was performed. For these tests, the same downstage receiver position was used to simulate the “soloist” position. In each hall, along with the cross-stage measurement, a source position at a 1-meter distance (“soloist” position as described in Section 3.3.1) was also recorded. This was the impulse response used to convolve the self-generated signal from the instrument in real-time as the subject played. Due to the nature of the stimuli, the auralization of self-generated real-time sound is more complex than the offline convolution of pre-recorded anechoic audio as described in Section 4.3.1.

When the performer generates a sound using an instrument or his/her own voice, the direct sound enters the ears by air-conducted paths and bone-conducted paths, which are properties of the instrument and performer and unaffected by the space itself. The air-conducted sound from the instrument also propagates out into the space and returns to the ear as reflections and reverberance, which are determined by the acoustic properties of the space. It would be extremely difficult to reproduce the bone-conducted signal to the ears no matter what reproduction method is used. Additionally, the blocking out of the bone-conducted and air-conducted direct sound would be difficult. Therefore, real-time auralization typically does not attempt to synthetically reproduce the direct sound. Instead, the direct sound is physically generated by the performer (as it is unaffected by the space) and only the reflections and reverberance are reproduced. This requires the truncation of the impulse response to remove the direct sound. Then the truncated impulse response is convolved in real-time with the signal from the instrument and played

back to the performer over the selected reproduction system. This will be called the “Real-Time Auralization System,” or RTA System.

4.3.2.1 RTA Signal Capture

The instrument signal must be captured at a fixed distance from the source (instrument). In order to eliminate feedback, the microphone should be placed as close to the source as possible. However, proximity effects may occur if the microphone is too close to the source. Additionally, instrument directivity may influence the spectral distribution of the signal depending on the microphone location and physical motion by the musician while playing. Methods of microphone placement were investigated in previous work by Laird et al., where a distance of 8 cm was used to maximize the signal-to-noise ratio [63]. However, musicians reported feeling a “PA effect” (feeling that the reproduced room response sound was amplified or synthetic) even after a proximity correction filter was applied. This was potentially due to various effects on directivity, spectrum, instrument motion and non-musical sounds generated by the close-microphone position. For this research, a Neumann KM185 microphone with a hyper-cardioid directional pattern was used in order to provide good rejection of the loudspeaker signals. This allowed the microphone to be placed slightly further away from the instrument (18 inches) to allow for a more natural sounding signal. Adversely, this increased the physical latency of the system by adding distance to the source-receiver path.

4.3.2.2 RTA Latency

Any system using real-time convolution will have some latency. Two main sources of latency exist: processing latency due to hardware and software, and physical latency due to speed of sound in air. Real-time performer auralization has previously been implemented using headphones [96]. In this case, the latency of the system is limited to the hardware/software latency and the physical latency of the instrument-microphone distance (as the sound is reproduced directly at the ears). This provides a very short travel path for the reproduced sound, and physical latency is negligible. However, for reasons previously described, reproduction over loudspeakers was chosen for this research, and therefore the physical distance from

the loudspeakers to the ears generates additional latency.

The chain of system latency is shown in Figure 4.3.

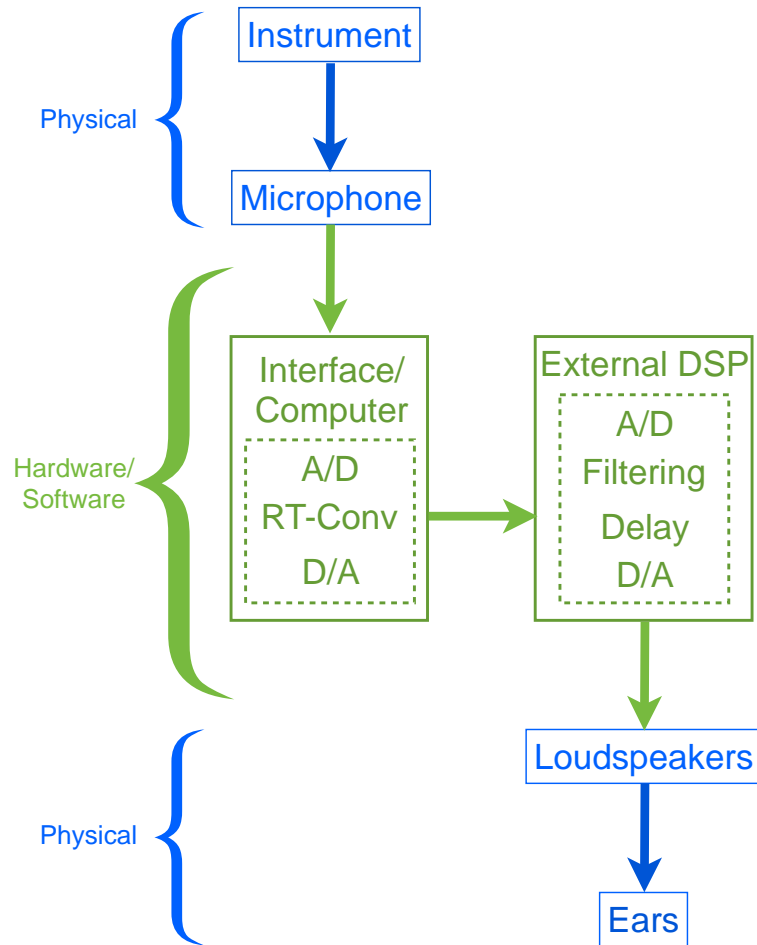


Figure 4.3: RTA System Latency Components

The latency of the entire system can be measured by determining the arrival time of a reference signal when played through the system and captured by a microphone at the head position. The physical latency can be determined by calculating the distance from the loudspeakers to the ears and the distance from the instrument to the microphone, which can be subtracted from the overall measured latency to determine the latency of the hardware/software. While the physical latency is based on fixed distances and cannot be changed unless the equipment is moved, hard-

ware/software latency can be minimized through various methods, dependent on the device chain and settings for each device.

4.3.2.3 Arup RTA Research

Based on work by Laird et al., and as part of an internal research grant by Arup, a real-time auralization (RTA) system was developed by Caulkins, Stetson and Guthrie for the Arup SoundLab [63]. The RTA system was developed in a previous version of the NY SoundLab (will be called “155AoA”) in New York, and tested in the LA SoundLab in Los Angeles. After the system was developed, a new NY SoundLab was constructed (called “77W”) in New York, where the resulting RTA system was modified for the new setup and used for the subjective testing described in this research.

In the development of the RTA system, latency was measured for several hardware/software combinations. The hardware/software chain of the initial system is described in Table 4.3.

Table 4.3: Initial RTA System Hardware/Software Chain

Device	Function
USB Interface (RME Fireface UC)	Pre-amplification, A/D Conversion
Mac Pro 8-Core 2.4 GHz running Max/MSP 5.1.9	Convolution, Decoding
MOTU 24 I/O with PCI-424 soundcard	D/A Conversion
Biamp Audia DSP	EQ/Level Calibration

The latency of each system configuration was measured by locating a reference loudspeaker and the auralization microphone (used for instrument signal capture) at a fixed distance (initial testing used 12 inches, although 18 inches was later used for increased perception of realism). These were located remotely in order to avoid feedback and maximize the signal-to-noise ratio. The microphone signal was convolved with each ambisonic channel using non-truncated Dirac impulses (generated in Matlab), to preserve the integrity of the signal. The decoded signal

was reproduced at the loudspeaker array and a measurement microphone was located at the center of the sphere. The time delay of signal at the measurement microphone compared to the reference signal produced by the loudspeaker was determined using EASERA SysTune software. The signal between the interface and the EASERA software creates additional latency and was measured separately using a loopback signal in order to subtract this from the final latency measurement. A schematic diagram of this process is shown in Figure 4.4.

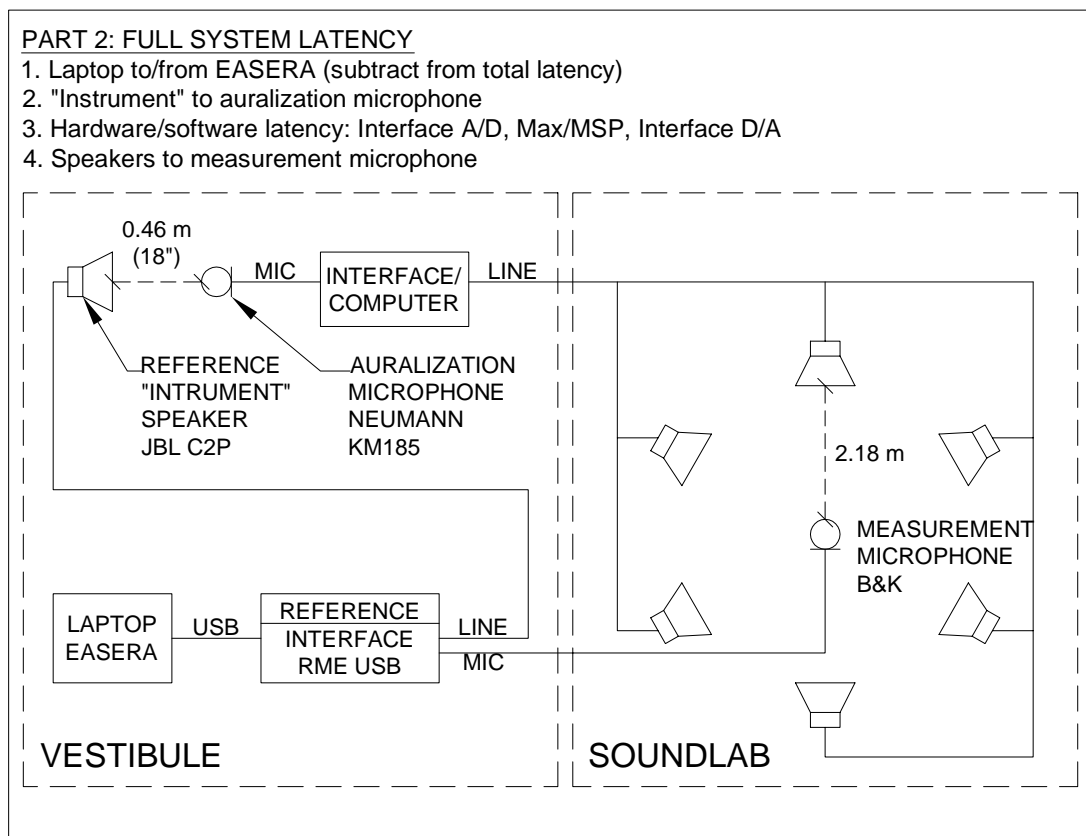
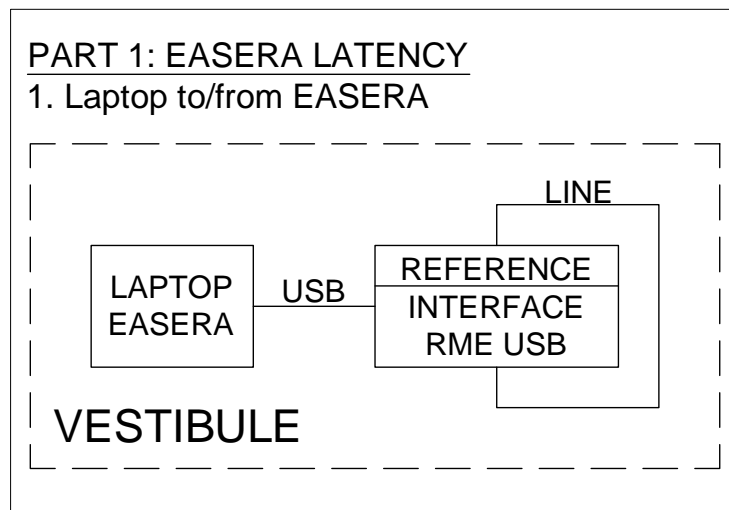


Figure 4.4: Schematic Diagram of RTA System Latency Measurement Setup

Based on these measurements, it was determined that the largest source of

hardware/software latency in the system were the conversions between analog and digital audio. The minimum required conversions are two (one from the microphone and one to the loudspeakers). However, in the system shown above, an additional two conversions occur at the external DSP unit. To minimize system latency, the individual loudspeaker filters and delays necessary for a calibrated playback system were implemented directly in Max/MSP. This decreased the overall latency by 4.45 ms.

The second largest source of hardware/software latency was found to be buffer size and sampling rate settings in the software. Low latencies can be achieved using small buffer sizes and high sampling rates, at the cost of increased CPU usage. At high levels of usage (>50%) unacceptable audio artefacts, such as drop-outs and stutter, were found to occur. Multiple real-time convolution methods (VST plug-ins and Max/MSP externals) were tested. At the time of testing, in Spring 2012, at a setting of 96 kHz sampling rate and 32-tap vector size for nine channels of convolution, the “AHarker” externals showed the lowest CPU usage, averaging around 25% CPU. Therefore, AHarker objects were implemented to drive the system [49].

The loudspeaker array for the 155AoA NY SoundLab at the time of testing had a radius of 2.18 meters. Therefore, the total latency was 0.8 ms (instrument to microphone) + 4.6 ms (hardware/software, set to 96 kHz/128 taps) + 6.4 ms (loudspeakers to ears) or 11.8 ms. The revised chain of system latency is shown in Figure 4.5.

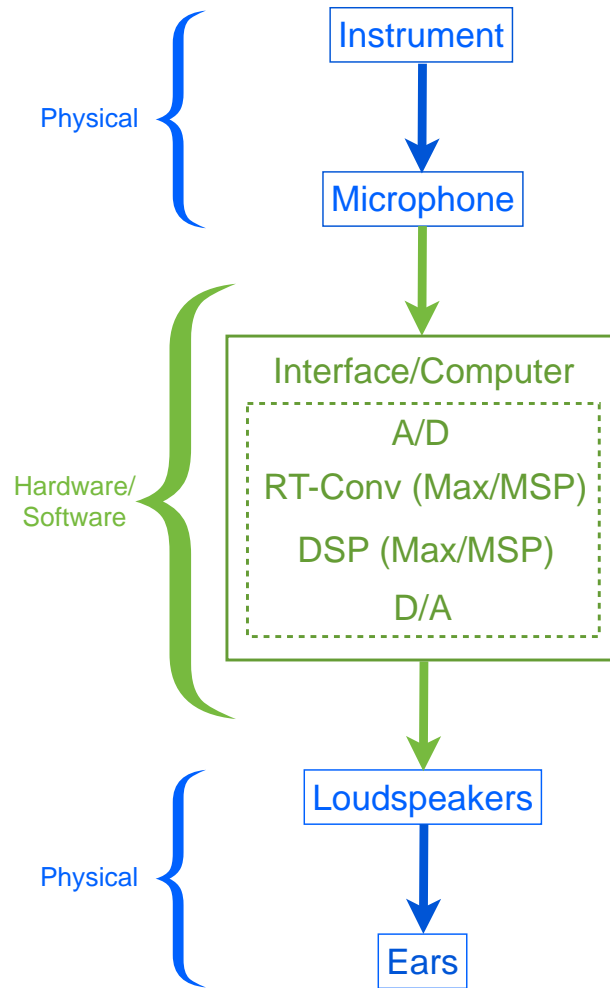


Figure 4.5: Revised RTA System Latency Components

Due to the removal of direct sound from the impulse response, the playback of the room response should be delayed by the length of the removed portion in order for reflections to arrive at the ear at the correct times. This naturally provides a margin of allowable system latency. However, the reflection off the stage floor at a 1-meter source-receiver distance for a seated musician (average 1.1 meters to ear height) should arrive only 4.1 ms after the direct sound. Therefore, given the overall system latency of 11.8 ms, it is not viable to include the floor reflection in the convolved response. It was assumed that with some minor variations, most stage floors would provide reflections similar to that of a layer of 5/8" MDF mounted

on the floor of the laboratory under test (carpet). Stage floor vibration is also simulated using this construction, which is valuable to creating a sense of realism in the virtual environment [1]. Assuming that no surfaces were closer than the radius of the loudspeakers (2.18 meters), any energy beyond the first floor reflection would arrive after propagating from the instrument and reflecting back from a surface at least 2.18 meters away, a delay of 12.7 ms. Therefore, the impulse responses could be truncated up to 12.7 ms and still provide a realistic room response. Comparison of this distance with the measured stage enclosures is shown in plan in Figure 4.6 and in section in Figure 4.7.

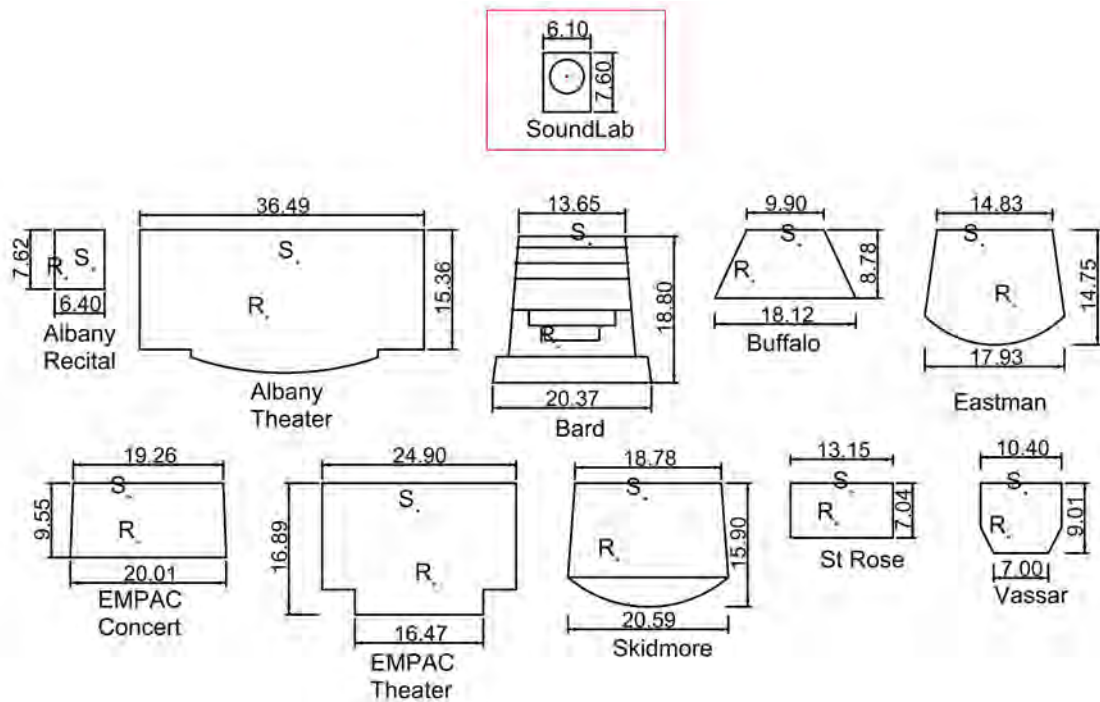


Figure 4.6: Measured Stage Enclosure Plans Comparison with RTA System Setup

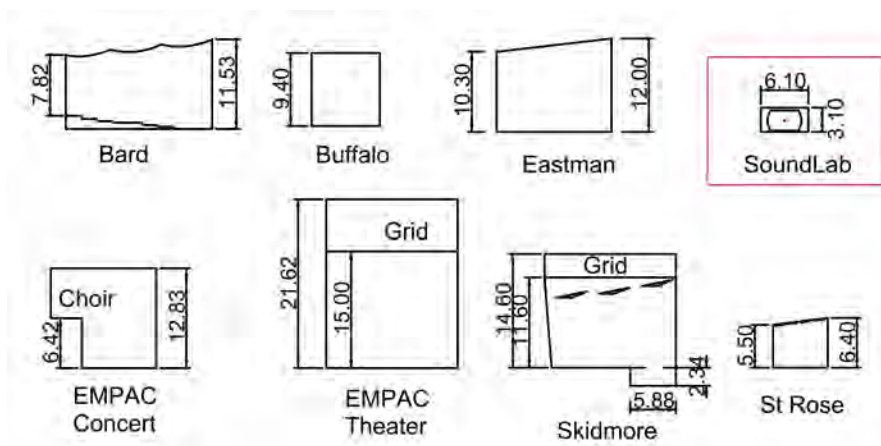


Figure 4.7: Measured Stage Enclosure Sections Comparison with RTA System Setup

A schematic diagram of the final RTA system is shown in Figure 4.8 (image reproduced courtesy Terence Caulkins).

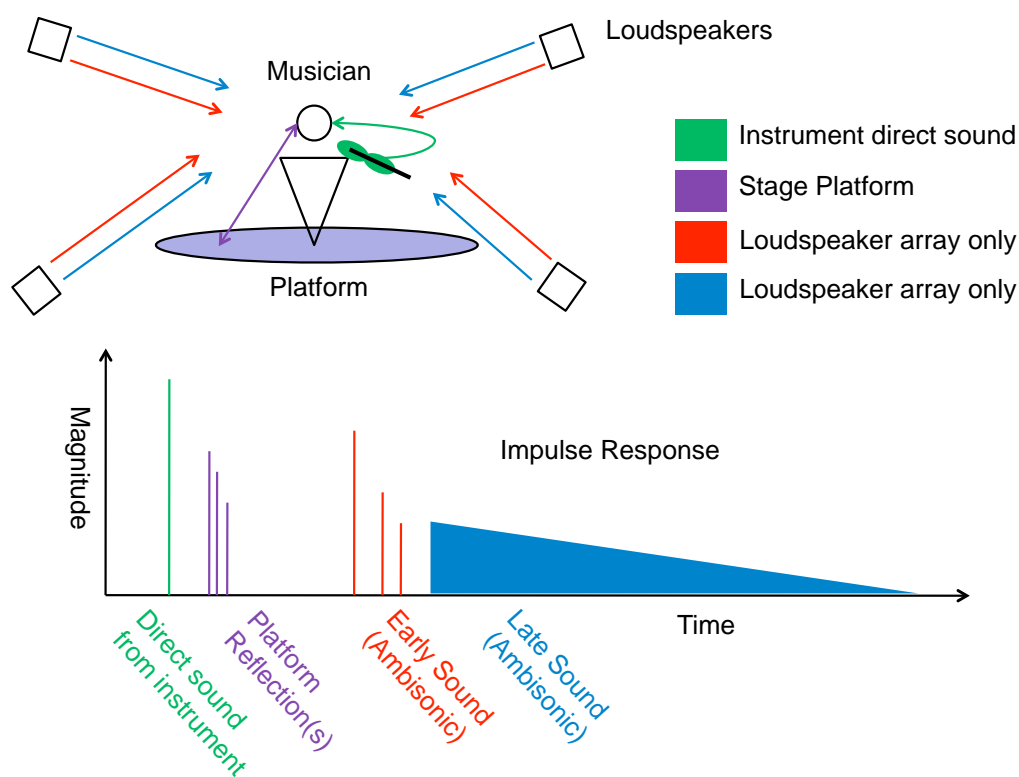


Figure 4.8: Schematic Diagram: RTA System

4.3.2.4 RTA Power Spectrum Corrections

Another factor that was determined to influence the realism of the RTA system is related to the directivity of the instrument. In a hall, sound radiates differently in each direction at different frequencies from an instrument, and the frequency-dependent directivity produces different spectra in different directions. As the sound mixes in the far field of the hall, the contribution from off-axis directions increases and the overall spectrum of the response shifts. Because the microphone is only positioned on axis, even at a distance of 18 inches, the frequency response of the on-axis direction dominates the spectrum. The early portion of the sound is not significantly affected by this discrepancy, but the late portion can be perceived as unnatural as a result, particularly for instruments with strong variations in directivity such as flutes and French horns. Two methods were explored to alleviate this issue. The first consisted of placing four microphones in the corners of the listening room to pick up the far field response and convolving the resulting mixed signal with the late portion of the IR instead of the close-microphone signal. Investigations of this method did not improve the overall perception of realism, perhaps because the energy from the loudspeakers was adding significantly to the far-field signal picked up by these microphones and increasing the perceived “PA effect.”

The second method consisted of finding the average power spectrum of each instrument over all directions and using this spectrum to filter the close-microphone signal for the late portion of the IR. Directivity measurements were captured by the Helsinki University of Technology were used for several instruments [81]. These measurements contain dB values for the energy in each octave band at equiangular spacing in 10° increments around the instrument. In order to calculate the power spectrum, the energy in each octave band was summed over all directions (because the spacing was not equidistant, each direction e_i was weighted by its percentage of total surface area ω_i on a sphere before summing). Area weightings are shown in Figure 4.9.

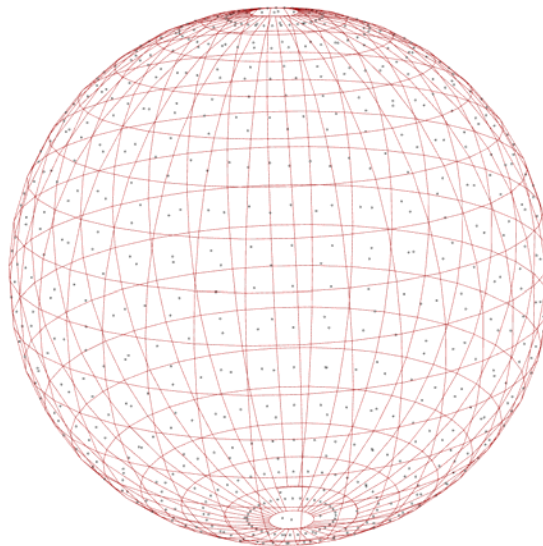


Figure 4.9: Spherical Distribution of Area Weightings for Power Spectrum Calculations

This was then compared to the on-axis energy e_0 for that octave band multiplied by the total surface area of the sphere ω_T in order to determine the difference between the far-field spectrum and the on-axis spectrum, as shown below:

$$10 \log_{10} \left(\frac{\sum_{i=1}^N e_i * \omega_i}{e_0 * \omega_T} \right) \quad (4.20)$$

For each instrument, a single dB value was generated for each octave band. FIR filters were generated in Max/MSP that would apply these power spectrum corrections to the signal before convolving with the late part of the IR. This method was found to increase the perceptual realism of the auralization for the instruments tested. Correction values for the instruments tested are in Table 4.4.

Table 4.4: Instrument Power Spectrum Corrections in dB

	Octave Band Center Frequency in Hz							
	63	125	250	500	1000	2000	4000	8000
Flute	−3.3	−3.3	0.0	0.0	−6.3	−8.7	−10.1	−4.3
Horn	0.0	0.0	−2.3	−3.9	−1.2	−10.3	−8.4	−4.9
Violin	−1.8	−1.8	−2.3	−2.9	0.0	−6.1	−3.2	−3.2
Cello	−1.3	−2.5	0.0	−2.2	−2.7	−7.7	−4.9	−3.8

4.3.2.5 Listening Room Setup

As mentioned in Section 4.3.2.3, a new SoundLab was constructed in New York in between the time of RTA system development and the subjective tests. Subjective testing was conducted in the new 77W SoundLab, using the settings listed in Table 4.5.

Table 4.5: Subjective Test Settings Implemented in the Arup 77W NY SoundLab

Parameter	Value
W x D x H	6.1 m x 7.6 m x 3.1 m
Ceiling	Fabric-wrapped 4" Thermafiber Panels on walls and ceiling
Walls	Fabric-wrapped 4" Thermafiber Panels on walls and ceiling
Floor	Wood Flooring on RIM isolators, carpet in listening area
Noise Level	NC15
T_{30} (seconds)	0.15 mid-frequency average (0.6 at 63 Hz)
Loudspeakers	Genelec 8030A (18)
Subwoofers	Genelec 7050B (4)

The loudspeakers were mounted in three rings of 6 at low, mid and high. Four subwoofers were located at floor level. The speaker locations from the tests are shown in Figure 4.10. The resulting radius of the sphere was 2.18 meters, the same

radius as that used for the system development testing in the 155AoA lab.

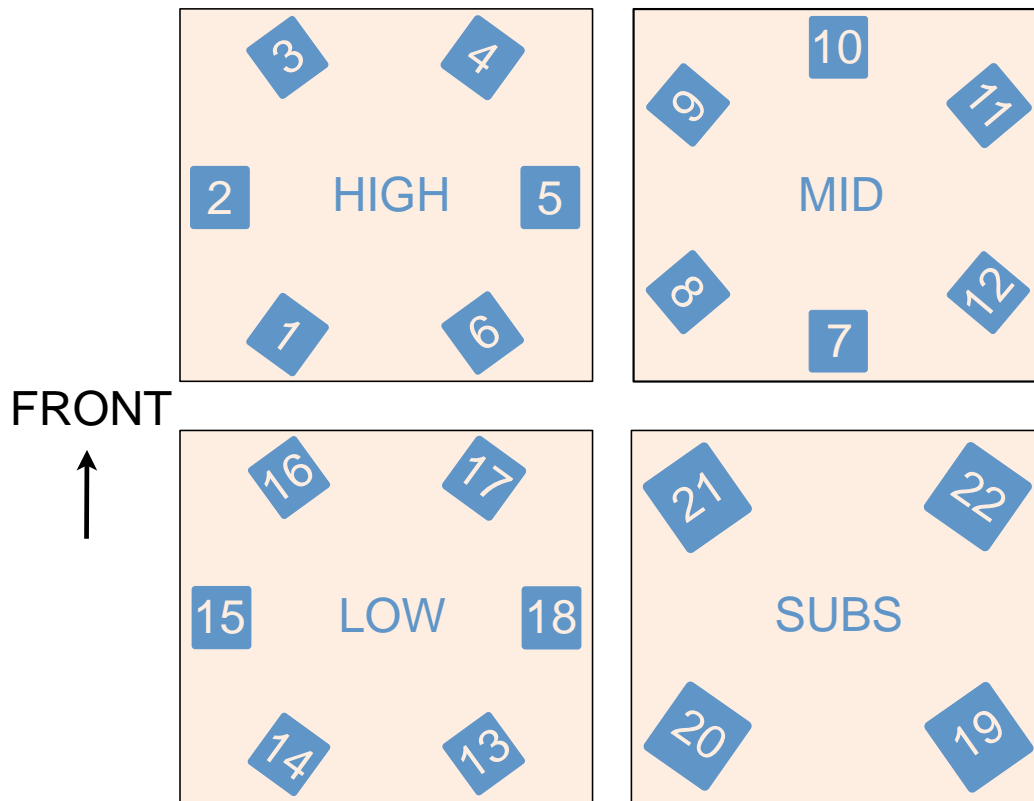


Figure 4.10: Speaker Layout for Subjective Tests

The decoder used for the tests is a commercial software for the Max/MSP environment provided by IRCAM called Spat. Spat 4.4 provides multiple decoder settings, as described in Section 4.2.3. The four subwoofers were decoded using standard 1st-Order BFormat decoding. The 18 speakers were decoded using HOA 2nd-Order decoding. The settings used for the subjective tests were as follows:

- HOA 2nd-Order Decoding
- Pseudo-inverse Matrix Inversion
- SN3D Encoding Weights
- Mode-matching Equations
- Max r_E Decoding Type

4.3.2.6 Listening Room Acoustics

The influence of the playback room acoustics is a non-negligible factor in real-time auralization. Effectively, the reproduced impulse response is a convolution of the target (measured) room, the playback system response, and the playback room response as summarized below:

$$h_{reproduced}(t) = h_{target\ room}(t) * h_{playback\ room}(t) * h_{playback\ system}(t) \quad (4.21)$$

If the playback room is anechoic, the only compounding factor is the playback system and associated artefacts, and the equation becomes:

$$h_{reproduced}(t) = h_{target\ room}(t) * h_{playback\ system}(t) \quad (4.22)$$

Due to the discomfort related to playing in anechoic conditions, it was decided to conduct this research in a typical listening room with a relatively controlled acoustic, to balance increased musician comfort with interference from the playback room.

In the 155AoA NY Soundlab, where the first tests were conducted, the walls were treated with fabric-wrapped, perforated-wood panels with 2-inch fiberglass backing. The floor consisted of a removable carpet over a wood floor on concrete. The ceiling and corners were also treated with various thicknesses (2-8 inches) of acoustic foam. The reverberation time of the room was <0.2 seconds at mid frequencies and <0.7 seconds at low frequencies. However, especially for instruments with strong directivity patterns facing towards the front or rear wall (brass instruments, for example), the first reflections from the walls were found to be quite distracting. Previous work with small, relatively dry rooms has shown that RT is not a good indicator of the impact of these early reflections [17]. Instead, a variation on G where a 3-meter free-field reference measurement (instead of the standard 10-meter measurement) is used. For the 155AoA SoundLab, G was measured with and without a temporary installation of 16 2-inch foam panels on the rear wall. The average decrease in G with the panels was about 2 dB, as shown in Figure 4.11. The lab is

shown with and without the foam panels in Figure 4.12.

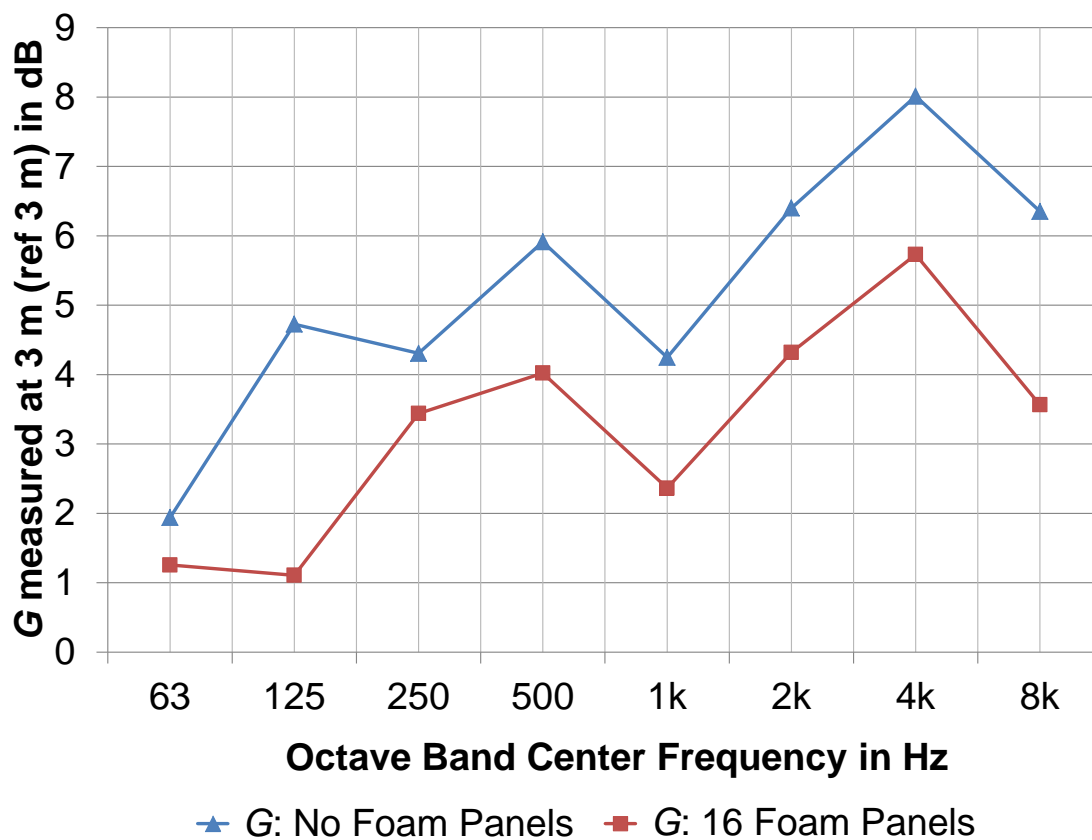


Figure 4.11: G with and without Temporary Foam Panels



Figure 4.12: Arup SoundLab NY with and without Temporary Foam Panels

Even with additional treatment, the response of a non-anechoic listening room cannot be completely eradicated. As a result, even with the foam panels, initial perceptual evaluations of the RTA system in the 155AoA lab revealed a lack of balance between early and late energy. These perceptual evaluations were conducted by the researchers using speech, vocals, and French horn in order to obtain initial impressions of the system. When the system levels were set so that the early energy levels felt natural, then the late energy felt too quiet. When the system levels were increased so that the late energy felt natural, the “PA effect” or a feeling of amplified or synthetic response occurred.

In order to address this perceived imbalance, the impulse response was separated into two parts, an early and a late part, convolved with the input signal and added together as shown in Figure 4.13.

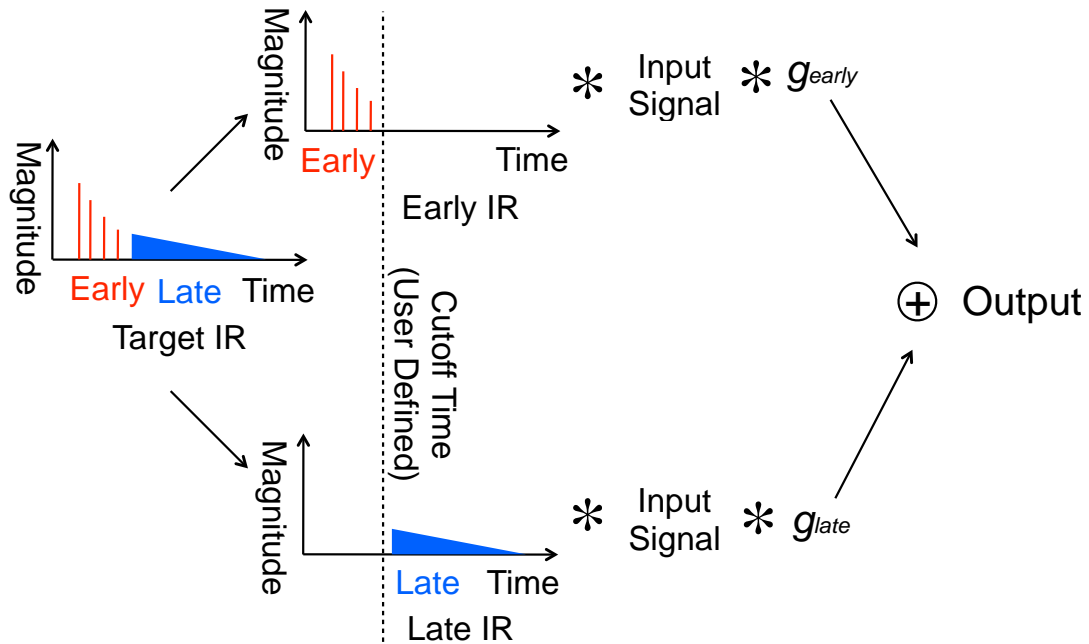


Figure 4.13: Schematic Diagram of Impulse Response Separation

For a unity gain $g_{early} = g_{late} = 1$, the output of the summed convolutions is identical to the non-separated target IR convolved with the input signal. This scheme offers an independent gain stage for early and late portions of the target room response, and offers a relatively simple means of compensating for the influence of the listening room in the early part of the response. Additionally, as described in Section 4.3.2.4, dividing the IR as described allows power spectrum corrections to be applied to the late portion of the signal.

A second set of perceptual evaluations were conducted, which were used to determine the cutoff time for the late convolution (see Figure 4.13). Cutoff times of 50 ms, 75 ms, 100 ms, 125 ms, and 150 ms were evaluated using both synthetic reverb (generated in IRCAM Spat 4.4) and convolution of real room IRs for the late part. It was determined that the 100-ms cutoff time with increased late energy levels provided the most realistic experience.

4.3.3 Physical Test Setup

Because the tests were expected to be at least 2 hours in length, and the goal was to simulate onstage ensemble performance conditions, subjects were expected to play in a seated position. Because the height of the sweet spot is actually higher than normal seated head height (1.4 m), custom chairs are typically used in the SoundLab for listening purposes. These chairs are not feasible for most musicians in typical performance postures. In order to raise the musicians so that their ears were at the sweet spot but still allow typical performance seating postures, a raised platform was constructed. This platform also served to simulate the necessary stage floor reflection. The platform was constructed as a hollow box with dimensions $48'' \times 48'' \times 12''$ with two layers of $3/4''$ plywood nailed together on top. The hollow nature also served to provide some typical stage floor vibration (especially for instruments coupled to the stage, like violoncellos), as this is shown to influence realistic perception of musicians [1]. The box was painted black and black fabric was mounted around the outside of the box to resemble a stage riser. Additional $24'' \times 48'' \times 3/4''$ plywood boards were laid out on the carpet surrounding the platform to extend the reflecting floor condition out to the edges of the sphere (the carpet could not be removed). Images of the platform are in Appendix C.3. The 16 $2''$ foam panels used in the RTA testing were also installed behind the screen for additional reflection control.

In order to provide some repeatability between subjects, performers were restricted to four instrument types: Flute, French horn, Violin and Violoncello. These instrument types were chosen to represent a wide range of directivity, timbre, dynamic and orchestral position. The microphone used for testing was a Neumann KM185 condenser microphone with a hypercardioid pattern. The microphone was located 18 inches from the axis of the instrument. For flute, the microphone was located in front of the musician, facing the mouthpiece. For French horn, the microphone was located behind the musician, facing the bell. For violin and cello, the microphone was located perpendicular to the instrument body (in front for cellos, above for violins), facing the bridge. The microphone was sent through a Sound Devices USB Pre2 (interface used in RTA testing was unavailable). Because the

latency through the USB port on the device was significant, the optical output was used instead, although this still added some latency beyond the original tests. The same computer and sound card were used, as described in Section 4.3.2.3.

Because the testing setup required additional processing and routing from the Max/MSP patch (an iPad was used for musician control, as described below), the CPU usage increased and the tested sampling rate of 96 kHz generated audio artefacts. Instead, a 48 kHz sampling frequency was used. The buffer size was 64 taps. Because of the added latency from the lower sampling rate and from the pre-amp device, the total latency was measured at 13.9 ms, even though the physical latency had not changed. The allowable latency was still 12.7 ms, but it was determined that a delayed room response of 1.2 ms would not significantly impact the perception of the virtual space, whereas the deletion of any reflections occurring in that time (in order to properly align the rest of the IR) would have a stronger influence on the impression of the space. Therefore, only the first 12.7 ms of each impulse response were removed.

The impulse responses from all 10 halls were prepared as described in Section 4.3.2.3. For the RTA impulse responses, the 1-meter downstage measurements from each hall were normalized to the direct sound. The first 12.7 ms were removed and the truncated IRs were normalized again to the W component of the loudest truncated IR such that relative levels were maintained between each hall. 32-bit files were required to prevent quantization artefacts from arising during the second normalization process (the reflected and reverberant energy are significantly lower in level when compared to the direct sound at 1 meter). Then the files were split into early and late portions (cutoff set to 100 ms after the arrival of the direct sound).

Some artefacts were present in the recorded IRs that were amplified in the normalization process and were particularly audible in the convolution process. These artefacts likely arose due to inconsistencies in the source signal spectrum that were not removed during the deconvolution process. They took the form of narrow-band “ringing” sounds and “ghost sweeps” present in the end of the decay. Notch filters were applied to each ambisonic channel to remove the ringing and low-pass filters controlled by time envelopes applied to the end of the decay to remove the ghosting

effects. Spectrograms of the W and R components of one IR before and after these corrections are shown in Figure 4.14.

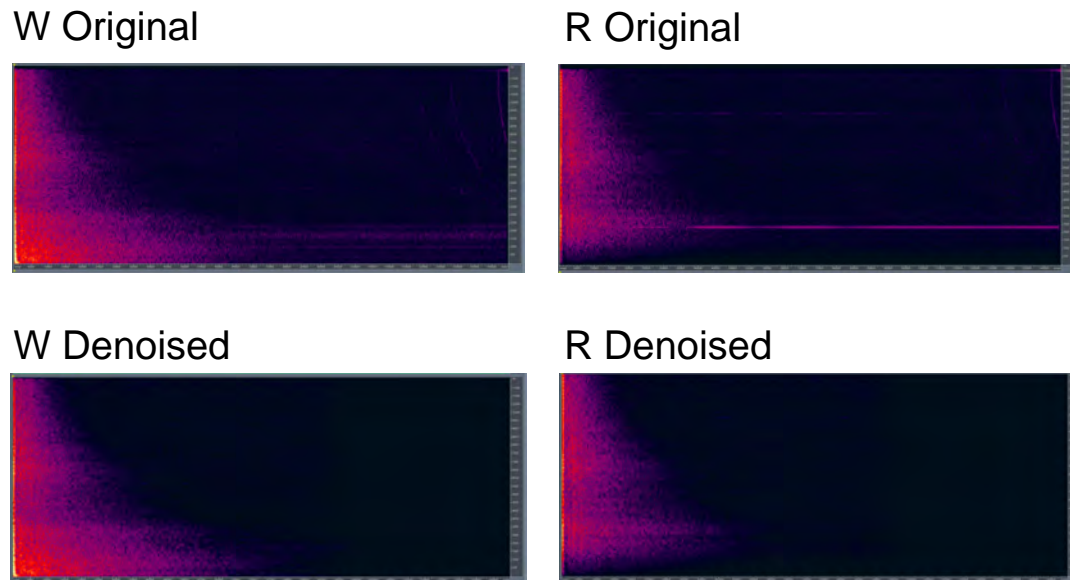


Figure 4.14: IRs Before and After Denoising

It was determined that abstracted images of the halls would be projected on the SoundLab screen in order to provide the listeners with some sense of orientation. The images were hand-traced from photographs, such that no color information or surface detail could influence judgement. Additionally, as shown in previous research, a complete lack of visual information can detract from feelings of immersion in virtual environments [48], [76], [104]. The drawings used in all three tests are shown Appendix C.3. For reference, an image of the testing setup is shown from the ensemble playing test in Figure 4.15.



Figure 4.15: Ensemble Playing Test Setup

4.4 Results

4.4.1 Objective Characterization of RTA System

In order to determine the performance of the RTA System and its reliability for the subjective tests, follow-up measurements in the 77W SoundLab using the same omnidirectional source used in the hall measurements were captured at 1-meter distance for comparison. Measurement setup attempted to match the hall measurements, with the spherical microphone placed in the sweet spot at the listener head position, and the dodec source located 1-meter in front of the spherical microphone. This setup is shown in Appendix C.3.

The W, X, Y and Z components of $h_{\text{playback room}}$ or the dry SoundLab impulse response have been overlaid with the same components of an example $h_{\text{target room}}$ (the “soloist” measurement from Eastman) in Figures 4.16 - 4.19. These IRs have

been normalized to the direct sound and truncated to the first 200 milliseconds for comparison.

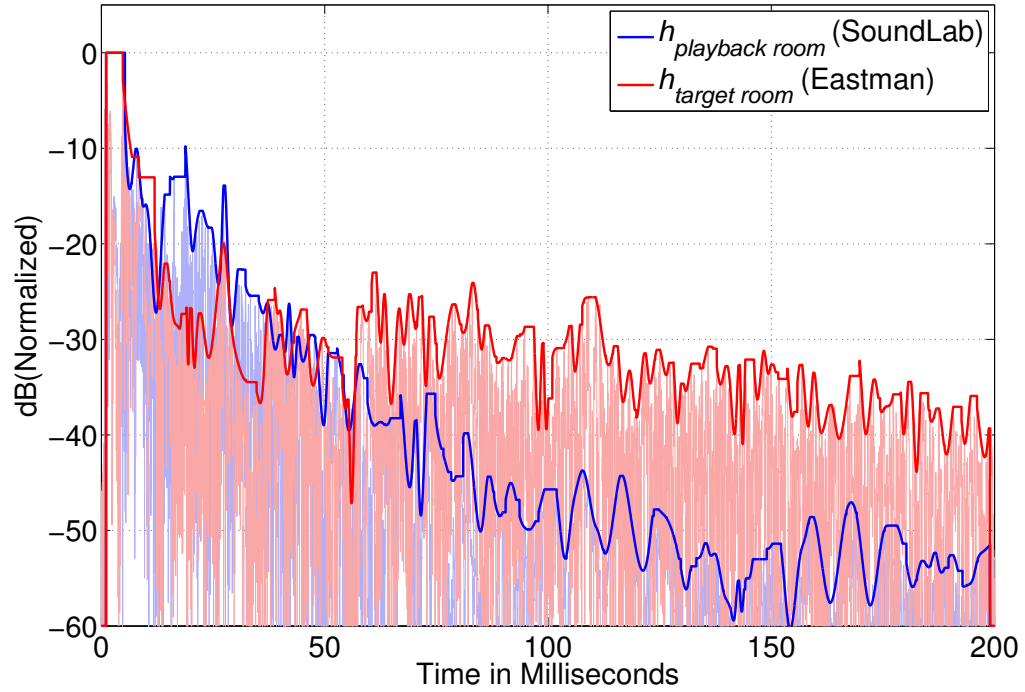


Figure 4.16: 1-meter Impulse Responses from Playback Room Alone (Arup SoundLab NY) and Target Room Alone (Kodak Hall, Eastman), W Channel

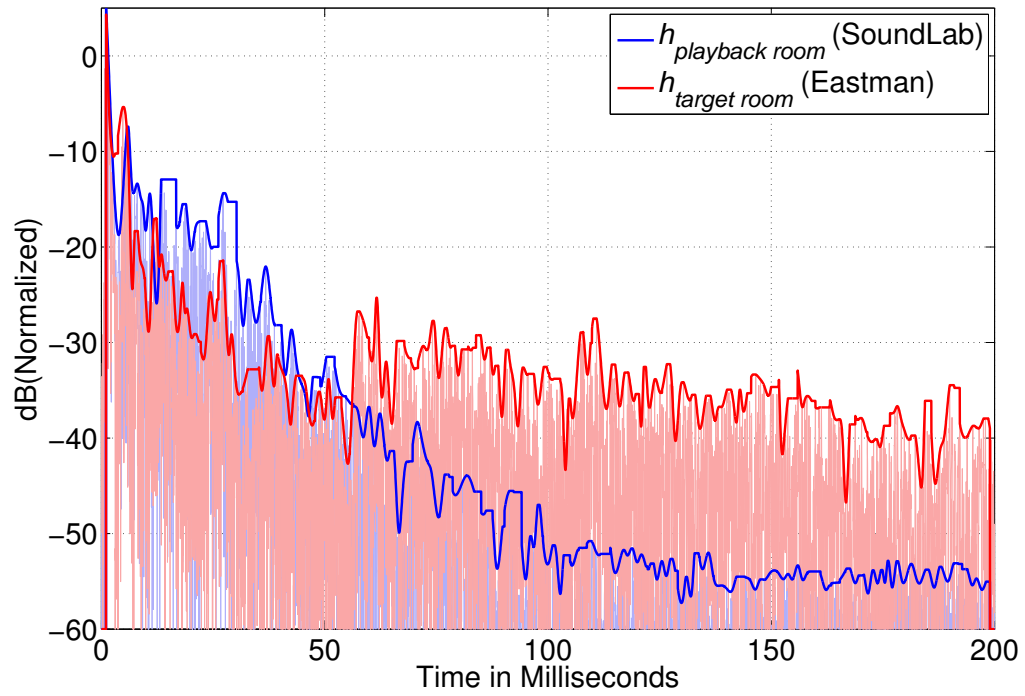


Figure 4.17: 1-meter Impulse Responses from Playback Room Alone (Arup SoundLab NY) and Target Room Alone (Kodak Hall, Eastman), X Channel

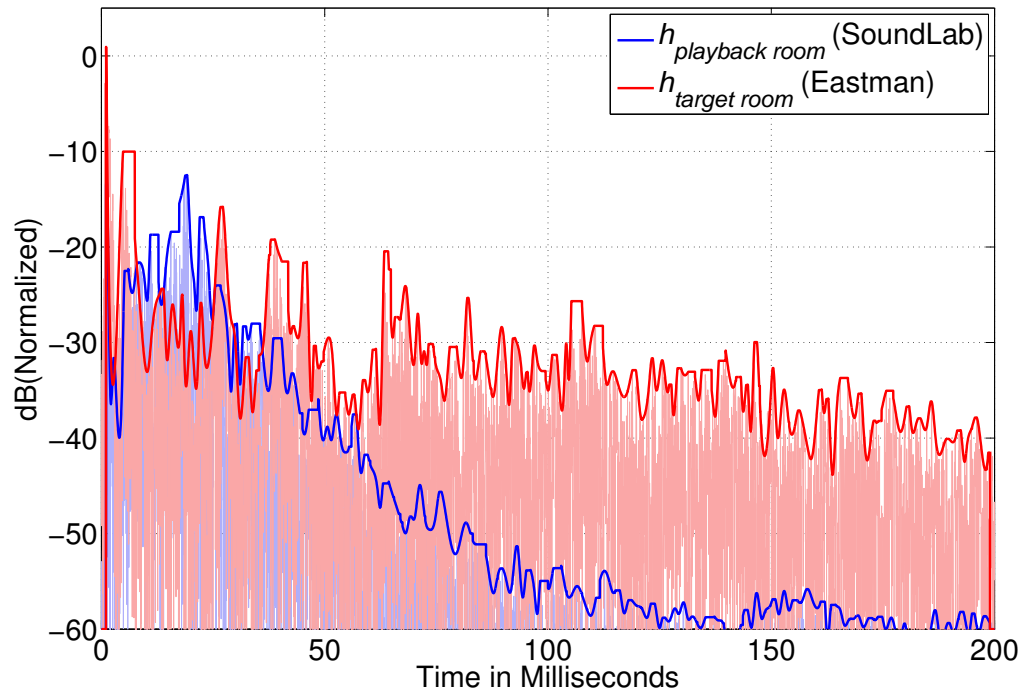


Figure 4.18: 1-meter Impulse Responses from Playback Room Alone (Arup SoundLab NY) and Target Room Alone (Kodak Hall, Eastman), Y Channel

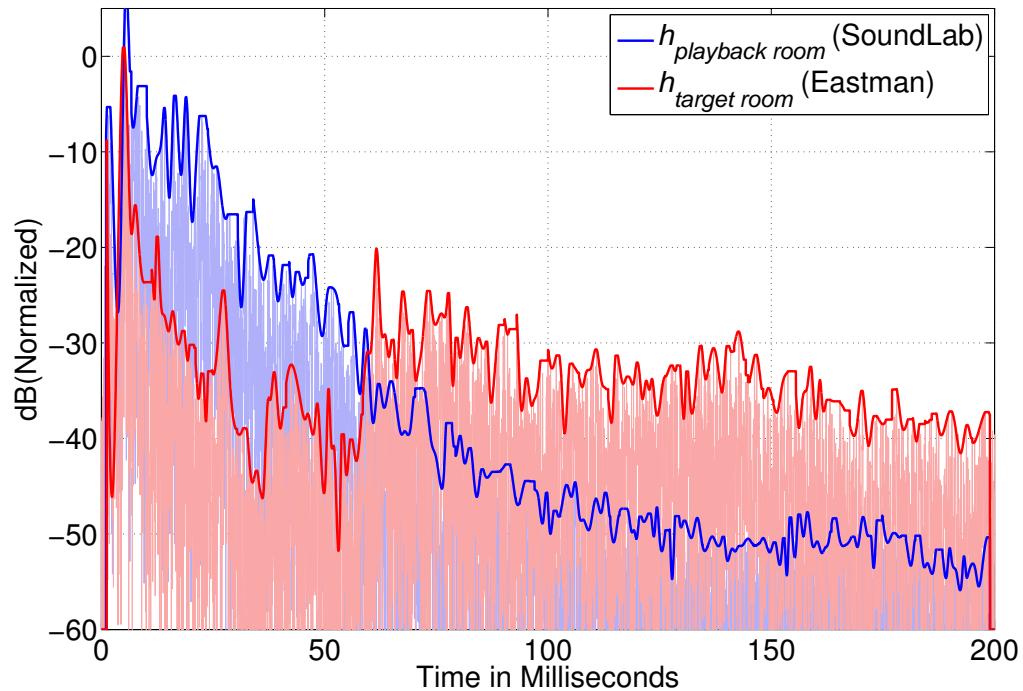


Figure 4.19: 1-meter Impulse Responses from Playback Room Alone (Arup SoundLab NY) and Target Room Alone (Kodak Hall, Eastman), Z Channel

As shown in this example, the energy from the SoundLab dominates the response until about 60 milliseconds, and continues to display comparable levels to the target room IR until approximately 100 ms, after which point it drops >10 dB below the Eastman IR. The difference between the playback room levels and target room levels are dependent on the measured hall. Due to the smaller stage enclosure, Vassar levels dominate the response after only about 40 milliseconds. In the subjective tests, values for g_{early} and g_{late} were set at 0 dB and +1 dB, based on user preference. More work remains to be done in order to determine an accurate method for setting these values. These values could potentially be set dynamically in relation to measured loudness of the target IR. Additionally, Figure 4.19 shows that the playback room contribution in the vertical direction is significantly higher than the horizontal directions. This is likely due to the relatively low ceiling in the SoundLab and future implementations of the RTA system could benefit from

listening rooms with higher ceilings.

Additionally, auralized IRs from each hall were measured in the 77W NY Soundlab using a directional loudspeaker (JBL Control 2P) in the instrument position with a microphone 12 inches away on axis. This setup is shown in Appendix C.3.

Early/late ratio and overall gain have been adjusted to match subjective test conditions and plotted against the target room IRs from the halls. The comparison of each ambisonic channel for Skidmore Hall is shown in Figure 4.20, and for Vassar Hall in Figure 4.21.

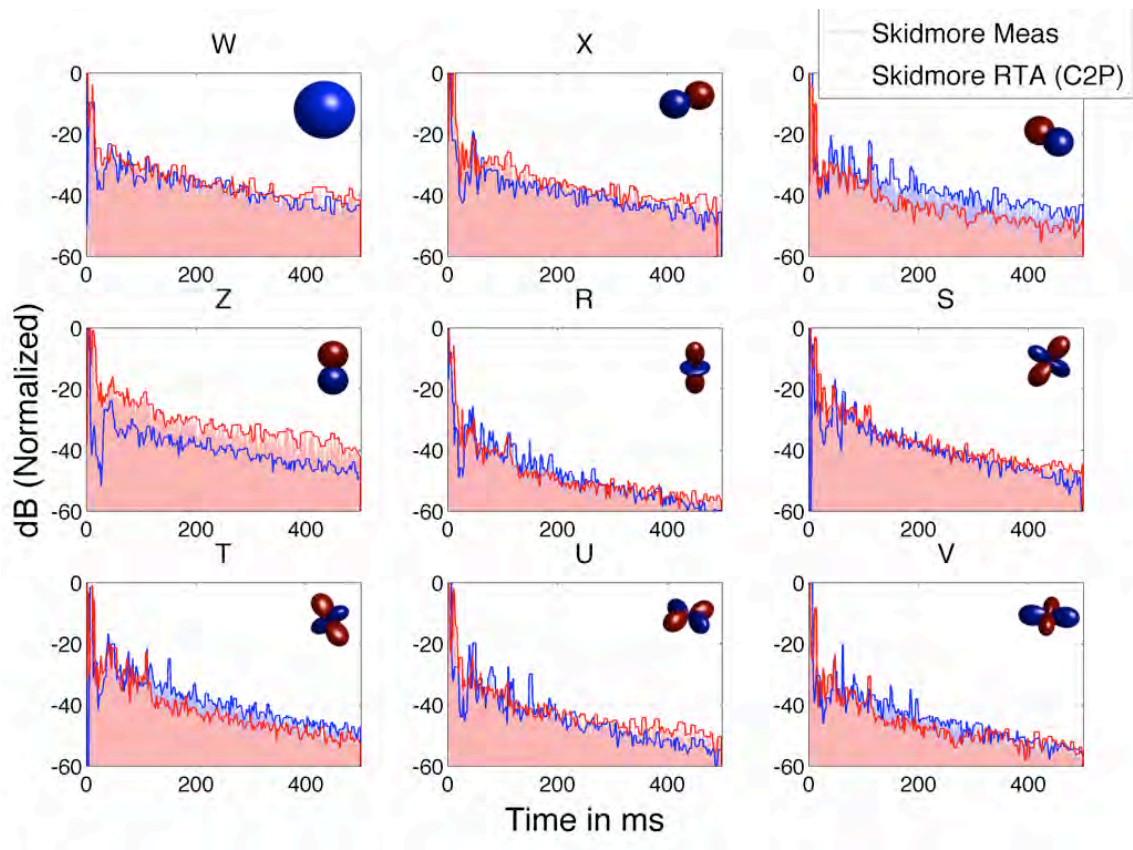


Figure 4.20: 1-meter Measured IR from Skidmore Hall Compared to Auralized IR of Skidmore Hall Using RTA

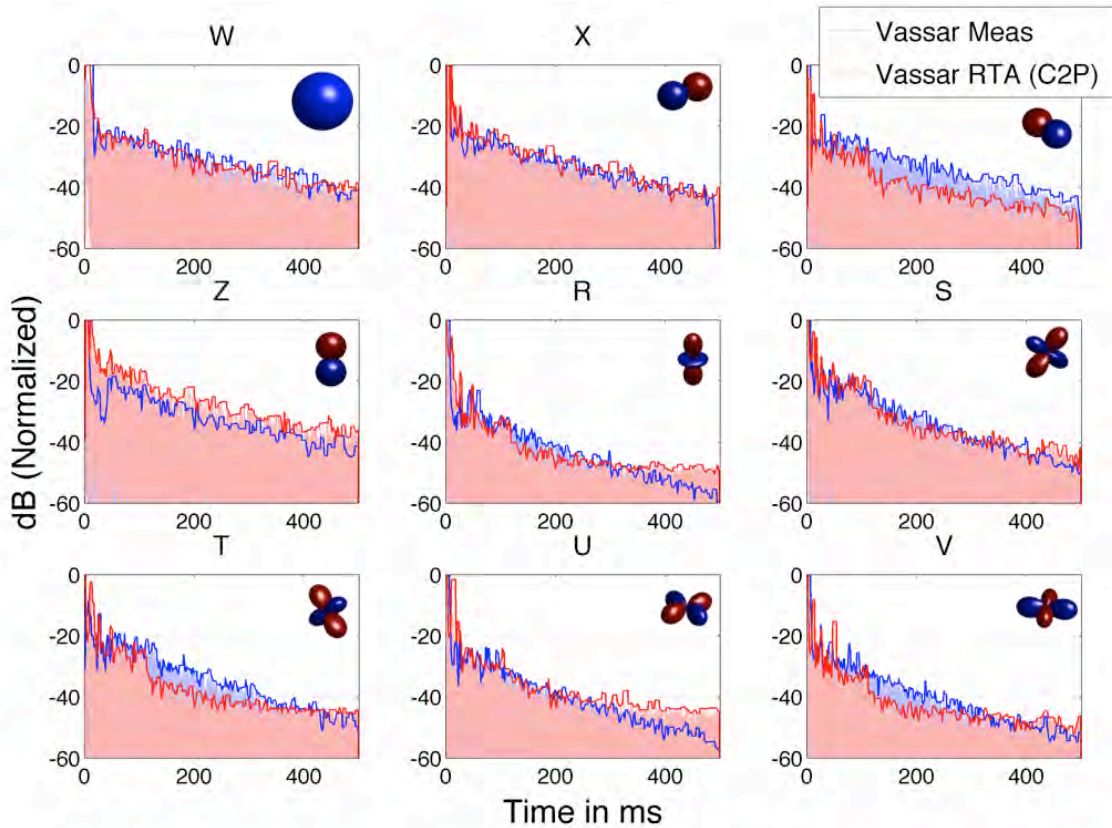


Figure 4.21: 1-meter Measured IR from Vassar Hall Compared to Auralized IR of Vassar Hall Using RTA

The energy in the W, X, S, and U harmonics are fairly consistent between measured and auralized responses. An overall increase in the energy in the Z channel in the auralized response can be attributed to the proximity of the SoundLab ceiling, as shown in Figure 4.19. However, the energy in the Y, R, T, and V harmonics show a drop in energy of about 5 dB after 100 milliseconds. This is likely due to the filtering of the auralized late part by the instrument power spectrum, described in Section 4.3.2.4. As shown in Figure 4.22 (W Channel) and Figure 4.23 (R Channel), the software output for Skidmore Hall (subtracting all physical phenomena including loudspeaker directivity, microphone placement, decoding artifacts, and SoundLab acoustics) is plotted (smoothed curves shown for ease of comparison) against the measured IR and the recorded RTA IR described above. The software output has been recorded with no power spectrum applied (cyan) and with the power spectrum

of Violin (black). Although the energy level for the W channel is consistent with the application of the power spectrum, an overall decrease in energy of about 5 dB is seen in the broadband spectrum of the R Channel, and the decrease in energy for each octave band is dependent on the instrument. Therefore, it can be concluded that the auralized IR is within a margin of 5 dB for each ambisonic channel, and the discrepancies in some harmonics are consistent between halls, implying that the relative differences between halls remain intact and hall comparisons can still be made.

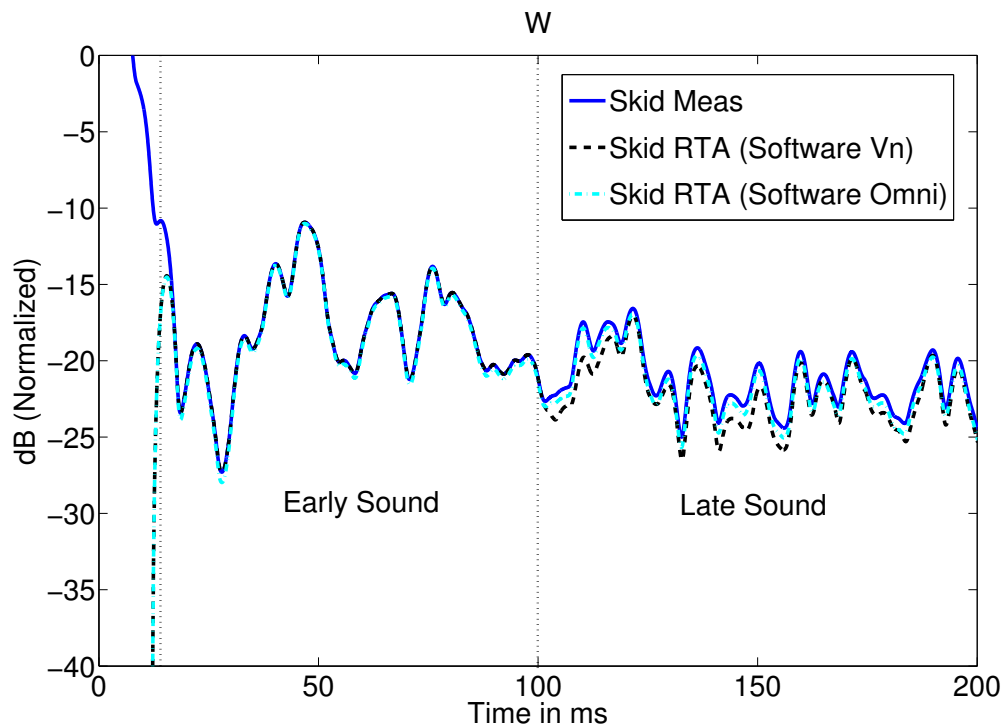


Figure 4.22: Smoothed IR Comparisons for Skidmore Hall, W Channel

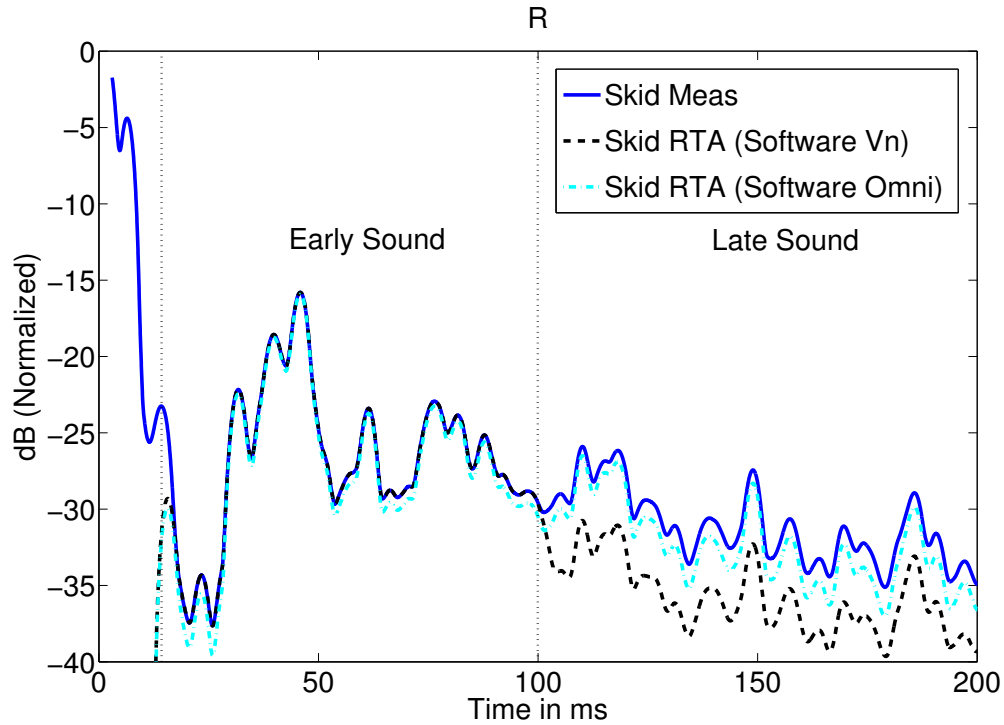


Figure 4.23: Smoothed IR Comparisons for Skidmore Hall, R Channel

4.5 Discussion and Future Work

The two methods described in this chapter combine to form a powerful system for the virtual reproduction of the onstage performer experience. Although the real-time performer auralization system is still in a prototype stage, it is already being used to help musicians from orchestras in existing venues improve their own onstage experience. Measured and modeled acoustic information can be used to raise and lower canopies, test orchestra shell configurations and riser heights, move around onstage and play with different ensembles, all within the convenience and repeatability of a laboratory. Variable acoustics are often used in design to provide flexibility onstage, but the optimization of these elements is time-consuming and under-utilized. The real-time auralization system creates the potential for virtual optimization of these elements. Another benefit of real-time auralization is that it can be used for parametric design using modeled spaces. While the limitations of ray-tracing have already been described, some work is being done into real-time

wave-based modeling, which could be beneficial to this research [3].

The system could also be used for purely virtual performance. In this case, measured or accurately modeled spaces are not required. Instead, more creative and artistic acoustic signatures could be created and used that take advantage of the spatial abilities of the ambisonic technology. Additionally, the system need not be limited to music alone. Speech and ambient noise sources can also be used as input to the system. An intuitive understanding of the acoustics of a space is much more accessible when the signal is produced by the participant in real-time.

To move the RTA system beyond the prototype stage, a great deal of work is required to improve its robustness and flexibility. Feedback control is a crucial concern, as is the tradeoff between on-axis and average instrument directivity created by the close-microphone technique. The effect of the listening room on the overall energy is problematic as well. In particular, the effect of the low ceiling increases the amount of early energy coming from above in relation to other directions. A listening room with a higher ceiling should be used to provide more accurate spatial energy distribution. Additionally, increasing the database of onstage measured IRs is crucial to improving the robustness of the system.

General improvements to ambisonic encoding and decoding methods are also possible and can improve the overall quality of the system. Ambisonic decoding improvements for wider listening areas, better frequency ranges, and near-field sources are widely researched, with promising refinements in recent work [109], [50]. Beyond ambisonics, the use of wavefield-synthesis or directional audio encoding, while not yet feasible for real-time auralization, may provide increased spatial realism for onstage sources [18]. At this time, the Arup Soundlab has recently installed a wavefield-synthesis system and future hybrid combinations of wavefield-synthesis and ambisonics are possible that could maximize the advantages of both technologies.

To improve the overall quality of the reproduction of the onstage experience, the measurement methodology can be refined. Some refinements are reliant on technological and computational improvements, which are under constant study across the field. One topic of research is the reproduction of source directivity in the

measurement process. The current measurement source used to record the impulse responses for this system is omnidirectional, which does not accurately represent the excitation of the hall by individual instruments. It serves as a good approximation of ensemble directivity at large receiver distances such as those found in audience measurements, but the accuracy of measurements for onstage receivers suffer from this lack of directivity. Dodecahedral sources with individually-controlled drivers are being investigated for the creation of individual instrument directivities, as are the use of loudspeaker orchestras to record individual IRs for each instrument in order to create more accurate ensemble auralizations [70], [83]. It is difficult to simulate ensemble playing with a single point source on the other side of the stage. Typical conditions for orchestral performers involve sources from all directions.

4.6 Conclusions

This chapter outlined the theory and methodology behind the system used for higher-order ambisonic stage acoustic auralizations. This system allows for the simultaneous auralization of real-time self-generated sound and pre-convolved sound from other musicians onstage. The flexibility of the design allows multiple combinations of these elements to be utilized in the subjective tests. The physical setup of the laboratory to create the appropriate test conditions has been described. The design of the tests themselves, as well as the analysis of the subjective preference data and proposed correlation with objective parameters, will be described in Chapter 5.

CHAPTER 5

SUBJECTIVE TESTS

5.1 Introduction

In Chapter 4, the design of a system was outlined for the real-time auralization of the musician experience onstage. This system has been utilized to create and execute subjective tests with musicians listening and playing to spatial impulse responses from 10 different concert halls and theatres. The measurement of these impulse responses is described in Chapter 3, and the development of the spherical array used to take the measurements is outlined in Chapter 2.

The subjective tests were designed specifically with the goal of using multi-dimensional scaling (MDS) for the analysis. This is an ideal statistical method for exploratory analysis with a complex set of stimuli, because stimuli variables do not need to be determined in advance. The method is not as rigorous as more standard statistical tests in terms of determining effect size and significance, but it works well for this research because the relevant parameters differentiating hall preferences are not yet known. Additionally, the sample size is quite small compared to most statistical tests due to the complexity of the test and the expert skill required to participate.

Based on several precedents in the field of concert hall acoustics, this method is ideal for initial investigations into the ecologically and cognitively complex experience of onstage acoustics from the performer perspective. While a number of omnidirectional parameters have been developed for the measurement and prediction of ideal onstage acoustics, as described in Section 3.2.1, the complexity of the experience increases when spatial information is included. Additionally, when measured impulse responses are used rather than controlled combinations of synthetic reflections and reverberation, the number of potential attributes used by the subject to differentiate between the halls increases exponentially. This chapter describes the utilized test design and analysis methodologies and presents the results of the preference tests. It also attempts to propose some objective attributes that show

correlation with the preferences of the participating musicians and could potentially be used to improve the design of stage enclosures and halls for a higher-quality performer experience.

5.2 Precedents

Two groundbreaking studies that show the contribution of MDS to the field of psychoacoustics and room acoustics are the timbre studies by Grey in 1976 and the stage acoustics studies by Gade in 1982. Grey used INDSCAL for his research, whereas Gade used a combination of MDPREF and PREFMAP [43], [37]. Factor analysis, a similar method, was also used by Schroeder et al in 1973 along with MDPREF to analyze preference judgements for 12 listeners comparing the transaural reproduction of 22 concert halls in a laboratory setting and also by Yamaguchi in 1972 to investigate the variations in multiple room acoustics parameters across multiple seat locations in the same hall [93], [108]. More recent work by Morimoto & Asaoka has shown that even seemingly uni-dimensional acoustical parameters can be multi-dimensional by examining “reverberance” and describing its influence separately in terms of temporal and spatial components [74].

Grey’s study compares two forms of data, one made of similarity judgements between pairs of stimuli and applied to MDS, and one made of confusions between pairs in an identification task [43]. His goal was to explore the leading elements contributing to perception of timbre, which was previously considered too complex for such classifications, although its perception was considered crucial to the identity of a musical instrument. In the study, tones from different musical instruments were synthesized and equalized to eliminate differences in pitch, loudness, and duration, to focus on unknown parameters. A three-dimensional mapping of similarities between 16 instruments proved most significant, and matched a hierarchical cluster analysis performed on the data. The confusion test appeared to confirm these clusters. The three dimensions were interpreted as follows:

- **Dimension 1:** Spectral Energy Distribution (narrow spectral bandwidth and concentration of low-frequency energy (French horn, strings) vs. wide spectral bandwidth and less low frequency energy (oboe, trombone)).

- **Dimension 2:** Spectral Fluctuation (harmonics that attack and decay in close alignment (oboe, clarinet, saxophone) vs. harmonics that attack and decay at different points throughout the note (flute, horn, strings)).
- **Dimension 3:** Attack Patterns (high-frequency inharmonicity in transient (strings, flute, single-reeds, high double-reeds) vs. low frequency inharmonicity in transient (brass, low double-reeds)).

Gade’s research involved extensive subjective testing with performers (rather than listeners) and proved instrumental in the creation of the Stage Support parameters defined in Section 3.2.1.2 [37]. His experiments included both solo and ensemble performances, and using PREFMAP he was able to correlate preference data to measured values of these new parameters in three concert halls. Stage support is a ratio of energy of direct sound and early reflections for the soloist (measured at the same receiver position), and early ensemble level is a ratio of energy of direct sound emitted from the other player and early received energy (including the delayed direct sound from the other player) for the ensemble performer. The sound fields used in the experiments were digitally manipulated versions of impulse responses from the aforementioned concert halls. For example, four trios of flute, violin and cello performed in four sound fields with different sound levels of reverberation and early energy. MDPREF vector mappings showed that musicians were divided into two clusters, cluster one preferring strong early reflections and strong reverberation (professional musicians) and cluster two preferring strong early reflections and weak reverberation (amateur musicians).

PREFMAP confirms this with objective values of reverberation time and stage support at 1kHz correlating to these dimensions. In another experiment, subjects made preference judgements based on manipulations in the frequency content of the early reflections. Two clusters appear in the MDPREF mapping, with violinists preferring the high frequency content, and the cellos and flutes preferring the low-frequency content. PREFMAP confirms this by placing ideal points for stage support at 2 kHz and 500 Hz along the extremes of this dimension. Experiments including the direct sound (basis for EEL parameter) resulted in three-dimensional mappings, where Dimension 1 (strongest dimension) indicated correla-

tion in PREFMAP with the level of direct and reflected energy received from the other player, Dimension 2 indicated weak correlations to reverberation level, and Dimension 3 indicated low-frequency early reflections. In this case, preference was strongly correlated with high levels of direct and early reflected sound, whereas instrumentalists were divided on the importance of the other two dimensions. In summary, the two most significant parameters were the level and arrival time of early reflections for the performer's own sound, and the level and arrival time of direct and reflected sound from the other performers.

5.3 Theory

Multidimensional Scaling (MDS) encapsulates a wide variety of (mainly iterative) methods for the interpretation of proximities between stimuli. These proximities can be obtained indirectly or directly through subjective testing. A matrix (roughly symmetric, with the exception of order effects, with zeroes on the diagonal) of proximities is mapped into R dimensions (typically two or three dimensions are used, although more dimensions can be used depending on the number of stimuli). The map can be interpreted by determining the subjective meaning of the x-y-z axes. The map can be further transformed and axes can be rotated in order to improve the clarity of the interpretation. In most MDS algorithms, a regressive method is used to place the stimuli at initial points in the R -dimensional space based on the experimental proximities (interpreted as spatial distances) between stimuli. Then the geometrical distances are measured and compared to the original proximity data. Using a specified metric, the “goodness-of-fit” is determined and the points are shifted using an iterative process until this goodness-of-fit is optimized (the difference between geometrical distance and experimental proximity is minimized). There are many processes that achieve this goal for different types of data, with varying success. A more detailed description of the theory and process behind MDS can be found in [14].

The input data for MDS can be presented in different forms. The description above uses data in the form of proximities or similarities between stimuli. This research produces dominance data, which show the relationship between stimuli in

terms of preference, which can also be redefined as the distance or proximity between recorded preferences and some ideal preference. Typically, preference data is of the ordinal type (the relationship between data points is only categorized by rankings of greater or lesser values, not the ratio or absolute numerical relationship between values). It can be recorded as a three-way matrix of paired comparisons data, or a two-way matrix of rank-orderings or scores for the stimuli for each individual. In the pair-comparison case, the score matrix must be computed by summing the columns of each individual matrix before the data can be used. Whereas proximity data is typically square (rows and columns both contain stimuli), the score matrix is rectangular, as it contains different entries for the rows (individuals) and columns (stimuli). In order to use the dominance data in a proximity model, the data would need to be considered part of larger diagonal matrix where rows and columns contain both individuals and stimuli, but with significant chunks of missing data (individual-individual dominances, for example, do not exist). Additionally, the individuals are thought to have the same perceptual experience of the stimuli but have different preferences for the ideal combination of attributes (dimensions) for these stimuli. For these reasons, dominance data is usually analyzed using an unfolding model.

There are two main types of unfolding models: ideal-point models, and vector models. The ideal-point model iteratively places the individuals and stimuli as points in the MDS space, where the absolute distance from the individual point to each stimuli (shown by drawing concentric circles known as “iso-preference contours” around the individual point) represents preference [14]. Programs such as MINIRSA and PREFSCAL use this ideal point model. However, due to the conditional nature of the matrix (rows and columns cannot be treated equally), the use of a typical iterative model in this case often provides a trivial or degenerate solution, where the stress value is quite low (indicating a good model) but the data is not accurately reproduced. PREFSCAL applies certain penalty functions to minimize the chances of such solutions. However, an additional issue with this model is a difficulty in visual interpretation when it comes to finding agreement among individuals.

MDPREF (the software used in this research) is a vector model. It is a metric model, and uses an analytical solution rather than an iterative process [94].

Instead of a point of ideal preference, each individual is represented by a vector pointing in the direction of infinite preference. It uses the Eckart-Young method of singular-value decomposition (SVD) which attempts to essentially down-sample the fully-dimensional space (N stimuli = N dimensions) into an R -dimensional reconstruction. Typically, this method can destroy relations of incidence by stretching the individual preferences differently, and create a map that is very difficult to interpret. This failure can be prevented by restricting the vectors to unit vectors; however, this may create a situation where the data is not robust and cannot create a significant model. One downside of MDPREF is that, because the method scales down the vectors *after* mapping, it will *always* provide a significant model, even when the map cannot be interpreted in any meaningful way.

MDPREF categorizes dominance data using score matrices made directly of rank-orderings or culled from paired-comparisons. If paired comparisons are used, it constructs an $N \times M$ matrix of N stimuli and M subjects (where preferences fall on a normalized -1:1 scale) by summing the rows of each subject's $N \times N$ pair-comparison matrix (where preferred stimuli for each pair receives a 1, and non-preferred receives a 0). Once the stimuli have been mapped in an R -dimensional space, the interpretation of this mapping can be conducted in multiple ways. The axes can be rotated (oblique or orthogonal rotations) to line up with natural clusters present in the data or with external parameters. External analysis compares the mapping of similarities or preferences for stimuli with measured attributes of the stimuli [94]. Values for these attributes can be objectively determined for all stimuli (profile data) and ideal points can be determined that optimize the correlation between these values for stimuli in the mapping.

One consequence of using the vector model is that the space is arranged based on a “more is better” concept, such that increasing values of each dimension always lead to higher preference. In reality, this is often untrue for acoustical parameters. For example, increasing reverberation time is only preferred up to a certain point (2.2 seconds for symphonic music, for example), after which point increasing reverberance is less preferred again. This was an issue encountered by Schroeder et al. when using MDPREF in a qualitative listening experiment (described above) [93]. Schroeder et

al. resolved this issue by assuming an ideal value for reverberation time and mapping the stimuli above and below this value separately. Another possible method (used in this research, described in Section 5.5.2) is to apply an inversely proportional correction to data above the ideal value to “fold” it over so that previously increasing values above the ideal value now decrease below. For example, if an ideal value of reverberation time is 2.2 seconds, a 2.5 second value would now be assigned a value of 1.9 seconds. This assumes that the relationship between values is linear.

It is important to keep in mind that MDS is mainly an exploratory method, and given the absence of a hypothesis at the beginning, the possibility of false positives is high. Additionally, assumptions about the ideal values of objective parameters can have a strong influence on the results. Further tests should be conducted to confirm the conclusions drawn from these experiments.

5.4 Methodology

The system used for the subjective tests was outlined in Chapter 4. Specifically, the physical structure and laboratory setup for the tests is outlined in Section 4.3.3. In summary, each experiment lasted 2 hours total, divided into three sections, which could be completed sequentially or in separate sessions depending on schedule and subject fatigue. The order of the sections remained the same for all subjects due to practical concerns. Within each section, the order of stimuli was randomized to prevent order effects. The sections were:

- **Test 1:** Listening Tests (Pre-convolved cross-stage audio).
- **Test 2:** Solo Playing Test (Real-time self-generated audio).
- **Test 3:** Ensemble Playing Test (Simultaneous real-time, self-generated audio and pre-convolved, cross-stage audio).

Twenty (20) subjects were recruited for these tests. In order to provide some repeatability between subjects, instruments were restricted to four types (five players of each type): Flute, French horn, Violin and Violoncello. These instrument types

were chosen to represent a wide range of directivity, timbre, dynamic and orchestral position.

Test 1, the listening test, took an average of 40 minutes to complete. In this test, the musicians were seated without an instrument at the sweet spot. They were presented with four sets of stimuli. For each set, they ranked the stimuli within that set from favorite to least-favorite. The order of the sets was randomized, and the order of stimuli within each set was also randomized to prevent test error. Each set contained 10 stimuli, one for each measured hall. The sets were as follows (in no particular order):

1. Front-Back Cross-stage IR: Xenakis Violin excerpt (39 seconds).
2. Front-Back Cross-stage IR: Bach Violin excerpt (23 seconds).
3. Side-Side Cross-stage IR: Xenakis Violin excerpt (39 seconds).
4. Side-Side Cross-stage IR: Bach Violin excerpt (23 seconds).

For each set, an anechoic violin recording (described in Chapter 4) convolved with all 10 halls was played simultaneously on loop and the iPad selection muted the non-selected halls. This had the effect of a “continuous” playback that moved from hall to hall. This method was chosen for ease of comparison. A Bruel & Kjaer 2236 Type II Meter was also installed in the room to monitor the levels of the playback and prevent them from exceeding OSHA accepted levels.

Musicians were provided with an instruction document at the beginning of the test and also provided with verbal instructions. For Test 1, they were asked to make preference judgements based on the following factors:

1. **Support:** how much the musician’s performance sounds supported by the stage.
2. **Reverberance:** how much the reverberance adds to (or detracts) the performance.
3. **Timbre:** how much the pitch or tone coloration and balance adds to (or detracts) the quality of the musician’s sound.

4. **Hearing each other:** how clearly you can hear the musician and would be able to play with them.
5. **Dynamics:** how well the dynamic range of the music is enhanced by the hall (does *forte* sound loud and *piano* sound soft?).
6. **Spatial response:** how well the stage provides a spatial image that balances between the feeling of envelopment/spaciousness and ease of hearing the other musician.

For each test, an iPad interface was prepared that would allow the performer to control the stimuli and submit their ratings. The interface was designed using MMF-Fantastick, an object in the Max/MSP environment that would transmit information over an ad-hoc local wireless network (not the LAN) between the Mac Pro computer and the iPad [19]. The iPad interface used for the listening tests is shown in Figure 5.1. An image of the corresponding Max/MSP patch for the test is in Appendix C.3.

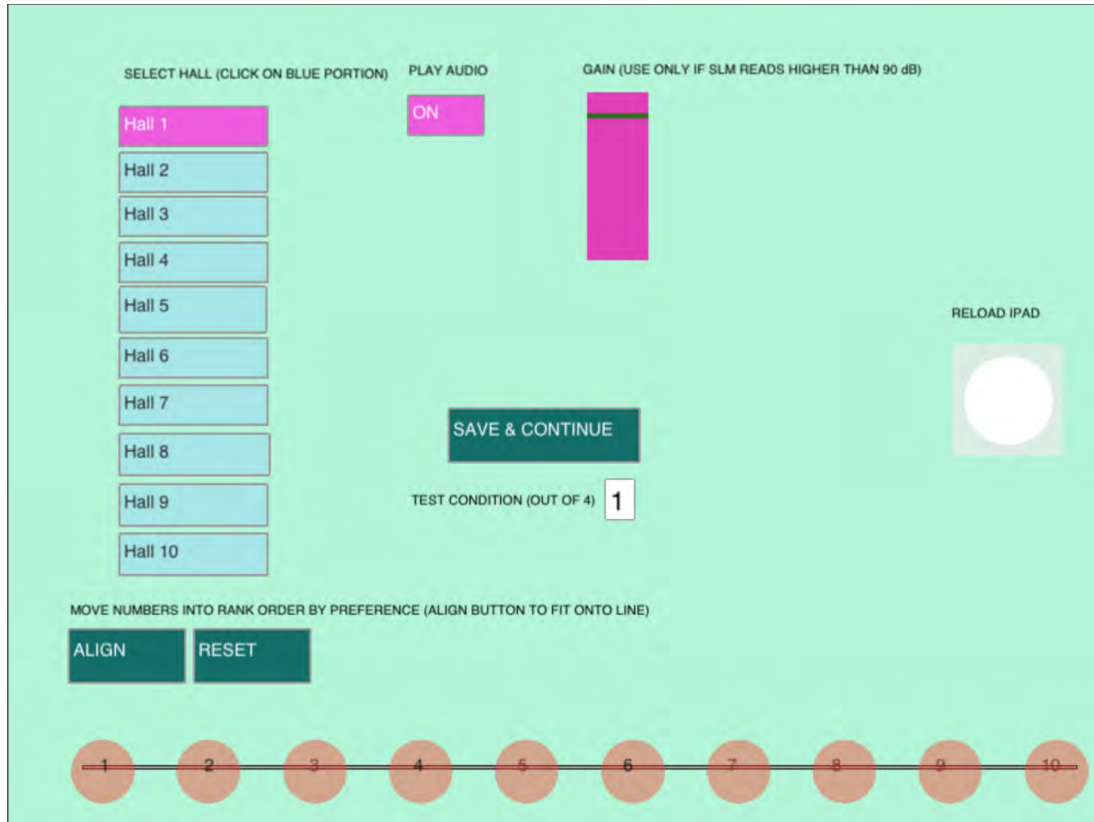


Figure 5.1: iPad Interface for Test 1: Listening Tests

The ranking was chosen by moving numbered circles along a bar on the interface. The circles were ordered by hall preference (distance between circles was not relevant) from “favorite” on the left side to “least favorite” on the right side. When the subjects were satisfied with the ranking for that set, they would continue to the next set and their rankings were saved in a text file, along with the hall information. Hall information was not disclosed to the subjects and the numbers corresponding to each hall changed with each set (Hall 1 was not always the same hall).

Due to the high cognitive load of real-time performance, Tests 2 and 3 used pair-comparison testing instead of rank-order testing. In order to reduce the test length and prevent fatigue, each stimuli was only compared with each other stimuli one time. The order of stimuli for each pair and the order of pairs were randomized. Stimuli were never compared with themselves. This produced a total number of $(S^N - S)/N$ pairs, where S is the number of stimuli (10) and N is the number

of stimuli in each comparison (2). The total number of comparisons in this case was 45. The average lengths of Test 2 and Test 3 were each approximately 30 minutes. Given 10 minute breaks in between each test, the total length of the session averaged 2 hours. Most subjects completed the entire test in one session, although for scheduling purposes, some subjects completed the tests over multiple sessions.

For Test 2, musicians were seated with their instrument in the sweet spot with the microphone positioned as described above. The musician was asked to play at a *forte* dynamic while the level on the pre-amp was adjusted to a level just below clipping (consistent for all subjects). The iPad was positioned on a stand nearby. Two “soloist” impulse responses were loaded by the Max/MSP patch and assigned to Halls A and B. The musician selected one of the two available stimuli using the iPad and played a musical selection of their own choosing. They were not required to play the same selection for all comparisons, but it was suggested that they play the same selection in A and B for any given comparison in order to make a fair judgement. They were instructed to judge their preference for Hall A or B based on the following factors:

1. **Support:** how much your sound feels supported by the stage.
2. **Reverberance:** how much the reverberance adds to (or detracts) your performance.
3. **Timbre:** how much the pitch or tone coloration and balance adds to (or detracts) the quality of your sound.
4. **Dynamics:** how well the dynamic range of your sound is enhanced by the hall (does *forte* sound loud and *piano* sound soft?).
5. **Spatial response:** how well the stage provides a spatial image that balances between the feeling of envelopment/spaciousness and ease of hearing yourself.

Subjects then selected their preference for the current pair and continued to the next comparison. The iPad interface used for the soloist playing test is shown in Figure 5.2.

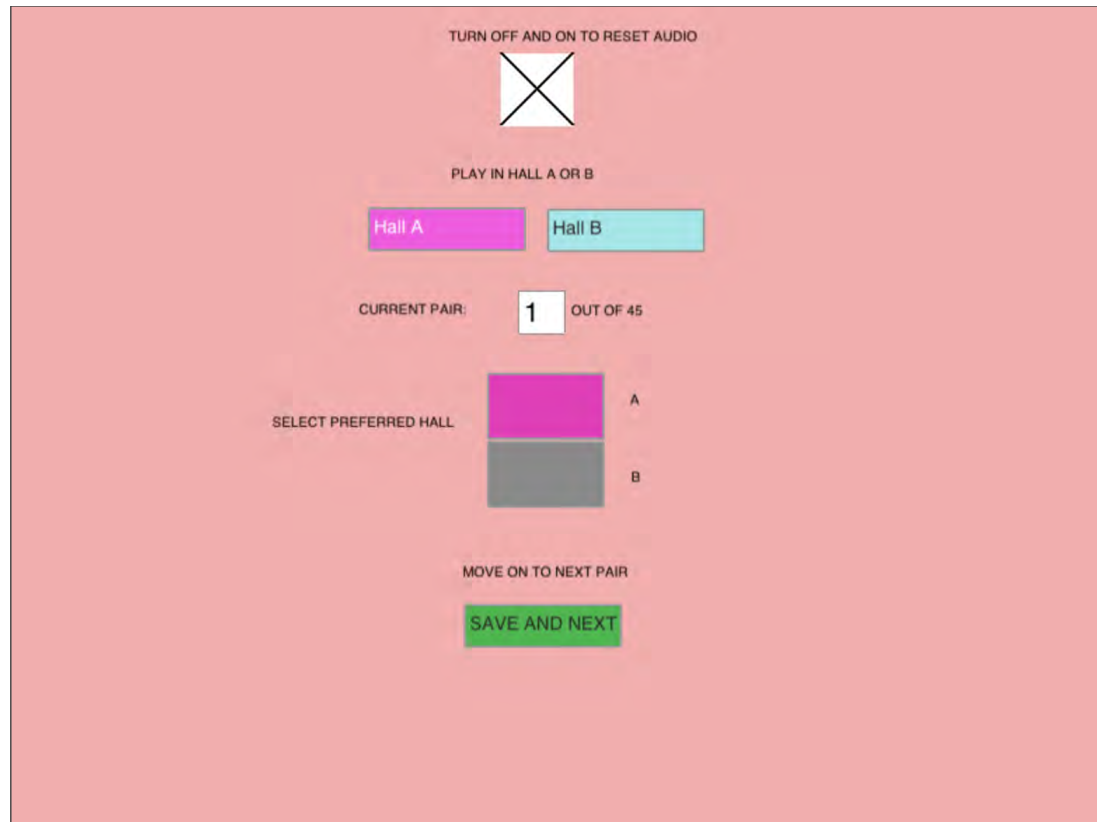


Figure 5.2: iPad Interface for Test 2: Solo Playing Test

For Test 3, musicians were seated with their instrument as in Test 2. In addition to the iPad, a printed score was placed on a stand showing the Mahler excerpt to be played. Two “soloist” impulse responses were loaded by the Max/MSP patch and assigned to Halls A and B. The accompanying pre-convolved orchestral excerpt was also loaded for each corresponding hall. The musicians selected one of the two available stimuli using the iPad. They could then trigger the playback and attempt to perform their respective part along with the recording (The first-chair part was suggested, but if the musicians did not feel capable or suffered from fatigue, they were allowed to play the other parts for their instrument as necessary. The goal was to provide a consistent cognitive load to that of a performance. After playing through the excerpt, they switched halls and repeated the exercise as many times as necessary for each comparison. They were instructed to judge their preference for Hall A or B based on the following factors:

1. **Support:** how much the your performance feels supported by the stage.
2. **Reverberance:** how much the reverberance adds to (or detriments) the performance (yours and the other musicians).
3. **Timbre:** how much the pitch or tone coloration and balance adds to (or detriments) the quality of the sound (yours and the other musicians).
4. **Hearing each other:** how clearly you can hear the musician and are be able to play along with them.
5. **Dynamics:** how well the dynamic range of your sound and that of the other musician is enhanced by the hall (does *forte* sound loud and *piano* sound soft?).
6. **Spatial response:** how well the stage provides a spatial image that balances between the feeling of envelopment/spaciousness and ease of hearing yourself and the other musician.

Subjects then selected their preference for the current pair and continued to the next comparison.

5.5 Results

5.5.1 Subjective Preference Mapping

Although 20 subjects took part in the tests, the data files for three subjects (Violoncello) were corrupted and it was not possible due to time constraints to test additional subjects. Therefore, 17 subjects were used in this analysis: 5 Flutes, 5 French Horns, 5 Violins, and 2 Violoncellos. The software used for the preference analysis was NewMDSx, running an MDPREF routine as described in Section 5.3 [24]. The preferences of each subject was entered as a binary matrix of all pair comparisons. In order to determine the dimensionality of the results, a scree test was performed on the data, by determining the amount of variance described by each dimension. For a test with N stimuli, the data will always be explained perfectly

with N dimensions. However, this is not very useful for interpreting common factors driving subjective preferences. Therefore, the number of dimensions should be minimized such that the majority of variance is explained but interpretation is still possible. The dimension corresponding to the “elbow” of the curve dictates the best proportion of dimension number to explained variance. All three tests were analyzed using $N = 10$ dimensions and the scree plot of the explained variance (normalized to the maximum for comparison) for each dimension is shown in Figure 5.3. A 10×17 matrix of randomly generated numbers was also analyzed for comparison.

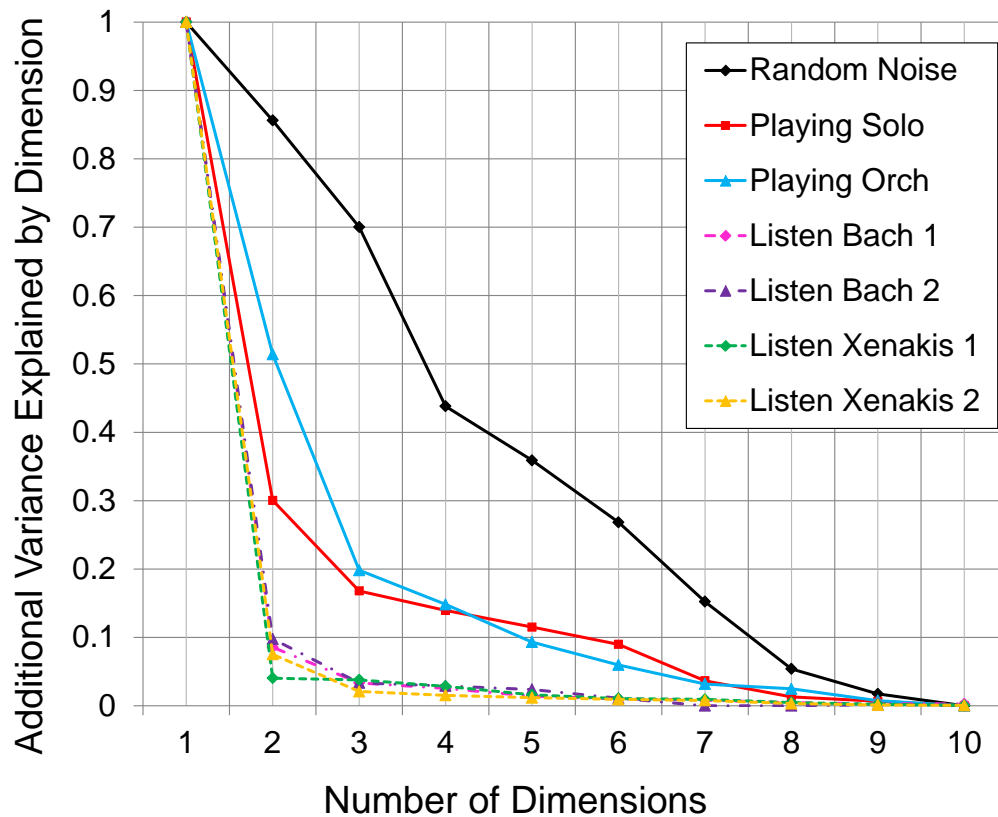


Figure 5.3: Scree Test for Dimensionality (Normalized Variance Explained by Each MDS Dimension)

All four conditions tested in the Listening portion (Test 1) have a very distinct elbow at Dimension 2. Therefore, these results should be mapped in two dimensions, and in fact, the first dimension alone explains over 80% of the variance, so the second dimension is not adding significantly to the model. Both solo and ensemble playing

tests (Tests 2 and 3) have an elbow at Dimension 3, and all three dimensions are required to account for 80% of variance. Therefore, these results should be mapped in three dimensions. The percentage of variance (un-normalized) for each test is listed in Table 5.1:

Table 5.1: Absolute Percentage of Variance Explained by Each MDS Dimension

MDPREF Routine	Dimensions			
	1	2	3	4-10
Listening Test: Bach Receiver 1	84%	<10%	<5%	<5%
Listening Test: Bach Receiver 2	82%	<10%	<5%	<5%
Listening Test: Xenakis Receiver 1	87%	<5%	<5%	<5%
Listening Test: Xenakis Receiver 2	87%	<10%	<5%	<5%
Solo Playing Test	54%	16%	10%	<10%
Ensemble Playing Test	48%	25%	10%	<10%

The results of the MDPREF analysis have been plotted in Figures 5.5 - 5.16. For the three-dimensional plots, multiple two-dimensional views are also shown so that the relationships between all three dimensions can be seen. The 10 stimuli (halls) are shown as red asterisks with the accompanying hall name. The subjective preferences are shown as vectors from the origin (Flute = F1-5 in cyan, Horn = H1-5 in black, Violin = V1-5 in magenta, Cello = C1-2 in blue). These vectors indicate the direction of increasing positive preference. The vectors are terminated at the origin for ease of viewing only.

If each vector were extended in the opposite direction through the origin (negative preference), and all halls were projected as normals to that vector, the rank order in which the halls projected onto that vector should match the preferences for that subject. A diagram showing the projection of sample stimuli (red dots) onto three sample subject vectors (negative preference extended past the origin, shown as dashed lines) is shown in Figure 5.4. Depending on the vector direction, the order of preference differs for some of the stimuli. The two vectors that cluster closer to-

gether towards the left have similar preference orders, indicating higher agreement along that dimension. The distance between the projected stimuli are irrelevant. Only the rank orders on the subject vectors are important. These projected orders make up the second score matrix.

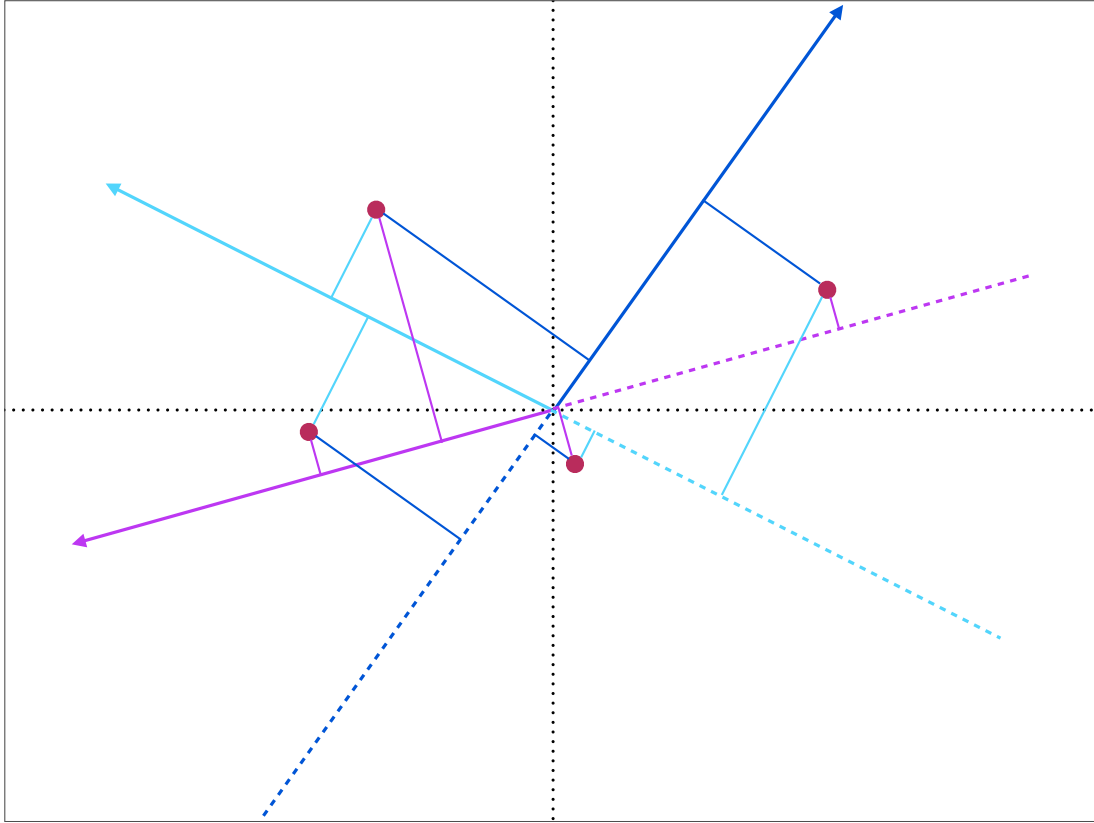


Figure 5.4: Diagram of Sample MDPREF Mapping (Stimuli Dots Projected onto Subject Vectors)

The extent to which the second score matrix, or the revised preferences for each subject (as determined from the model shown in the plots) accurately reproduces the first score matrix, or the actual recorded preferences, is represented by the Pearson correlation coefficient, or r . The coefficient of determination, or the square of the Pearson correlation coefficient, r^2 , represents the amount of variability in preferences explained by the model, and is shown in each plot.

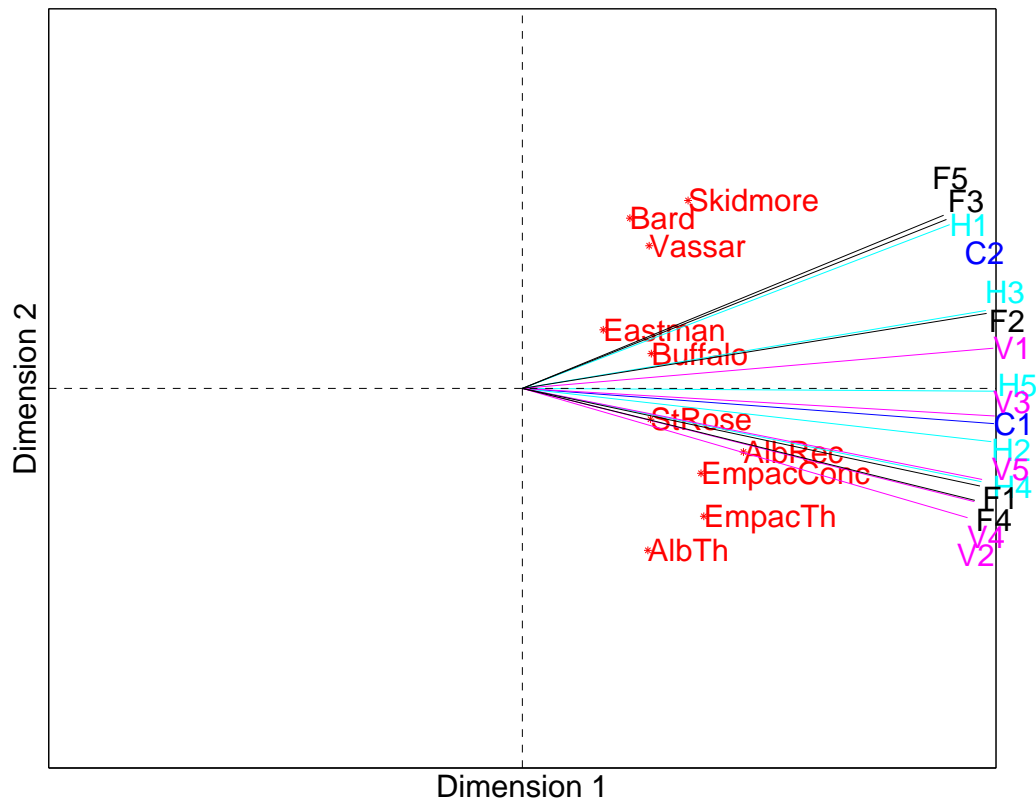


Figure 5.5: Listening Test MDPREF Results, Bach Position 1: $r^2 = 0.59$ (Flute = F1-5, Horn = H1-5, Violin = V1-5, Cello = C1-2, AlbRec = SUNY Albany Recital Hall, AlbTh = SUNY Albany Theatre, EmpacConc = EMPAC Concert Hall, EmpacTh = EMPAC Theatre)

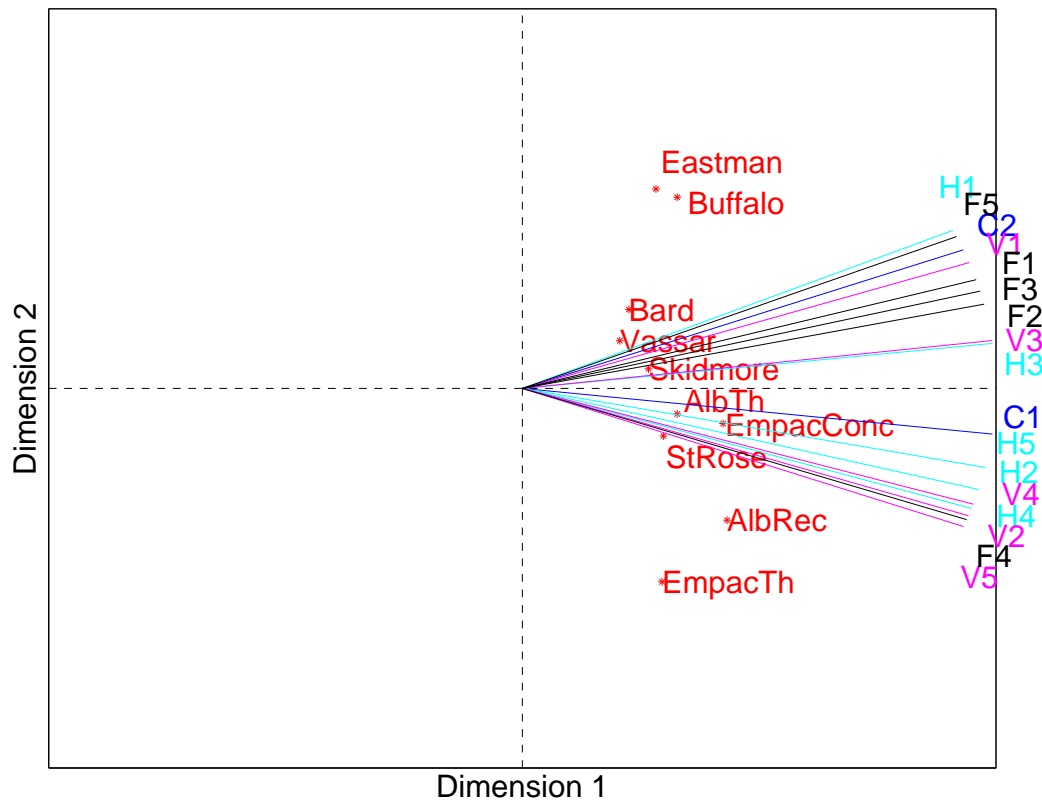


Figure 5.6: Listening Test MDPREF Results, Bach Position 1: $r^2 = 0.56$ (Flute = F1-5, Horn = H1-5, Violin = V1-5, Cello = C1-2, AlbRec = SUNY Albany Recital Hall, AlbTh = SUNY Albany Theatre, EmpacConc = EMPAC Concert Hall, EmpacTh = EMPAC Theatre)

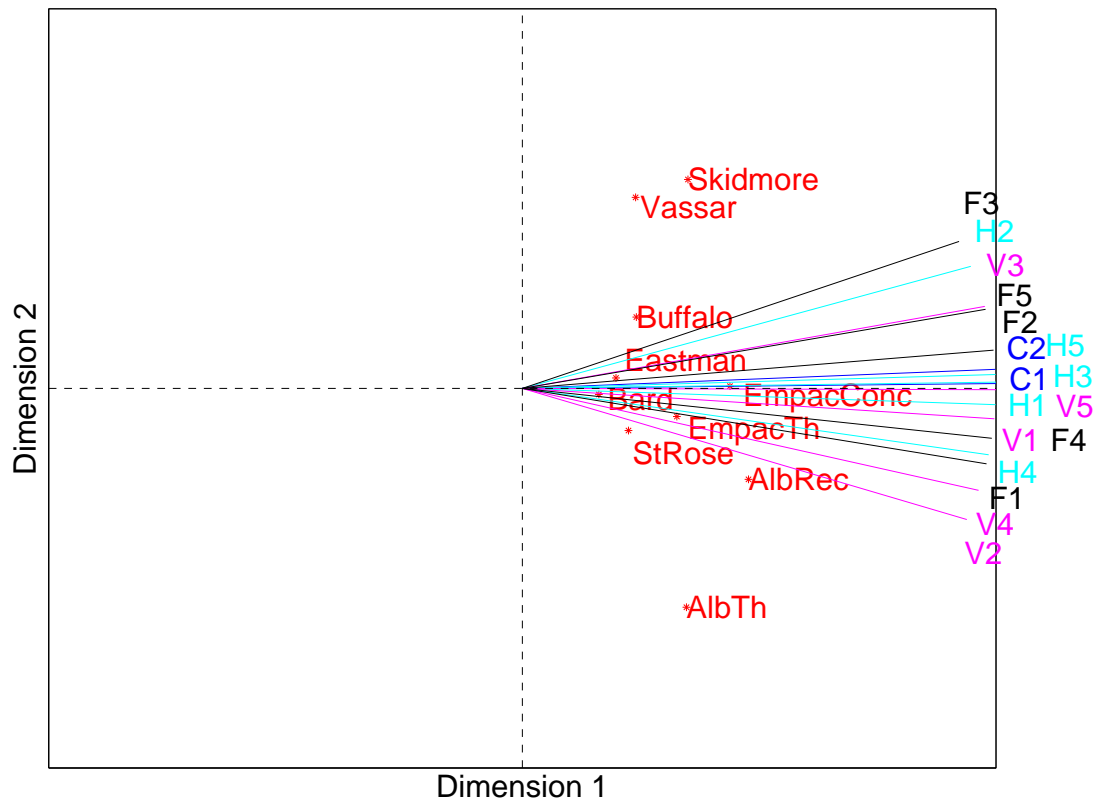


Figure 5.7: Listening Test MDPREF Results, Xenakis Position 1: $r^2 = 0.54$ (Flute = F1-5, Horn = H1-5, Violin = V1-5, Cello = C1-2, AlbRec = SUNY Albany Recital Hall, AlbTh = SUNY Albany Theatre, EmpacConc = EMPAC Concert Hall, EmpacTh = EMPAC Theatre)

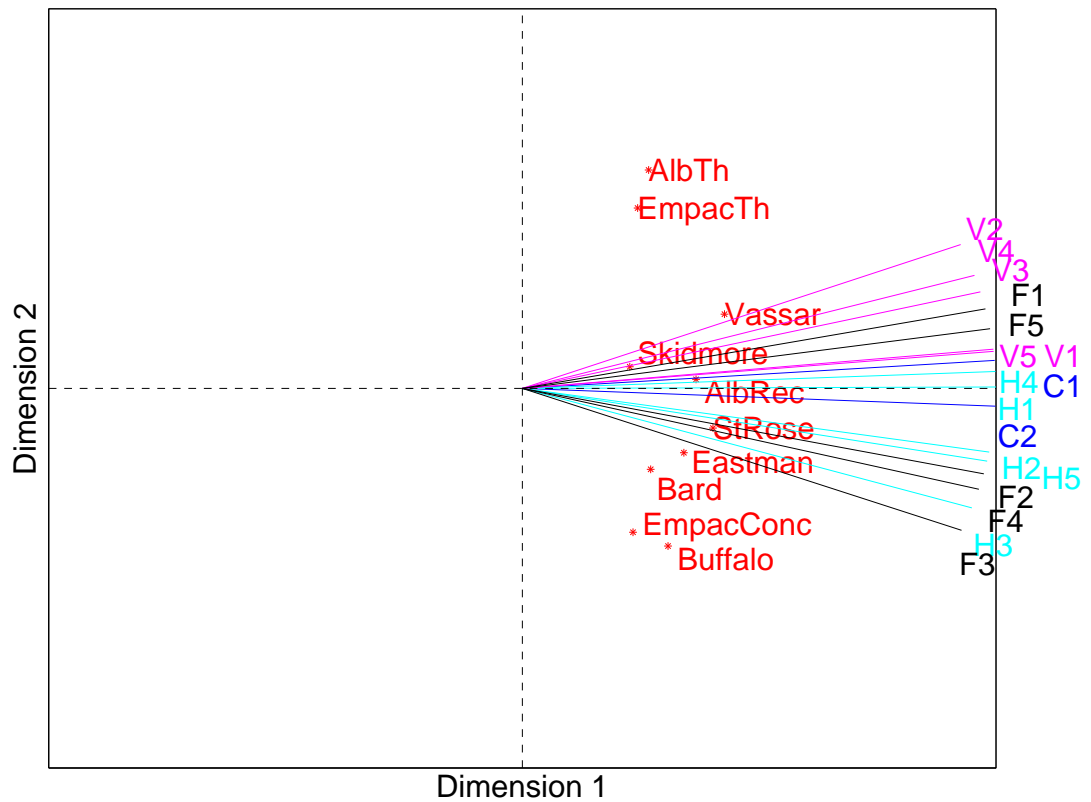


Figure 5.8: Listening Test MDPREF Results, Xenakis Position 2: $r^2 = 0.38$ (Flute = F1-5, Horn = H1-5, Violin = V1-5, Cello = C1-2, AlbRec = SUNY Albany Recital Hall, AlbTh = SUNY Albany Theatre, EmpacConc = EMPAC Concert Hall, EmpacTh = EMPAC Theatre)

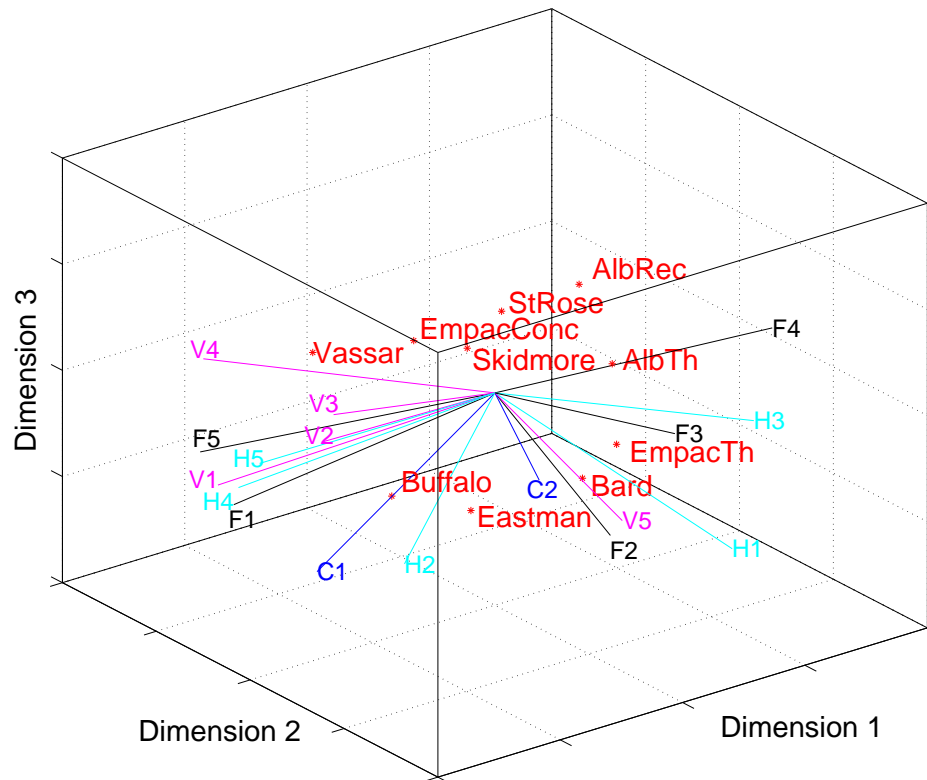


Figure 5.9: Solo Playing Test MDPREF Results: $r^2 = 0.74$ (Flute = F1-5, Horn = H1-5, Violin = V1-5, Cello = C1-2, AlbRec = SUNY Albany Recital Hall, AlbTh = SUNY Albany Theatre, EmpacConc = EMPAC Concert Hall, EmpacTh = EMPAC Theatre)

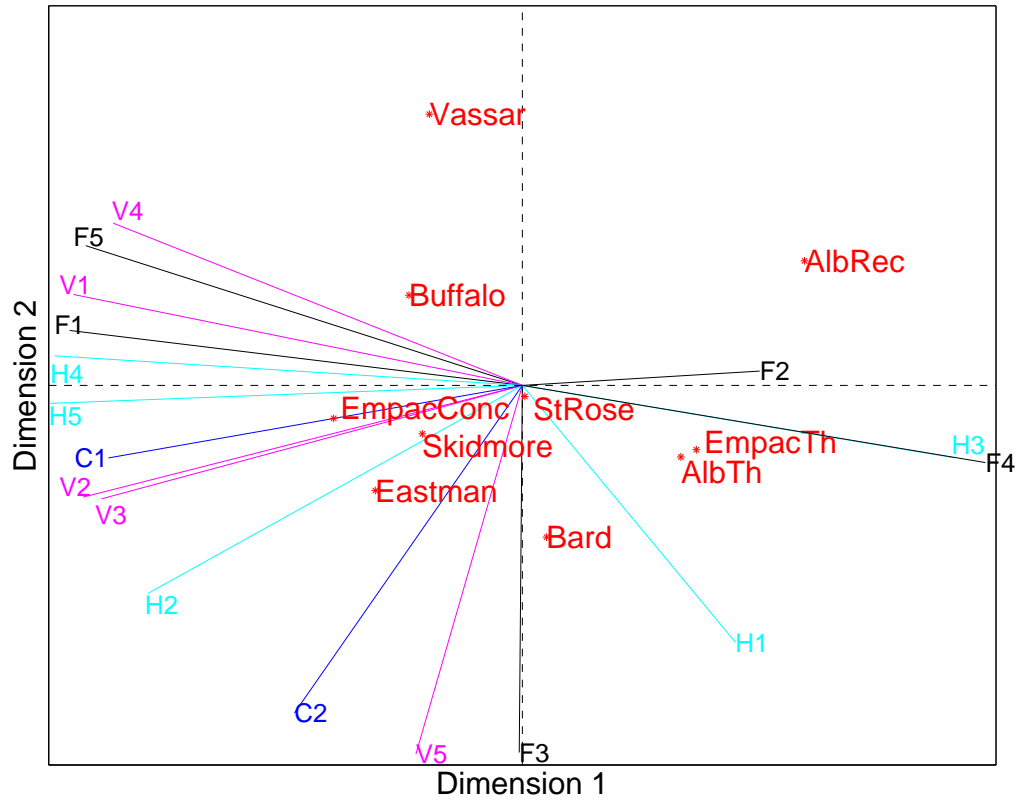


Figure 5.10: Solo Playing Test MDPREF Results: $r^2 = 0.74$ (Flute = F1-5, Horn = H1-5, Violin = V1-5, Cello = C1-2, AlbRec = SUNY Albany Recital Hall, AlbTh = SUNY Albany Theatre, EmpacConc = EMPAC Concert Hall, EmpacTh = EMPAC Theatre)

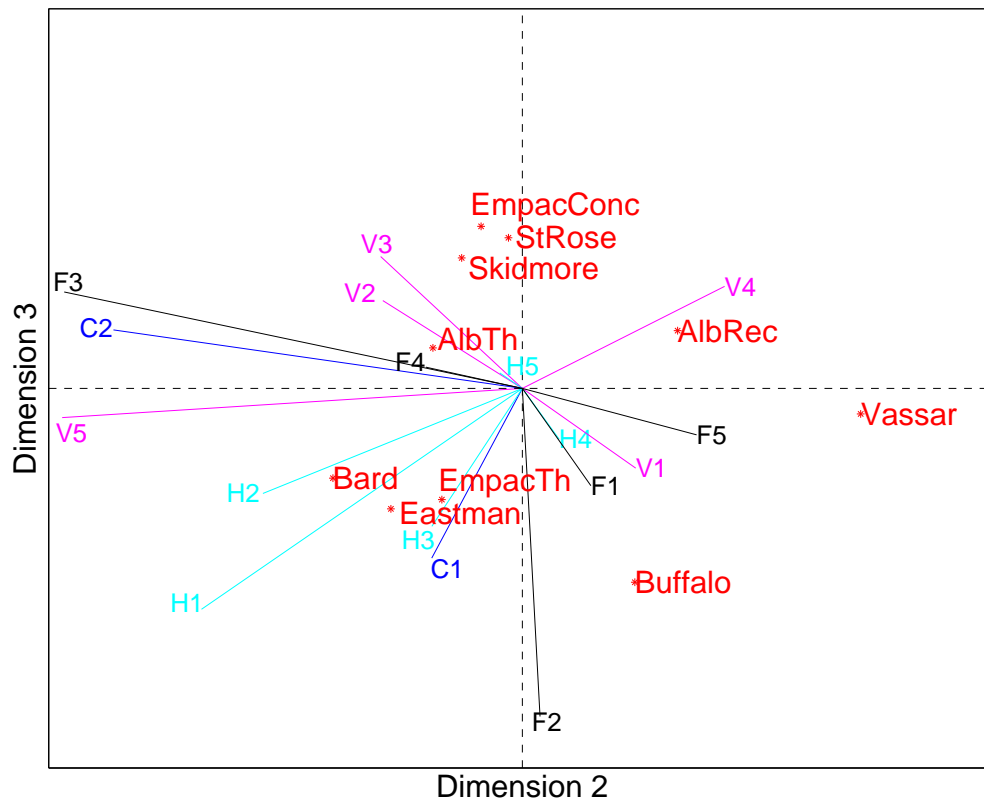


Figure 5.11: Solo Playing Test MDPREF Results: $r^2 = 0.74$ (Flute = F1-5, Horn = H1-5, Violin = V1-5, Cello = C1-2, AlbRec = SUNY Albany Recital Hall, AlbTh = SUNY Albany Theatre, EmpacConc = EMPAC Concert Hall, EmpacTh = EMPAC Theatre)

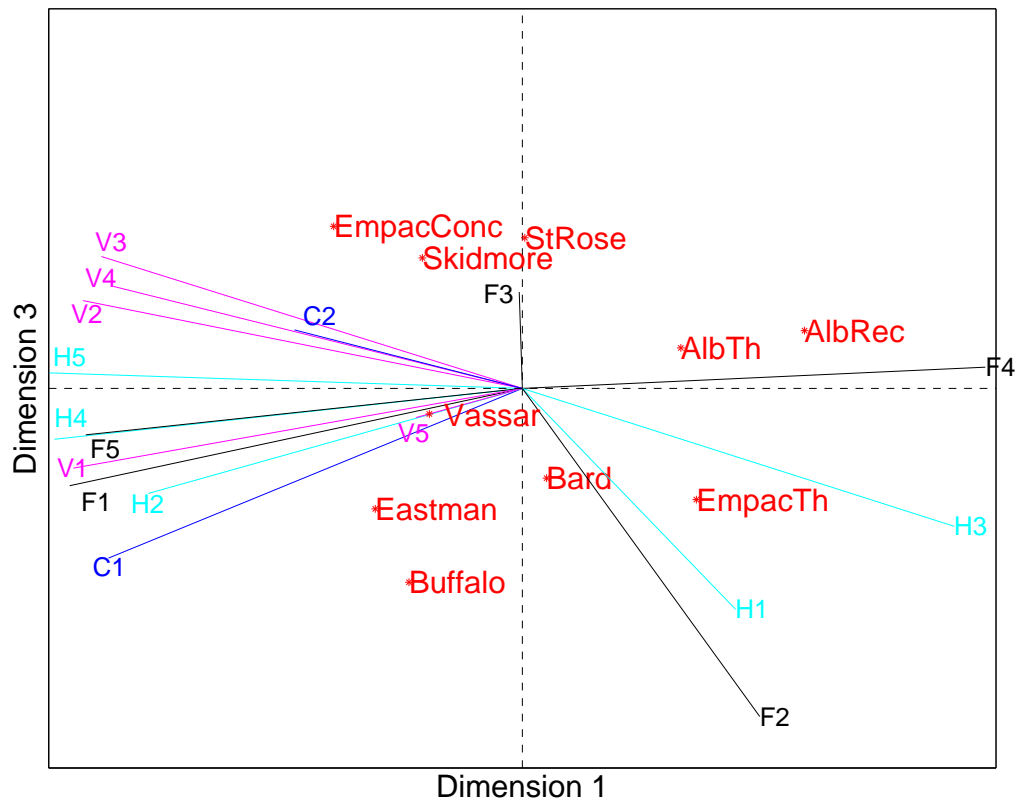


Figure 5.12: Solo Playing Test MDPREF Results: $r^2 = 0.74$ (Flute = F1-5, Horn = H1-5, Violin = V1-5, Cello = C1-2, AlbRec = SUNY Albany Recital Hall, AlbTh = SUNY Albany Theatre, EmpacConc = EMPAC Concert Hall, EmpacTh = EMPAC Theatre)

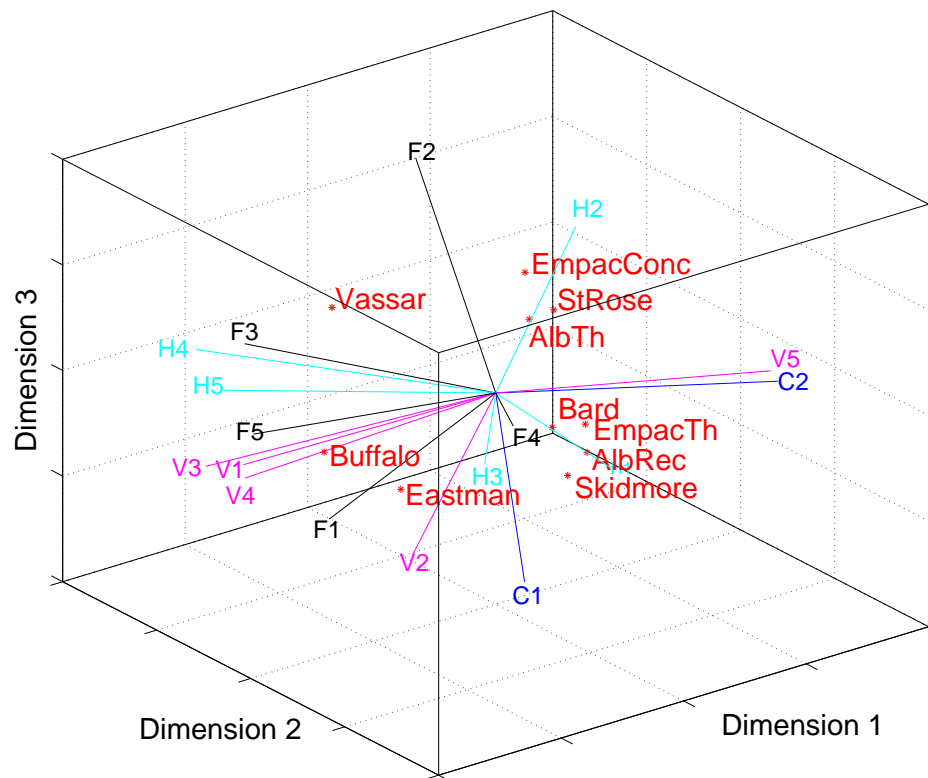


Figure 5.13: Ensemble Playing Test MDPREF Results: $r^2 = 0.77$ (Flute = F1-5, Horn = H1-5, Violin = V1-5, Cello = C1-2, AlbRec = SUNY Albany Recital Hall, AlbTh = SUNY Albany Theatre, EmpacConc = EMPAC Concert Hall, EmpacTh = EMPAC Theatre)

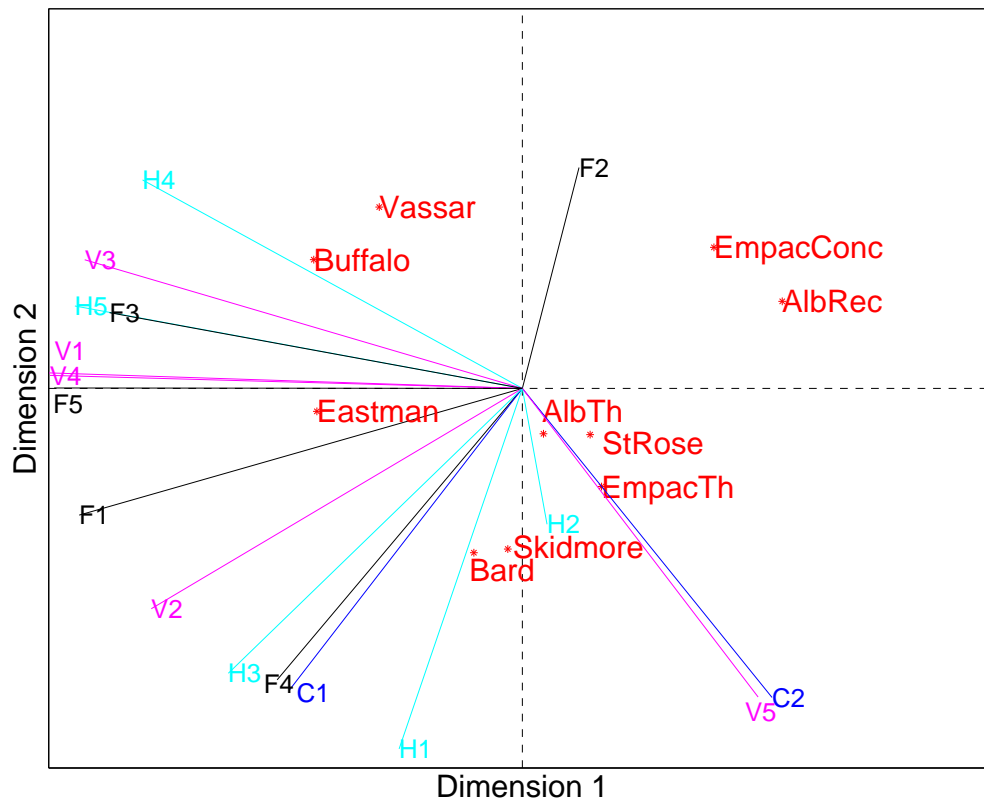


Figure 5.14: Ensemble Playing Test MDPREF Results: $r^2 = 0.77$ (Flute = F1-5, Horn = H1-5, Violin = V1-5, Cello = C1-2, AlbRec = SUNY Albany Recital Hall, AlbTh = SUNY Albany Theatre, EmpacConc = EMPAC Concert Hall, EmpacTh = EMPAC Theatre)

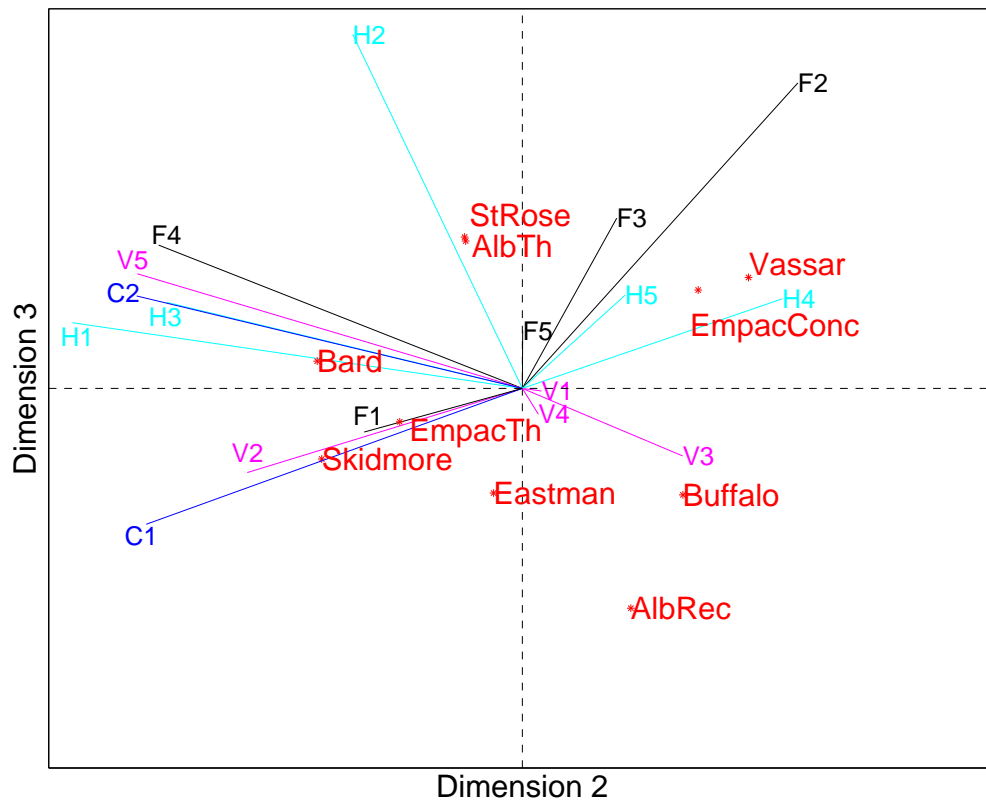


Figure 5.15: Ensemble Playing Test MDPREF Results: $r^2 = 0.77$ (Flute = F1-5, Horn = H1-5, Violin = V1-5, Cello = C1-2, AlbRec = SUNY Albany Recital Hall, AlbTh = SUNY Albany Theatre, EmpacConc = EMPAC Concert Hall, EmpacTh = EMPAC Theatre)

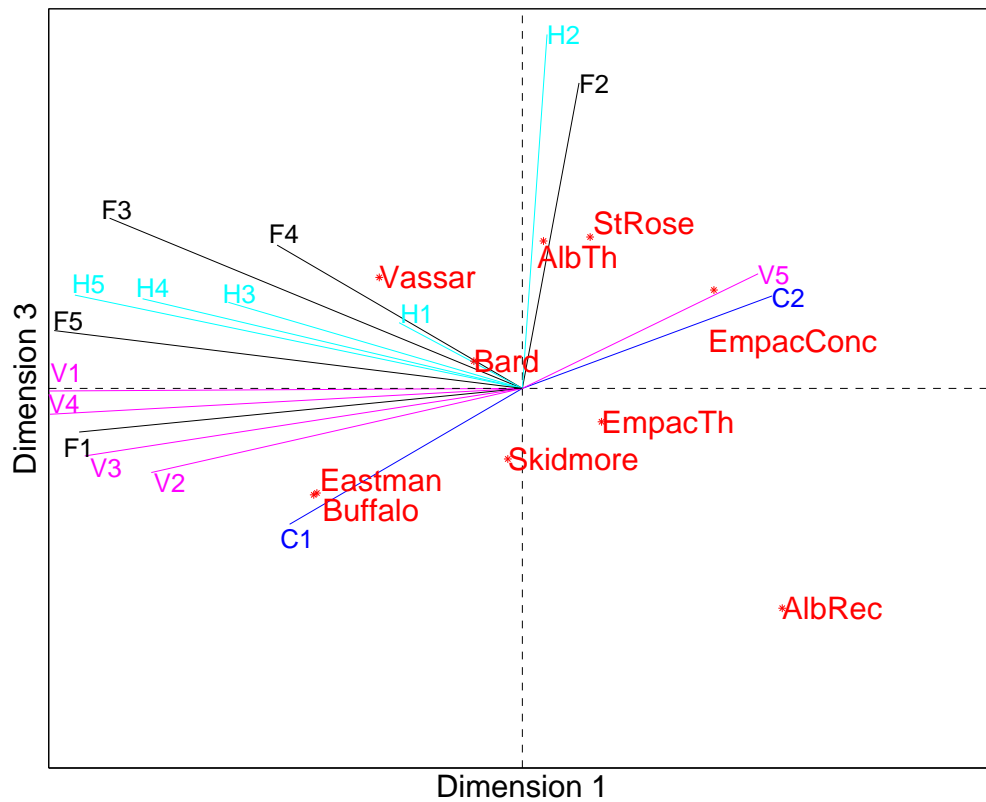


Figure 5.16: Ensemble Playing Test MDPREF Results: $r^2 = 0.77$ (Flute = F1-5, Horn = H1-5, Violin = V1-5, Cello = C1-2, AlbRec = SUNY Albany Recital Hall, AlbTh = SUNY Albany Theatre, EmpacConc = EMPAC Concert Hall, EmpacTh = EMPAC Theatre)

The values for r , r^2 and p are collated in Table 5.2:

Table 5.2: Correlation of MDPREF First and Second Score Matrices

MDPREF Routine	Dimensions	r	r^2	p
Listening Test: Bach Receiver 1	2	0.77	0.59	< 0.01
Listening Test: Bach Receiver 2	2	0.75	0.56	< 0.01
Listening Test: Xenakis Receiver 1	2	0.74	0.54	< 0.01
Listening Test: Xenakis Receiver 2	2	0.62	0.38	< 0.01
Solo Playing Test	3	0.86	0.74	< 0.01
Ensemble Playing Test	3	0.88	0.77	< 0.01

All tests showed significant correlation between the measured data and the MDPREF model at a $p < 0.01$ level. The coefficient of determination shows the amount of variability explained by the tests, and while there is not a clear threshold for “good” values of r^2 , especially given the small sample size, it is clear that the models for the playing tests (both solo and ensemble tests show values of $r^2 \geq 0.7$) are more accurate than those for the listening tests (values of $r^2 \geq 0.60$) [31].

However, the results for this correlation test only show that the models can be trusted to accurately describe the measured data, not that the individuals agree on a ranking of preferred stimuli in each test. Visually, the agreement of individuals can be estimated by comparing the distribution of halls in space on the graph. For the listening tests, the halls are distributed very close together along the Dimension 1 axis. If the stimuli points are projected onto each vector, it can be seen that this arrangement provides a great deal of variation in individual preference order. For the playing tests, on the other hand, a much wider distribution of halls along the individual vectors can be seen in all three dimensions, showing consistent inter-individual preferences for specific halls. As previously mentioned, one issue with MDPREF is that it always provides a solution, even when the interpretation is not meaningful. Due to the difficulty in interpretation of the listening test maps, as well as questionable reliability of the rank-ordering test method (the large number of stimuli per comparison increased listener fatigue and potential for errors), only the performance tests will be analyzed in more detail for this research.

While traditional tests of significance (t-test, F-test) are not usable in MDS, circular statistics can be used to determine whether the distribution of preferences is significantly different from a random distribution in each dimension. In this case, a Rayleigh test is performed which tests angular distribution of a sample against the null hypothesis of a uniform circular distribution. This test assumes that in order to reject the null hypothesis, the distribution must be unimodal and sampled from a von Mises distribution (the circular equivalent to normal distribution) [10]. For both Solo and Ensemble results, the 2-dimensional projections of X-Y (Dimensions 1 and 2) and X-Z (Dimensions 1 and 3) are both significant at a $p < 0.05$ level, whereas the projections of Y-Z (Dimensions 2 and 3) are not. This could indicate that Dimensions 2 and 3 are factors describing individual taste or potential consensus among instrument groups. In order to compare groups, a Watson-Williams test can be performed to reject the null hypothesis that two or more groups have the same mean direction (the circular analog to the two-sample t-test). In this case, for the Ensemble tests, the projection in the Y-Z (Dimensions 2 and 3) plane shows a significant difference between Winds (Flutes and French horns) and strings, which can be visually confirmed by looking at both the Y-Z plane and the X-Z plane, which may indicate that the Z-axis is influencing group preferences.

However, the initial locations of X-Y-Z axes generated by MDPREF are arbitrary. Rotation of the coordinates in 3-Dimensional space is contingent on objective parameter mapping, where the direction of the three orthogonal axes can be optimized to fit specific parameters. At that point, the circular statistics can be re-calculated to determine the relevance of each dimension.

5.5.2 Objective Parameter Mapping

Once the coordinates have been determined for the stimuli and subjects in multi-dimensional space, multiple linear regression can be applied using objective hall characteristics as the dependent variable and individual halls as the independent variable. In MDS software, this property fitting takes the form of one phase of a multi-step procedure known as PREFMAP. However, as the procedure is identical to multiple-regression procedures, the MatLab “regress” function is used for reasons

of flexibility. The output for each parameter tested is a set of three coefficients corresponding to cartesian coordinates in the multidimensional space. The location of the parameter coordinates indicates the direction of increasing value. As mentioned previously, this can be deceptive if the optimal value of a parameter is the lowest value or if the optimal values follow a bell curve.

At this point, initial assumptions must be made regarding the optimal values of specific parameters in order to gain meaningful information from the mapping. In order to do this, all the parameters tested were first scaled between 0 and 1 for ease of display. The resultant vector was generated for all subject responses to find the direction of highest overall preference. The stimuli were projected onto this line to determine the order of hall preference, and then the parameter values were sorted into this order. Any parameters which then did not follow a relatively straight line in terms of value (where the highest value fell into the middle of the distribution) was corrected such that the most preferred hall had the highest value and all higher values were folded back down over this center point (for example, if the most preferred hall had a value of 0.5, then the corrected values would be $0.5 = 1$, $0.6 = 0.8$, $0.4 = 0.8$, etc.).

Because the number of parameters was extremely high due to various spatial permutations described in Section 3.4 (293 solo parameters and 568 ensemble parameters were prepared), an initial hierarchical cluster analysis was first performed to determine whether any parameters could be grouped together or eliminated due to high correlations with other parameters.

5.5.2.1 Solo Parameters

The dendrogram in Figure 5.17 shows the distribution of the 30 highest branches of the cluster analysis. Based on this, 22 clusters were formed (as labeled in the dendrogram) and the average of all parameter values in that cluster was determined for each hall.

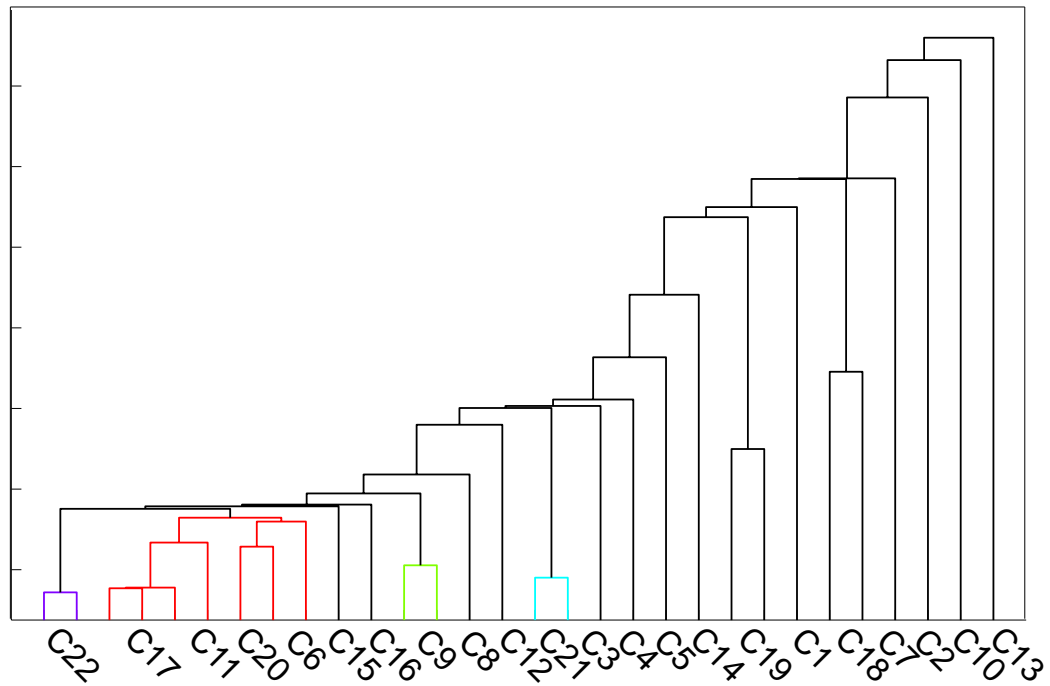


Figure 5.17: Dendrogram From Hierarchical Cluster Analysis: Solo Parameters (Clusters on Abscissa Labeled C1-C22)

The only clusters with a F-statistic significant at a $p < 0.05$ level were C1 and C5, both of which explained $>70\%$ of the data in each dimension ($r^2 > 0.7$). Setting the Dimension 1 axis to C1 and rotating the stimuli and subject coordinates to match, the next orthogonal cluster was determined by taking the product of the r^2 value and the angle between each cluster and C1. C5 was found to be nearest to orthogonal, and this was set to the Dimension 2 axis. The coordinates were rotated again to fit these axes. These two clusters are shown in Figure 5.18.

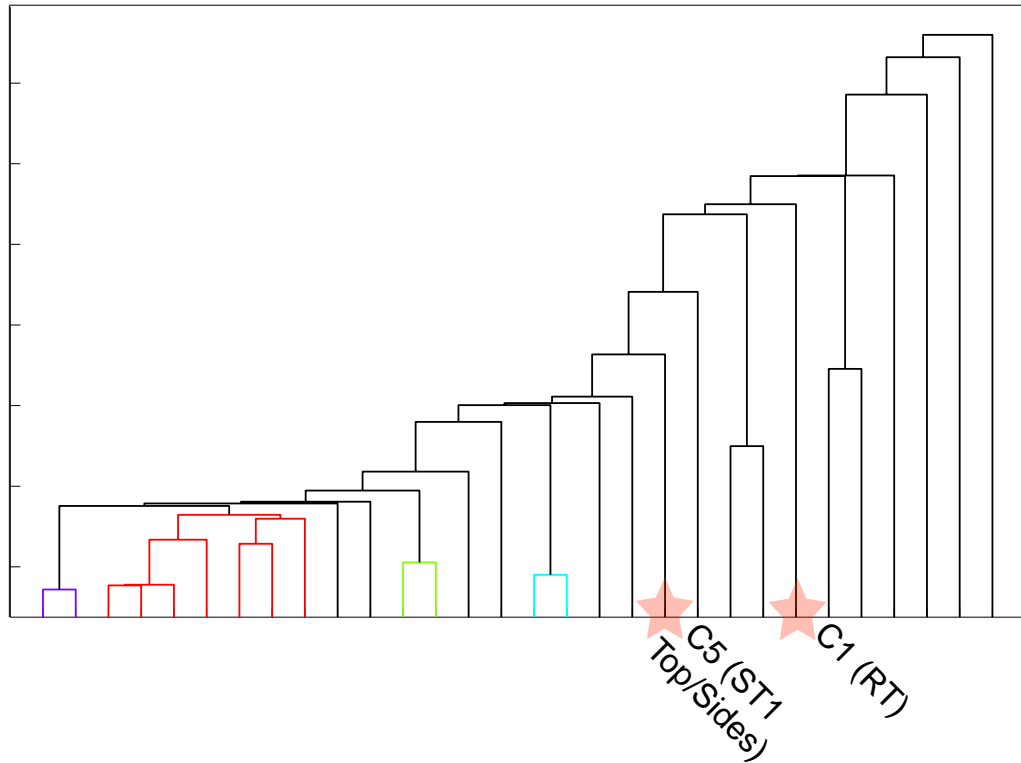


Figure 5.18: Dendrogram From Hierarchical Cluster Analysis: Solo Parameters (Starred Clusters on Abscissa Corresponding to Dimensions 1 and 2)

The final cluster was determined in the same way. Although no other clusters had a significant p -value, C17 had the highest r^2 value at 0.49. The cluster analysis was refined to show the 80 largest branches in order to narrow the range of parameters defined by C17, as shown in Figure 5.19. This maximized the r^2 value at 0.52.

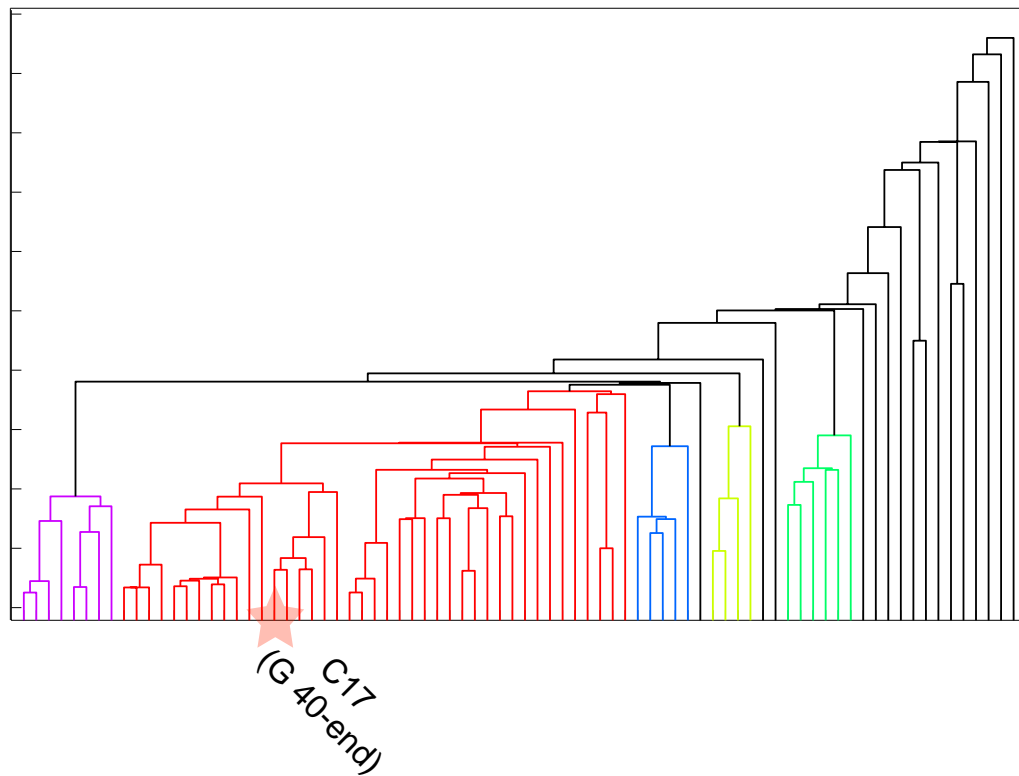


Figure 5.19: Dendrogram From Hierarchical Cluster Analysis: Solo Parameters (Starred Cluster on Abscissa Corresponding to Dimension 3)

The clusters (using the re-defined C17) are named by the dominant elements in Table 5.3.

Table 5.3: Clusters of Solo Parameters

Cluster	Dominant Elements	r^2	ANOVA ($df = 3$)	
			F	p
C1	T_{30} , EDT	0.88	14.03	< 0.01
C2	T_c	0.35	1.06	0.43
C3	DD	0.12	0.26	0.85
C4	ST2-3 Rear	0.16	0.39	0.77
C5	ST1-3 Top/Sides	0.71	4.80	< 0.05
C6	ST1 Left	0.20	0.49	0.70
C7	ST1-3 Front	0.37	1.17	0.39
C8	ST1-3 Right	0.14	0.32	0.81
C9	ST1 Rear	0.15	0.34	0.80
C10	G_{late} Top/Rear	0.48	1.85	0.24
C11	G_{late} Front/Sides	0.48	1.88	0.23
C12	G_{late} Top/Bottom	0.11	0.24	0.87
C13	$G_{40-\infty}$ Top/Sides	0.13	0.30	0.82
C14	$G_{40-\infty}$ Top/Bottom	0.08	0.17	0.92
C15	Early Energy Front, Late Energy Sides	0.10	0.21	0.88
C16	LQ_{740} Front	0.23	0.59	0.64
C17	$G_{40-\infty}$ all directions	0.52	2.10	0.20
C18	LQ_{740}	0.41	1.39	0.33
C19	ST3 Front/Rear	0.37	1.18	0.39
C20	T_c/RR_{160} Front	0.26	0.69	0.59
C21	T_c/RR_{160} Top, Right	0.07	0.15	0.93
C22	$T_c/RR_{160}/ST2$ Rear, Left	0.08	0.17	0.91

The rotated space with the orthogonal clusters is shown in Figures 5.20 - 5.23.

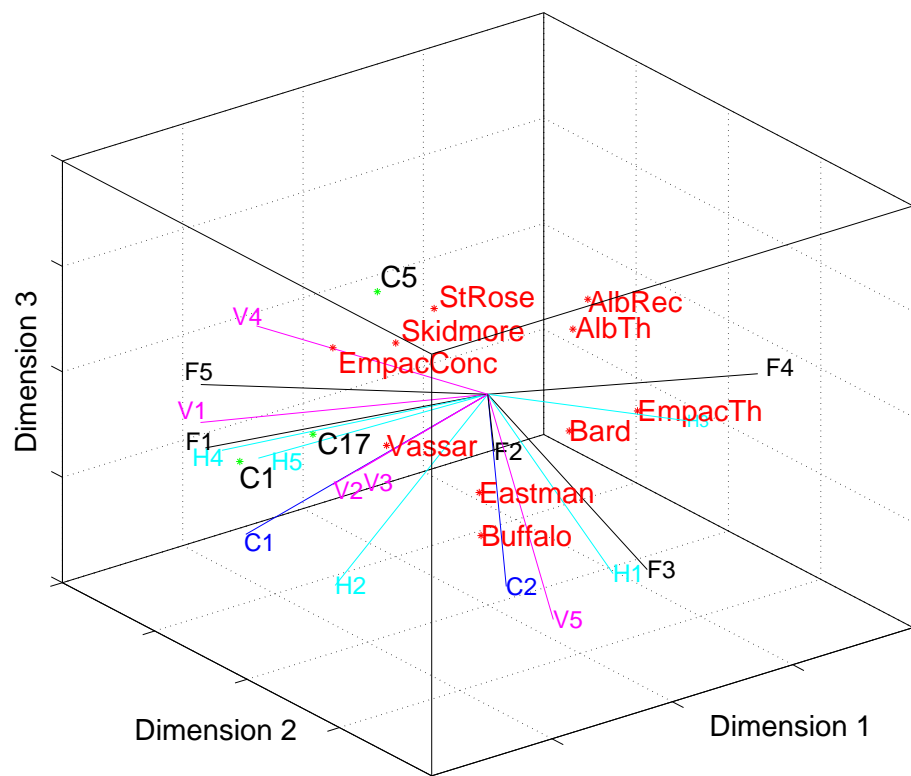


Figure 5.20: Solo Playing Test Parameter Cluster Mapping (Flute = F1-5, Horn = H1-5, Violin = V1-5, Cello = C1-2, AlbRec = SUNY Albany Recital Hall, AlbTh = SUNY Albany Theatre, EmpacConc = EMPAC Concert Hall, EmpacTh = EMPAC Theatre, Clusters = Green Points with Black Text)

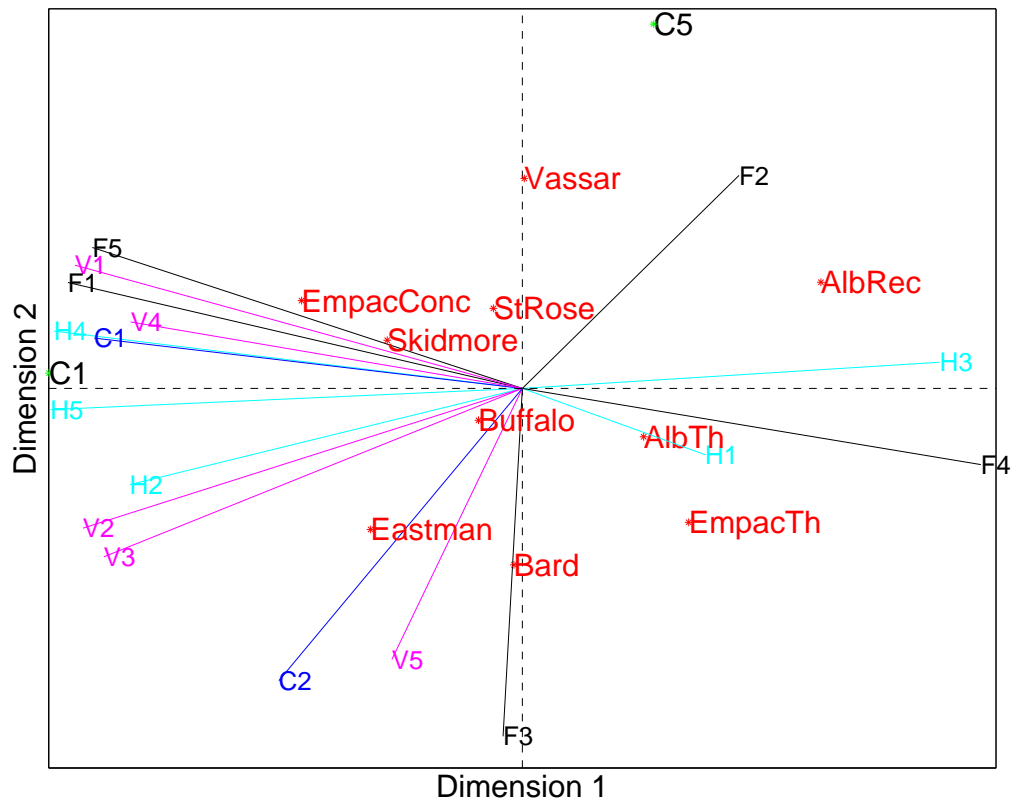


Figure 5.21: Solo Playing Test Parameter Cluster Mapping (Flute = F1-5, Horn = H1-5, Violin = V1-5, Cello = C1-2, AlbRec = SUNY Albany Recital Hall, AlbTh = SUNY Albany Theatre, EmpacConc = EMPAC Concert Hall, EmpacTh = EMPAC Theatre, Clusters = Green Points with Black Text)

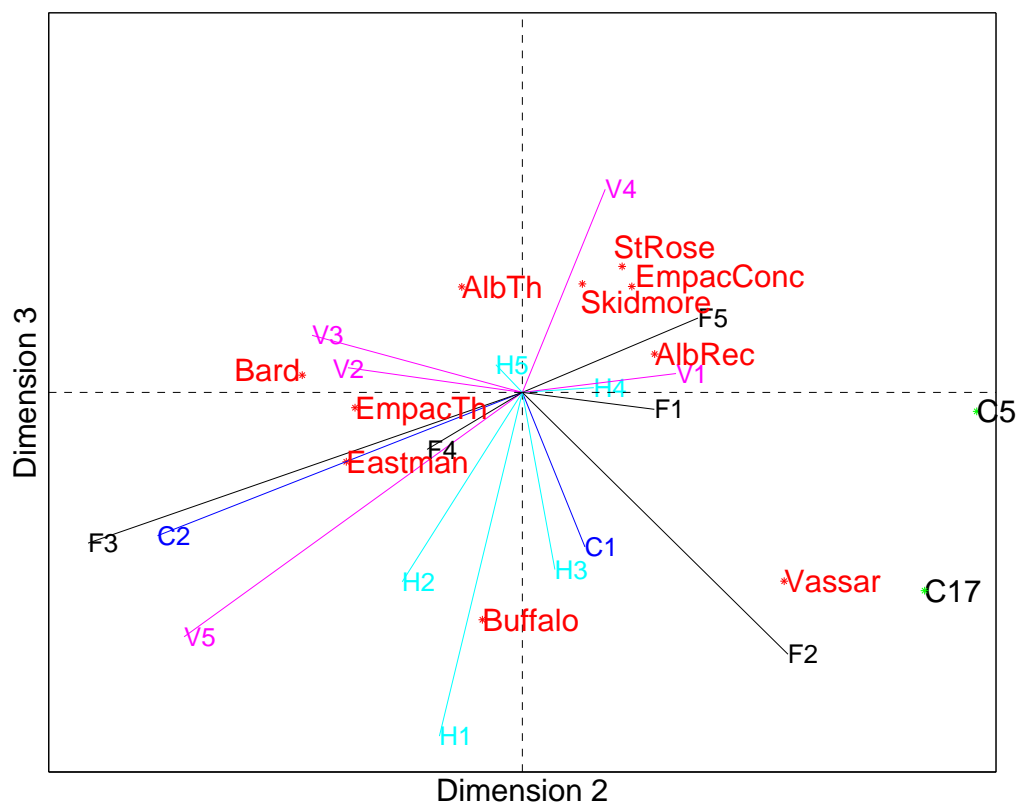


Figure 5.22: Solo Playing Test Parameter Cluster Mapping (Flute = F1-5, Horn = H1-5, Violin = V1-5, Cello = C1-2, AlbRec = SUNY Albany Recital Hall, AlbTh = SUNY Albany Theatre, EmpacConc = EMPAC Concert Hall, EmpacTh = EMPAC Theatre, Clusters = Green Points with Black Text)

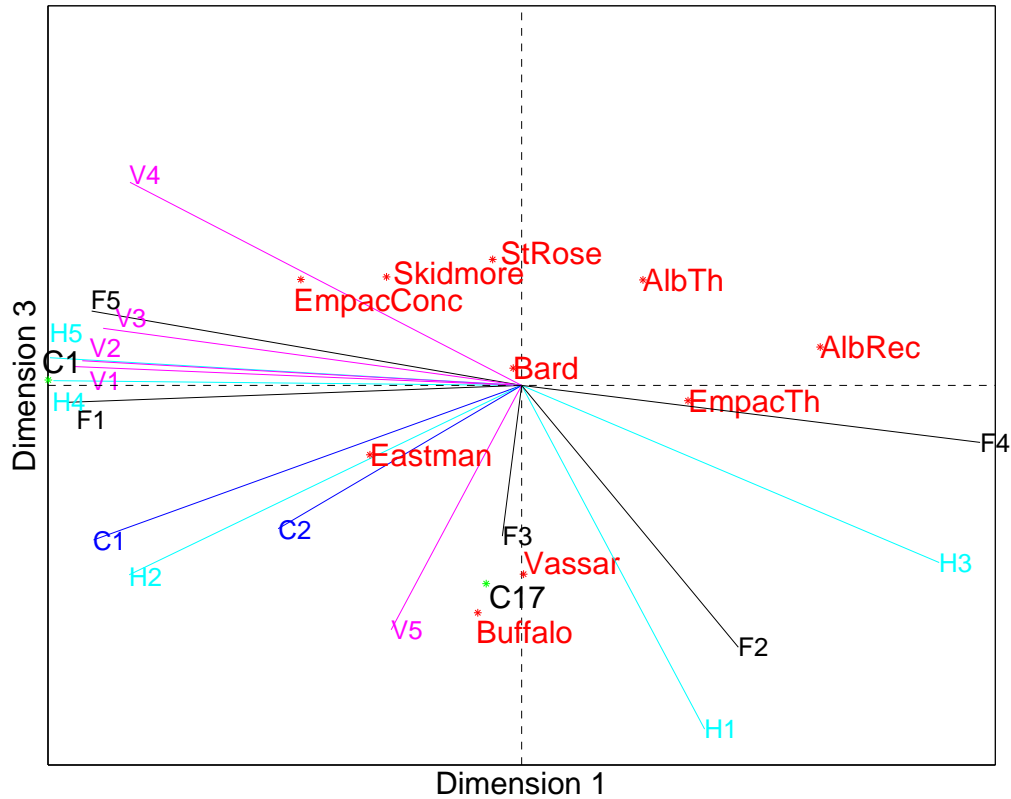


Figure 5.23: Solo Playing Test Parameter Cluster Mapping (Flute = F1-5, Horn = H1-5, Violin = V1-5, Cello = C1-2, AlbRec = SUNY Albany Recital Hall, AlbTh = SUNY Albany Theatre, EmpacConc = EMPAC Concert Hall, EmpacTh = EMPAC Theatre, Clusters = Green Points with Black Text)

Cluster C1 is linear in terms of values: increased reverberation and early decay time is preferred. The range for T_{30} from least to most preferred is 0.9 seconds to 2.2 seconds. 2.2 seconds is considered the maximum desirable reverberation time for symphonic music [8]. It is possible that eventually some threshold of decay time would be reached and preference would decrease, but that cannot be determined from the available stimuli, as there is no stimuli with values higher than this threshold, as there were in the Schroeder et al. study [93].

Cluster C5 follows a bell curve. The range of values for ST1 Top/Sides for the tested halls was -7 dB to $+2$ dB, with the most preferred hall being -3 dB.

Cluster C17 also follows this shape, with $G_{40-\infty}$ ranging from 12.6 dB to 18.8 dB and the most preferred hall at 16.2 dB.

Circular statistics were re-calculated for the rotated subject vectors. The Rayleigh test on all subject vectors as a single group found that the rotation had little effect on clustering. The 2-dimensional projection of X-Y (Dimensions 1 and 2) is still significant at a $p < 0.05$ level, the projection of X-Z (Dimensions 1 and 3) is slightly improved with a significance at a $p < 0.01$ level, and the projection of Y-Z (Dimensions 2 and 3) is not significant. However, examination of instrument groups shows that the X-Y and X-Z projections are now significant for the strings group alone and not significant for the winds alone. The X-Z projection also shows a significant Watson-Williams test result for the difference between winds and strings. The Y-Z projection is significant for flutes alone, and shows significant difference between winds and strings as well. Although the small test sample makes such instrument-based comparisons difficult, visual inspection could lead to the following observations:

- **Dimension 1:** Strings dominate with strong preference for increased reverberance, with weak agreement for other instruments.
- **Dimension 2:** No strong agreement for ST1 Top/Sides (personal preference appears to dominate).
- **Dimension 3:** Winds (flutes especially) dominate with strong preference for mid-range values of $G_{40-\infty}$, with little agreement from other instruments.

5.5.2.2 Ensemble Parameters

Due to the large number of parameters computed for the ensemble tests (568), the parameters were first tested individually against the MDPREF results to eliminate un-correlated parameters that might add noise to the hierarchical clustering. All parameters where $r^2 < 0.7$ after multiple regression tests (corresponding to a non-significant F-statistic) were eliminated, leaving 111 parameters.

On visual observation of the tested halls, some additional parameters were considered. It was thought that the frequency distribution of early energy may

have some effect on ensemble playing, so individual parameters were tested in four different octave bands (500, 1kHz, 2kHz, and 4kHz), but the results were similar for each octave band, suggesting that frequency was not affecting preference judgement in these tests (potentially due to the limits of the available stimuli). Therefore, the 1kHz parameters were used.

Additionally, it was considered that the Directional Diffuseness parameter (DD , defined in Section 3.2.2) was not relevant for stage acoustics when examining the entire length of the decay. DD was therefore also computed for shorter time windows (0-100 ms, 0-80 ms, 0-50 ms, and 0-30 ms) in order to determine the length of time in which spatial homogeneity has an influence on ensemble playing. When these parameters were included in the multiple regression, DD_{0-30} was found to have a high r^2 value (0.93), bringing the number of parameters to 112.

These parameters were then divided into clusters using cluster analysis. An iterative process was used to find the optimal number of clusters that maximized their r^2 values from multiple regression. Based on this process, 15 clusters were formed. These clusters are described in Table 5.4. For clarity, measurement positions are labeled Cross-Stage (Left-Right S-R Pair) and UpDown-Stage (Front-Back S-R Pair) and the directional sectors are labeled Front, Back, Top, Bottom, Front, Rear, Left and Right as defined in Section 3.4.

Table 5.4: Clusters of Ensemble Parameters

Cluster	Dominant Elements	r^2	ANOVA ($df = 3$)	
			F	p
C1	EDT Cross-Stage Rear, Left, Front; Tc Cross-Stage Bottom	0.85	11.58	< 0.01
C2	Tc Cross-Stage Left	0.75	5.89	< 0.05
C3	Tc UpDown-Stage Left; RR_{160} UpDown-Stage Front	0.78	7.11	< 0.05
C4	G_{7-40} UpDown-Stage Top/Rear	0.77	6.85	< 0.05
C5	G (all time windows) Cross-Stage (all directions)	0.78	6.93	< 0.05
C6	Tc UpDown-Stage Right	0.93	26.07	< 0.01
C7	LQ_{740} Cross-Stage Top/Sides	0.90	17.11	< 0.01
C8	RR_{160} Cross-Stage Rear	0.76	6.38	< 0.05
C9	MTF Cross-Stage Top, Bottom, Rear, Left, Front	0.77	6.57	< 0.05
C10	MTF Cross-Stage Left (Normalized)	0.72	5.10	< 0.05
C11	EDT, EDTR Cross-Stage Left (Normalized)	0.77	6.53	< 0.05
C12	EDT UpDown-Stage Top	0.81	8.37	< 0.05
C13	EDT UpDown-Stage Top/Rear	0.74	5.59	< 0.05
C14	G (all time windows) UpDown-Stage (all directions); DD_{0-30} Cross-Stage	0.80	7.96	< 0.05
C15	Omnidirectional Tc	0.75	6.07	< 0.05

Through an iterative process, the optimal rotation of the MDPREF space was determined using the defined clusters. All clusters were mapped on the 3-dimensional MDPREF space. 3D and 2D projections of the rotated space are shown

in Figures 5.24 - 5.27.

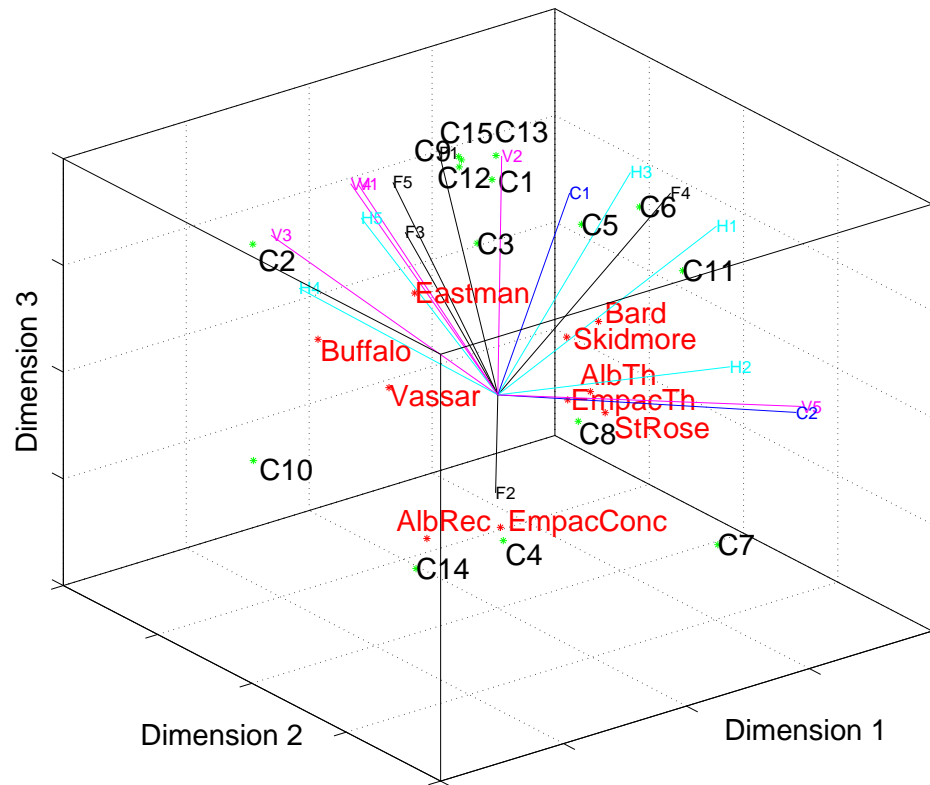


Figure 5.24: Ensemble Playing Test Parameter Cluster Mapping (Flute = F1-5, Horn = H1-5, Violin = V1-5, Cello = C1-2, AlbRec = SUNY Albany Recital Hall, AlbTh = SUNY Albany Theatre, EmpacConc = EMPAC Concert Hall, EmpacTh = EMPAC Theatre, Clusters = Green Points with Black Text)

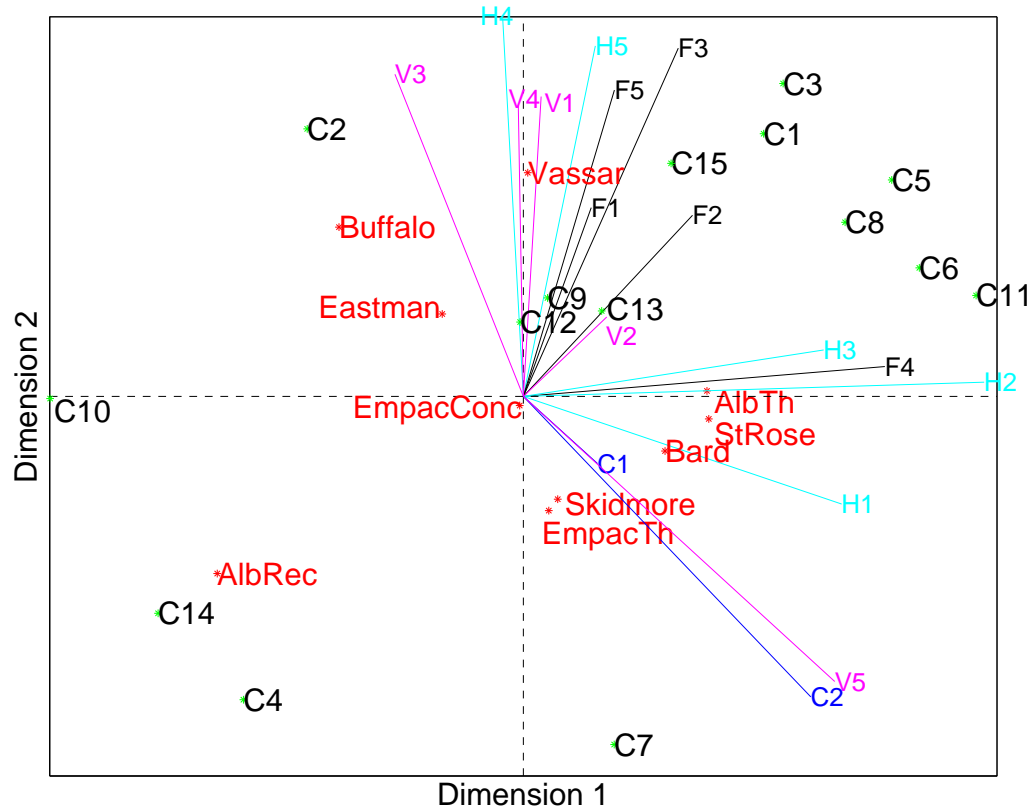


Figure 5.25: Ensemble Playing Test Parameter Cluster Mapping (Flute = F1-5, Horn = H1-5, Violin = V1-5, Cello = C1-2, AlbRec = SUNY Albany Recital Hall, AlbTh = SUNY Albany Theatre, EmpacConc = EMPAC Concert Hall, EmpacTh = EMPAC Theatre, Clusters = Green Points with Black Text)

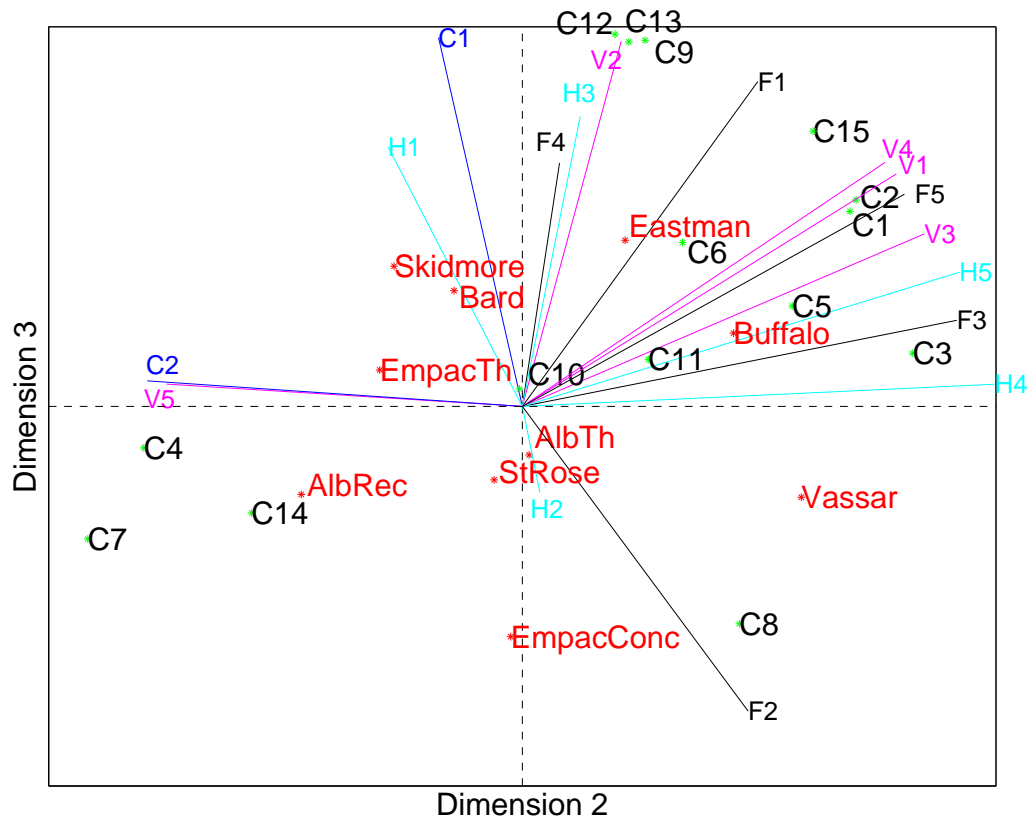


Figure 5.26: Ensemble Playing Test Parameter Cluster Mapping (Flute = F1-5, Horn = H1-5, Violin = V1-5, Cello = C1-2, AlbRec = SUNY Albany Recital Hall, AlbTh = SUNY Albany Theatre, EmpacConc = EMPAC Concert Hall, EmpacTh = EMPAC Theatre, Clusters = Green Points with Black Text)

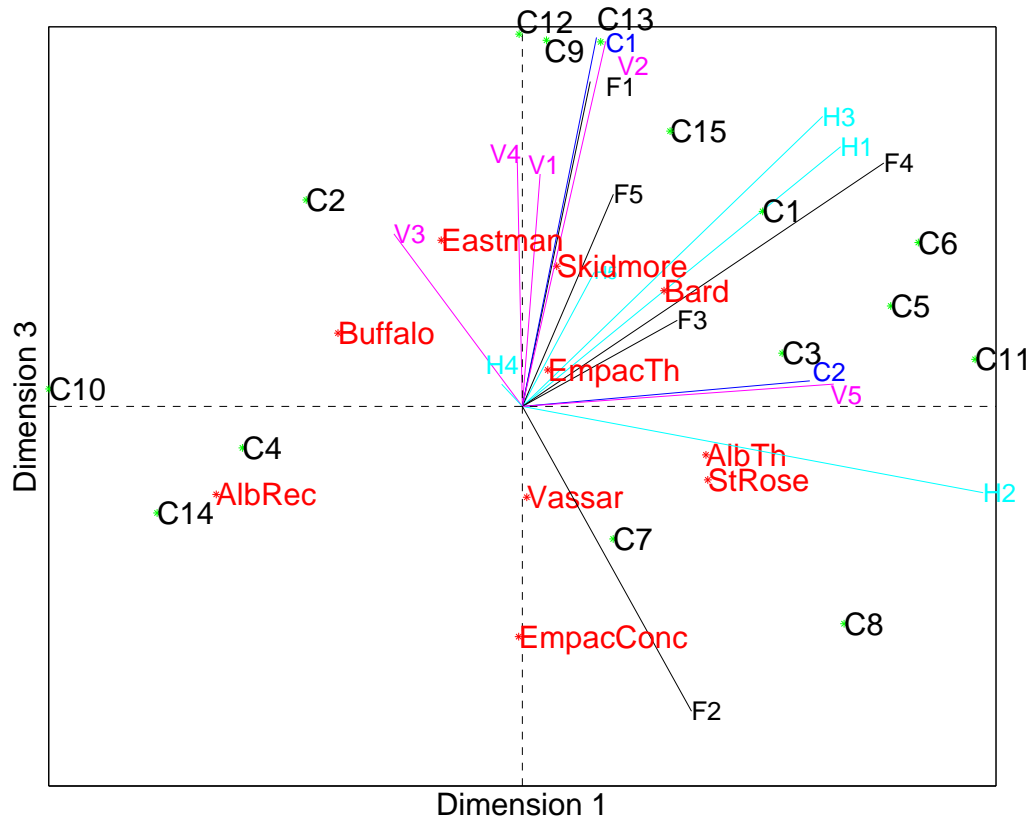


Figure 5.27: Ensemble Playing Test Parameter Cluster Mapping (Flute = F1-5, Horn = H1-5, Violin = V1-5, Cello = C1-2, AlbRec = SUNY Albany Recital Hall, AlbTh = SUNY Albany Theatre, EmpacConc = EMPAC Concert Hall, EmpacTh = EMPAC Theatre, Clusters = Green Points with Black Text)

The rotated preference vectors were tested again using circular statistics and, for the rotated space, all three dimensions showed statistically significant differences from uniform distribution at a $p < 0.01$ level. This implies that all three axes contribute significantly to the determination of preference. The clusters that appear to align best with Dimension 1 include C14, C10, C4 on the negative side and C5 on the positive side (C14 has the highest r^2 value of this group). The cluster that aligns best with Dimension 2 is C7 (negative). The clusters that align with Dimension 3 are C9, C12 and C13 on the positive side and C8 on the negative side. A dendrogram of the clusters is shown in Figure 5.28.

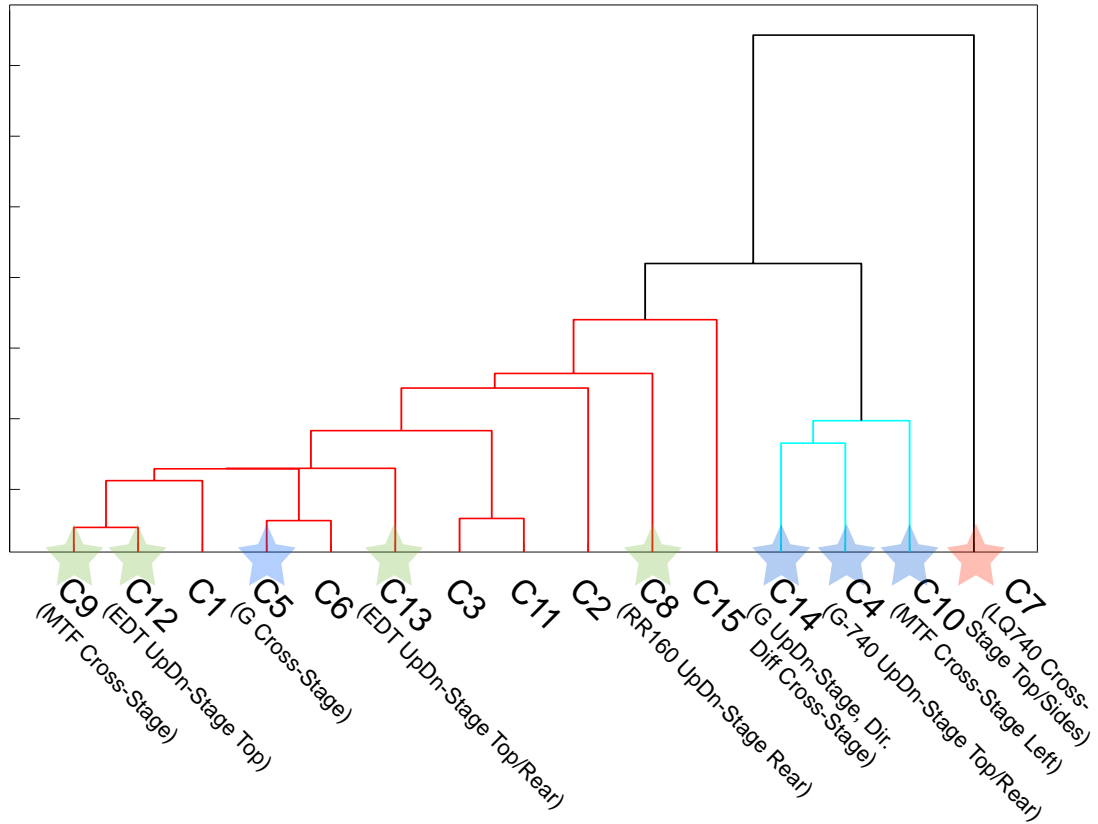


Figure 5.28: Dendrogram From Hierarchical Cluster Analysis: Ensemble Parameters (Starred Clusters Corresponding to MDPREF Dimensions)

Dimension 1 can be summarized in terms of a combination of clusters C5 and C14 (see Table 5.4):

Dimension 1 was most highly correlated with cluster C14. As shown in Figure 5.25, this correlation is negative, indicating that lower values of the parameters in C14 are preferred. Dimension 1 was also highly correlated with cluster C5, although the correlation in this case was positive, indicating that higher values of the parameters in C5 are preferred.

DD_{0-30} (cross-stage measurement) is the dominant parameter in C14, with the highest individual correlation coefficient. Lower values of spatial homogeneity in the first 30 milliseconds are preferred. Larger time windows for DD were not significantly correlated. This implies that spatial differentiation in the early portion of the decay is important for ensemble playing. The initial 30 milliseconds are

most likely to consist of low-order reflections from the stage enclosure, and the presence of diffusion or lack of specular energy from nearby surfaces may contribute to increased homogeneity. Spatial differentiation in this early time window may help with cues and synchronization between musicians due to spatial un-masking between self-generated sound and that generated by others.

C14 also contains multiple versions of up-down-stage G (almost all tested spatial sectors and time windows were correlated). Again, lower values of these parameters, measured with a source at the back of the stage and the receiver at the front, were preferred.

C5, on the other hand, contains almost all spatial and time-windowed variations on cross-stage G , measured with a source-receiver pair horizontally separated on the stage. Higher values of these parameters were preferred.

The opposing preference for cross-stage G over up-down-stage G could be due to the fact that preferred halls have better buildup of energy at the sides of the stage and less at the front, which would provide good balance as the directivity of the loudest instruments is already contributing to high levels of direct sound at the front of the stage.

Dimension 2 shows negative correlation with cluster C7, which contains only one parameter, LQ_{740} Top/Sides. This indicates that lower values of LQ_{740} Top/Sides are preferred, which implies that more energy from the sides is preferred to energy from the top of the stage. As LQ_{740} is essentially a measure of onstage clarity with the time limits adjusted to reflect the arrival of sound from other musicians, this is similar to the soloist condition, in which ST1 Top/Sides was found to have significance (a measure of onstage clarity for self-generated sound). As described in Section 3.2.1.3, this also matches the architectural findings from work by Dammerud, who determined that higher ceilings and narrow side walls proved beneficial for ensemble communication [26].

Dimension 3 can be summarized in terms of Clusters C8, C9, C12, and C13, as described in Table 5.4:

Cluster C9 is well aligned with positive preference. This cluster consists of multiple spatial variations on the cross-stage measurement of MTF (Modulation

Transfer Function). The preferences of MTF fall on a bell curve. Values of 0.75 (out of range from 0 to 1) were most preferred, and values higher and lower were increasingly less preferred. As MTF is a variation on the traditional Speech Intelligibility measure with the self-generated sound considered as noise and the ensemble sound as signal, intelligibility of the ensemble is important to performance only to a level where it does not mask the sound of the performer's instrument, which could be equally detrimental to synchronization and intonation.

Clusters C12 and C13 fall closely along the positive axis for dimension 3. Both clusters show preference for increased reverberance (EDT) from above and less from the rear of the stage. Cluster C8, on the other hand, falls on the negative axis, showing preference for decreased reverberance (RR_{160}) from the rear of the stage. This could indicate a preference for less buildup of energy from the back of the stage (similar to the preferences along Dimension 1) and a preference for higher upper volume in contrast to the walls of the stage enclosure (similar to Dimension 2).

In summary, the three dimensions for the ensemble playing test conditions were interpreted as follows:

- **Dimension 1:** Early spatial homogeneity (decreasing values of DD_{0-30} are preferred), Strength (lower values of up-downstage G and higher values of cross-stage G preferred).
- **Dimension 2:** Spatial ratio of LQ_{740} from Top/Sides (decreasing values preferred).
- **Dimension 3:** Cross-stage signal preservation (ideal value of $MTF = 0.75$ on a scale of 0-1), Spatial ratio of reverberance (increased Top EDT reverberance, decreased Rear EDT and RR_{160} reverberance preferred).

5.6 Discussion and Future Work

Given the large number of parameters and parameter clusters that were significantly correlated with the 3D mapping of the halls in the solo and ensemble playing tests, conclusions with regards to any individual parameter or cluster driving the

subjective preferences is purely exploratory. The sample set of 10 halls, while large enough to show that certain stages are definitely preferred for a variety of characteristics, is not large enough to determine without question the few parameters that drive these preferences. However, this work can be used as a method proof-of-concept and a starting point for more exhaustive measurements and controlled experiments. The potential acoustic attributes used to describe each dimension in the MDS spaces can be used to control specific parameters in a virtual model in CATT for more precise evaluations. Additional measurements in a wide variety of halls can also enrich the understanding of the architectural implications of the parameters described above.

Previous research using MDS in acoustics (including the outlined studies by Grey, Yamaguchi, and Morimoto & Asaoka) often utilizes proximity data, which focuses on the differences between stimuli (instrument type, seat position, and hall type, respectively) rather than preference. These studies have been instrumental in showing that auditory perception in concert halls is a complex combination of several factors, but they did not attempt to order these factors in terms of priority for individual listener preference. In this research, the main goal is to provide a method for improving stage acoustic design, which requires some preferential judgement from the test subjects. In this area, previous research is less prevalent. The outlined study by Schroeder et al. focuses on listening tests, which again is less valuable for stage acoustics as it does not accurately replicate the conditions experienced by musicians in performance.

The Gade research described in Section 5.2 is the benchmark study most directly related to this research. The stage support parameters have long been considered the final word on stage acoustics. However, experience has increasingly shown that acoustic design should not be informed on one parameter alone. Design for ideal audience acoustics is certainly not limited to an optimization of reverberation time, but rather aims to optimize a large group of parameters simultaneously. This research attempts to expand upon Gade's work by refining the laboratory conditions and resolution of the auditory stimuli as described in Chapter 4, and testing correlations with additional objective parameters, in the hope of finding additional

parameters that may improve the process of stage enclosure design. A natural outcome of this goal is an increase in uncertainty due to the additional complexity of the stimuli. This method should be developed further and used to measure and test additional stimuli to improve the robustness of the results.

In the test setup, it was shown by the difference between the listening and playing tests that paired-comparison method was much more robust in preventing listener confusion than the rank-order method. In the future, paired-comparisons should be used for all tests. Additionally, adjective comparisons or more descriptive responses from the subjects (attempting to define during the test what caused the subjects to prefer one hall over another) could be elicited to further restrict the range of possible attributes in the analysis.

In the auralizations, some potential improvements could include wider instrument variety and larger test groups. To provide some repeatability within the small number of musicians tested, instruments were limited to four types. Increasing the number of tested instruments could improve the robustness of the preference judgments. Testing other non-traditional types of music could also influence judgement, as the only tested type was in the late-romantic symphonic style. Chamber music, non-Western styles, contemporary classical or even amplified music could produce very different preferences. Including multiple musicians in the same or co-located rooms could also have a significant effect on preference [52].

The analysis methodology can be refined, as well. The use of the vector model has limitations, as described in Section 5.3. Additional analysis using ideal-point models such as PREFSCAL, which avoid degenerate solutions, should be considered. Tests of the same data for subjective perception of dissimilarities could in fact be used to generate an external map of the halls, onto which an external unfolding of the preference data could be mapped. Additionally, further tests that are more statistically robust could be conducted that either use measurements made in controlled conditions (for example, multiple canopy heights on the same stage) or acoustic models where only a few known parameters are varied. The parameters found to be significant in this research could serve as the starting point for such tests.

5.7 Conclusions

This chapter described the subjective test methodology and analysis of preference results in an attempt to determine acoustic attributes correlated to subjective preference. In summary, the results of the preference mapping led the author to focus on the playing tests (solo and ensemble conditions). For each test, a 3-dimensional perceptual space was determined using MDPREF that was then correlated with objective parameters. These parameters were initially grouped into clusters using hierarchical clustering analysis, and the significant clusters were then mapped into the perceptual space using multiple regression to determine the best interpretation for each axis.

The three dimensions for the solo playing test conditions were interpreted as described in Table 5.5:

Table 5.5: Summary of Perceptual Dimensions, Soloist Condition

Dimension	Name	Parameter	Range	Preferred Values	Group
1	Omni Reverberance	T_{30} (s) EDT (s)	0.97 - 2.25 0.90 - 2.24	High	Strings
2	Spatial Support	ST1 Top/ Sides (dB)	-7 - 2	Mid	Individual
3	Omni Late Strength	$G_{40-\infty}$ (dB)	12.6 - 18.8	Mid	Winds

The three dimensions for the ensemble playing test conditions were interpreted as described in Table 5.6:

Table 5.6: Summary of Perceptual Dimensions, Ensemble Condition

Dimension	Name	Parameter (Preferred Values)	Group
1	Spatial Homogeneity, Strength	DD_{0-30} (Low), UpDn-Stage G (Low), Cross-Stage G (High)	All
2	Spatial Support	LQ_{740} Top/Sides (Low)	All
3	Signal Transfer, Spatial Reverberance	MTF (Mid), EDT Top/Rear (High), RR_{160} Rear (Low)	All

CHAPTER 6

ARCHITECTURAL INVESTIGATIONS

6.1 Introduction

The previous chapters outlined and tested a methodology for high-resolution spatial auralization in subjective testing with musicians. The subjects evaluated a set of measurements from 10 different concert hall and theatre stages and ranked the measurements in order of preference. Based on a multidimensional analysis, musician preference was best described using three perceptual factors, aligning with orthogonal axes in 3-dimensional space. These parameters correlating with these factors differ under solo playing or ensemble playing conditions. To summarize, the factors for each condition are shown in Table 6.1.

Table 6.1: Subjective Test Results: Perceptual Factors

	Soloist	Ensemble
Dimension 1	Reverberance	DD_{0-30} , G Cross-stage vs. UpDown-Stage
Dimension 2	ST1 Top/Sides	LQ_{740} Top/Sides
Dimension 3	$G_{40-\infty}$	MTF, Running Reverberance Top/Rear

Although parametric differences have been examined between the measured halls, and preference has been organized in terms of perceptual factors, it is still difficult to determine what salient architectural parameters align with objective parameters and influence subjective preferences without testing these parameters in a controlled environment. Given a different set of halls with a different range of architectural variations, different perceptual factors may be aligned with preference. It is not possible to determine with certainty whether specific geometric elements or surface types in these halls were major drivers in the parameters listed above. This chapter attempts to hypothesize what relationships are possible between architecture and these measured parameters by creating a computer model of one

hall and testing architectural variations. However, in order to determine whether these relationships are truly driving subjective preference, further tests are necessary. Conclusions regarding the influence of architectural changes on subjective preference would require performing controlled experiments with new stimuli, in which only predetermined architectural elements were varied.

At the time of this research, several limitations prevented such tests. First, as this chapter will show, currently available computer modeling techniques mainly consist of ray-tracing algorithms, which are limited in their ability to accurately model spatial variations. The computer models are still used for design purposes and could be used for real-time optimization of architectural elements, but these sessions would likely be supplemented by real-life design expertise and not based on setting criteria for acoustic parameters. Wave-based methods or physical scale models would be more accurate for producing test stimuli, but are not technologically feasible at this time. Measurements in real spaces, while time consuming and costly, can provide the most accurate virtual auralization experience. It seems logical that a space with variable elements (canopies, shells, risers) is accessible, it would make more sense to bring the musicians into the actual space and complete tests in the real environment. However, as shown in previous chapters, the major benefits of virtual reproduction in the SoundLab are that stimuli are repeatable and A-B comparisons can be made without time lapse. The same music can be heard or played in multiple spaces within a short span of time. Even if variations are made within the same hall, canopies, acoustic banners, and risers can take several minutes to move in and out, during which time the auditory memory of the test subject is strained and comparisons may be suspect.

This chapter attempts to show the possible application of the test method described in Chapter 5 to architectural design. It aims to show the benefit of such methodology for future experiments with more controlled stimuli, such as measurements from a single space with variable acoustics, and how such tests could benefit the field of architectural design for optimal stage acoustics. It attempts to lay out initial observations and hypotheses regarding architectural elements that may be relevant for such test measurements. As mentioned above, the best available method

for this initial study is a computer model using ray-tracing algorithms. With this method, 2nd-order ambisonic impulse responses can be generated and analyzed using the same beamforming methodology applied to the measured IRs. There are several limitations to ray-tracing algorithms, namely when modeling scattering surfaces and short source-receiver distances. Both limitations have significant influences on the absolute accuracy of onstage source-receiver pairs. However, some initial observations can be made about relative differences between IRs due to architectural variations.

6.2 Methodology

For this study, a computer model was created in CATT-Acoustic of the highest-ranked hall, Kodak Hall at Eastman. Multiple variations (8) were made to the stage enclosure while the architecture of the house remained constant. The reverberation time of the model was calibrated to that of the unoccupied measured hall. In the measurements, several chairs were arranged on the stage floor, although they were unoccupied. This has been approximated in the model with higher absorption and scattering coefficients applied to the stage floor. The CATT model is shown in comparison to the measured space in Figure 6.1.

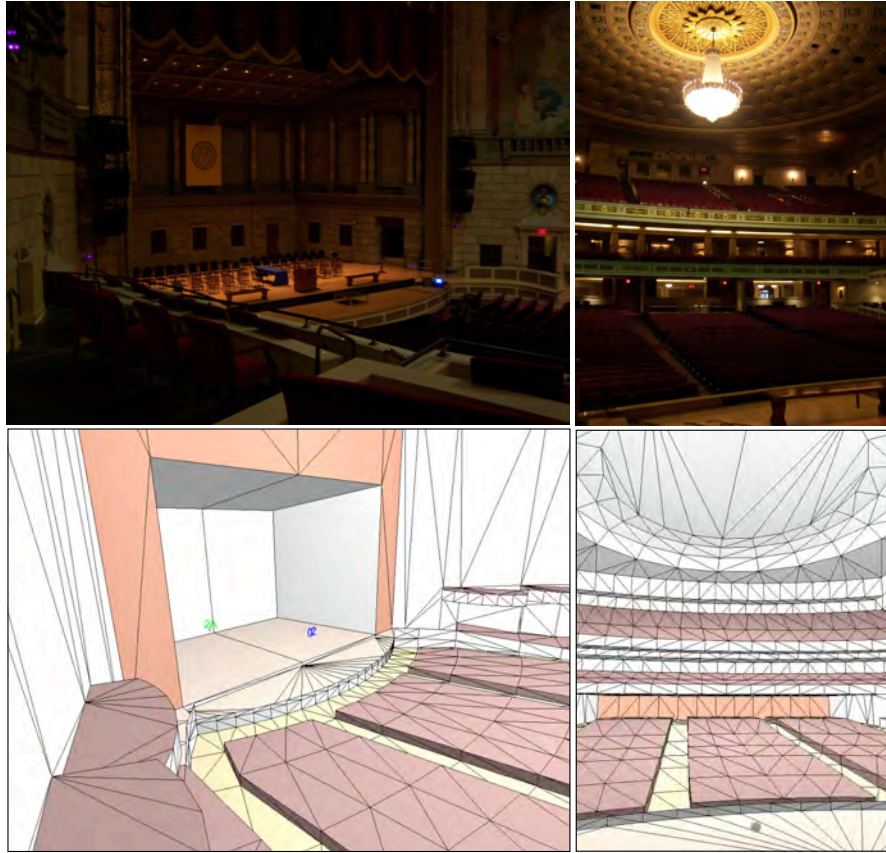


Figure 6.1: Kodak Hall, Eastman: CATT-Acoustic Model

The variations made to the stage enclosure are shown in Figure 6.2. The variations are described below. In each case, all other elements remain the same as the existing enclosure:

1. **Existing:** Calibrated to existing Eastman Stage Enclosure.
2. **High:** Enclosure ceiling raised 3 meters.
3. **Wide:** Enclosure side walls moved out 1.5 meters each (3 meters total).
4. **Deep:** Enclosure rear wall moved back 3 meters.
5. **Diffuse:** Existing enclosure with increased scattering coefficients on walls and ceiling.
6. **Small:** Enclosure walls and ceiling moved in by 3 meters.

7. **Flat:** Enclosure wall and ceiling angles changed to 90° .
8. **Curved:** Enclosure walls and ceiling replaced with convex elements.
9. **Angled:** Enclosure wall and ceiling angles increased by decreasing the rear wall size by 3 meters (height and width).

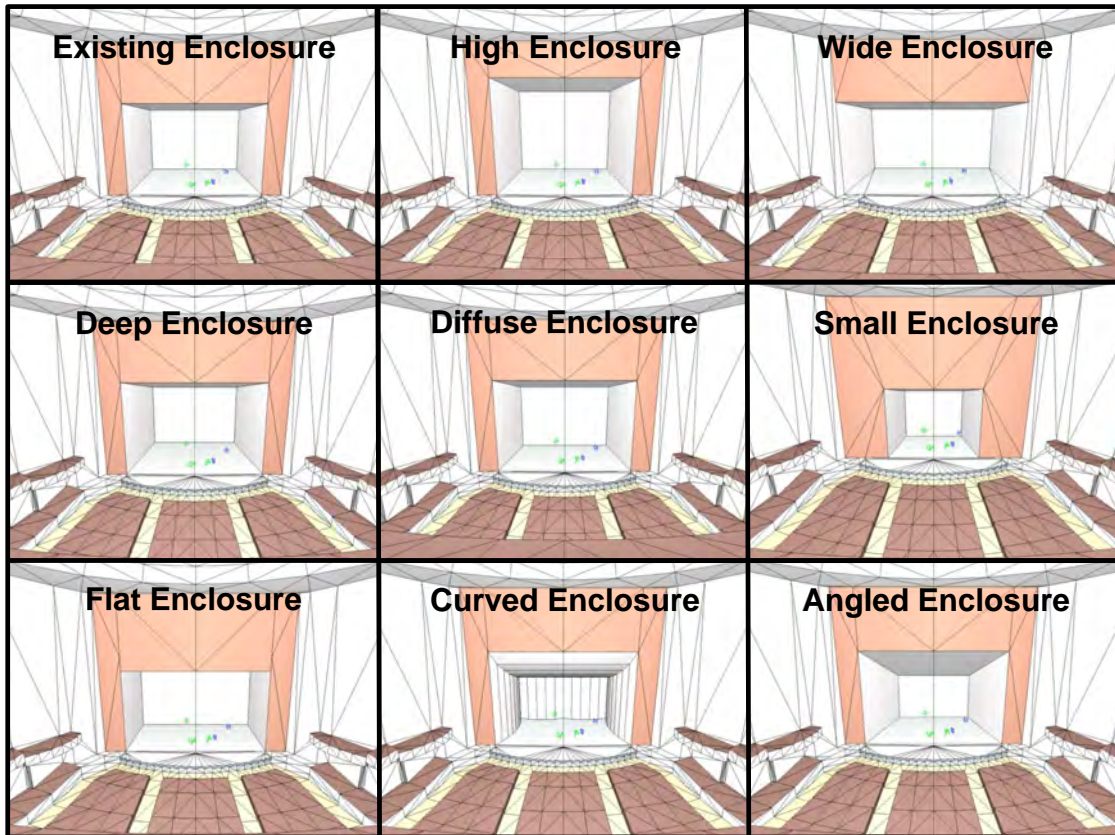


Figure 6.2: Kodak Hall, Eastman: Variations on Stage Enclosures Modeled in CATT-Acoustic

6.3 Results

The parameters described in Section 3.4 were calculated for each variation. The most relevant parameters determined by multiple regression in Section 5.5.2 are shown below. For the soloist source-receiver pair, the parameters aligning with each dimension are shown in Figures 6.3 - 6.6.

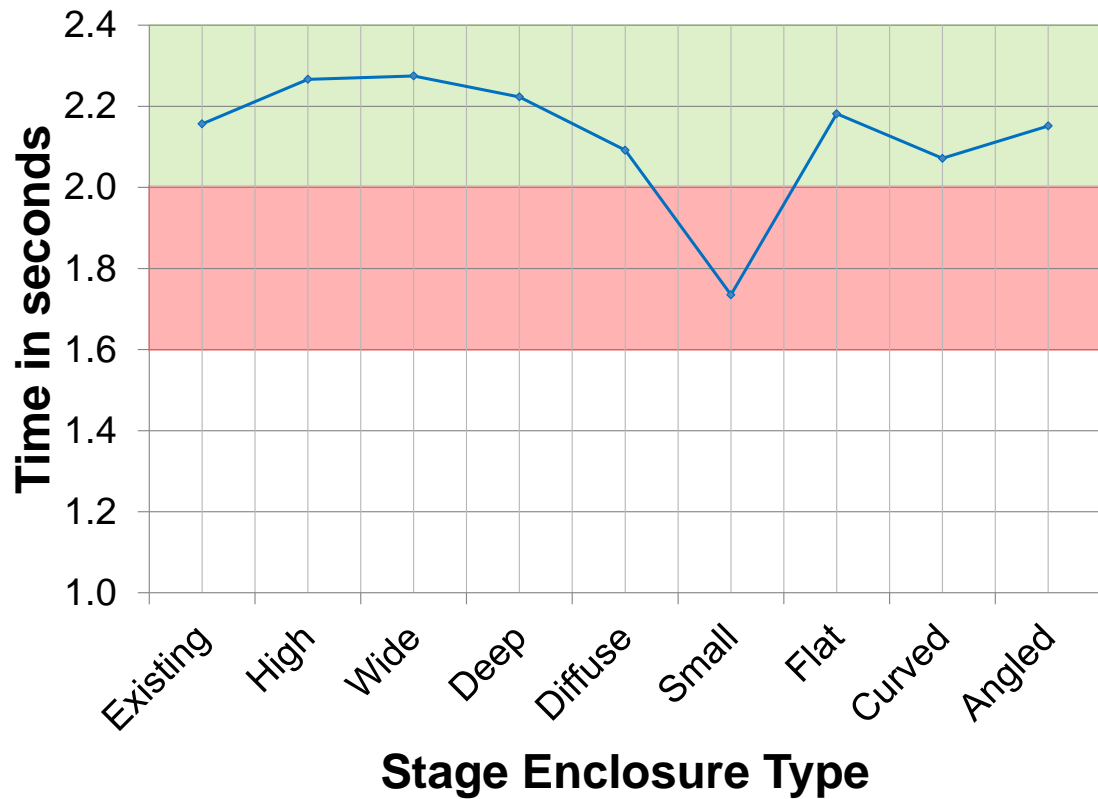


Figure 6.3: Eastman Model: Solo Parameters (Modeled Onstage T_{30})

The first parameter, T_{30} , is the parameter that most closely matches that of the measured IR. Variations in T_{30} by stage enclosure (Figure 6.3) are most likely due to the overall changes in volume created by moving the enclosure walls in or out. As expected, the changes that increase that volume (high, wide, deep, and flat) have higher values of T_{30} , and those that decrease the volume or increase the diffusion level (small, curved, diffuse, angled) have lower values. Of course, T_{30} is strongly affected by changes in the house as well, so any correlation between T_{30} and stage enclosure design is likely driven by volumetric increases and increased coupling between the stage enclosure and the house.

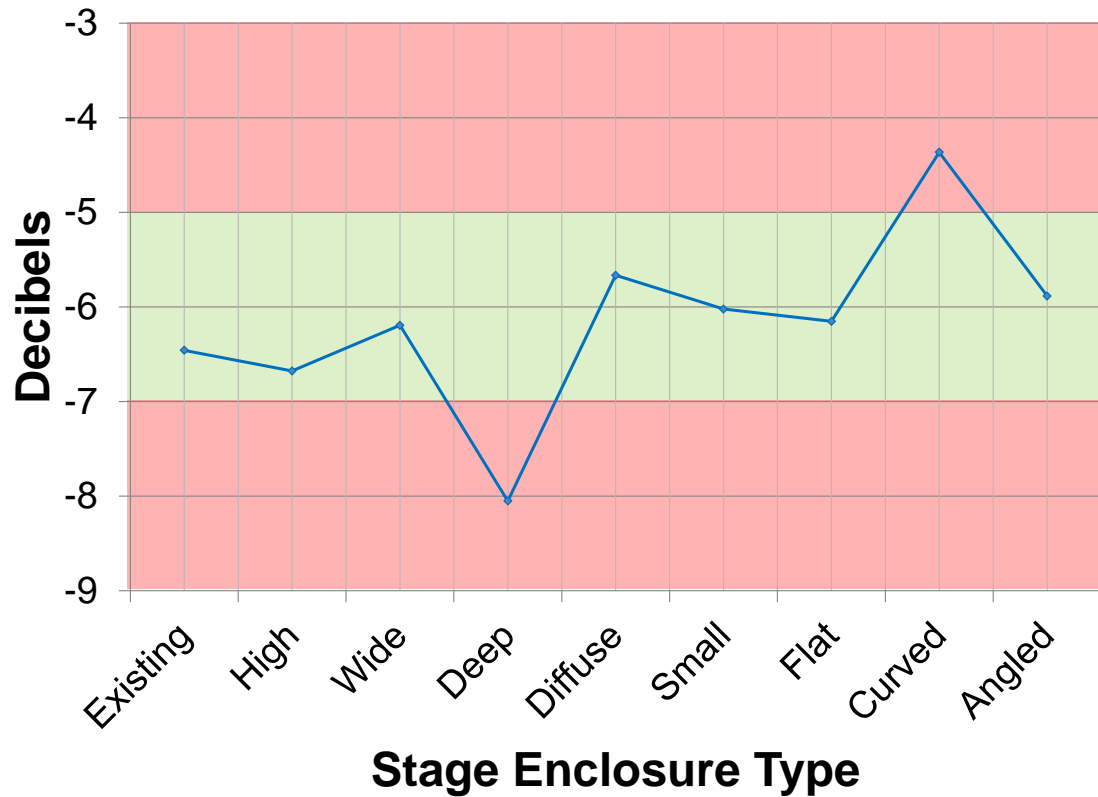


Figure 6.4: Eastman Model: Solo Parameters (Modeled ST1 Top/Sides)

For the second parameter, ST1 Top/Sides, preferred values formed a bell curve, with -3 dB as an ideal value out of a range between -7 dB and $+2$ dB. The measured IR for Eastman has a STI Top/Sides value of -2.6 dB. In the CATT model, this parameter has a value of -6.5 dB, as the source-receiver distance of only 1 meter creates an unrealistically high direct sound level in relation to the early energy due to the limitations of the ray-tracing algorithm (Figure 6.4). However, it is still possible to compare the relative differences in ST1 for the various CATT models. As expected, the high enclosure has less supporting early energy from the top, whereas the wide enclosure has less from the sides. The increase in scattering (Diffuse, Curved) actually serves to decrease the relative amount of lateral support. Interestingly, it is the increase in enclosure depth that decreases the ratio the most. This could be because the energy of second-order reflections from the rear wall to the ceiling is decreased. Looking back at the measured halls, the highest value of

ST1 Top/Sides is from Bard, where the stage is 5 meters deeper than it is wide. On the other hand, the ceiling is relatively low and there are convex reflectors on both the walls and ceiling, both criteria that have been shown by the CATT study to increase the ST1 value. This shows that combinations of these architectural criteria may have different effects than indicated by the individual changes. The lowest values for ST1 Top/Sides are found in the theatre spaces (Albany and EMPAC), where the presence of a fly tower prevents strong early energy from reflecting off the ceiling. For reference, the omnidirectional values of ST1 are shown in Figure 6.5.

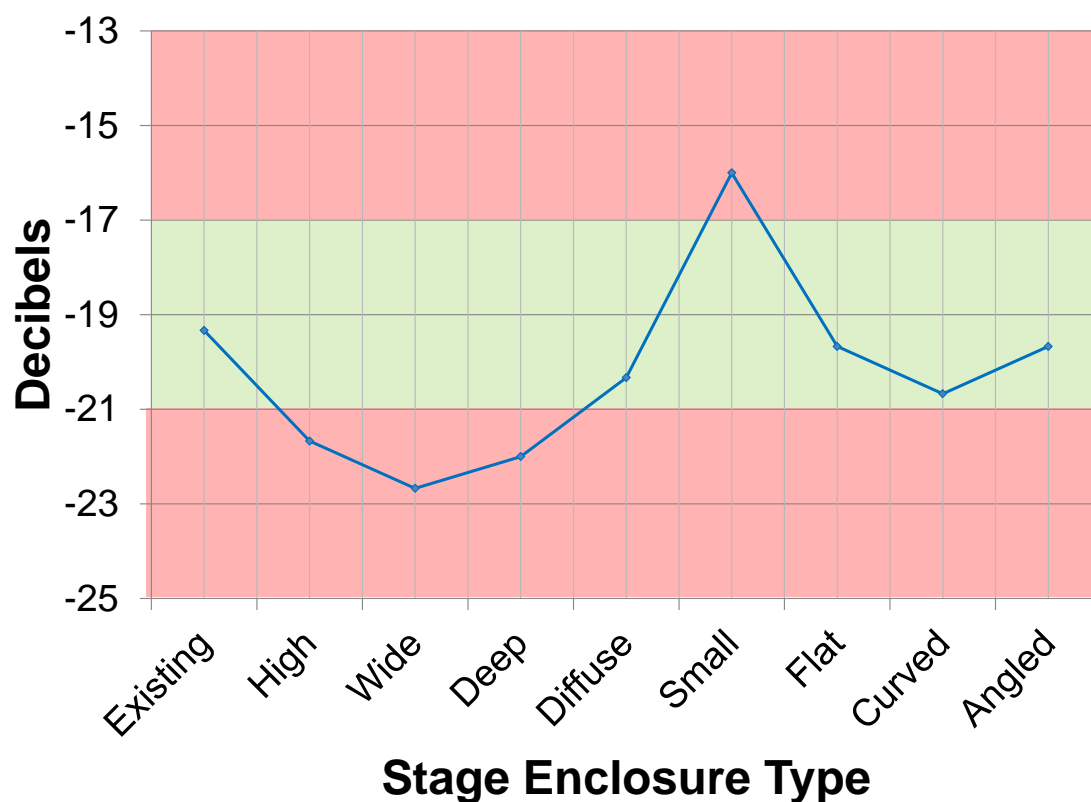


Figure 6.5: Eastman Model: Solo Parameters (Modeled ST1)

As shown above, the overall value of ST1 is lowest for the wide, deep and high enclosures, and highest for the small enclosure. This correlates well with the measurements, where Vassar and St Rose have both the smallest enclosures and the highest ST1, and value continues to decrease in roughly inverse proportion to stage size. Scattering and angles seem to have little effect on the overall ST1

value, indicating these have more influence over the spatial distribution of supporting energy.

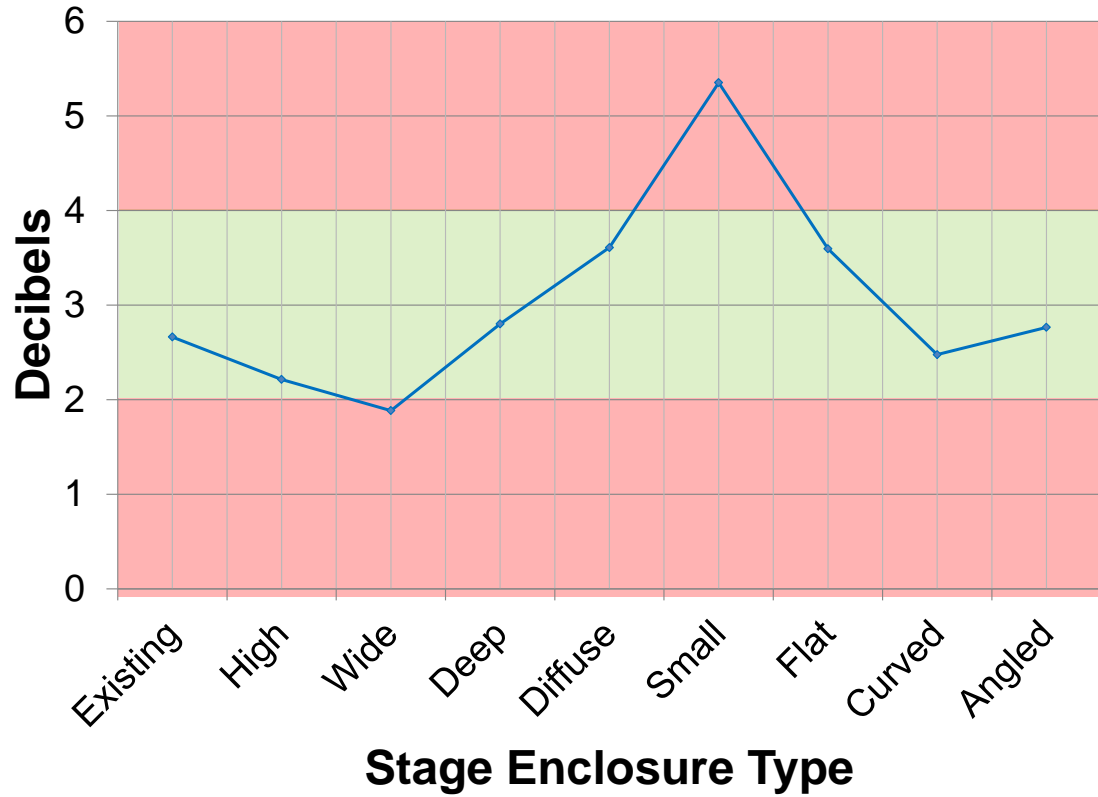


Figure 6.6: Eastman Model: Solo Parameters (Modeled $G_{40-\infty}$)

For the third parameter, $G_{40-\infty}$, preferred values again followed a bell curve for the measured halls, with ideal values of approximately +16 dB in a range between +12 dB and +18 dB. In the measured IRs, Eastman had a value of +16.2 dB, whereas the CATT model produces a value of +2.7 dB. Again, an unrealistically high direct sound produces lower levels of late energy in CATT (Figure 6.6). For this parameter, the high and wide enclosures have the lowest values of late strength and the small enclosure has the highest. Diffuse and flat enclosures are higher than the existing enclosure. Evenly applied scattering in the enclosure could serve to increase the amount of higher-order reflections between enclosure surfaces. This is also true of smaller enclosures and those with parallel walls/ceiling. Although it would need to be investigated in a measured scenario, these higher values are likely to be less

desirable than the existing enclosure values. Deep, angled and curved enclosures all provide little change to the late strength from the existing enclosure, implying that some of this parameter is driven by the energy from the house, which is likely to be driven by reflections from the sides and top of the enclosure (thus the low values in high and wide enclosures).

Looking at the measured halls, the highest value of $G_{40-\infty}$ was found in Vassar, which has a small enclosure with parallel side walls. St. Rose (curved reflectors), Buffalo (strong sidewall angles) and Eastman all have similar values centered around the top of the bell curve. The theatres have slightly lower values, likely due to the fly tower and wings, and Skidmore is also low, perhaps because of the lack of solid ceiling surface (the actual ceiling is 3 meters above the grid of small, modular reflectors). However, Bard has the lowest value of $G_{40-\infty}$ despite the presence of a low ceiling, curved elements and a deep stage (as shown in Figure 6.7. In this case, it is possible that the house has more influence on the late strength, which was not addressed in the CATT study due to the large increase in possible architectural criteria. The volume of the Bard house is larger than halls with higher late strength, such as Vassar and St. Rose. Additionally, a quick observation shows that while some of the other large halls have a relatively constant ceiling height throughout the house, the ceiling at the rear of the Bard house forms a set of reverse convex reflectors, sending sound down into the audience where it can be more quickly absorbed. Also the balconies, where early sound is often reflected to the stage from the house area, are broken up, causing the reflected sound to scatter. More investigation would be necessary to isolate any architectural criteria from the house influencing the acoustics onstage.



Figure 6.7: Bard House Ceiling: Curved Panels

For the two tested ensemble source-receiver pairs (cross-stage and up-down-stage), the parameters best aligned with each dimension are shown in Figures 6.8 - 6.24.

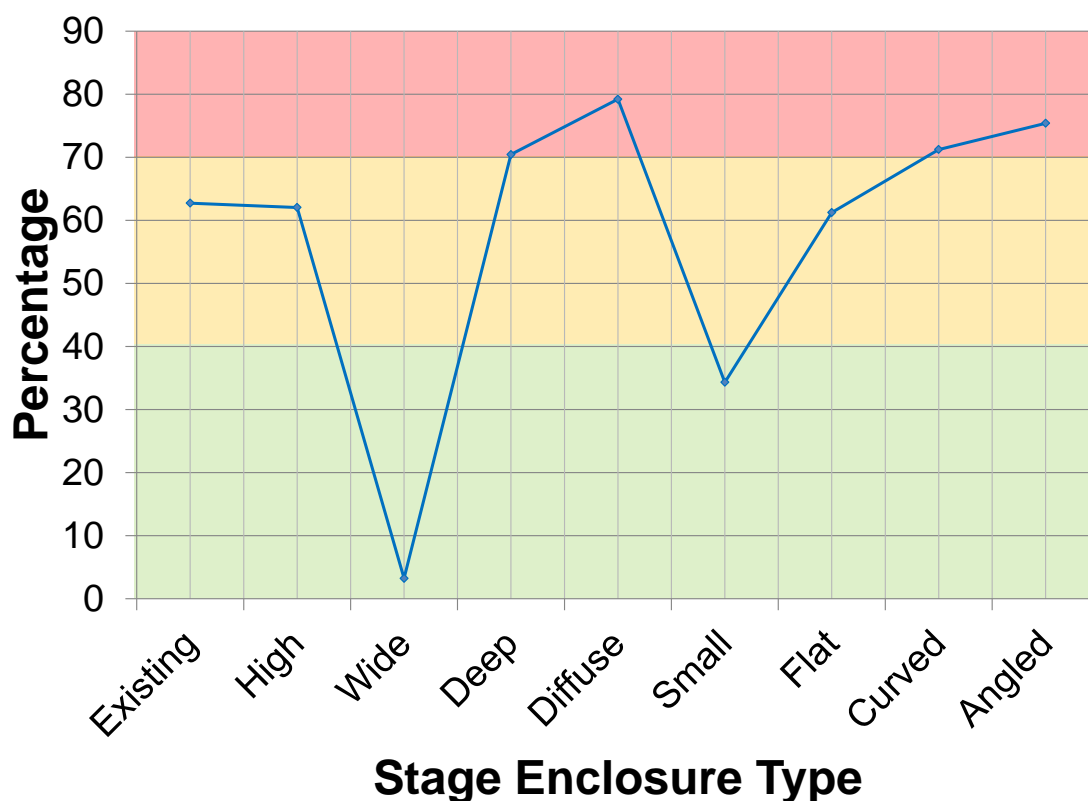


Figure 6.8: Eastman Model: Ensemble Parameters (Modeled Cross-Stage DD_{0-30})

The first dimension is best aligned with cross-stage values of early directional diffuseness, or DD_{0-30} , shown in Figure 6.8. Lower values were preferred. Measured values ranged from 0.4% to 70%, with Eastman at the lowest, or 0.4%. In the CATT study, the value of the existing enclosure was 62%. At first, this seems counter-intuitive, given CATT's tendency to underestimate diffuse energy in the early part of the IR. However, on closer examination of the model using image source modeling, it becomes apparent that DD_{0-30} can be increased just as much by a few strong reflections in opposition to the source location as it can by a large amount of small diffuse reflections. Some images of the early reflections in the model are shown in Figure 6.9.

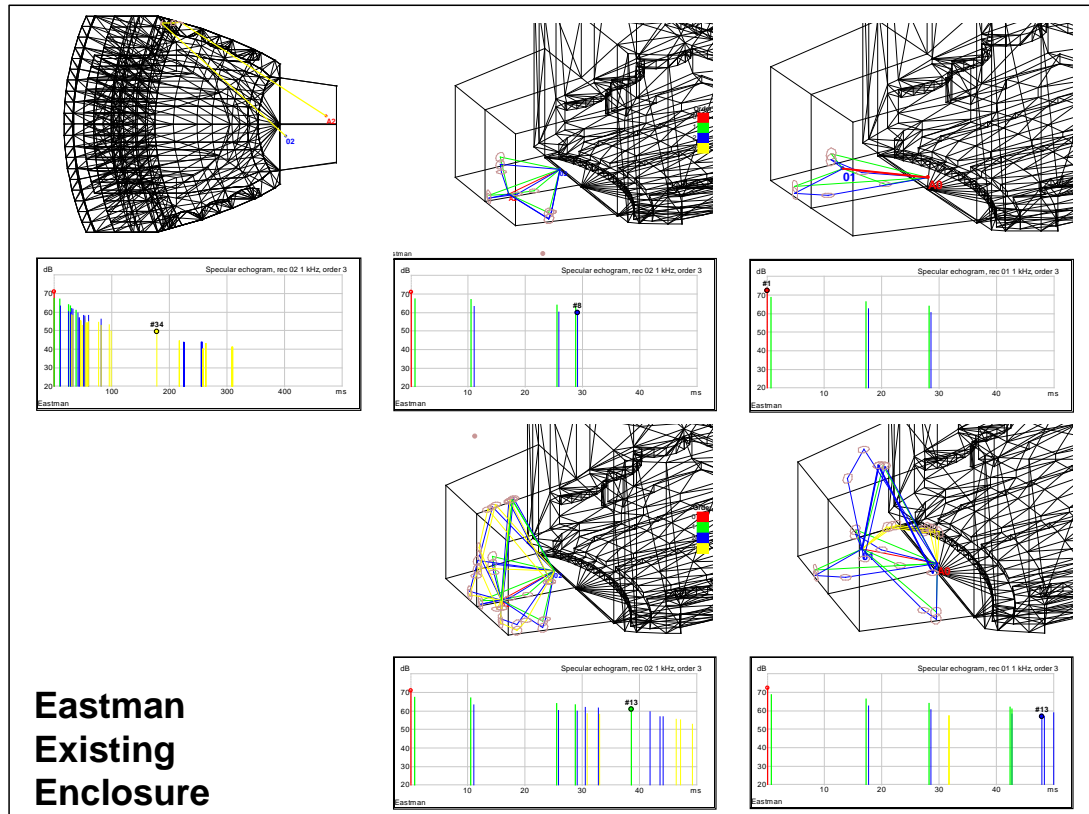


Figure 6.9: Eastman Existing Model: Image Sources (Direct Sound = Red, Reflections: 1st Order = Green, 2nd Order = Blue, 3rd Order = Yellow)

These specular reflections are all at a relatively low level, which in the measurements were likely obscured by chairs onstage, as shown in Figure 6.1. While the stage floor is given higher scattering properties in the model, it cannot account for the grazing incidence at the chairs above the floor. This kind of arrangement was not present in any of the other measured halls and could account for the extremely low levels of early *DD*. In spite of this, the measurements still showed a wide range of values for this parameter, indicating that the Eastman measurement was not an outlier. Additionally, even with the limitations of ray-tracing for this type of parameter, it is still possible to make direct comparisons between the modeled variations.

In the CATT model of the existing enclosure, the energy is relatively even in the horizontal plane, with more energy distributed from the front (source) and rear

(rear wall reflection) and slightly less from the sides. Energy from the ceiling does not arrive within the 30 millisecond window, and therefore the homogeneity is 62%. In comparison, the models with the lowest values of DD_{0-30} are the wide and small enclosure (Figures 6.10 and 6.11).

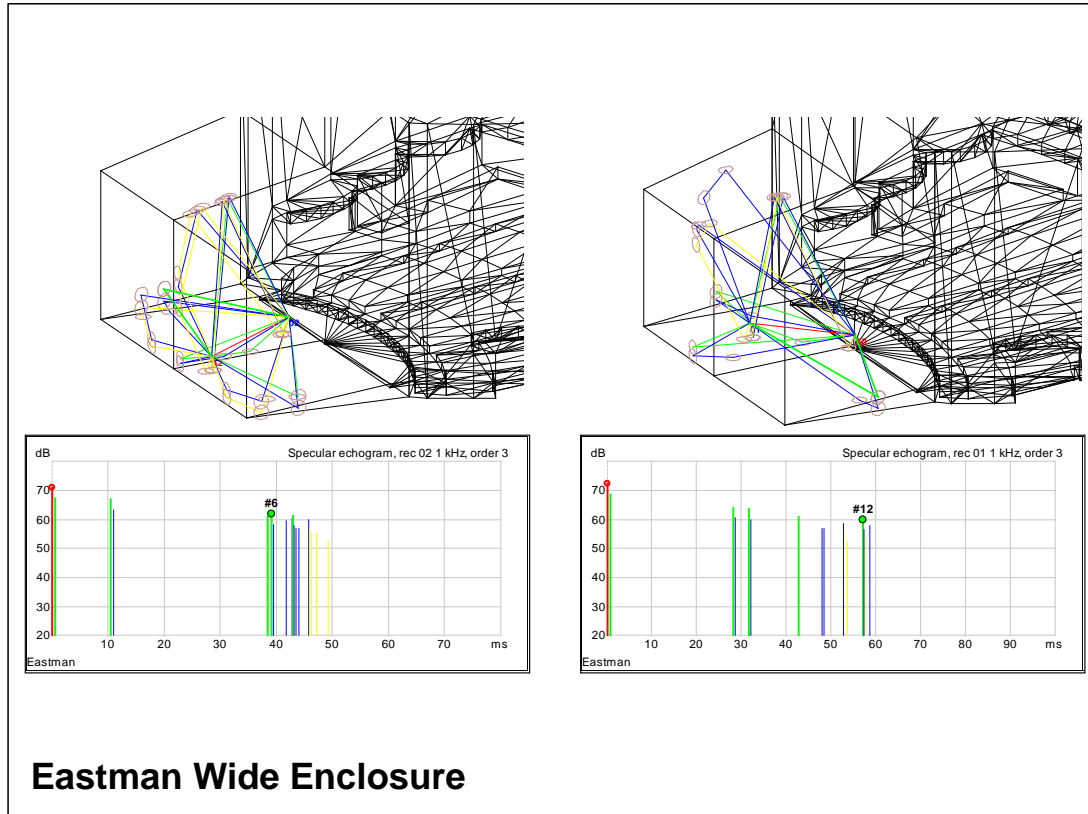


Figure 6.10: Eastman Wide Model: Image Sources (Direct Sound = Red, Reflections: 1st Order = Green, 2nd Order = Blue, 3rd Order = Yellow)

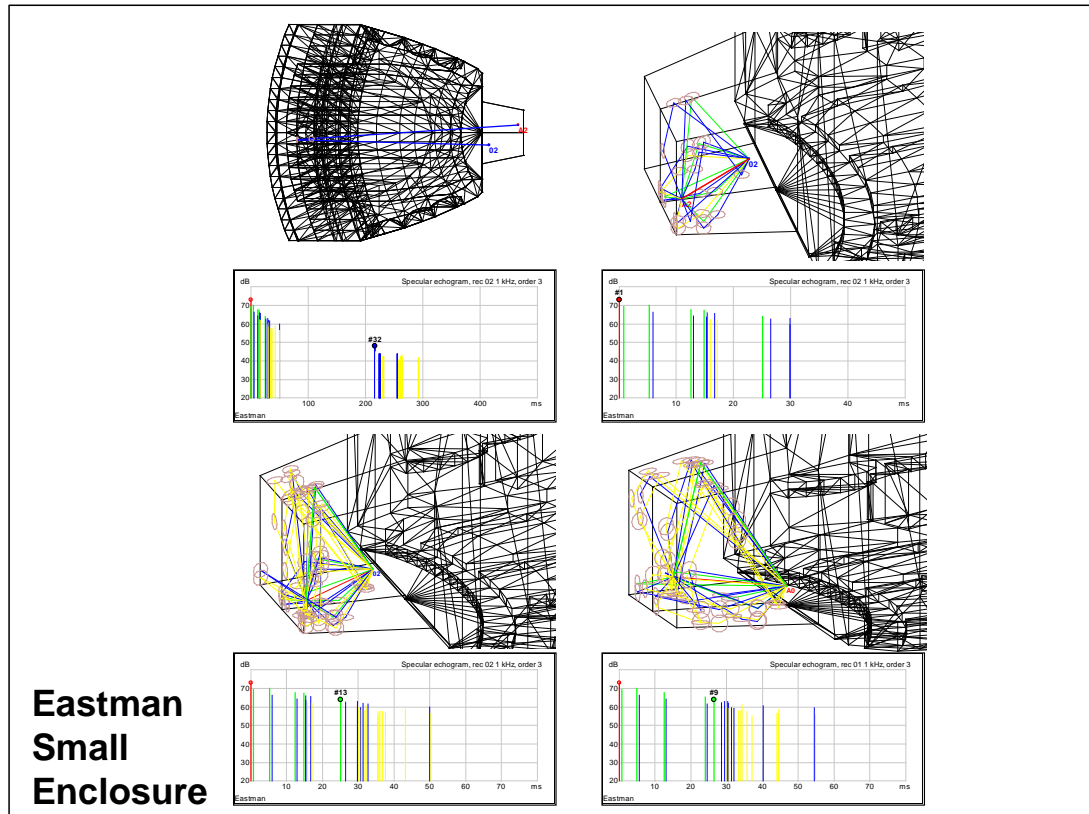


Figure 6.11: Eastman Small Model: Image Sources (Direct Sound = Red, Reflections: 1st Order = Green, 2nd Order = Blue, 3rd Order = Yellow)

The wide enclosure is clearly less spatially homogenous, as the distance to the side walls pushes the lateral reflected energy outside of the 30 millisecond window, resulting in skewed distribution from the front and rear. However, in the case of the small enclosure, the opposite is true, as all surfaces are brought within a distance allowing first-order and even a few second-order reflections from every surface to arrive within 30 milliseconds. However, the proportionate distances are still not even, as the rear wall is closest and the ceiling is furthest away, and the differences are magnified within the earlier time range. Additionally, these strong reflections all come from the rear of the enclosure, skewing the distribution behind the receiver.

Diffuse, angled and curved enclosures all had increased values of DD_{0-30} . Image sources for the curved and angled models are shown in Figures 6.12 and 6.13.

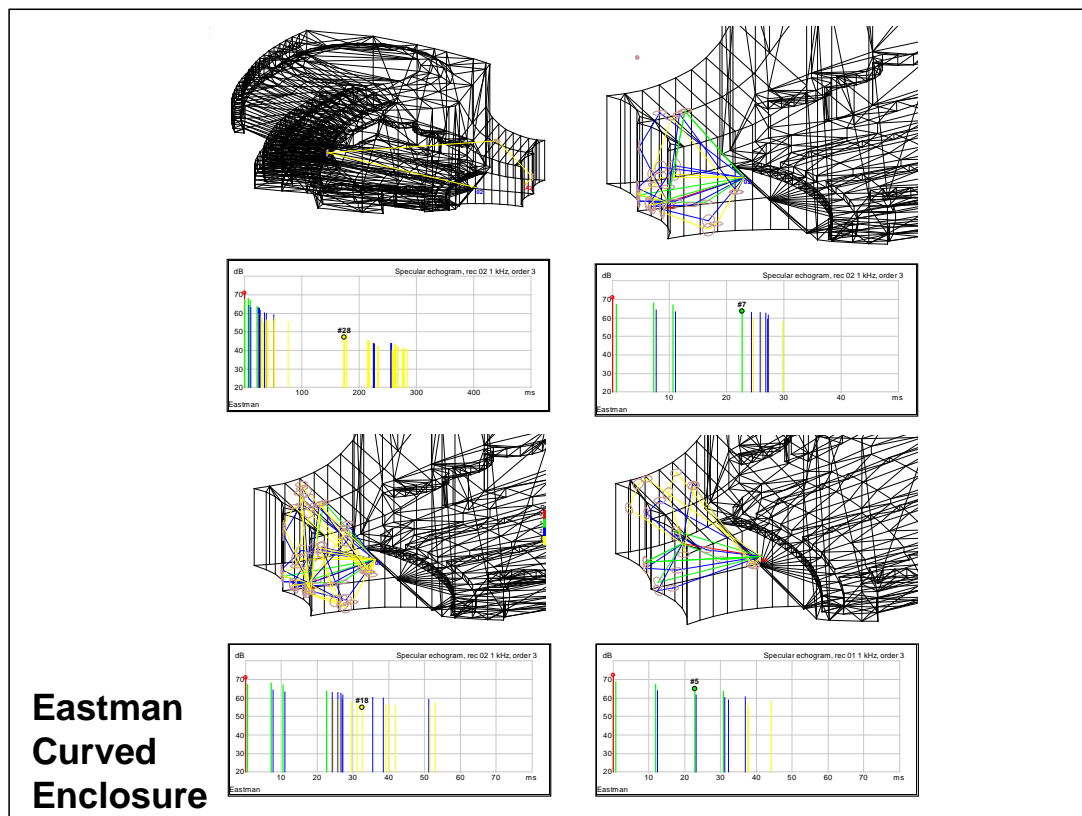


Figure 6.12: Eastman Curved Model: Image Sources (Direct Sound = Red, Reflections: 1st Order = Green, 2nd Order = Blue, 3rd Order = Yellow)

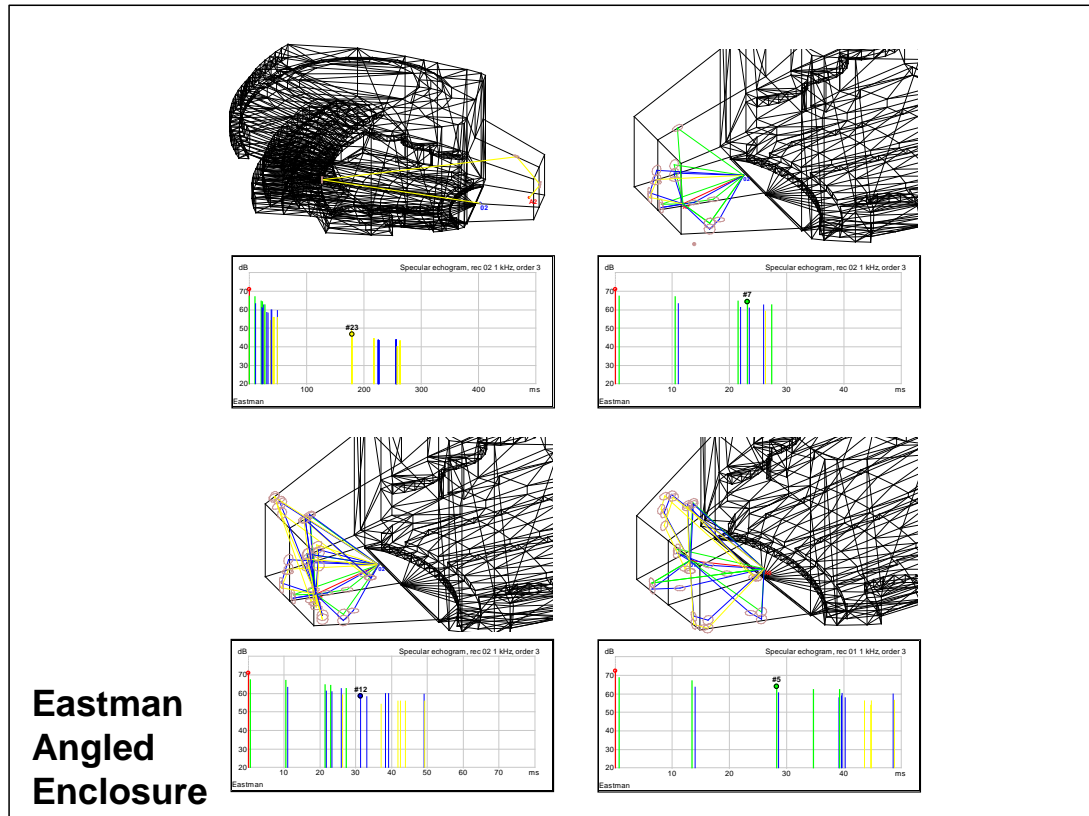


Figure 6.13: Eastman Angled Model: Image Sources (Direct Sound = Red, Reflections: 1st Order = Green, 2nd Order = Blue, 3rd Order = Yellow)

The curved and diffuse enclosures are expected to become directionally diffuse at a faster rate, because there are more available paths for early reflections. The angled enclosure can be explained by the particular source-receiver arrangement, as the particular angle used brings the adjacent side wall closer to the receiver, allowing the reflection to arrive earlier and offset the distribution from the direct sound.

The deep enclosure also had increased early *DD* (Figure 6.14). This is logical as the rear wall was disproportionately close to the receiver in relation to the other surfaces.

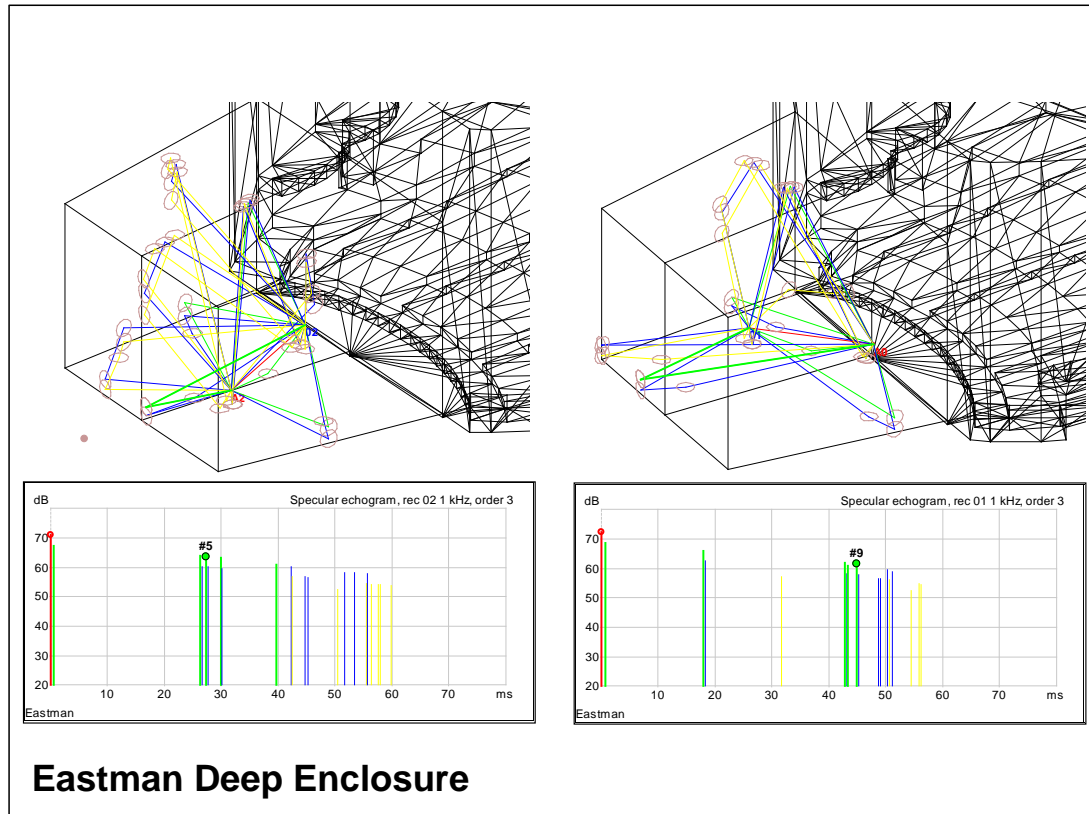


Figure 6.14: Eastman Deep Model: Image Sources (Direct Sound = Red, Reflections: 1st Order = Green, 2nd Order = Blue, 3rd Order = Yellow)

The high and flat enclosures showed little change from the existing enclosure (Figures 6.15 and 6.16). Again, this is logical as the ceiling height was already out of the 30 millisecond range in the existing enclosure, and the flat enclosure does not change the arrival time of any enclosure reflections.

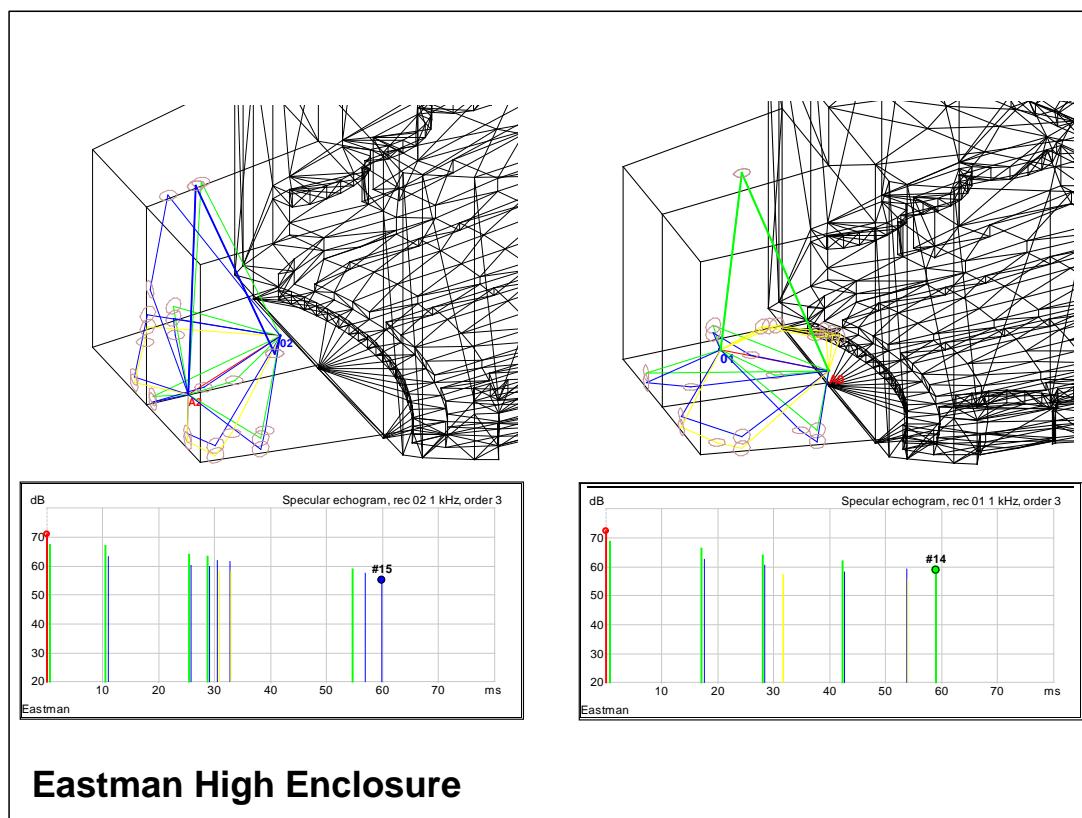


Figure 6.15: Eastman High Model: Image Sources (Direct Sound = Red, Reflections: 1st Order = Green, 2nd Order = Blue, 3rd Order = Yellow)

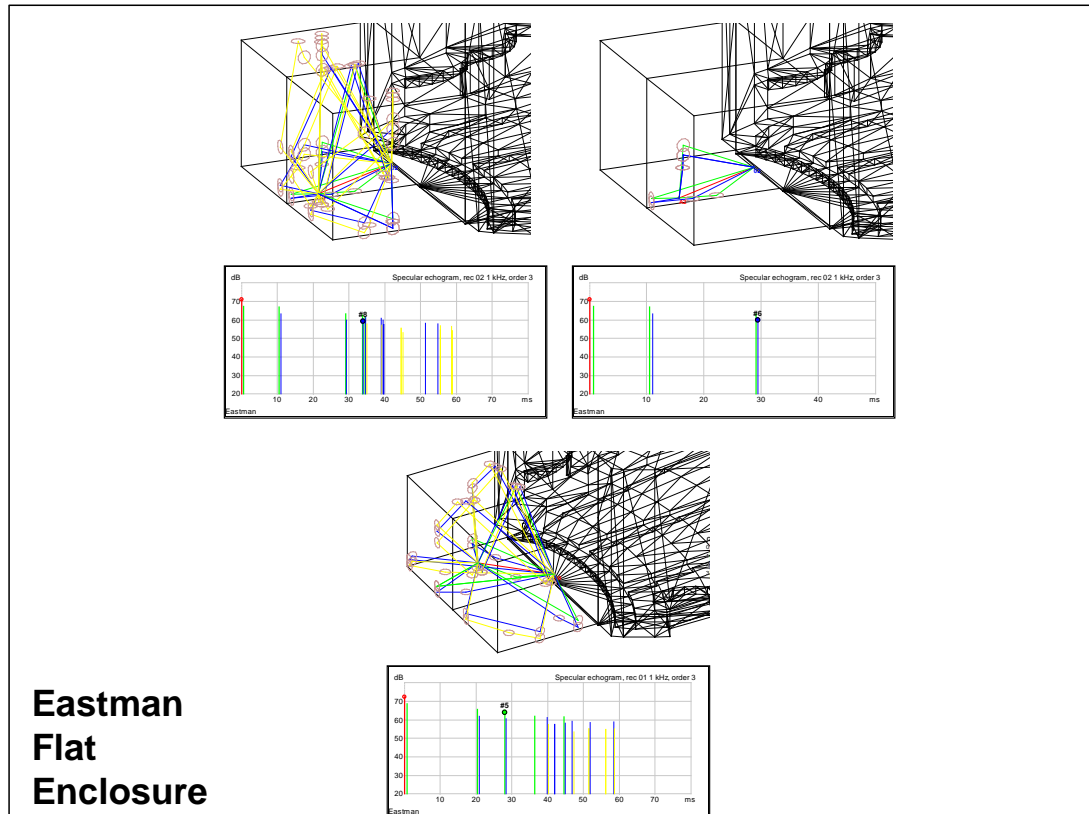


Figure 6.16: Eastman Flat Model: Image Sources (Direct Sound = Red, Reflections: 1st Order = Green, 2nd Order = Blue, 3rd Order = Yellow)

One other hypothesis for DD_{0-30} differences was that directional diffuseness could be influenced by higher energy levels from the house, but as shown in Figures 6.9, 6.11, 6.12, and 6.13 above, specular energy from the house does not arrive until after 180 milliseconds in Eastman. Although this is a relatively large space compared to some of the other measured halls, any reflecting surface from the house would need to be within approximately 30 feet of the stage (for the cross-stage source receiver pair) to contribute to the parameter. However, it could certainly contribute to the high level of early DD in Albany Recital Hall. Albany Recital has the highest value of early DD , has no real enclosure to separate it from the hall volume and also has the smallest house, with several house surfaces within that distance.

Looking to the other halls for reference, Eastman, Vassar, and Albany Theatre have the lowest values of DD_{0-30} . All of these spaces have proportionately high

ceilings. In addition, Albany Theatre has side wings to prevent strong lateral energy, and Vassar loses potential for high rear energy due to the organ chamber above the stage. Surprisingly, Bard and St. Rose, which have curved reflectors in the stage enclosure, have relatively low values of DD_{0-30} . Bard measurements were taken with risers, which may create some diffraction at stage level, obstructing reflections from the rear of the stage. Bard also has a disproportionately deep enclosure, which creates an imbalance of spatial energy as the rear wall reflections are pushed outside the 30 millisecond window. A basic CATT model was also made of Bard to demonstrate this, and is shown in Figure 6.17.

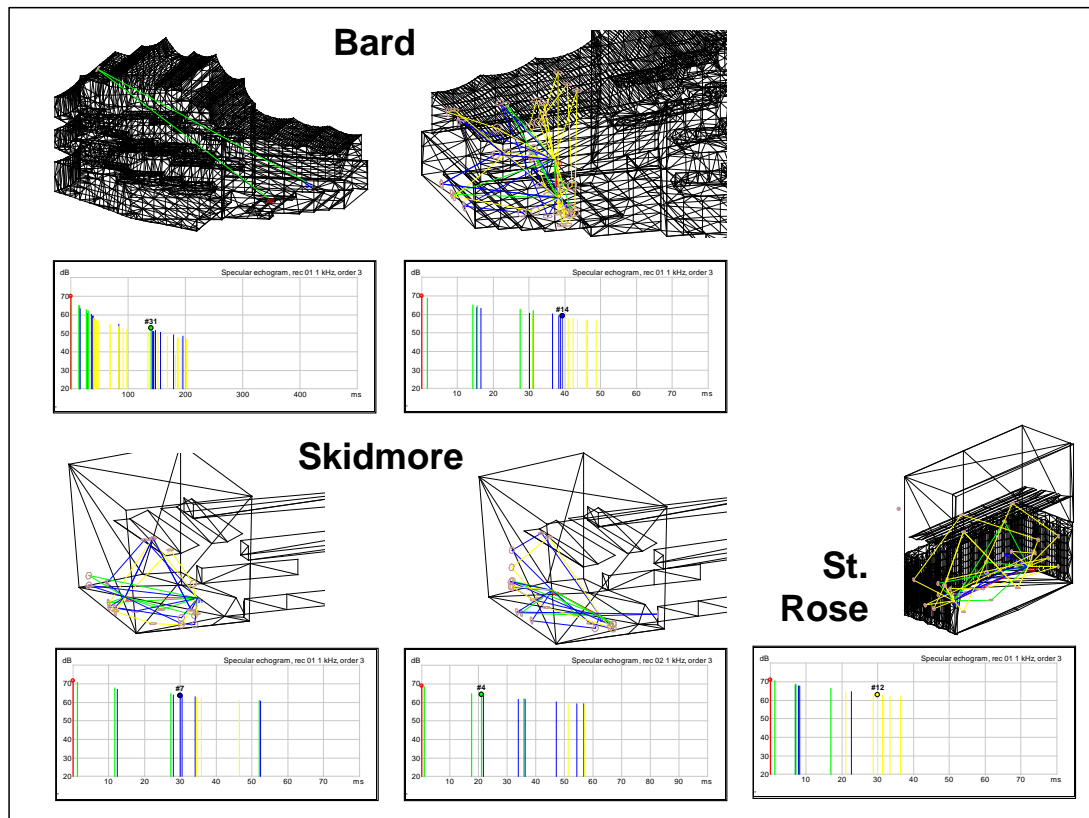


Figure 6.17: Bard, St. Rose, and Skidmore Models: Image Sources (Direct Sound = Red, Reflections: 1st Order = Green, 2nd Order = Blue, 3rd Order = Yellow)

St. Rose, also shown in Figure 6.17 (stage only) shows a significant amount of early energy, similar to the Eastman small enclosure. However, all this energy

is from the rear, because the enclosure is so short relative to its height and width, which may again have the counter-intuitive effect of lowering the levels of early DD . EMPAC Concert and Skidmore, with higher values, have more evenly proportioned enclosures.

However, another compounding factor is apparent when examining the measurements, which is that the source-receiver arrangement is not (due to the variation in stage size) ever exactly the same distance, meaning that the level and arrival time of the direct sound varies from hall to hall. As shown in the image source models, the direct sound has a significant impact on the spatial distribution. Therefore, it is possible that this parameter could be made more robust by removing the direct sound from the calculated time window. Additionally, it shows that DD_{0-30} in its current form may not be as robust as it appears at first due to the wide variation depending on location onstage. More investigation is needed to determine the best format for this parameter.

Along the same dimension, low values of all time windows for UpDown-Stage G and high values of all time windows for Cross-Stage G were preferred. In fact, it seemed unexpected that the late and early values of G for a single source-receiver pair would be more correlated than the early or late portions of G for different stage locations, as shown in Figure 6.18.

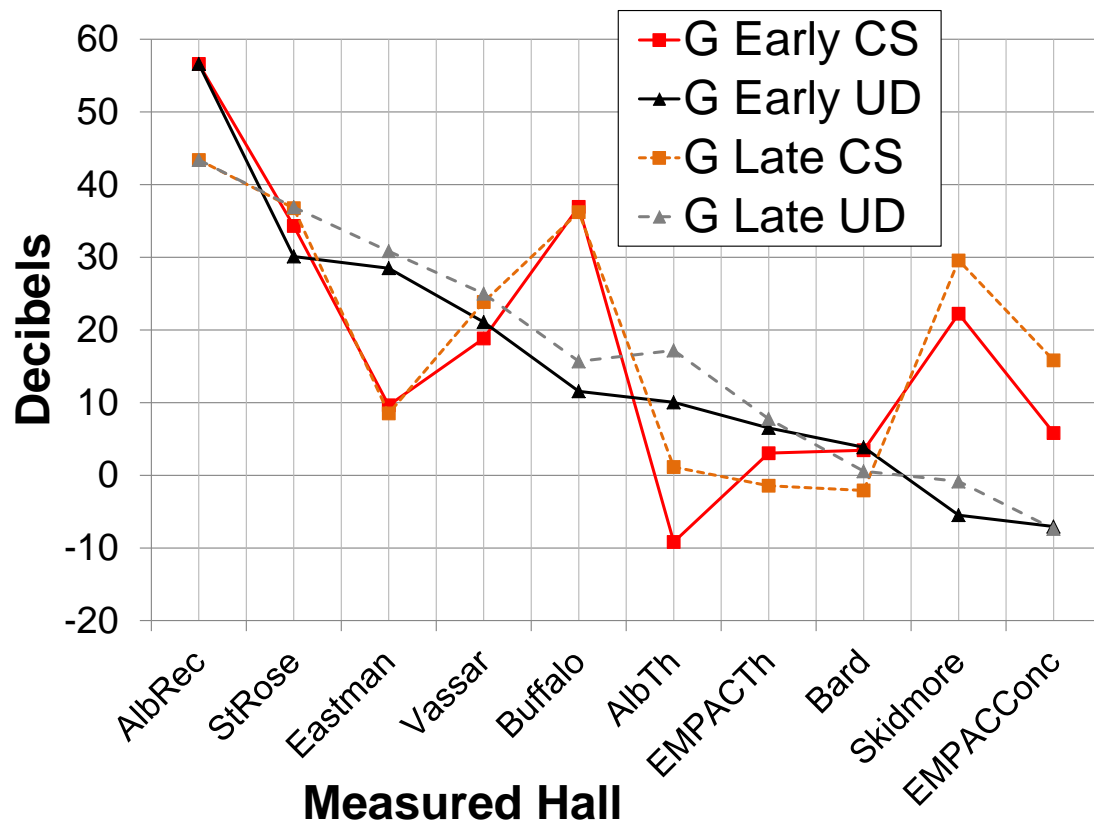


Figure 6.18: Eastman Measurements: Ensemble Parameters (Measured G , UD = UpDown-Stage, CS = Cross-Stage, Halls: AlbRec = SUNY Albany Recital Hall, AlbTh = SUNY Albany Theatre, EmpacConc = EMPAC Concert Hall, EmpacTh = EMPAC Theatre)

When examining the modeled variations, G behaves more as expected, with the early time windows for both Cross-Stage and UpDown-Stage well correlated and the late time windows correlated, but with a wide gap between the early and late portions for both positions, as shown in Figures 6.19 and 6.20.

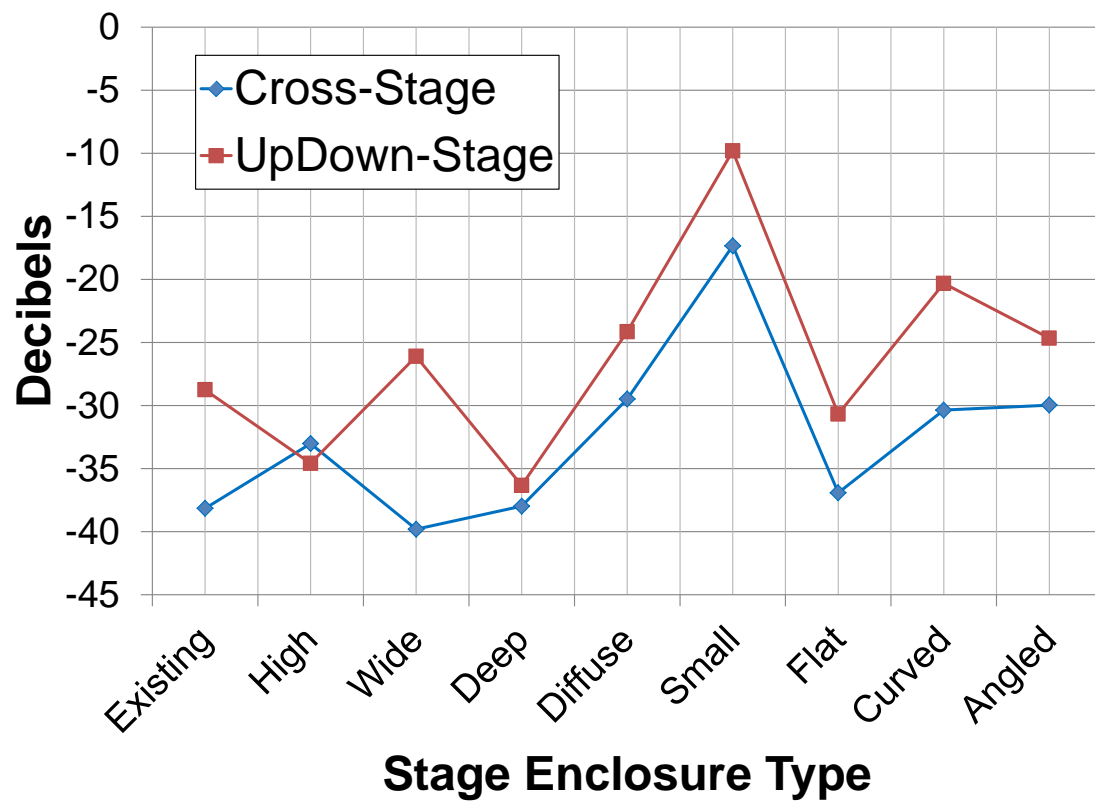


Figure 6.19: Eastman Model: Ensemble Parameters (Modeled Early G)

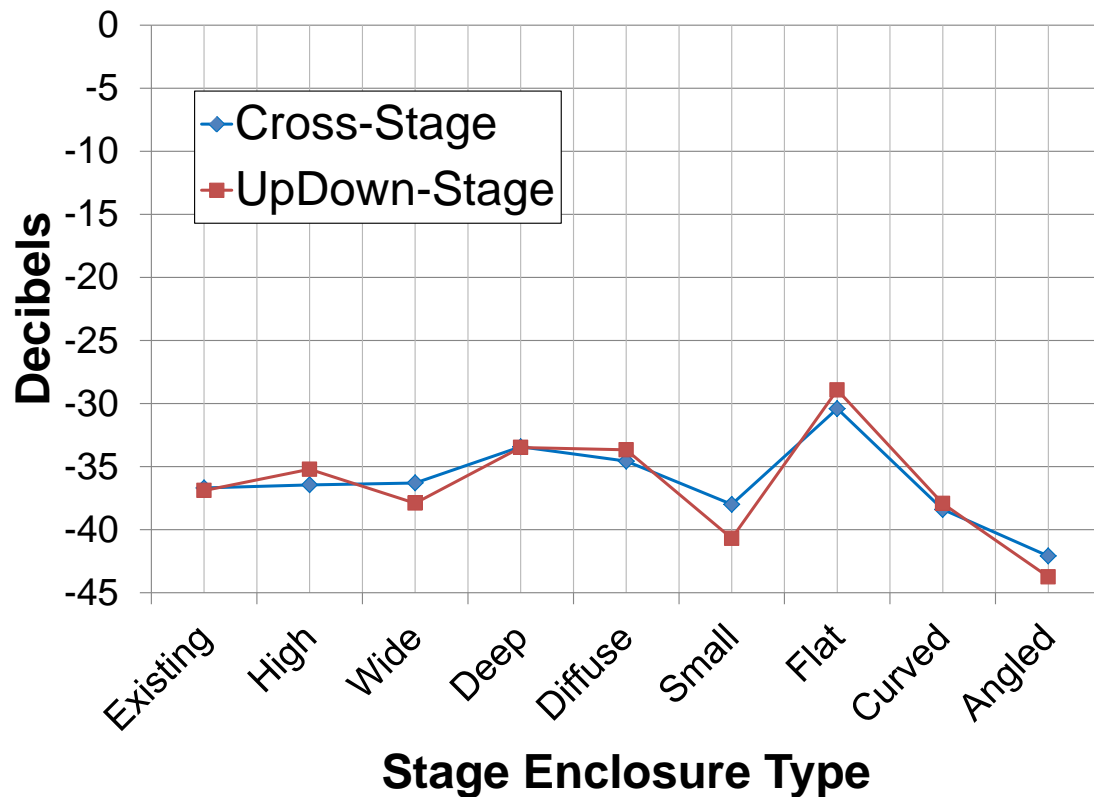


Figure 6.20: Eastman Model: Ensemble Parameters (Modeled Late G)

The differences in G for a single hall are smaller than those between halls. This indicates that G is highly dependent on hall size, stage size, and factors at a scale that were not examined in the CATT model. Also, the differences between cross-stage and up-down-stage positions seem to be driven by distance to nearby enclosure surfaces, which can increase the values of G . More investigation would be needed with a larger sample set of halls to determine the true influence of this parameter. However, basic examination of the modeled variations shows that stage location more strongly influences early G than it does late G . Additionally, the strongest contributor to late G appears to be the flat enclosure (perhaps due to late flutter echoes) whereas the small enclosure creates the highest early G , which is logical given the increased energy of reflections from closer surfaces. It also appears that enclosures with better coupling to the hall through angled surfaces actually increase early and decrease late G . The late energy is logical as the angle prevents

significant energy from returning from the hall and reflecting off enclosure surfaces. The increase in early energy could be related to the stage position.

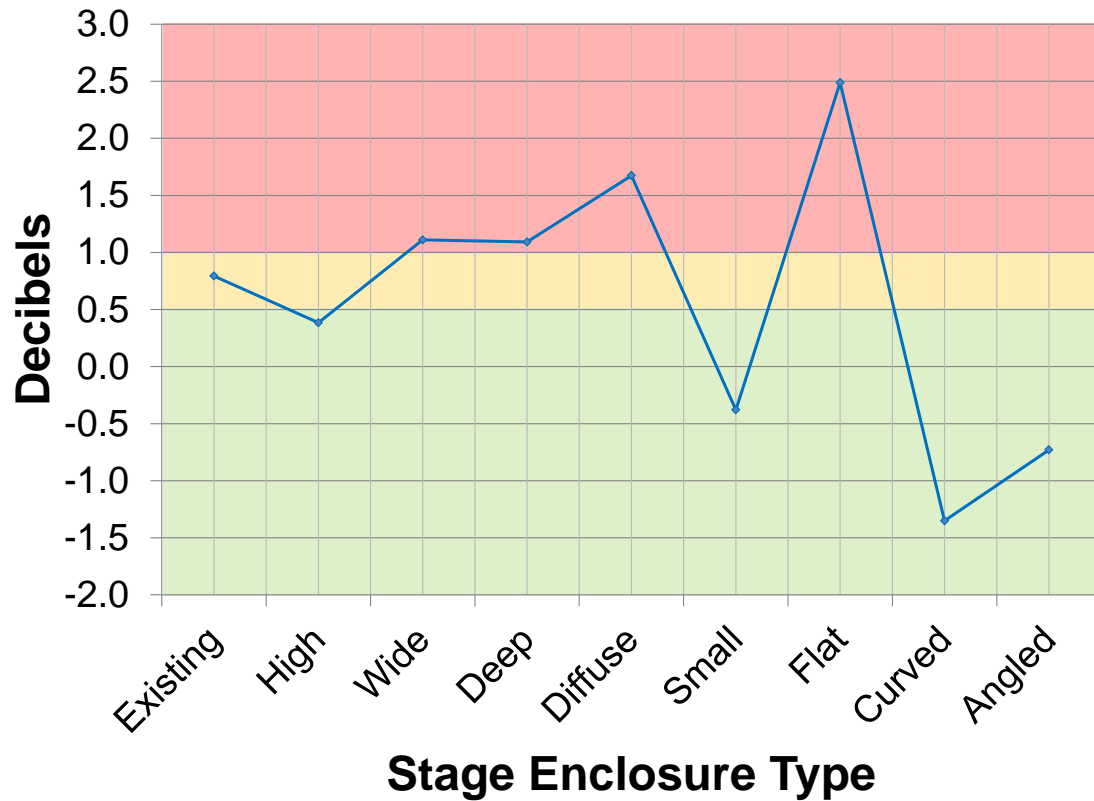


Figure 6.21: Eastman Model: Ensemble Parameters (Modeled Cross-Stage LQ_{740} Top/Sides)

The second dimension is correlated with cross-stage values of LQ_{740} Top/Sides, for which lower values (more early lateral energy, less early overhead energy) is preferred (Figure 6.21). This parameter is similar to the soloist preference for low values of ST1 Top/Sides. In the measurements, values ranged from +0.5 (Albany Recital) to -2.6 dB (Vassar), with Eastman falling at -2.3 dB. In the model, the variations range from +2.5 dB to -1.35 dB, with the existing Eastman enclosure at 0.8 dB. This could be due to the lack of diffuse energy in the early portion of the model skewing the energy distribution. However, relative comparisons can still be made.

As expected, the high enclosure decreases this value and the wide enclosure

increases it. The deep enclosure also increases the parameter, likely because the 2nd-order rear-side reflections that occurred before 40 milliseconds in the existing enclosure are pushed back to the late side of the ratio. Diffuse and flat enclosures are also marked by increases in this parameter. Diffuse enclosure increases are likely due to the particular stage geometry in that the early energy from both the sides and the top is decreased by scattering but the top is already arriving later so the sides are more strongly affected. The flat enclosure increases overhead energy due to the increase in overhead reflections while the sides remain relatively unaffected. The small, curved, and angled enclosures decrease the levels of this parameter. The small enclosure maintains proportions but moves all the energy earlier, where the level differences between top and sides are magnified. Curved and angled enclosures provide more reflection paths off the side walls while pushing the energy off the ceiling out into the hall.

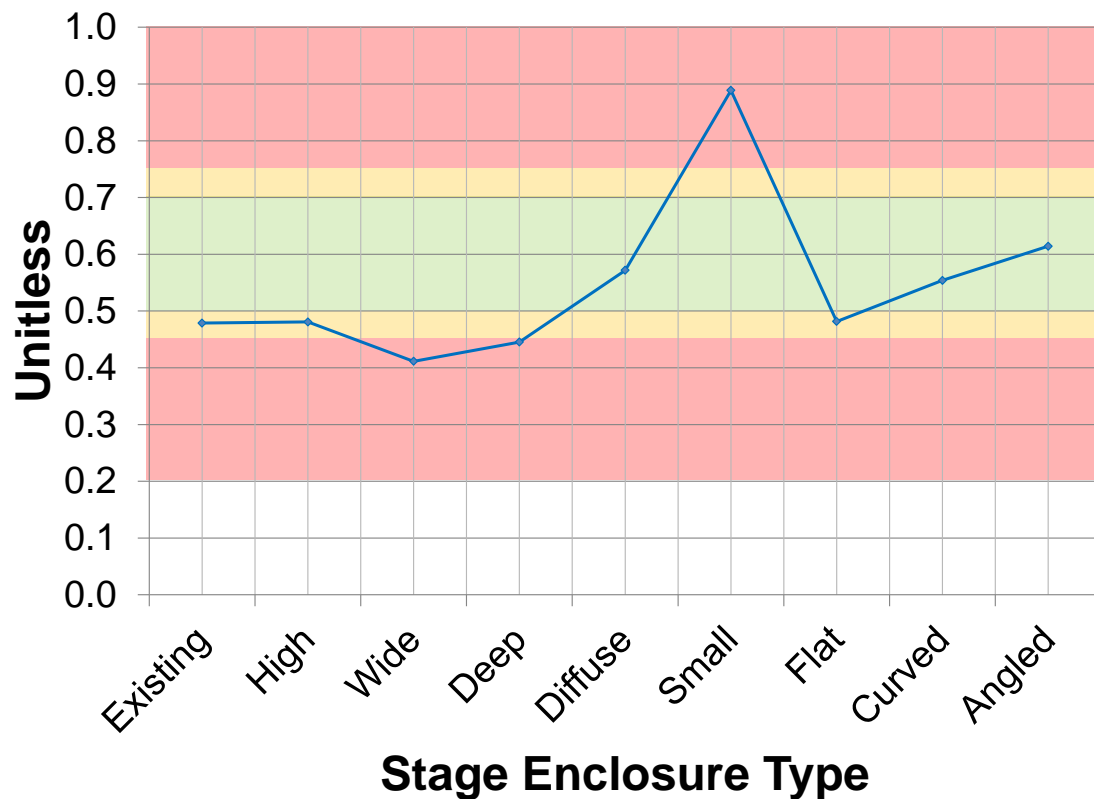


Figure 6.22: Eastman Model: Ensemble Parameters (Modeled Cross-Stage MTF)

The third dimension is correlated with cross-stage values of MTF (Figure 6.22). In the measured halls, the preferred values followed a bell curve, with ideal values around 0.75 (MTF is a unitless parameter that ranges from 0 to 1), indicating that a small amount of signal degradation is preferred, as it allows for good balance between self-produced sound and that produced by the ensemble. For the measured halls, values ranged from 1.00 (Albany Recital) to 0.09 (EMPAC Concert Hall), with Eastman at 0.71. In the modeled variations, values ranged from 0.41 to 0.89 with the existing enclosure at 0.48. Again, this is likely due to the over-estimation of the direct sound in relation to the reflected energy by the ray-tracing algorithm. High, deep and flat enclosures have little affect on this parameter. The wide enclosure has the lowest value, but the variation is small. The parameter is highest in the small enclosure, but the value falls above the preferred range, indicating that the

intelligibility of the ensemble signal could mask the self-generated sound. Diffuse, curved and angled enclosures also increase the value of MTF, while remaining in an ideal range of 0.50 to 0.75, indicating that some scattering or asymmetry onstage could improve cross-stage communication. Looking at the measured halls, Skidmore, Eastman and Bard all fall in this ideal range, and are characterized by small levels of diffusion and asymmetrical angles or curves. St. Rose, Vassar and Buffalo have values above the ideal range and are characterized by symmetry, small enclosures or flat surfaces. The theatres (Albany and EMPAC) have lower than ideal values, as they do not have enough reflecting surfaces to generate cross-stage communication. EMPAC Concert Hall, with the lowest value, is characterized by a wide enclosure with very little angle on the walls, creating a lower signal-to-noise ratio onstage.

Another parameter that was correlated with the third dimension was directional running reverberance or liveness, represented by preferred increase in overhead EDT and a preferred decrease in rear RR_{160} . As shown in Figure 6.23, the measured halls show a wide range of differences between these parameters, whereas the modeled variations (Figure 6.24) are not diverse enough to create a strong difference between overhead and rear reverberance. The difference is greatest in the deep enclosure, where the rear volume can build up higher levels of reverberant energy, and second-highest in the angled enclosure, where the overhead reverberant energy cannot build up before being driven into the house. Overhead levels are highest in the high enclosure, where more overhead energy can build up, and the flat enclosure, where more higher-order reflections can contribute to overhead energy.

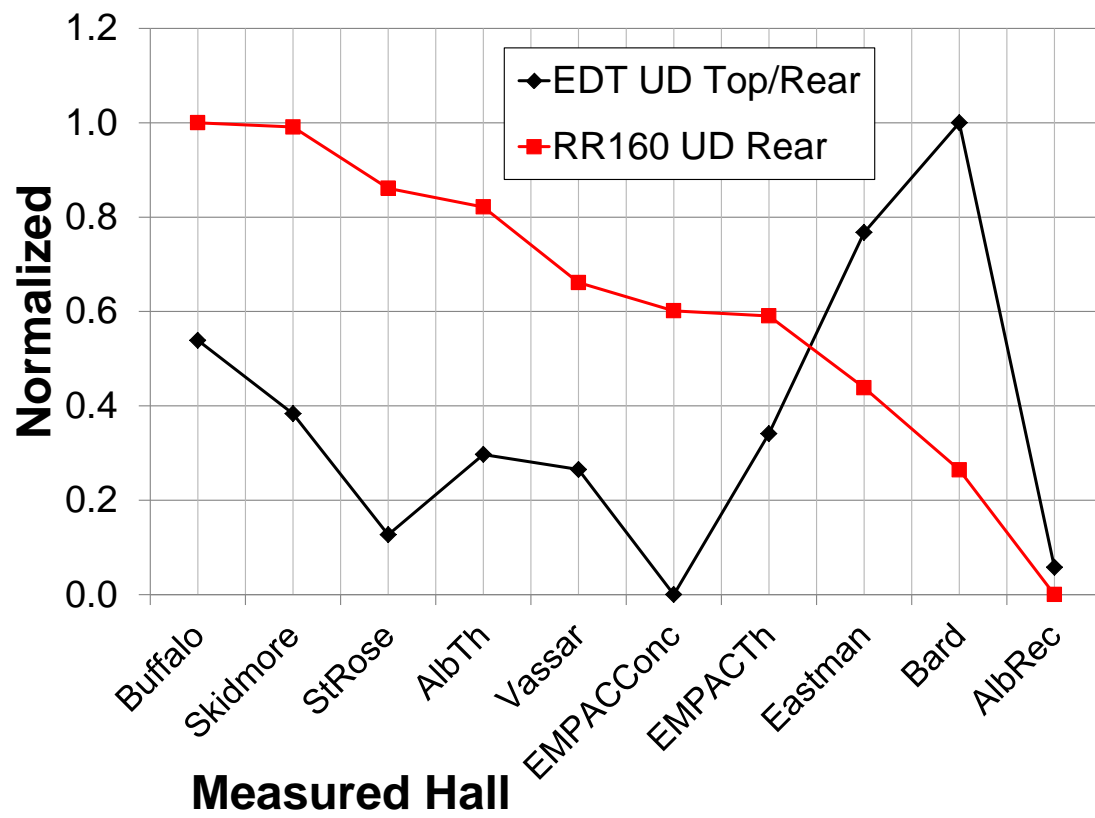


Figure 6.23: Eastman Measurements: Ensemble Parameters (Measured Running Reverberance, UD = UpDown-Stage, Halls: AlbRec = SUNY Albany Recital Hall, AlbTh = SUNY Albany Theatre, EmpacConc = EMPAC Concert Hall, EmpacTh = EMPAC Theatre)

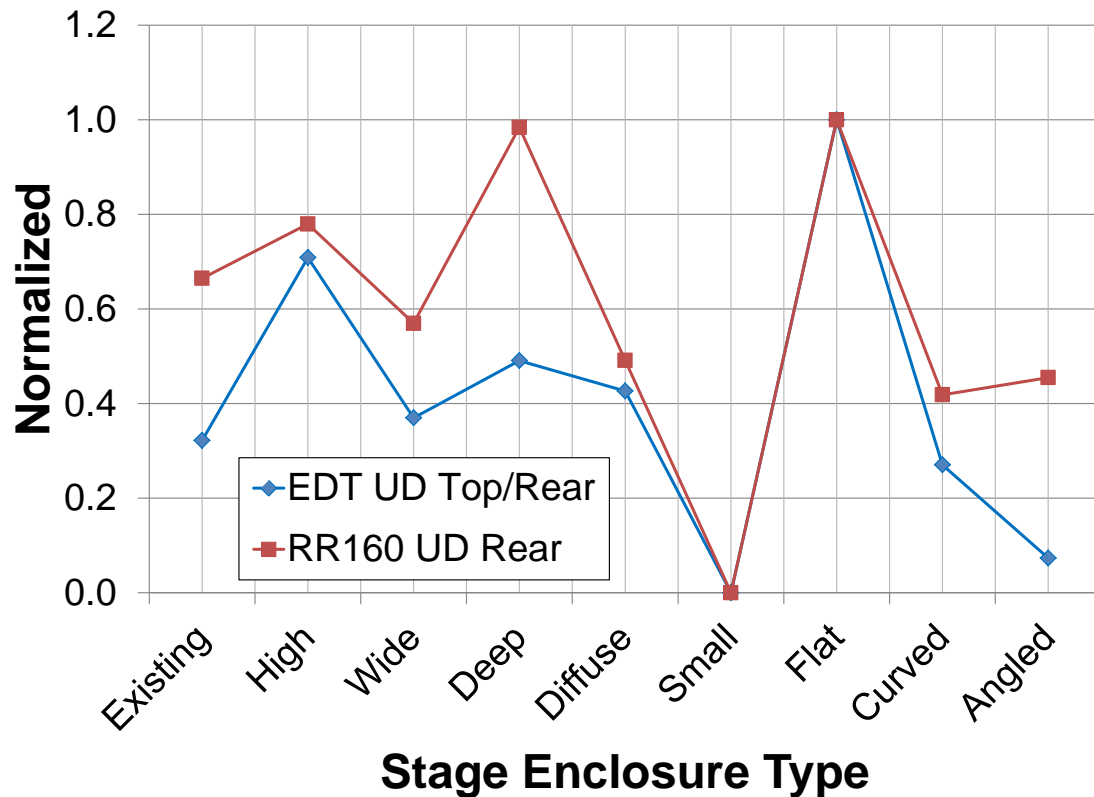


Figure 6.24: Eastman Model: Ensemble Parameters (Modeled Running Reverberance, UD = UpDown-Stage)

6.4 Discussion and Future Work

Given the study above, it appears that some characteristics are consistently providing optimum values of the preferred parameters within the confines of the computer model and the subjective preference tests. These characteristics should be considered in future collection of onstage measurements for comparison tests. If possible, conditions should be generated in which these architectural elements can be varied individually and with control, whether using wave-based modeling or physical measurements. The proposed characteristics are listed below.

- Wall surfaces with good early reflections (within 30 milliseconds after the direct sound).
- Proportionately high ceiling (approximately 13-14 meters) and narrow walls

(stage width no greater than 14 meters).

- Small amounts of asymmetrical scattering.
- Moderate coupling of the enclosure to the hall using to angles or curves.
- Evenly-proportioned width and depth of enclosure.
- Larger house volume with symphonic reverberance (1.8-2.2 seconds at mid frequencies).

Other architectural elements that are common to stage acoustics design but were not thoroughly tested here include overhead reflectors, orchestra shells, ledges, banners, risers, and orchestra pits. While some of these elements were present in some of the halls, they were not used in the tests because adding halls to the tests would have increased test subject fatigue. More controlled tests should be conducted, where individual elements are varied. For example, several measurements of the same hall with different shell configurations or reflector heights could be used to generate a single test.

6.5 Conclusions

The architectural investigations outlined in this chapter are limited to the preferences for the 10 stage enclosures measured in the concert hall survey as described in Chapter 3. In order to make strong architectural conclusions about stage acoustics design, more testing needs to be completed with larger data sets and more enclosure variations. The data set examined here is limited and parameter variations highly dependent on source-receiver locations. Some initial architectural elements have been proposed for use in further studies, based on their apparent relationship to the acoustic parameters correlating with musician preference within the given data set.

Again, while computer models are not ideal for this testing, measurement surveys are costly and time-intensive. It is possible that scale-modeling could be utilized. The spherical microphone array has been successfully used in scale modeling for other research [107]. However, in the case of concert hall scale models, which

rely on measurements at very high frequencies (range is dependent on model scale), the current microphone array would likely not be sufficient due to spatial aliasing. It is possible that a higher-order array that minimized the distance between capsules could be developed for this use. It is also possible that ray-tracing models can be utilized for basic analysis of spatial parameters, with the understanding that although absolute values of spatial energy distribution may be inaccurate, relative differences can still be compared between models with architectural variations.

CHAPTER 7

CONCLUSIONS

The research described in this document attempted to provide insight into the relevance of spatial acoustics for onstage performer experience. It also outlined a methodology for utilizing improved measurement and reproduction technologies to provide a more realistic testing environment for stage acoustics research. The author presented the work as five self-contained studies, divided into separate chapters. Chapter 2 began by outlining the development of a spherical microphone array built and tested for stage acoustics measurements of spatial impulse responses. Chapter 3 described the use of this array to record onstage impulse responses in 10 concert halls around New York State. Beamforming analysis was used to determine the spatial characteristics of each hall and several acoustic parameters were developed or adapted from previously established parameters for comparison with subjective preferences. In Chapter 4, a testing setup was defined and utilized for subjective preference testing using a real-time performer auralization system.

In Chapter 5, the subjective tests were described, in which musicians rated their preferences for the 10 measured halls in the virtual laboratory environment in three conditions with varying cognitive loads: passive listening, soloist performance, and ensemble performance. The subjective ratings from each musician were grouped and analyzed using multidimensional scaling, to establish the main dimensions influencing performer preference. It was determined that passive listening alone was not enough to create strong stage preferences. Additionally, soloist and ensemble playing conditions resulted in different sets of preferences. Based on these multidimensional analyses, the predefined objective parameters were examined in comparison using multiple regression to determine whether specific parameters could be used to predict subjective performer preferences. Due to the large number of parameters tested, clusters of highly-correlated parameters were established in order to provide high-level descriptions of relevant acoustic concepts. In the soloist conditions, reverberation (EDT and T_{30}) was found to be the strongest predictor of

subjective preference, with higher reverberation time preferred. Other predictors of preference included a ratio of stage support from overhead and from the sides, with mid-range levels preferred, and strength or G after 40 ms, again with preference for mid-range levels.

For the ensemble conditions, relationships between subjective and objective parameters were much more complex. A cluster analysis provided the dominant dimensions: Dimension 1 was driven by a combination of early spatial homogeneity, described by the parameter Directional Diffuseness windowed to the first 30 milliseconds (DD_{0-30}), for which low values were preferred, and several variations on G . Dimension 2 was correlated with a Top/Sides spatial ratio of the modified stage support parameter, LQ_{740} , with higher relative lateral energy preferred. Dimension 3 was driven by two acoustic concepts, spatial distribution of running reverberance (higher top reverberance preferred, lower rear reverberance preferred) and cross-stage communication as defined by a modified version of the Modulation Transfer Function (MTF), for which a mid-range value was preferred. The three dimensions for the solo playing conditions are summarized in Table 7.1, and the three dimensions for the ensemble playing conditions are summarized in Table 7.2:

Table 7.1: Soloist Perceptual Dimensions

Dimension	Name	Parameters	Preferred Values
1	Reverberance	T_{30} EDT	High High
2	Spatial Support	ST1 Top/Sides	Mid
3	Late Strength	$G_{40-\infty}$	Mid

Table 7.2: Ensemble Perceptual Dimensions

Dimension	Name	Parameters	Preferred Values
1	Spatial Homogeneity, Strength	DD_{0-30} UpDn-Stage G Cross-Stage G	Low Low High
2	Spatial Support	LQ_{740} Top/Sides	Low
3	Signal Transfer, Spatial Reverberance	MTF EDT Top/Rear RR_{160} Rear	Mid High Low

The design of these tests were based on previous research in the field by Gade and others [37]. The results of these tests are supported in some aspects by similar outcomes from those benchmark studies. However, these tests supplement the benchmarks by providing additional information beyond the benchmark studies with regards to spatial parameters.

Chapter 6 outlined the results of a preliminary modeling study using the most consistently-preferred hall of the measured set. A virtual model of this hall was created and calibrated in CATT-Acoustics and 8 geometrical variations were made to the stage enclosure to investigate the effects of basic enclosure design on the preferred parameters. Based on this study, some initial observations were made about stage enclosure design, many of which align with previous ad-hoc understanding and research by Dammerud and others, such as the preference for high ceiling and narrow walls, as well as a moderate level of asymmetrical scattering and coupling of the enclosure to the larger hall volume. It is proposed that further tests should include more detailed investigations using controlled variations of these and other architectural elements. Possible extensions of this work and applications of the outlined method were also proposed.

REFERENCES

- [1] C. Abercrombie, “Influence of vibration and stage construction on the perception of musical performance,” M.S. thesis, Sch. of Arch., Rensselaer Polytechnic Inst., Troy, NY, 2009.
- [2] T. Abhayapala and D. Ward, “Theory and design of high order sound field microphones using spherical microphone array,” in *Proc. IEEE Int. Conf. Acoust., Speech, and Signal Process.*, Orlando, FL, 2002, pp. 1949–1952.
- [3] L. Antani *et al.*, “Validation of adaptive rectangular decomposition for three-dimensional wave-based acoustic simulation in architectural models,” in *Proc. 21st Int. Congr. Acoust.*, no. 015099, Montreal, Canada, 2013.
- [4] M. Barron and L. Lee, “Energy relations in concert auditoriums 1,” *J. Acoust. Soc. Amer.*, vol. 84, no. 2, pp. 618–628, Aug. 1988.
- [5] A. Bassuet, “New acoustical parameters and visualization techniques to analyze the spatial distribution of sound in music spaces,” *J. Building Acoust.*, vol. 18, no. 3, pp. 329–347, Dec. 2011.
- [6] A. Bassuet *et al.*, “New implementation of multi-microphone recording technique to simulate music ensembles in room acoustic auralizations,” in *Proc. 21st Int. Congr. Acoust.*, no. 015135, Montreal, Canada, 2013.
- [7] E. Benjamin *et al.*, “Localization in horizontal-only ambisonic systems,” in *Proc. 121st Audio Eng. Soc. Conv.*, no. 6967, San Francisco, 2006.
- [8] L. Beranek, *Concert Halls and Opera Houses: Music, Acoustics, and Architecture*, 2nd ed. New York: Springer, 2004.
- [9] L. Beranek *et al.*, *Music, Acoustics & Architecture*. New York: Wiley, 1962.
- [10] P. Berens, “CircStat: a MATLAB toolbox for circular statistics,” *J. Statistical Software*, vol. 31, no. 10, pp. 1–21, Sep. 2009.
- [11] S. Bertet *et al.*, “Investigation of the perceived spatial resolution of higher order ambisonics sound fields: a subjective evaluation involving virtual and real 3D microphones,” in *Proc. 30th Int. Conf. Audio Eng. Soc.*, no. 26, Saariselkä, Finland, 2007.
- [12] J. Blauert, Ed., *Communication Acoustics*. Berlin, Germany: Springer-Verlag, 2005.

- [13] W. Boning and M. Bertsch, "From the sound up: generating form from acoustic preferences," unpublished.
- [14] I. Borg and P. J. F. Groenen, *Modern Multidimensional Scaling: Theory and Applications*, 2nd ed., ser. Springer Series in Statistics. New York: Springer, 2005.
- [15] J. Braasch *et al.*, "A loudspeaker-based projection technique for spatial music applications using virtual microphone control," *J. Comput. Music*, vol. 32, no. 3, pp. 55–71, Fall 2008.
- [16] D. S. Brungart and B. D. Simpson, "The effects of spatial separation in distance on the informational and energetic masking of a nearby speech signal," *J. Acoust. Soc. Amer.*, vol. 112, no. 2, pp. 664–676, Aug. 2002.
- [17] D. Cabrera *et al.*, "Considerations in characterising an almost anechoic room for interactive spatial audio reproduction," in *Proc. Int. Symp. Room Acoust.*, no. P4g, Melbourne, Australia, 2010.
- [18] T. Caulkins, "Caractérisation et contrôle du rayonnement d'un système de wave field synthesis pour la situation de concert," These de doctoral d'état, Institut de Recherche et Coordination Acoustique/Musique, Univ. Pierre et Marie Curie, Paris, France, 2007.
- [19] M. Chamagne. (2010) MMF-Fantastick. (Date Last Accessed Mar. 29, 2014). [Online]. Available: <http://www.mathieuchamagne.com/2010/08/25/mmf-fantastick/>
- [20] S. Chiles and M. Barron, "Sound level distribution and scatter in proportionate spaces," *J. Acoust. Soc. Amer.*, vol. 116, no. 3, pp. 1585–1595, Sep. 2004.
- [21] S. Clapp, "Three-dimensional spherical harmonic analysis of concert and recital halls," Ph.D dissertation, Sch. of Arch., Rensselaer Polytechnic Inst., Troy, NY, 2014, unpublished.
- [22] S. Clapp *et al.*, "Using spherical microphone array beamforming and bayesian inference to evaluate room acoustics (invited)," *J. Acoust. Soc. Amer.*, vol. 132, no. 3, pp. 2058–2058, Sep. 2012.
- [23] T. Cox and P. D'Antonio, *Acoustic Absorbers and Diffusers: Theory, Design and Application*, 2nd ed. London, UK: Taylor & Francis, 2009.
- [24] A. Coxon. (2004) NewMDSX. (Date Last Accessed Mar. 29, 2014). [Online]. Available: <http://www.newmdsx.com/>
- [25] B. I. Dalenback *et al.*, "A macroscopic view of diffuse reflection," *J. Audio Eng. Soc.*, vol. 42, no. 10, pp. 793–807, Oct. 1994.

- [26] J. Dammerud, "Stage acoustics for symphony orchestras in concert halls," Ph.D dissertation, Dept. Architecture and Civil Eng., Univ. Bath, Bath, UK, 2009.
- [27] J. Dammerud and M. Barron, "Early subjective and objective studies of concert hall stage conditions for orchestral performance," in *Proc. 19th Int. Congr. Acoust.*, no. RBA-06-026, Madrid, Spain, 2007.
- [28] J. Daniel, "Représentation de champs acoustiques, application à la transmission et à la reproduction de scènes sonores complexes dans un contexte multimédia," These de doctoral d'état, Laboratoire d' Acoustique Musicale, Univ. Pierre et Marie Curie, Paris, France, 2000.
- [29] J. Daniel, "Spatial sound encoding including near field effect: Introducing distance coding filters and a viable, new ambisonic format," in *Proc. 23rd Int. Audio Eng. Soc. Conf.*, no. 16, Copenhagen, Denmark, 2003, pp. 1–15.
- [30] D. de Vries, *Wave Field Synthesis*, ser. AES Monograph. New York: Audio Engineering Society, 2009.
- [31] A. Field, *Discovering Statistics Using SPSS for Windows: Advanced Techniques for the Beginner*, 2nd ed. London: Sage Publications Ltd., 2000.
- [32] E. Fisher and B. Rafaely, "The nearfield spherical microphone array," in *Proc. IEEE Int. Conf. Acoust., Speech and Signal Process.*, Las Vegas, 2008, pp. 5272–5275.
- [33] J. Fliege and U. Maier, "A two-stage approach for computing cubature formulae for the sphere," Dept. Math., Univ. Dortmund, Dortmund, Germany, Rep. Mathematik 139T, 2009.
- [34] A. C. Gade, "Investigations of musicians room acoustic conditions in concert halls 1: Methods and laboratory experiments," *Acta Acustica*, vol. 69, no. 5, pp. 193–203, Nov. 1989.
- [35] A. C. Gade, "Investigations of musicians room acoustic conditions in concert halls 2: Field experiments and synthesis of results," *Acta Acustica*, vol. 69, no. 6, pp. 249–262, Dec. 1989.
- [36] A. Gade, "Musicians ideas about room acoustic qualities," Acoust. Lab., Tech. Univ. Denmark, Copenhagen, Denmark, Tech. Rep. 31, 1981.
- [37] A. Gade, "Subjective room acoustics experiments with musicians," Acoust. Lab., Tech. Univ. Denmark, Copenhagen, Denmark, Tech. Rep. 32, 1982.
- [38] M. Gerzon, "Periphony: with-height sound reproduction," *J. Audio Eng. Soc.*, vol. 21, no. 1, pp. 2–10, Jan. 1973.

- [39] M. Gerzon, "Practical periphony: the reproduction of full-sphere sound," *J. Audio Eng. Soc.*, vol. 28, no. 5, pp. 364–364, May 1980.
- [40] B. Gover *et al.*, "Microphone array measurement system for analysis of directional and spatial variations of sound fields," *J. Acoust. Soc. Amer.*, vol. 112, no. 5, pp. 1980–1991, Nov. 2002.
- [41] B. Gover *et al.*, "Designing a spherical microphone array for the directional analysis of reflections and reverberation," in *Proc. 115th Audio Eng. Soc. Conv.*, no. 5862, New York, NY, 2003.
- [42] B. Gover *et al.*, "Measurements of directional properties of reverberant sound fields in rooms using a spherical microphone array," *J. Acoust. Soc. Amer.*, vol. 116, no. 4, pp. 2138–2148, Oct. 2004.
- [43] J. M. Grey, "Multidimensional perceptual scaling of musical timbres," *J. Acoust. Soc. Amer.*, vol. 61, no. 5, pp. 1270–1277, May 1977.
- [44] D. Griesinger, "Subjective loudness of running reverberation in halls and stages," in *Proc. Wallace Clement Sabine Centennial Symp.*, Cambridge, MA, 1994, p. 89.
- [45] D. Griesinger, "Further investigation into the loudness of running reverberation," in *Proc. Inst. Acoust. Conf.*, London, UK, 1995, pp. 10–17.
- [46] D. Griesinger, "How loud is my reverberation?" in *Proc. 98th Audio Eng. Soc. Conv.*, no. 3943, Paris, France, 1995.
- [47] D. Griesinger, "The psychoacoustics of apparent source width, spaciousness and envelopment in performance spaces," *Acta Acustica*, vol. 83, no. 4, pp. 721–731, July 1997.
- [48] A. Guthrie, "Using telepresence to evaluate the relevance of acoustic parameters for musician communication in indeterminate music," M.S. thesis, Sch. of Arch., Rensselaer Polytechnic Inst., Troy, NY, 2008.
- [49] A. Harker and P. A. Tremblay, "The HISSTools impulse response toolbox: Convolution for the masses," in *Proc. Int. Comput. Music Conf.*, Ljubljana, Slovenia, 2012, pp. 148–155.
- [50] A. Heller *et al.*, "Is my decoder ambisonic?" in *Proc. 125th Audio Eng. Soc. Conv.*, no. 7553, San Francisco, CA, 2008.
- [51] P. Henderson, "Achieving perceptually-accurate aural telepresence," Ph.D dissertation, Sch. of Arch., Rensselaer Polytechnic Inst., Troy, NY, 2006.
- [52] F. Hollerweger, "Periphonic sound spatialization in multi-user virtual environments," M.F.A. Thesis, Dept. Music, Univ. California Santa Barbara, Santa Barbara, CA, 2006.

- [53] T. Houtgast and H. Steeneken, "The modulation transfer function in room acoustics as a predictor of speech intelligibility," *J. Acoust. Soc. Amer.*, vol. 54, no. 2, pp. 557–557, Aug. 1973.
- [54] E. Hulsebos, "Auralization using wave field synthesis," Ph.D dissertation, Dept. Physics, Tech. Univ. Delft, Delft, Netherlands, 2004.
- [55] *Acoustics: Measurement of the reverberation time of rooms with reference to other acoustical parameters*, ISO Standard 3382, 1997.
- [56] V. Jordan, "Einige bemerkungen uber anhall und anfangsnachhall in musikraumen," *Appl. Acoust.*, vol. 1, no. 1, pp. 29–36, Jan. 1968.
- [57] Y. Jurkiewicz, "Investigation of musician's conditions and acoustical environments on orchestra platforms," M.S. thesis, Dept. Acoust., École Centrale de Lyon, Lyon, France, 2005.
- [58] E. Kahle and J.-P. Jullien, "Some new considerations on the subjective impression of reverberance and its correlation with objective criteria," in *Proc. Wallace Clement Sabine Centennial Symp.*, Cambridge, 1994, pp. 239–242.
- [59] K. Kato *et al.*, "Musicians' adjustment of performance to room acoustics, part 2: Acoustical analysis of performed sound signals," in *Proc. 19th Int. Congr. Acoust.*, no. MUS-03-005, Madrid, Spain, 2007.
- [60] K. Kato *et al.*, "Musicians' adjustment of performance to room acoustics, part 3: Understanding the variations in musical expressions," *J. Acoust. Soc. Amer.*, vol. 123, no. 5, pp. 3610–3610, May 2008.
- [61] Y. Kim *et al.*, "Evaluation of stage acoustics in concert halls by investigating performer's preference," in *Proc. 19th Int. Congr. Acoust.*, no. RBA-06-029, Madrid, Spain, 2007.
- [62] L. Kinsler, *Fundamentals of Acoustics*, 4th ed. New York: John Wiley, 2000.
- [63] I. Laird *et al.*, "Development of a virtual performance studio with application of virtual acoustic recording methods," in *Proc. 130th Audio Eng. Soc. Conv.*, no. 8358, London, UK, 2011.
- [64] Z. Li and R. Duraiswami, "Flexible and optimal design of spherical microphone arrays for beamforming," *IEEE Trans. Audio, Speech and Language Process.*, vol. 15, no. 2, pp. 702–714, Feb. 2007.
- [65] T. Lokki *et al.*, "Concert hall acoustics assessment with individually elicited attributes," *J. Acoust. Soc. Amer.*, vol. 130, no. 2, pp. 835–849, Aug. 2011.

- [66] T. Lokki *et al.*, “Recording of anechoic symphony music,” *J. Acoust. Soc. Amer.*, vol. 123, no. 5, pp. 3936–3936, May 2008.
- [67] D. G. Malham, “Higher order ambisonic systems for the spatialisation of sound,” in *Proc. Int. Comput. Music Conf.*, Beijing, China, 1999, pp. 484–487.
- [68] D. Malham, “Experience with large area 3D ambisonic sound systems,” in *Proc. Inst. Acoust. Conf.*, Windermere, UK, 1992, pp. 209–216.
- [69] A. H. Marshall *et al.*, “Acoustical conditions preferred for ensemble,” *J. Acoust. Soc. Amer.*, vol. 64, no. 5, pp. 1437–1442, Nov. 1978.
- [70] J. Meyer, *Acoustics and the Performance of Music*. Frankfurt, Germany: Verlag das Musikinstrument, 1978.
- [71] J. Meyer and E. Biassoni de Serra, “Verderckungseffekt bei instrumentalmusikern,” *Acta Acustica*, vol. 46, no. 2, pp. 130–140, Oct. 1980.
- [72] J. Meyer *et al.*, “Spherical microphone array for spatial sound recording,” in *Proc. 115th Audio Eng. Soc. Conv.*, no. 5975, New York, NY, 2003.
- [73] S. Moreau *et al.*, “3D sound field recording with higher order ambisonics – objective measurements and validation of a 4th order spherical microphone,” in *Proc. 120th Audio Eng. Soc. Conv.*, no. 6857, Paris, France, 2006.
- [74] M. Morimoto and A. Asaoka, “Multi-dimensional analysis of reverberance,” in *Proc. 18th Int. Congr. Acoust.*, Kyoto, Japan, 2004, pp. 2469–2472.
- [75] P. Morse and K. Ingard, *Theoretical Acoustics*, ser. International Series in Pure and Applied Physics. New York: McGraw-Hill, 1968.
- [76] S. Myrbeck, “The impact of lighting and room acoustics parameters on the perceived intimacy of a musical performance,” M.S. thesis, Sch. of Arch., Rensselaer Polytechnic Inst., Troy, NY, 2009.
- [77] G. M. Naylor, “Modulation transfer and ensemble music performance,” *Acta Acustica*, vol. 65, no. 3, pp. 127–137, Feb. 1988.
- [78] G. M. Naylor and R. J. M. Craik, “The effects of level difference and musical texture on ease of ensemble,” *Acta Acustica*, vol. 65, no. 2, pp. 95–100, Jan. 1988.
- [79] M. Nyman, *Experimental Music: Cage and Beyond*, 2nd ed. Cambridge, UK: Cambridge Univ. Press, 1999.
- [80] F. Otondo and B. Kirkwood, “Perceived influence of changes in musical instrument directivity representation,” in *Proc. Stockholm Music Acoust. Conf.*, Stockholm, Sweden, 2003, pp. 655–658.

- [81] J. Pätynen and T. Lokki, “Directivities of symphony orchestra instruments,” *Acta Acustica*, vol. 96, no. 1, pp. 138–167, Jan. 2010.
- [82] J. Pätynen *et al.*, “Anechoic recording system for symphony orchestra,” *Acta Acustica*, vol. 94, no. 6, pp. 856–865, Nov. 2008.
- [83] J. Pätynen *et al.*, “Analysis of concert hall acoustics via visualizations of time-frequency and spatiotemporal responses,” *J. Acoust. Soc. Amer.*, vol. 133, no. 2, pp. 842–857, Feb. 2013.
- [84] N. Peters *et al.*, “Spatial sound rendering in Max/MSP with ViMiC,” in *Proc. Int. Comput. Music Conf.*, Belfast, N. Ireland, 2008.
- [85] B. Rafaely, “Plane-wave decomposition of the sound field on a sphere by spherical convolution,” *J. Acoust. Soc. Amer.*, vol. 116, no. 4, pp. 2149–2157, Oct. 2004.
- [86] B. Rafaely, “Analysis and design of spherical microphone arrays,” *IEEE Trans. Speech and Audio Process.*, vol. 13, no. 1, pp. 135–143, Jan. 2005.
- [87] B. Rafaely and A. Avni, “Interaural cross correlation in a sound field represented by spherical harmonics,” *J. Acoust. Soc. Amer.*, vol. 127, no. 2, pp. 823–828, Feb. 2010.
- [88] B. Rafaely *et al.*, “Spatial aliasing in spherical microphone arrays,” *IEEE Trans. Signal Process.*, vol. 55, no. 3, pp. 1003–1010, Mar. 2007.
- [89] J. Rathsam and B. Rafaely, “Analysis of in-situ acoustic absorption using a spherical microphone array,” *J. Acoust. Soc. Amer.*, vol. 125, no. 4, pp. 2544–2544, Apr. 2009.
- [90] V. M. Richards and D. L. Neff, “Cuing effects for informational masking,” *J. Acoust. Soc. Amer.*, vol. 115, no. 1, pp. 289–300, Jan. 2004.
- [91] J. Rindel and C. Christensen, “Auralisation of a symphony orchestra with ODEON, the chain from musical instruments to the eardrums,” in *Proc. EAA Symp. Auralization*, Espoo, Finland, 2009.
- [92] M. Schroeder, “Modulation transfer functions: Definition and measurement,” *Acta Acustica*, vol. 49, no. 3, pp. 179–182, Nov. 1981.
- [93] M. Schroeder *et al.*, “Comparative study of european concert halls: Correlation of subjective preference with geometric and acoustic parameters,” *J. Acoust. Soc. Amer.*, vol. 56, no. 4, pp. 1195–1201, Oct. 1974.
- [94] R. Shepard *et al.*, *Multidimensional Scaling: Theory and Applications in the Behavioral Sciences*. New York: Seminar Press, 1972.

- [95] J. Solway, "Predicting speech transmission indices in non-diffuse spaces," M.S. thesis, Inst. Sound & Vibration Res., Univ. Southampton, Southampton, UK, 1997.
- [96] K. Stetson, "Singers' preferences for acoustical characteristics of concert halls," M.S. thesis, Sch. of Arch., Rensselaer Polytechnic Inst., Troy, NY, 2008.
- [97] S. Ternström, "Preferred self-to-other ratios in choir singing," *J. Acoust. Soc. Amer.*, vol. 105, no. 6, pp. 3563–3574, June 1999.
- [98] S. Ternström *et al.*, "Self-to-other ratios measured in an opera chorus in performance," *J. Acoust. Soc. Amer.*, vol. 118, no. 6, pp. 3903–3911, Dec. 2005.
- [99] S. Thomasson, "Kan god podieakustik mätas?" in *Proc. Nordic Acoust. Soc. Meeting*, Lund, Sweden, 1974, pp. 181–184.
- [100] K. Ueno *et al.*, "Experimental study on stage acoustics for ensemble performance in chamber music," *Acoust. Sci. and Tech.*, vol. 26, no. 4, pp. 345–352, July 2005.
- [101] K. Ueno *et al.*, "Musicians adjustment of performance to room acoustics, part 1," in *Proc. 19th Int. Congr. Acoust.*, no. MUS-03-004, Madrid, Spain, 2007.
- [102] K. Ueno and H. Tachibana, "Experimental study on the evaluation of stage acoustics by musicians using a 6-channel sound simulation system," *Acoust. Sci. and Tech.*, vol. 24, no. 3, pp. 130–138, May 2003.
- [103] K. Ueno and H. Tachibana, "Cognitive modeling of musicians perception in concert halls," *Acoust. Sci. and Tech.*, vol. 26, no. 2, pp. 156–161, Mar. 2004.
- [104] D. Valente, "Listeners' expectation of room acoustical parameters based on visual cues," Ph.D dissertation, Sch. of Arch., Rensselaer Polytechnic Inst., Troy, NY, 2009.
- [105] E. Van Den Braak and L. Van Luxemburg, "New (stage) parameter for conductor's acoustics," *J. Acoust. Soc. Amer.*, vol. 123, no. 5, pp. 3198–3198, May 2008.
- [106] E. Williams, *Fourier Acoustics: Sound Radiation and Nearfield Acoustical Holography*. San Diego: Academic Press, 1999.
- [107] N. Xiang *et al.*, "Bayesian characterization of multiple-slope sound energy decays in coupled-volume systems," *J. Acoust. Soc. Amer.*, vol. 129, no. 2, pp. 741–752, Feb. 2011.

- [108] K. Yamaguchi, “Multivariate analysis of subjective and physical measures of hall acoustics,” *J. Acoust. Soc. Amer.*, vol. 52, no. 5A, pp. 1271–1279, Nov. 1972.
- [109] F. Zotter and M. Frank, “All-round ambisonic panning and decoding,” *J. Audio Eng. Soc.*, vol. 60, no. 10, pp. 807–820, Nov. 2012.
- [110] F. Zotter *et al.*, “Ambisonic decoding with and without mode-matching: A case study using the hemisphere,” in *Proc. 2nd Int. Ambisonics Symp.*, Paris, France, 2010.

APPENDIX A

SOLO PARAMETERS

Solo parameters used in this study, calculated from the 1-meter “soloist” impulse responses, shown here for the 1 kHz octave band. “Normalized” versions of spatial parameters were divided by the total omnidirectional energy in the given parameter if units were in dB, or the average value over all directions if units were time or percent.

PARAMETER				HALL									
Parameter	Direction	Normalized	Units	Alb Recital	Alb Theatre	Bard	Buffalo	Eastman	EMPAC C	EMPAC Th	Skidmore	St. Rose	Vassar
CenterTime	Top		ms	23.56	42.09	115.54	50.56	58.06	30.68	15.05	62.56	77.78	78.80
CenterTime	Bottom		ms	18.21	24.11	59.09	51.54	26.99	33.56	28.61	83.24	34.54	46.94
CenterTime	Front		ms	25.85	43.38	62.51	71.58	43.34	32.78	19.46	66.10	51.50	58.49
CenterTime	Rear		ms	22.70	52.08	100.75	65.16	46.07	46.29	21.67	88.86	51.53	62.98
CenterTime	Left		ms	20.33	60.31	91.37	71.36	37.68	40.51	19.73	73.30	72.60	71.44
CenterTime	Right		ms	27.15	52.80	86.46	83.79	33.27	29.41	29.78	56.53	67.70	74.39
CenterTime	Audience		ms	29.99	48.99	59.92	43.32	44.92	26.84	18.10	82.15	57.82	72.30
CenterTime	SideWallsL		ms	18.71	60.99	76.85	60.92	51.09	31.17	28.40	110.45	93.52	88.75
CenterTime	SideWallsR		ms	31.07	60.30	86.06	73.84	42.47	35.11	25.52	59.52	93.63	103.44
CenterTime	Top	X	ms	0.60	-3.70	29.59	-15.10	17.16	-4.86	-7.33	-9.20	18.50	13.29
CenterTime	Bottom	X	ms	-4.76	-21.68	-26.86	-14.13	-13.91	-1.98	6.23	11.47	-24.74	-18.56
CenterTime	Front	X	ms	2.89	-2.41	-23.45	5.91	2.44	-2.76	-2.93	-5.67	-7.77	-7.02
CenterTime	Rear	X	ms	-0.27	6.29	14.80	-0.50	5.17	10.75	-0.71	17.10	-7.75	-2.52
CenterTime	Left	X	ms	-2.64	14.52	5.42	5.69	-3.23	4.98	-2.66	1.54	13.33	5.94
CenterTime	Right	X	ms	4.18	7.00	0.50	18.13	-7.63	-6.13	7.40	-15.23	8.43	8.88
CenterTime	Audience	X	ms	7.02	3.20	-26.03	-22.34	4.02	-8.70	-4.28	10.39	-1.45	6.79
CenterTime	SideWallsL	X	ms	-4.26	15.19	-9.10	-4.75	10.19	-4.37	6.01	38.68	34.24	23.24
CenterTime	SideWallsR	X	ms	8.10	14.50	0.11	8.17	1.56	-0.43	3.13	-12.25	34.35	37.93
CenterTime	Top/Bottom		ms	5.35	17.98	56.45	-0.98	31.07	-2.88	-13.56	-20.68	43.24	31.86
CenterTime	Front/Rear		ms	3.16	-8.70	-38.25	6.41	-2.73	-13.51	-2.21	-22.76	-0.03	-4.50
CenterTime	Left/Right		ms	-6.82	7.52	4.91	-12.43	4.41	11.11	-10.05	16.77	4.90	-2.94
CenterTime	Front/Sides		ms	5.10	-11.65	-21.53	-24.05	-1.86	-6.30	-8.86	-2.83	-35.75	-23.79
CenterTime	Top/Sides		ms	-1.33	-18.55	34.08	-16.82	11.28	-2.46	-11.90	-22.42	-15.80	-17.29
CenterTime	Top/Rear		ms	0.87	-9.99	14.79	-14.60	11.99	-15.61	-6.62	-26.30	26.25	15.82
CenterTime	FrontTop/ RearBottom		ms	4.26	4.64	9.10	2.72	14.17	-8.19	-7.89	-21.72	21.61	13.68
Gearly	Top		dB	48.85	40.64	7.94	53.94	39.13	58.42	62.79	39.39	46.17	51.17
Gearly	Bottom		dB	54.80	53.76	28.77	53.49	62.92	56.62	42.81	25.16	66.76	65.00
Gearly	Front		dB	47.91	47.60	26.64	44.24	49.80	55.28	50.07	34.80	57.43	58.39
Gearly	Rear		dB	44.92	39.65	16.93	48.19	44.77	46.21	52.76	21.51	56.10	54.69
Gearly	Left		dB	48.35	35.01	13.93	39.11	53.39	54.57	47.76	32.79	48.80	54.99
Gearly	Right		dB	49.10	38.85	19.61	36.86	56.33	57.14	48.58	37.33	48.56	50.65
Gearly	Audience		dB	27.88	31.20	16.68	34.79	35.22	48.57	38.32	20.67	37.91	38.34
Gearly	SideWallsL		dB	39.33	23.06	13.53	36.66	30.28	39.55	29.38	13.10	29.69	34.13
Gearly	SideWallsR		dB	36.22	19.49	15.07	26.01	35.24	40.24	34.68	25.83	26.35	25.98
Gearly	Top	X	dB	-98.11	-87.11	-48.97	-83.97	-114.04	-105.70	-89.59	-56.09	-115.74	-116.27
Gearly	Bottom	X	dB	-92.16	-74.00	-28.14	-84.42	-90.25	-107.50	-109.58	-70.32	-95.15	-102.45
Gearly	Front	X	dB	-99.06	-80.15	-30.27	-93.68	-103.37	-108.84	-102.32	-60.68	-104.48	-109.06
Gearly	Rear	X	dB	-102.05	-88.11	-39.98	-89.73	-108.40	-117.91	-99.63	-73.97	-105.81	-112.76
Gearly	Left	X	dB	-98.61	-92.74	-42.98	-98.80	-99.78	-109.55	-104.62	-62.70	-113.11	-112.46
Gearly	Right	X	dB	-97.87	-88.90	-37.30	-101.06	-96.84	-106.97	-103.80	-58.15	-113.36	-116.80
Gearly	Audience	X	dB	-119.09	-96.56	-40.23	-103.12	-117.94	-115.55	-114.07	-74.81	-124.00	-129.11
Gearly	SideWallsL	X	dB	-107.64	-104.69	-43.38	-101.25	-122.89	-124.57	-123.01	-82.38	-132.22	-133.32
Gearly	SideWallsR	X	dB	-110.74	-108.26	-41.84	-111.90	-117.93	-123.87	-117.71	-69.65	-135.56	-141.47
Gearly	Top/Bottom		dB	-5.95	-13.11	-20.83	0.45	-23.79	1.80	19.99	14.23	-20.59	-13.83
Gearly	Front/Rear		dB	2.99	7.95	9.72	-3.95	5.03	9.07	-2.68	13.29	1.32	3.69
Gearly	Left/Right		dB	-0.75	-3.84	-5.68	2.26	-2.94	-2.57	-0.82	-4.54	0.25	4.34
Gearly	Front/Sides		dB	-47.68	-11.35	-11.91	-27.88	-30.30	-31.22	-25.74	-18.26	-18.13	-21.77
Gearly	Top/Sides		dB	-26.70	-1.91	-20.65	-8.72	-26.39	-21.37	-1.26	0.46	-9.88	-8.94
Gearly	Top/Rear		dB	3.93	1.00	-8.98	5.76	-5.64	12.21	10.04	17.88	-9.93	-3.52
Gearly	FrontTop/ RearBottom		dB	-2.96	-5.16	-11.11	-3.50	-18.76	10.87	17.30	27.52	-19.27	-10.13
Gsupport	Top		dB	12.44	-1.76	-7.41	23.91	10.62	5.46	9.34	6.17	24.18	36.44
Gsupport	Bottom		dB	12.88	-1.74	-1.00	22.72	20.76	7.67	6.96	1.81	28.16	34.00
Gsupport	Front		dB	11.93	6.60	-6.88	20.73	15.58	8.10	6.46	8.34	25.04	34.87
Gsupport	Rear		dB	10.27	2.37	-0.03	20.96	19.80	4.91	9.23	2.57	28.15	37.80
Gsupport	Left		dB	10.40	4.29	-2.54	15.21	23.68	7.75	1.09	10.13	26.15	40.59
Gsupport	Right		dB	13.26	-0.68	-5.87	20.17	21.81	6.48	16.97	1.24	23.32	33.44
Gsupport	Audience		dB	5.43	5.65	-6.49	7.69	13.88	9.91	3.75	6.84	18.50	25.78
Gsupport	SideWallsL		dB	8.90	0.13	-1.50	16.17	16.22	1.24	1.77	3.62	19.30	29.10
Gsupport	SideWallsR		dB	9.91	-2.10	-3.34	10.20	13.95	4.10	15.16	-1.81	16.43	20.88
Gsupport	Top	X	dB	-23.15	-6.30	4.45	-37.95	-45.50	-14.73	-15.68	-8.96	-53.33	-72.14
Gsupport	Bottom	X	dB	-22.71	-6.28	10.87	-39.13	-35.36	-12.51	-18.06	-13.32	-49.34	-74.57
Gsupport	Front	X	dB	-23.66	2.06	4.98	-41.12	-40.54	-12.09	-18.56	-6.80	-52.46	-73.70
Gsupport	Rear	X	dB	-25.32	-2.17	11.84	-40.89	-36.33	-15.27	-15.79	-12.56	-49.35	-70.77
Gsupport	Left	X	dB	-25.19	-0.25	9.32	-46.64	-32.44	-12.44	-23.93	-5.00	-51.35	-67.98
Gsupport	Right	X	dB	-22.34	-5.22	5.99	-41.69	-34.32	-13.71	-8.05	-13.89	-54.18	-75.13
Gsupport	Audience	X	dB	-30.16	1.12	5.37	-54.16	-42.25	-10.28	-21.27	-8.29	-59.01	-82.79
Gsupport	SideWallsL	X	dB	-26.70	-4.40	10.37	-45.68	-39.91	-18.95	-23.25	-11.51	-58.20	-79.47
Gsupport	SideWallsR	X	dB	-25.68	-6.64	8.52	-51.65	-42.17	-16.09	-9.87	-16.94	-61.07	-87.69

PARAMETER				HALL									
Parameter	Direction	Normalized	Units	Alb Recital	Alb Theatre	Bard	Buffalo	Eastman	EMPAC C	EMPAC Th	Skidmore	St. Rose	Vassar
Gsupport	Top/Bottom		dB	-0.44	-0.02	-6.41	1.18	-10.14	-2.22	2.37	4.36	-3.99	2.43
Gsupport	Front/Rear		dB	1.66	4.23	-6.86	-0.23	-4.21	3.19	-2.77	5.77	-3.11	-2.93
Gsupport	Left/Right		dB	-2.85	4.97	3.33	-4.95	1.87	1.27	-15.88	8.89	2.83	7.14
Gsupport	Front/Sides		dB	-13.38	7.62	-1.66	-18.69	-16.29	4.57	-13.17	5.03	-17.24	-24.21
Gsupport	Top/Sides		dB	-6.37	0.20	-2.57	-2.47	-19.55	0.12	-7.59	4.36	-11.56	-13.55
Gsupport	Top/Rear		dB	2.17	-4.13	-7.38	2.95	-9.18	0.54	0.11	3.60	-3.98	-1.36
Gsupport	FrontTop/ RearBottom		dB	1.22	4.20	-13.27	0.95	-14.36	0.97	-0.40	10.13	-7.10	-0.50
G740	Top		dB	29.49	13.85	-9.59	28.23	28.83	38.12	33.93	12.11	27.14	35.37
G740	Bottom		dB	32.73	22.99	8.19	27.89	48.12	34.68	22.18	6.65	41.00	47.95
G740	Front		dB	30.09	19.03	10.73	17.80	35.05	36.91	23.49	5.33	36.91	44.93
G740	Rear		dB	28.91	15.80	-2.40	22.93	32.37	28.83	29.32	0.42	35.18	39.91
G740	Left		dB	29.23	11.28	-5.12	12.21	41.84	32.94	23.33	12.24	28.95	39.54
G740	Right		dB	31.74	14.66	4.55	10.68	46.05	34.55	29.17	10.99	27.88	34.37
G740	Audience		dB	12.43	11.48	5.40	14.35	25.51	32.52	20.67	3.78	22.68	28.42
G740	SideWallsL		dB	25.80	8.04	1.49	17.34	24.93	21.35	15.79	-5.84	19.61	26.06
G740	SideWallsR		dB	22.63	5.77	2.21	7.22	27.60	23.65	20.52	6.65	10.78	13.70
G740	Top	X	dB	-61.61	-34.95	-12.77	-31.64	-87.30	-64.90	-46.78	-11.76	-71.39	-85.67
G740	Bottom	X	dB	-58.37	-25.81	5.01	-31.97	-68.01	-68.34	-58.53	-17.22	-57.53	-73.09
G740	Front	X	dB	-61.01	-29.77	7.55	-42.07	-81.08	-66.11	-57.21	-18.54	-61.62	-76.10
G740	Rear	X	dB	-62.19	-33.00	-5.58	-36.94	-83.76	-74.19	-51.38	-23.45	-63.35	-81.13
G740	Left	X	dB	-61.86	-37.52	-8.30	-47.66	-74.29	-70.08	-57.38	-11.63	-69.58	-81.49
G740	Right	X	dB	-59.35	-34.14	1.36	-49.19	-70.08	-68.47	-51.54	-12.87	-70.65	-86.66
G740	Audience	X	dB	-78.66	-37.32	2.22	-45.52	-90.62	-70.49	-60.03	-20.08	-75.85	-92.61
G740	SideWallsL	X	dB	-65.30	-40.76	-1.70	-42.53	-91.20	-81.67	-64.92	-29.71	-78.92	-94.97
G740	SideWallsR	X	dB	-68.46	-43.03	-0.98	-52.64	-88.53	-79.36	-60.19	-17.21	-87.75	-107.33
G740	Top/Bottom		dB	-3.25	-9.14	-17.78	0.34	-19.30	3.44	11.75	5.46	-13.86	-12.58
G740	Front/Rear		dB	1.18	3.23	13.13	-5.13	2.68	8.08	-5.83	4.91	1.74	5.03
G740	Left/Right		dB	-2.51	-3.39	-9.66	1.53	-4.21	-1.61	-5.84	1.24	1.07	5.17
G740	Front/Sides		dB	-36.00	-2.33	1.71	-10.21	-27.02	-12.48	-15.63	2.97	-7.70	-11.34
G740	Top/Sides		dB	-18.95	0.04	-13.28	3.67	-23.70	-6.88	-2.38	11.29	-3.25	-4.39
G740	Top/Rear		dB	0.58	-1.95	-7.19	5.30	-3.54	9.28	4.61	11.69	-8.04	-4.54
G740	FrontTop/ RearBottom		dB	-2.06	-5.91	-4.65	-4.79	-16.61	11.52	5.92	10.37	-12.13	-7.55
G40end	Top		dB	16.78	14.69	11.93	36.86	22.49	23.96	13.13	17.92	37.15	46.80
G40end	Bottom		dB	15.89	14.16	12.05	35.99	22.02	22.97	12.38	15.30	37.21	44.56
G40end	Front		dB	16.38	20.84	9.67	33.96	20.35	20.82	10.04	19.65	35.13	43.21
G40end	Rear		dB	10.94	17.36	16.90	35.65	21.97	20.37	11.25	14.37	37.69	44.29
G40end	Left		dB	12.43	18.87	10.95	29.57	23.19	22.84	7.81	21.93	38.03	46.86
G40end	Right		dB	16.94	14.18	12.86	32.62	27.99	21.47	15.45	14.81	35.73	43.98
G40end	Audience		dB	8.02	15.97	4.20	18.18	17.69	19.53	6.63	14.90	26.25	31.95
G40end	SideWallsL		dB	10.63	11.86	8.02	27.02	13.73	13.62	5.67	13.73	27.75	32.24
G40end	SideWallsR		dB	12.96	9.15	10.92	19.82	18.98	15.35	11.06	7.85	25.03	29.23
G40end	Top	X	dB	-27.90	-35.36	-25.25	-65.46	-46.52	-42.26	-21.90	-34.06	-73.32	-88.05
G40end	Bottom	X	dB	-28.78	-35.89	-25.13	-66.33	-46.98	-43.24	-22.65	-36.69	-73.25	-90.29
G40end	Front	X	dB	-28.30	-29.21	-27.51	-68.37	-48.66	-45.39	-24.99	-32.34	-75.34	-91.64
G40end	Rear	X	dB	-33.74	-32.69	-20.27	-66.67	-47.04	-45.85	-23.78	-37.62	-72.78	-90.56
G40end	Left	X	dB	-32.25	-31.18	-26.23	-72.76	-45.81	-43.38	-27.22	-30.06	-72.44	-87.99
G40end	Right	X	dB	-27.74	-35.86	-24.32	-69.71	-41.01	-44.75	-19.58	-37.18	-74.74	-90.87
G40end	Audience	X	dB	-36.65	-34.07	-32.97	-84.14	-51.32	-46.69	-28.40	-37.09	-84.22	-102.90
G40end	SideWallsL	X	dB	-34.04	-38.19	-29.16	-75.30	-55.27	-52.59	-29.36	-38.26	-82.72	-102.60
G40end	SideWallsR	X	dB	-31.72	-40.89	-26.25	-82.51	-50.03	-50.87	-23.96	-44.14	-85.44	-105.62
G40end	Top/Bottom		dB	0.89	0.53	-0.12	0.87	0.46	0.98	0.75	2.63	-0.06	2.24
G40end	Front/Rear		dB	5.44	3.48	-7.23	-1.69	-1.62	0.45	-1.21	5.28	-2.56	-1.08
G40end	Left/Right		dB	-4.51	4.69	-1.91	-3.05	-4.80	1.37	-7.64	7.12	2.30	2.89
G40end	Front/Sides		dB	-15.57	-5.04	-14.74	-28.66	-15.02	-9.45	-10.11	-6.68	-26.52	-29.53
G40end	Top/Sides		dB	-6.81	-6.32	-7.01	-9.97	-10.22	-5.02	-3.61	-3.66	-15.62	-14.67
G40end	Top/Rear		dB	5.84	-2.67	-4.97	1.21	0.52	3.59	1.88	3.56	-0.54	2.52
G40end	FrontTop/ RearBottom		dB	6.32	4.01	-7.35	-0.82	-1.16	1.44	-0.46	7.91	-2.63	1.16
LQ740	Top		dB	3.18	-0.21	-5.38	-2.16	1.59	3.54	5.20	-1.45	-2.50	-2.86
LQ740	Bottom		dB	4.21	2.21	-0.96	-2.03	6.52	2.93	2.45	-2.16	0.95	0.85
LQ740	Front		dB	3.43	-0.45	0.27	-4.04	3.68	4.02	3.36	-3.58	0.45	0.43
LQ740	Rear		dB	4.49	-0.39	-4.83	-3.18	2.60	2.12	4.52	-3.49	-0.63	-1.09
LQ740	Left		dB	4.20	-1.90	-4.02	-4.34	4.66	2.53	3.88	-2.42	-2.27	-1.83
LQ740	Right		dB	3.70	0.12	-2.08	-5.49	4.52	3.27	3.43	-0.95	-1.96	-2.40
LQ740	Audience		dB	1.47	-1.50	0.40	-1.28	2.61	4.33	4.68	-3.71	-1.19	-1.18
LQ740	SideWallsL		dB	5.06	-1.27	-2.18	-3.23	3.73	2.57	3.37	-6.52	-2.71	-2.06
LQ740	SideWallsR		dB	3.22	-1.13	-2.91	-4.20	2.87	2.77	3.15	-0.40	-4.75	-5.18
LQ740	Top	X	dB	-0.69	-0.11	-2.55	1.38	-2.34	0.47	1.39	0.89	-1.51	-1.71
LQ740	Bottom	X	dB	0.34	2.31	1.87	1.51	2.60	-0.14	-1.36	0.18	1.94	2.00

PARAMETER				HALL									
Parameter	Direction	Normalized	Units	Alb Recital	Alb Theatre	Bard	Buffalo	Eastman	EMPAC C	EMPAC Th	Skidmore	St. Rose	Vassar
LQ740	Front	X	dB	-0.44	-0.35	3.10	-0.50	-0.25	0.96	-0.44	-1.24	1.44	1.58
LQ740	Rear	X	dB	0.62	-0.29	-1.99	0.36	-1.33	-0.95	0.71	-1.14	0.37	0.06
LQ740	Left	X	dB	0.33	-1.79	-1.18	-0.80	0.74	-0.54	0.07	-0.08	-1.27	-0.68
LQ740	Right	X	dB	-0.17	0.22	0.75	-1.95	0.59	0.20	-0.38	1.39	-0.97	-1.25
LQ740	Audience	X	dB	-2.40	-1.39	3.23	2.26	-1.32	1.27	0.88	-1.36	-0.19	-0.02
LQ740	SideWallsL	X	dB	1.19	-1.17	0.66	0.31	-0.19	-0.49	-0.44	-4.18	-1.72	-0.91
LQ740	SideWallsR	X	dB	-0.64	-1.02	-0.07	-0.66	-1.05	-0.30	-0.66	1.94	-3.75	-4.02
LQ740	Top/Bottom		dB	-1.03	-2.42	-4.42	-0.13	-4.94	0.61	2.75	0.71	-3.45	-3.71
LQ740	Front/Rear		dB	-1.06	-0.06	5.09	-0.86	1.08	1.91	-1.16	-0.09	1.07	1.53
LQ740	Left/Right		dB	0.50	-2.02	-1.94	1.15	0.15	-0.74	0.45	-1.47	-0.31	0.57
LQ740	Front/Sides		dB	-2.67	-0.30	2.94	2.43	-0.70	1.66	1.42	-0.24	2.54	2.44
LQ740	Top/Sides		dB	-0.96	0.99	-2.84	1.56	-1.72	0.87	1.94	2.01	1.23	0.76
LQ740	Top/Rear		dB	-1.32	0.18	-0.55	1.02	-1.01	1.42	0.68	2.03	-1.88	-1.76
LQ740	FrontTop/ RearBottom		dB	-1.05	-1.24	0.34	-0.50	-1.93	1.26	0.80	0.31	-1.19	-1.09
Glate	Top		dB	3.32	11.26	7.68	29.30	16.71	20.28	5.73	10.10	32.18	39.65
Glate	Bottom		dB	1.17	10.56	6.53	28.85	15.95	19.51	4.50	9.20	31.14	38.57
Glate	Front		dB	4.38	16.48	5.74	26.81	13.31	17.12	4.13	11.39	29.27	36.44
Glate	Rear		dB	-3.17	13.45	12.34	28.94	15.50	16.24	2.24	7.07	31.29	37.59
Glate	Left		dB	-1.53	14.60	4.44	23.18	16.46	19.52	1.90	14.71	33.50	39.23
Glate	Right		dB	5.47	10.02	9.13	24.34	19.69	17.33	5.51	8.72	29.77	37.02
Glate	Audience		dB	-0.87	12.79	1.02	13.49	12.62	16.61	1.38	8.71	22.16	26.92
Glate	SideWallsL		dB	0.45	9.01	2.97	22.24	8.35	10.91	1.50	8.48	24.43	27.16
Glate	SideWallsR		dB	5.15	6.03	8.06	13.71	12.66	12.07	2.40	3.40	19.92	24.43
Glate	Top	X	dB	-1.50	-26.92	-15.25	-51.41	-32.10	-34.72	-6.27	-20.50	-61.40	-74.61
Glate	Bottom	X	dB	-3.65	-27.62	-16.40	-51.86	-32.86	-35.49	-7.51	-21.40	-62.44	-75.68
Glate	Front	X	dB	-0.44	-21.70	-17.19	-53.90	-35.50	-37.88	-7.88	-19.20	-64.31	-77.81
Glate	Rear	X	dB	-8.00	-24.73	-10.59	-51.77	-33.31	-38.76	-9.76	-23.53	-62.29	-76.66
Glate	Left	X	dB	-6.35	-23.58	-18.49	-57.53	-32.35	-35.48	-10.11	-15.89	-60.08	-75.02
Glate	Right	X	dB	0.65	-28.16	-13.80	-56.38	-29.12	-37.67	-6.50	-21.88	-63.81	-77.24
Glate	Audience	X	dB	-5.69	-25.40	-21.91	-67.22	-36.19	-38.39	-10.63	-21.89	-71.42	-87.34
Glate	SideWallsL	X	dB	-4.38	-29.17	-19.96	-58.47	-40.46	-44.09	-10.50	-22.11	-69.15	-87.09
Glate	SideWallsR	X	dB	0.33	-32.15	-14.87	-67.00	-36.15	-42.93	-9.60	-27.19	-73.66	-89.83
Glate	Top/Bottom		dB	2.15	0.70	1.15	0.45	0.76	0.77	1.24	0.90	1.04	1.07
Glate	Front/Rear		dB	7.56	3.03	6.61	-2.13	-2.19	0.88	1.89	4.32	-2.02	-1.15
Glate	Left/Right		dB	-7.00	4.58	-4.69	-1.16	-3.23	2.19	-3.61	5.99	3.72	2.21
Glate	Front/Sides		dB	-6.47	-2.25	-10.01	-22.47	-8.39	-6.37	-2.53	-3.18	-22.19	-24.67
Glate	Top/Sides		dB	-2.28	-3.78	-3.35	-6.65	-4.30	-2.70	1.83	-1.79	-12.16	-11.95
Glate	Top/Rear		dB	6.49	-2.19	-4.66	0.36	1.20	4.03	3.49	3.03	0.88	2.05
Glate	FrontTop/ RearBottom		dB	9.70	3.73	-5.46	-1.68	-1.43	1.65	3.12	5.22	-0.98	-0.08
RR160	Top		dB	-17.82	-12.58	-5.46	-11.24	-11.23	-14.08	-19.66	-12.30	-8.79	-8.48
RR160	Bottom		dB	-20.04	-16.30	-10.24	-11.21	-17.45	-13.64	-14.90	-8.60	-13.71	-11.69
RR160	Front		dB	-17.21	-13.48	-9.54	-9.89	-14.62	-13.58	-16.95	-10.53	-11.92	-10.93
RR160	Rear		dB	-18.09	-12.23	-6.40	-10.05	-13.64	-12.12	-17.63	-8.42	-11.11	-10.19
RR160	Left		dB	-19.16	-11.37	-7.11	-9.26	-15.39	-12.97	-16.62	-9.55	-9.24	-9.07
RR160	Right		dB	-17.08	-13.06	-7.79	-8.40	-15.51	-14.20	-16.33	-11.80	-9.62	-9.26
RR160	Audience		dB	-15.89	-11.75	-9.61	-12.23	-13.19	-14.70	-17.59	-9.18	-10.38	-9.27
RR160	SideWallsL		dB	-19.53	-10.90	-8.03	-9.90	-13.61	-13.92	-14.90	-7.13	-7.26	-7.97
RR160	SideWallsR		dB	-16.88	-10.36	-7.53	-8.96	-13.71	-13.77	-16.26	-12.11	-7.45	-7.68
RR160	Top	X	dB	0.41	0.59	2.29	-1.23	3.41	-0.65	-2.65	-2.10	1.94	1.45
RR160	Bottom	X	dB	-1.81	-3.13	-2.48	-1.20	-2.82	-0.21	2.12	1.60	-2.98	-1.75
RR160	Front	X	dB	1.02	-0.31	-1.78	0.12	0.02	-0.14	0.06	-0.33	-1.19	-1.00
RR160	Rear	X	dB	0.15	0.94	1.35	-0.04	1.00	1.31	-0.61	1.78	-0.38	-0.25
RR160	Left	X	dB	-0.93	1.80	0.65	0.75	-0.75	0.46	0.39	0.65	1.49	0.86
RR160	Right	X	dB	1.15	0.11	-0.03	1.61	-0.87	-0.77	0.69	-1.60	1.11	0.68
RR160	Audience	X	dB	2.35	1.42	-1.85	-2.22	1.45	-1.27	-0.57	1.02	0.35	0.67
RR160	SideWallsL	X	dB	-1.30	2.27	-0.27	0.11	1.03	-0.49	2.12	3.07	3.47	1.97
RR160	SideWallsR	X	dB	1.36	2.81	0.23	1.05	0.93	-0.34	0.75	-1.91	3.28	2.26
RR160	Top/Bottom		dB	2.22	3.72	4.77	-0.03	6.22	-0.44	-4.77	-3.70	4.92	3.20
RR160	Front/Rear		dB	0.87	-1.25	-3.14	0.15	-0.98	-1.46	0.68	-2.11	-0.81	-0.75
RR160	Left/Right		dB	-2.08	1.69	0.68	-0.86	0.12	1.23	-0.29	2.25	0.38	0.18
RR160	Front/Sides		dB	2.32	-1.12	-1.83	-2.80	0.47	-0.86	-2.01	0.44	-3.02	-1.44
RR160	Top/Sides		dB	0.38	-1.96	2.31	-1.82	2.43	-0.24	-4.08	-2.68	-1.44	-0.66
RR160	Top/Rear		dB	0.26	-0.35	0.94	-1.19	2.41	-1.97	-2.04	-3.88	2.31	1.70
RR160	FrontTop/ RearBottom		dB	1.55	1.24	0.82	0.06	2.62	-0.95	-2.05	-2.91	2.05	1.23
ST1	Top		dB	-8.16	-10.19	-1.47	-6.71	-5.90	-12.96	-13.06	-7.15	-4.00	-1.28
ST1	Bottom		dB	-9.62	-13.62	-6.15	-6.74	-9.60	-11.64	-8.07	-4.32	-9.13	-6.89
ST1	Front		dB	-7.94	-9.05	-7.43	-4.19	-7.19	-11.21	-10.52	-5.51	-7.03	-4.13
ST1	Rear		dB	-7.26	-8.11	-2.53	-5.29	-4.60	-9.58	-10.07	-2.84	-6.06	-2.51

PARAMETER				HALL									
Parameter	Direction	Normalized	Units	Alb Recital	Alb Theatre	Bard	Buffalo	Eastman	EMPAC C	EMPAC Th	Skidmore	St. Rose	Vassar
ST1	Left		dB	-8.45	-6.27	-1.92	-4.57	-6.01	-11.12	-11.23	-4.42	-4.21	-0.80
ST1	Right		dB	-7.82	-8.68	-4.74	-1.91	-7.58	-12.37	-6.57	-8.20	-4.94	-2.24
ST1	Audience		dB	-6.14	-7.74	-6.51	-8.40	-5.28	-12.51	-11.05	-2.59	-5.21	-1.28
ST1	SideWallsL		dB	-9.31	-6.63	-3.30	-5.93	-1.01	-12.41	-8.34	-0.04	-1.36	3.68
ST1	SideWallsR		dB	-7.46	-6.31	-4.80	-3.45	-5.52	-11.64	-5.23	-8.02	-0.15	2.13
ST1	Top	X	dB	0.05	-0.87	2.57	-1.81	0.92	-1.48	-3.14	-1.74	1.89	1.69
ST1	Bottom	X	dB	-1.41	-4.30	-2.11	-1.84	-2.79	-0.16	1.85	1.08	-3.23	-3.92
ST1	Front	X	dB	0.27	0.27	-3.39	0.71	-0.38	0.27	-0.60	-0.10	-1.13	-1.15
ST1	Rear	X	dB	0.95	1.21	1.51	-0.39	2.21	1.90	-0.15	2.57	-0.16	0.47
ST1	Left	X	dB	-0.24	3.06	2.12	0.33	0.81	0.36	-1.31	0.99	1.68	2.18
ST1	Right	X	dB	0.39	0.64	-0.71	2.99	-0.77	-0.89	3.35	-2.79	0.96	0.74
ST1	Audience	X	dB	2.07	1.58	-2.47	-3.50	1.53	-1.03	-1.13	2.82	0.69	1.70
ST1	SideWallsL	X	dB	-1.11	2.69	0.74	-1.03	5.81	-0.93	1.58	5.36	4.54	6.65
ST1	SideWallsR	X	dB	0.75	3.01	-0.76	1.45	1.30	-0.16	4.69	-2.61	5.75	5.11
ST1	Top/Bottom		dB	1.46	3.43	4.68	0.03	3.70	-1.32	-4.99	-2.82	5.12	5.61
ST1	Front/Rear		dB	-0.68	-0.94	-4.91	1.10	-2.59	-1.63	-0.45	-2.67	-0.97	-1.62
ST1	Left/Right		dB	-0.63	2.42	2.83	-2.66	1.57	1.25	-4.67	3.78	0.72	1.44
ST1	Front/Sides		dB	2.25	-1.28	-2.46	-3.71	-2.02	-0.48	-4.26	1.44	-4.46	-4.18
ST1	Top/Sides		dB	0.23	-3.72	2.58	-2.02	-2.64	-0.93	-6.28	-3.12	-3.25	-4.19
ST1	Top/Rear		dB	-0.90	-2.08	1.06	-1.42	-1.30	-3.38	-2.99	-4.31	2.05	1.22
ST1	FrontTop/ RearBottom		dB	0.39	1.25	-0.11	0.57	0.56	-1.47	-2.72	-2.75	2.08	1.99
ST2	Top		dB	-11.54	-7.93	1.80	-5.94	-4.99	-9.76	-15.01	-6.83	-2.74	-1.58
ST2	Bottom		dB	-13.54	-11.54	-4.96	-5.71	-11.74	-9.14	-9.73	-3.08	-9.10	-6.93
ST2	Front		dB	-10.85	-7.70	-4.70	-3.24	-8.52	-9.36	-12.27	-5.47	-6.54	-4.74
ST2	Rear		dB	-11.67	-6.47	0.02	-3.91	-6.52	-7.20	-13.03	-2.32	-6.11	-3.76
ST2	Left		dB	-12.46	-4.83	-0.64	-3.11	-8.55	-8.56	-12.06	-4.13	-3.20	-1.87
ST2	Right		dB	-10.69	-7.15	-1.56	-1.47	-9.04	-10.10	-10.49	-7.07	-4.07	-2.21
ST2	Audience		dB	-9.38	-6.50	-4.49	-6.97	-6.45	-10.69	-12.92	-2.75	-4.54	-1.79
ST2	SideWallsL		dB	-13.11	-4.67	-2.32	-4.46	-4.22	-9.57	-9.60	0.74	-0.43	2.25
ST2	SideWallsR		dB	-9.96	-4.74	-1.51	-2.83	-6.71	-9.40	-10.57	-7.05	0.24	2.51
ST2	Top	X	dB	0.25	-0.33	3.47	-2.04	3.24	-0.74	-2.91	-2.02	2.55	1.94
ST2	Bottom	X	dB	-1.75	-3.93	-3.29	-1.82	-3.52	-0.12	2.37	1.74	-3.81	-3.42
ST2	Front	X	dB	0.94	-0.10	-3.02	0.66	-0.29	-0.33	-0.17	-0.65	-1.25	-1.23
ST2	Rear	X	dB	0.12	1.13	1.69	-0.01	1.71	1.82	-0.93	2.50	-0.81	-0.24
ST2	Left	X	dB	-0.66	2.78	1.03	0.78	-0.32	0.46	0.04	0.69	2.09	1.65
ST2	Right	X	dB	1.11	0.45	0.11	2.43	-0.82	-1.08	1.61	-2.25	1.23	1.30
ST2	Audience	X	dB	2.41	1.10	-2.82	-3.07	1.78	-1.67	-0.82	2.07	0.76	1.73
ST2	SideWallsL	X	dB	-1.32	2.94	-0.65	-0.56	4.00	-0.55	2.50	5.55	4.87	5.77
ST2	SideWallsR	X	dB	1.83	2.86	0.17	1.07	1.52	-0.38	1.53	-2.24	5.54	6.02
ST2	Top/Bottom		dB	2.00	3.61	6.76	-0.23	6.76	-0.62	-5.27	-3.75	6.36	5.35
ST2	Front/Rear		dB	0.82	-1.23	-4.72	0.67	-2.00	-2.15	0.76	-3.15	-0.44	-0.98
ST2	Left/Right		dB	-1.77	2.33	0.92	-1.65	0.49	1.54	-1.57	2.94	0.87	0.35
ST2	Front/Sides		dB	2.16	-1.80	-2.58	-3.33	-0.98	-1.21	-2.83	0.41	-4.45	-4.16
ST2	Top/Sides		dB	0.00	-3.23	3.71	-2.30	0.48	-0.28	-4.92	-3.67	-2.65	-3.96
ST2	Top/Rear		dB	0.13	-1.46	1.78	-2.03	1.53	-2.56	-1.97	-4.51	3.37	2.18
ST2	FrontTop/ RearBottom		dB	1.41	1.19	1.02	0.22	2.38	-1.38	-2.26	-3.45	2.96	2.19
ST3	Top		dB	-6.49	-5.90	3.50	-3.27	-2.39	-8.05	-10.78	-3.93	-0.28	1.60
ST3	Bottom		dB	-8.11	-9.45	-2.48	-3.13	-7.50	-7.20	-5.79	-0.56	-6.08	-3.89
ST3	Front		dB	-6.14	-5.29	-2.83	-0.68	-4.68	-7.16	-8.24	-2.44	-3.74	-1.41
ST3	Rear		dB	-5.89	-4.20	1.96	-1.45	-2.31	-5.20	-8.26	0.46	-3.06	-0.03
ST3	Left		dB	-6.98	-2.44	1.81	-0.73	-3.99	-6.60	-8.60	-1.25	-0.64	1.78
ST3	Right		dB	-5.99	-4.84	0.17	1.38	-5.21	-8.07	-5.06	-4.51	-1.47	0.80
ST3	Audience		dB	-4.45	-4.04	-2.34	-4.61	-2.70	-8.49	-8.82	0.35	-1.83	1.50
ST3	SideWallsL		dB	-7.80	-2.50	0.23	-2.10	0.87	-7.70	-5.92	3.39	2.16	6.08
ST3	SideWallsR		dB	-5.51	-2.44	0.17	-0.04	-3.04	-7.37	-4.09	-4.49	3.09	5.41
ST3	Top	X	dB	0.11	-0.54	3.15	-1.96	1.96	-1.00	-2.99	-1.89	2.26	1.79
ST3	Bottom	X	dB	-1.50	-4.10	-2.83	-1.82	-3.15	-0.15	2.00	1.48	-3.54	-3.70
ST3	Front	X	dB	0.46	0.06	-3.19	0.64	-0.34	-0.11	-0.45	-0.40	-1.19	-1.22
ST3	Rear	X	dB	0.71	1.15	1.61	-0.14	2.03	1.84	-0.47	2.50	-0.51	0.16
ST3	Left	X	dB	-0.38	2.91	1.45	0.59	0.35	0.45	-0.81	0.78	1.90	1.97
ST3	Right	X	dB	0.61	0.51	-0.19	2.69	-0.86	-1.02	2.73	-2.47	1.08	1.00
ST3	Audience	X	dB	2.15	1.31	-2.70	-3.30	1.65	-1.44	-1.03	2.39	0.72	1.69
ST3	SideWallsL	X	dB	-1.20	2.85	-0.12	-0.79	5.22	-0.65	1.87	5.43	4.70	6.28
ST3	SideWallsR	X	dB	1.10	2.91	-0.18	1.27	1.31	-0.32	3.69	-2.45	5.63	5.60
ST3	Top/Bottom		dB	1.61	3.55	5.98	-0.14	5.12	-0.85	-4.99	-3.37	5.80	5.49
ST3	Front/Rear		dB	-0.25	-1.09	-4.79	0.77	-2.37	-1.95	0.01	-2.90	-0.68	-1.38
ST3	Left/Right		dB	-0.99	2.40	1.64	-2.11	1.21	1.47	-3.54	3.25	0.83	0.97
ST3	Front/Sides		dB	2.20	-1.57	-2.55	-3.54	-1.61	-0.95	-3.81	0.90	-4.45	-4.25
ST3	Top/Sides		dB	0.16	-3.42	3.30	-2.20	-1.30	-0.51	-5.78	-3.38	-2.90	-4.15

PARAMETER				HALL									
Parameter	Direction	Normalized	Units	Alb Recital	Alb Theatre	Bard	Buffalo	Eastman	EMPAC C	EMPAC Th	Skidmore	St. Rose	Vassar
ST3	Top/Rear		dB	-0.60	-1.70	1.54	-1.82	-0.07	-2.84	-2.53	-4.39	2.78	1.63
ST3	FrontTop/ RearBottom		dB	0.68	1.23	0.59	0.32	1.37	-1.40	-2.49	-3.13	2.56	2.06
DD (0-30 ms)			%	24.06	18.01	4.24	24.56	6.45	27.13	32.79	26.88	27.05	18.87
Gtotal	Omni		dB	27.88	27.68	27.24	26.23	27.90	26.98	28.16	25.32	25.36	27.19
Gearly	Omni		dB	27.77	27.56	27.13	25.93	27.71	26.80	28.04	25.11	25.00	26.76
Glate	Omni		dB	11.78	12.03	11.08	14.55	14.24	13.01	12.41	11.99	14.36	16.95
Gsupport	Omni		dB	14.95	9.91	10.09	13.63	15.26	11.88	13.36	11.41	13.95	16.45
G740	Omni		dB	20.63	20.36	17.33	19.28	23.89	20.41	21.82	18.13	19.17	21.73
G40end	Omni		dB	14.59	13.22	12.66	16.19	16.25	14.78	14.36	14.10	16.14	18.77
LQ740	Omni		dB	6.04	7.14	4.67	3.09	7.64	5.63	7.46	4.03	3.04	2.96
RR160	Omni		dB	-22.20	-19.93	-21.00	-15.77	-20.10	-18.02	-20.88	-17.43	-15.13	-14.38
ST1	Omni		dB	-14.30	-18.70	-17.70	-13.00	-12.70	-16.30	-14.30	-15.00	-10.70	-10.30
ST2	Omni		dB	-19.30	-18.30	-16.70	-12.30	-15.00	-14.70	-16.00	-14.30	-10.30	-9.70
ST3	Omni		dB	-13.00	-15.00	-14.30	-9.70	-10.70	-12.30	-12.00	-11.30	-7.00	-7.00
C80	Omni		dB	3.20	0.37	1.93	1.33	1.40	4.57	2.40	2.73	2.10	1.33
D50	Omni		%	53.67	39.67	48.67	47.67	42.33	68.67	50.00	53.33	52.00	49.00
Tc	Omni		ms	63.67	101.67	95.67	100.00	102.00	60.67	67.00	85.67	82.33	85.67
EDT	Omni		s	0.90	1.49	1.47	1.96	1.71	2.15	1.11	2.24	1.60	1.52
T30	Omni		s	0.97	1.53	1.78	2.05	2.01	2.25	1.07	2.18	1.64	1.56
BR	Omni		none	1.31	1.18	0.91	0.98	1.15	1.19	1.39	1.03	1.22	0.93

APPENDIX B

ENSEMBLE PARAMETERS

Ensemble parameters used in this study, calculated from the cross-stage and up-down-stage “ensemble” impulse responses, shown here for the 1 kHz octave band. “Normalized” versions of spatial parameters were divided by the total omnidirectional energy in the given parameter if units were in dB, or the average value over all directions if units were time or percent.

PARAMETER					HALL									
Parameter	Location	Direction	Normalized	Units	Alb Recital	Alb Theatre	Bard	Buffalo	Eastman	EMPAC C	EMPAC Th	Skidmore	St Rose	Vassar
CenterTime	Cross-Stage	Top		ms	73.23	127.85	111.07	124.35	116.64	169.17	91.88	161.30	129.34	127.55
CenterTime	Cross-Stage	Bottom		ms	68.02	130.82	113.30	123.70	114.20	168.56	95.69	147.59	128.09	123.87
CenterTime	Cross-Stage	Front		ms	73.72	133.35	119.64	142.95	113.47	176.39	99.18	129.29	138.74	126.06
CenterTime	Cross-Stage	Rear		ms	65.44	131.11	119.77	125.65	112.70	166.11	92.74	139.75	132.80	125.33
CenterTime	Cross-Stage	Left		ms	58.73	138.57	104.70	125.90	106.25	177.48	95.57	155.08	141.02	120.75
CenterTime	Cross-Stage	Right		ms	88.79	122.94	115.44	129.12	97.69	164.42	95.96	161.26	127.53	128.21
CenterTime	Cross-Stage	Audience		ms	75.34	132.98	123.20	155.38	118.92	170.95	100.47	126.17	135.56	122.81
CenterTime	Cross-Stage	SideWallsL		ms	54.05	142.82	97.92	126.67	99.92	175.78	96.23	154.80	144.32	107.33
CenterTime	Cross-Stage	SideWallsR		ms	95.78	113.61	122.16	132.33	96.38	160.79	92.51	167.66	118.75	125.46
CenterTime	Cross-Stage	Top	X	ms	1.91	-2.92	-2.92	-4.26	6.48	-1.18	-3.29	12.25	-3.58	2.25
CenterTime	Cross-Stage	Bottom	X	ms	-3.30	0.04	-0.68	-4.92	4.04	-1.80	0.52	-1.45	-4.83	-1.42
CenterTime	Cross-Stage	Front	X	ms	2.40	2.57	5.66	14.34	3.31	6.03	4.01	-19.75	5.82	0.77
CenterTime	Cross-Stage	Rear	X	ms	-5.88	0.34	5.78	-2.96	2.54	-4.25	-2.43	-9.29	-0.12	0.03
CenterTime	Cross-Stage	Left	X	ms	-12.59	7.80	-9.29	-2.71	-3.91	7.12	0.40	6.04	8.10	-4.54
CenterTime	Cross-Stage	Right	X	ms	17.47	-7.83	1.45	0.51	-12.46	-5.93	0.79	12.21	-5.39	2.92
CenterTime	Cross-Stage	Audience	X	ms	4.01	2.20	9.22	26.77	8.76	0.59	5.30	-22.87	2.64	-2.49
CenterTime	Cross-Stage	SideWallsL	X	ms	-17.27	12.05	-16.07	-1.94	-10.23	5.43	1.06	5.76	11.39	-17.97
CenterTime	Cross-Stage	SideWallsR	X	ms	24.45	-17.17	8.17	3.71	-13.78	-9.57	-2.66	18.62	-14.17	0.16
CenterTime	Cross-Stage	Top/Bottom		ms	5.21	-2.96	-2.24	0.66	2.44	0.62	-3.81	13.71	1.25	3.68
CenterTime	Cross-Stage	Front/Rear		ms	8.28	2.24	-0.12	17.30	0.77	10.28	6.44	-10.46	5.95	0.73
CenterTime	Cross-Stage	Left/Right		ms	-30.06	15.63	-10.74	-3.22	8.56	13.06	-0.40	-6.18	13.49	-7.46
CenterTime	Cross-Stage	Front/Sides		ms	0.42	4.76	13.16	25.88	20.77	2.66	6.10	-35.06	4.03	6.42
CenterTime	Cross-Stage	Top/Sides		ms	-1.68	-0.36	1.03	-5.15	18.48	0.89	-2.49	0.07	-2.19	11.15
CenterTime	Cross-Stage	Top/Rear		ms	7.79	-3.26	-8.70	-1.30	3.94	3.07	-0.86	21.54	-3.45	2.22
CenterTime	Cross-Stage	FrontTop/ RearBottom		ms	6.75	-0.36	-1.18	8.98	1.60	5.45	1.31	1.62	3.60	2.20
CenterTime	UpDown-Stage	Top		ms	73.23	130.44	114.69	150.16	139.20	118.49	102.93	153.67	131.01	123.37
CenterTime	UpDown-Stage	Bottom		ms	68.02	142.98	115.23	164.58	113.37	158.63	104.14	169.87	123.13	116.36
CenterTime	UpDown-Stage	Front		ms	73.72	132.88	108.64	138.33	143.93	127.97	108.54	136.95	127.47	122.73
CenterTime	UpDown-Stage	Rear		ms	65.44	117.50	82.40	133.47	110.07	112.07	97.21	147.35	117.96	96.31
CenterTime	UpDown-Stage	Left		ms	58.73	144.07	117.28	144.11	126.56	125.62	96.05	123.30	133.23	122.95
CenterTime	UpDown-Stage	Right		ms	88.79	117.92	94.29	139.73	117.43	111.26	100.39	148.48	109.09	98.53
CenterTime	UpDown-Stage	Audience		ms	75.34	129.58	109.67	144.25	138.13	113.26	104.78	137.75	125.43	116.81
CenterTime	UpDown-Stage	SideWallsL		ms	54.05	139.67	106.34	138.47	132.24	121.89	92.47	115.23	132.23	127.21
CenterTime	UpDown-Stage	SideWallsR		ms	95.78	115.24	92.86	146.59	110.79	94.82	92.65	138.97	106.78	105.43
CenterTime	UpDown-Stage	Top	X	ms	1.91	-0.52	9.27	5.09	14.10	-7.18	1.39	7.07	7.36	9.99
CenterTime	UpDown-Stage	Bottom	X	ms	-3.30	12.02	9.80	19.51	-11.72	32.95	2.59	23.27	-0.52	2.98
CenterTime	UpDown-Stage	Front	X	ms	2.40	1.91	3.22	-6.73	18.83	2.30	7.00	-9.66	3.82	9.35
CenterTime	UpDown-Stage	Rear	X	ms	-5.88	-13.46	-23.02	-11.59	-15.02	-13.60	-4.33	0.75	-5.69	-17.07
CenterTime	UpDown-Stage	Left	X	ms	-12.59	13.11	11.86	-0.95	1.47	-0.05	-5.50	-23.31	9.58	9.58
CenterTime	UpDown-Stage	Right	X	ms	17.47	-13.05	-11.13	-5.33	-7.66	-14.41	-1.15	1.87	-14.55	-14.84
CenterTime	UpDown-Stage	Audience	X	ms	4.01	-1.39	4.25	-0.81	13.04	-12.42	3.24	-8.85	1.78	3.43
CenterTime	UpDown-Stage	SideWallsL	X	ms	-17.27	8.71	0.92	-6.59	7.15	-3.78	-9.07	-31.37	8.58	13.83
CenterTime	UpDown-Stage	SideWallsR	X	ms	24.45	-15.73	-12.56	1.53	-14.30	-30.85	-8.89	-7.63	-16.87	-7.94
CenterTime	UpDown-Stage	Top/Bottom		ms	5.21	-12.54	-0.53	-14.42	25.83	-40.14	-1.20	-16.20	7.88	7.01
CenterTime	UpDown-Stage	Front/Rear		ms	8.28	15.38	26.24	4.86	33.86	15.90	11.33	-10.40	9.51	26.42
CenterTime	UpDown-Stage	Left/Right		ms	-30.06	26.16	22.99	4.38	9.13	14.36	-4.34	-25.18	24.14	24.42
CenterTime	UpDown-Stage	Front/Sides		ms	0.42	2.12	10.07	1.72	16.61	4.90	12.22	10.65	5.93	0.49
CenterTime	UpDown-Stage	Top/Sides		ms	-1.68	2.99	15.09	7.62	17.68	10.13	10.37	26.57	11.51	7.05
CenterTime	UpDown-Stage	Top/Rear		ms	7.79	12.94	32.29	16.68	29.13	6.42	5.72	6.32	13.06	27.06
CenterTime	UpDown-Stage	FrontTop/ RearBottom		ms	6.75	1.42	12.85	-4.78	29.84	-12.12	5.06	-13.30	8.70	16.72
Gearly	Cross-Stage	Top		dB	56.61	-9.17	3.44	36.94	9.63	5.83	3.04	22.23	34.31	18.84
Gearly	Cross-Stage	Bottom		dB	58.53	-8.03	0.09	36.73	6.19	5.77	0.49	27.73	33.58	19.91
Gearly	Cross-Stage	Front		dB	56.94	-13.27	-1.94	30.00	9.30	6.20	-3.10	33.78	27.87	15.95
Gearly	Cross-Stage	Rear		dB	55.21	-11.50	2.12	40.57	6.55	8.08	1.10	27.23	28.77	16.94
Gearly	Cross-Stage	Left		dB	59.93	-7.29	-0.04	33.67	11.36	4.49	5.26	29.12	31.22	21.51
Gearly	Cross-Stage	Right		dB	51.67	-1.65	1.48	34.53	17.14	6.12	6.47	21.93	33.84	13.91
Gearly	Cross-Stage	Audience		dB	39.06	-6.83	-5.26	16.41	7.17	7.25	-1.23	26.08	21.49	12.10
Gearly	Cross-Stage	SideWallsL		dB	46.91	-9.15	1.35	24.54	7.49	0.37	0.12	20.11	19.83	18.68
Gearly	Cross-Stage	SideWallsR		dB	36.75	-0.72	-0.09	26.33	11.27	3.96	2.32	10.61	24.87	10.00
Gearly	Cross-Stage	Top	X	dB	-112.84	16.29	0.87	-69.28	-20.46	-12.41	-3.59	-58.78	-60.48	-34.69
Gearly	Cross-Stage	Bottom	X	dB	-110.91	17.43	-2.49	-69.49	-23.89	-12.47	-6.14	-53.28	-61.21	-33.62
Gearly	Cross-Stage	Front	X	dB	-112.50	12.19	-4.51	-76.22	-20.78	-12.04	-9.74	-47.23	-66.92	-37.58
Gearly	Cross-Stage	Rear	X	dB	-114.24	13.96	-0.46	-65.65	-23.54	-10.16	-5.53	-53.78	-66.02	-36.59
Gearly	Cross-Stage	Left	X	dB	-109.51	18.17	-2.61	-72.56	-18.73	-13.75	-1.38	-51.89	-63.58	-32.01
Gearly	Cross-Stage	Right	X	dB	-117.78	23.81	-1.10	-71.69	-12.94	-12.12	-0.16	-59.08	-60.96	-39.62
Gearly	Cross-Stage	Audience	X	dB	-130.38	18.63	-7.84	-89.81	-22.91	-10.99	-7.87	-54.93	-73.31	-41.43
Gearly	Cross-Stage	SideWallsL	X	dB	-122.53	16.31	-1.22	-81.68	-22.59	-17.86	-6.51	-60.90	-74.96	-34.84
Gearly	Cross-Stage	SideWallsR	X	dB	-132.69	24.74	-2.67	-79.89	-18.82	-14.28	-4.32	-70.40	-69.92	-43.52
Gearly	Cross-Stage	Top/Bottom		dB	-1.93	-1.14	3.36	0.21	3.44	0.06	2.55	-5.49	0.73	-1.07
Gearly	Cross-Stage	Front/Rear		dB	1.73	-1.76	-4.06	-10.57	2.76	-1.88	-4.21	6.55	-0.90	-0.99
Gearly	Cross-Stage	Left/Right		dB	8.26	-5.64	-1.51	-0.86	-5.79	-1.63	-1.21	7.19	-2.62	7.61
Gearly	Cross-Stage	Front/Sides		dB	-44.60	3.04	-6.52	-34.47	-11.58	2.92	-3.67	-4.64	-23.21	-16.59
Gearly	Cross-Stage	Top/Sides		dB	-27.05	0.70	2.18	-13.93	-9.13	1.49	0.61	-8.49	-10.38	-9.85
Gearly	Cross-Stage	Top/Rear		dB	1.40	2.33	1.32	-3.63	3.08	-2.25	1.94	-5.00	5.54	1.90
Gearly	Cross-Stage	FrontTop/ RearBottom		dB	-0.19	-2.91	-0.70	-10.35	6.20	-1.82	-1.66	1.06	-0.17	-2.06
Gearly	UpDown-Stage	Top		dB	56.61	10.04	3.85	11.56	28.49	-7.06	6.51	-5.49	30.11	21.09
Gearly	UpDown-Stage	Bottom		dB	58.53	3.04	2.90	5.88	36.84	-19.29	6.75	-10.73	33.56	23.46
Gearly	UpDown-Stage	Front		dB	56.94	11.81	3.55	12.04	26.28	-6.04	2.67	1.41	29.26	17.24

PARAMETER					HALL									
Parameter	Location	Direction	Normalized	Units	Alb Recital	Alb Theatre	Bard	Buffalo	Eastman	EMPAC C	EMPAC Th	Skidmore	St Rose	Vassar
Gearly	Up/Down-Stage	Rear		dB	55.21	18.76	21.31	16.72	36.17	-3.06	9.24	-5.28	36.11	29.15
Gearly	Up/Down-Stage	Left		dB	59.93	4.81	-0.13	7.47	32.19	-7.35	8.03	9.02	31.68	22.11
Gearly	Up/Down-Stage	Right		dB	51.67	16.27	12.35	11.56	37.95	-4.67	8.64	-4.59	36.93	27.97
Gearly	Up/Down-Stage	Audience		dB	39.06	11.08	-0.57	0.49	23.64	-0.21	1.97	0.88	21.99	14.80
Gearly	Up/Down-Stage	SideWallsL		dB	46.91	4.09	2.33	11.73	19.19	-8.06	8.09	6.09	22.77	13.52
Gearly	Up/Down-Stage	SideWallsR		dB	36.75	12.08	10.10	2.37	28.47	-1.19	8.33	-4.34	26.83	15.90
Gearly	Up/Down-Stage	Top	X	dB	-112.84	-22.33	-18.07	-21.05	-70.46	16.68	-14.41	2.34	-68.72	-49.42
Gearly	Up/Down-Stage	Bottom	X	dB	-110.91	-29.32	-19.02	-26.73	-62.12	4.45	-14.17	-2.89	-65.26	-47.05
Gearly	Up/Down-Stage	Front	X	dB	-112.50	-20.56	-18.37	-20.57	-72.68	17.70	-18.25	9.24	-69.57	-53.27
Gearly	Up/Down-Stage	Rear	X	dB	-114.24	-13.60	-0.60	-15.89	-62.78	20.68	-11.68	2.55	-62.72	-41.36
Gearly	Up/Down-Stage	Left	X	dB	-109.51	-27.56	-22.05	-25.14	-66.77	16.39	-12.89	16.85	-67.14	-48.40
Gearly	Up/Down-Stage	Right	X	dB	-117.78	-16.09	-9.57	-21.05	-61.01	19.07	-12.28	3.24	-61.89	-42.54
Gearly	Up/Down-Stage	Audience	X	dB	-130.38	-21.28	-22.48	-32.12	-75.32	23.53	-18.95	8.71	-76.83	-55.70
Gearly	Up/Down-Stage	SideWallsL	X	dB	-122.53	-28.27	-19.59	-20.88	-79.77	15.68	-12.83	13.92	-76.06	-56.99
Gearly	Up/Down-Stage	SideWallsR	X	dB	-132.69	-20.28	-11.81	-30.24	-70.49	22.55	-12.59	3.49	-72.00	-54.61
Gearly	Up/Down-Stage	Top/Bottom		dB	-1.93	6.99	0.95	5.68	-8.34	12.23	-0.24	5.24	-3.46	-2.37
Gearly	Up/Down-Stage	Front/Rear		dB	1.73	-6.95	-17.76	-4.68	-9.90	-2.99	-6.57	6.69	-6.85	-11.91
Gearly	Up/Down-Stage	Left/Right		dB	8.26	-11.46	-12.48	-4.09	-5.76	-2.68	-0.61	13.61	-5.25	-5.85
Gearly	Up/Down-Stage	Front/Sides		dB	-44.60	-5.09	-13.00	-13.61	-24.02	9.05	-14.45	-0.88	-27.60	-14.61
Gearly	Up/Down-Stage	Top/Sides		dB	-27.05	-6.14	-8.58	-2.54	-19.17	2.19	-9.91	-7.24	-19.49	-8.32
Gearly	Up/Down-Stage	Top/Rear		dB	1.40	-8.72	-17.46	-5.16	-7.68	-4.00	-2.73	-0.20	-6.00	-8.06
Gearly	Up/Down-Stage	FrontTop/ RearBottom		dB	-0.19	0.04	-16.81	1.00	-18.24	9.25	-6.81	11.93	-10.30	-14.28
Gsupport	Cross-Stage	Top		dB	54.05	-4.87	3.45	38.14	8.76	7.75	5.69	23.91	35.44	18.64
Gsupport	Cross-Stage	Bottom		dB	54.85	-4.10	-0.44	37.56	6.10	7.23	3.76	28.53	33.99	18.26
Gsupport	Cross-Stage	Front		dB	53.41	-8.44	-3.77	30.20	7.34	7.54	0.15	34.03	28.34	12.91
Gsupport	Cross-Stage	Rear		dB	48.86	-9.22	3.39	40.66	6.39	9.20	3.78	28.42	29.90	15.17
Gsupport	Cross-Stage	Left		dB	52.88	-1.34	-5.32	33.84	8.75	5.98	8.28	30.53	31.99	18.09
Gsupport	Cross-Stage	Right		dB	52.18	0.14	2.86	34.35	16.30	6.31	9.86	23.23	33.80	12.49
Gsupport	Cross-Stage	Audience		dB	36.38	-4.10	-6.36	16.47	6.47	7.94	1.28	26.28	21.75	9.04
Gsupport	Cross-Stage	SideWallsL		dB	41.07	-3.32	-4.69	24.35	3.18	1.43	2.31	20.93	19.72	12.51
Gsupport	Cross-Stage	SideWallsR		dB	38.01	-1.58	1.25	26.34	10.84	3.26	4.59	11.82	24.71	8.50
Gsupport	Cross-Stage	Top	X	dB	-104.06	9.05	3.37	-69.23	-18.06	-14.25	-10.06	-60.41	-61.29	-29.14
Gsupport	Cross-Stage	Bottom	X	dB	-103.26	9.81	-0.52	-69.81	-20.73	-14.78	-12.00	-55.79	-62.74	-29.52
Gsupport	Cross-Stage	Front	X	dB	-104.70	5.47	-3.86	-77.17	-19.48	-14.47	-15.60	-50.29	-68.39	-34.87
Gsupport	Cross-Stage	Rear	X	dB	-109.25	4.69	3.31	-66.71	-20.43	-12.81	-11.97	-55.90	-66.83	-32.61
Gsupport	Cross-Stage	Left	X	dB	-105.24	12.58	-5.40	-73.53	-18.07	-16.02	-7.47	-53.79	-64.75	-29.69
Gsupport	Cross-Stage	Right	X	dB	-105.93	14.06	2.78	-73.02	-10.52	-15.69	-5.90	-61.10	-62.94	-35.29
Gsupport	Cross-Stage	Audience	X	dB	-121.73	9.81	-6.44	-90.90	-20.35	-14.07	-14.47	-58.05	-74.98	-38.74
Gsupport	Cross-Stage	SideWallsL	X	dB	-117.05	10.59	-4.77	-83.01	-23.65	-20.58	-13.44	-63.40	-77.01	-35.28
Gsupport	Cross-Stage	SideWallsR	X	dB	-120.10	12.33	1.17	-81.03	-15.98	-18.74	-11.16	-72.50	-72.02	-39.28
Gsupport	Cross-Stage	Top/Bottom		dB	-0.80	-0.77	3.89	0.58	2.67	0.53	1.93	-4.61	1.45	0.38
Gsupport	Cross-Stage	Front/Rear		dB	4.54	0.78	-7.16	-10.46	0.95	-1.67	-3.63	5.61	-1.56	-2.25
Gsupport	Cross-Stage	Left/Right		dB	0.70	-1.48	-8.17	-0.51	-7.55	-0.33	-1.58	7.31	-1.81	5.60
Gsupport	Cross-Stage	Front/Sides		dB	-42.69	0.80	-2.91	-34.22	-7.55	3.25	-5.61	-6.47	-22.68	-11.96
Gsupport	Cross-Stage	Top/Sides		dB	-25.02	0.04	6.89	-12.55	-5.25	3.06	-1.21	-8.83	-8.98	-2.36
Gsupport	Cross-Stage	Top/Rear		dB	5.19	4.36	0.06	-2.52	2.37	-1.45	1.91	-4.50	5.54	3.48
Gsupport	Cross-Stage	FrontTop/ RearBottom		dB	3.75	0.01	-3.27	-9.88	3.62	-1.14	-1.69	1.00	-0.11	-1.87
Gsupport	Up/Down-Stage	Top		dB	54.05	12.68	3.93	9.91	30.28	-20.83	7.72	-11.10	28.07	21.87
Gsupport	Up/Down-Stage	Bottom		dB	54.85	6.33	3.44	6.33	37.91	-22.99	9.59	-13.52	30.42	21.92
Gsupport	Up/Down-Stage	Front		dB	53.41	14.58	1.85	9.00	27.71	-21.31	4.58	-6.83	25.12	14.03
Gsupport	Up/Down-Stage	Rear		dB	48.86	20.33	19.12	13.79	36.69	-21.86	10.02	-12.20	30.84	22.74
Gsupport	Up/Down-Stage	Left		dB	52.88	9.12	-1.35	4.59	33.91	-21.41	9.27	-2.25	29.98	21.35
Gsupport	Up/Down-Stage	Right		dB	52.18	17.73	10.53	8.11	39.57	-23.79	10.99	-13.24	30.78	19.82
Gsupport	Up/Down-Stage	Audience		dB	36.38	12.57	-2.36	-1.72	24.21	-13.78	2.77	-4.90	18.21	11.78
Gsupport	Up/Down-Stage	SideWallsL		dB	41.07	7.69	0.86	9.01	20.71	-18.03	8.92	-3.78	20.25	12.32
Gsupport	Up/Down-Stage	SideWallsR		dB	38.01	12.79	9.00	0.84	29.91	-18.97	9.62	-12.10	22.47	12.14
Gsupport	Up/Down-Stage	Top	X	dB	-104.06	-27.71	-14.83	-15.95	-72.74	45.26	-18.36	18.47	-59.54	-39.00
Gsupport	Up/Down-Stage	Bottom	X	dB	-103.26	-34.06	-15.32	-19.53	-65.12	43.10	-16.49	16.05	-57.19	-38.95
Gsupport	Up/Down-Stage	Front	X	dB	-104.70	-25.81	-16.91	-16.86	-75.32	44.78	-21.50	22.74	-62.48	-46.84
Gsupport	Up/Down-Stage	Rear	X	dB	-109.25	-20.06	0.36	-12.07	-66.34	44.23	-16.07	17.37	-56.76	-38.12
Gsupport	Up/Down-Stage	Left	X	dB	-105.24	-31.27	-20.11	-21.27	-69.12	44.69	-16.82	27.32	-57.62	-39.52
Gsupport	Up/Down-Stage	Right	X	dB	-105.93	-22.66	-8.23	-17.75	-63.46	42.30	-15.09	16.33	-56.82	-41.05
Gsupport	Up/Down-Stage	Audience	X	dB	-121.73	-27.82	-21.12	-27.58	-78.82	52.31	-23.31	24.67	-69.39	-49.09
Gsupport	Up/Down-Stage	SideWallsL	X	dB	-117.05	-32.70	-17.90	-16.85	-82.32	48.06	-17.16	25.79	-67.35	-48.54
Gsupport	Up/Down-Stage	SideWallsR	X	dB	-120.10	-27.60	-9.76	-25.02	-73.12	47.13	-16.46	17.47	-65.14	-48.72
Gsupport	Up/Down-Stage	Top/Bottom		dB	-0.80	6.35	0.49	3.58	-7.62	2.16	-1.86	2.42	-2.35	-0.06
Gsupport	Up/Down-Stage	Front/Rear		dB	4.54	-5.75	-17.27	-4.79	-8.98	0.55	-5.44	5.37	-5.72	-8.72
Gsupport	Up/Down-Stage	Left/Right		dB	0.70	-8.61	-11.88	-3.51	-5.66	2.38	-1.73	10.99	-0.79	1.53
Gsupport	Up/Down-Stage	Front/Sides		dB	-42.69	-7.91	-12.21	-11.57	-26.41	23.22	-15.78	10.98	-24.50	-12.69
Gsupport	Up/Down-Stage	Top/Sides		dB	-25.02	-7.80	-5.92	0.06	-20.34	16.17	-10.82	4.78	-14.65	-2.60
Gsupport	Up/Down-Stage	Top/Rear		dB	5.19	-7.65	-15.19	-3.89	-6.40	1.03	-2.29	1.10	-2.77	-0.88
Gsupport	Up/Down-Stage	FrontTop/ RearBottom		dB	3.75	0.60	-16.78	-1.22	-16.60	2.71	-7.30	7.79	-8.07	-8.77
G740	Cross-Stage	Top		dB	46.66	-30.40	-9.85	5.17	-4.26	-13.88	-16.62	9.48	18.13	2.96
G740	Cross-Stage	Bottom		dB	48.28	-27.60	-15.94	5.38	-7.15	-17.71	-17.96	18.14	19.42	3.66
G740	Cross-Stage	Front		dB	43.15	-32.09	-13.54	4.96	-0.34	-15.87	-23.57	23.28	14.72	2.12
G740	Cross-Stage	Rear		dB	44.02	-32.11	-14.87	15.19	-7.86	-12.09	-17.75	14.28	13.40	2.79
G740	Cross-Stage	Left		dB	49.14	-31.41	-9.12	5.81	-0.74	-15.83	-10.98	17.17	16.56	8.64
G740	Cross-Stage	Right		dB	39.68	-18.18	-14.50	5.40	7.94	-15.49	-13.86	8.41	16.76	-0.52

PARAMETER					HALL									
Parameter	Location	Direction	Normalized	Units	Alb Recital	Alb Theatre	Bard	Buffalo	Eastman	EMPAC C	EMPAC Th	Skidmore	St. Rose	Vassar
G740	Cross-Stage	Audience		dB	28.66	-24.27	-13.86	0.40	-1.31	-8.22	-15.65	19.49	10.05	2.70
G740	Cross-Stage	SideWallsL		dB	38.48	-28.93	-4.25	4.91	0.29	-18.10	-13.28	10.60	9.74	11.90
G740	Cross-Stage	SideWallsR		dB	27.95	-13.41	-12.35	7.63	3.24	-8.40	-10.35	-0.34	10.43	0.71
G740	Cross-Stage	Top	X	dB	-88.81	55.49	29.06	-15.78	1.95	31.55	33.75	-35.90	-31.36	-6.87
G740	Cross-Stage	Bottom	X	dB	-87.18	58.29	22.97	-15.58	-0.94	27.72	32.41	-27.24	-30.07	-6.17
G740	Cross-Stage	Front	X	dB	-92.32	53.80	25.37	-16.00	5.87	29.57	26.80	-22.11	-34.78	-7.71
G740	Cross-Stage	Rear	X	dB	-91.44	53.78	24.04	-5.77	-1.65	33.34	32.62	-31.10	-36.09	-7.04
G740	Cross-Stage	Left	X	dB	-86.32	54.48	29.79	-15.14	5.47	29.61	39.39	-28.21	-32.93	-1.19
G740	Cross-Stage	Right	X	dB	-95.78	67.71	24.41	-15.55	14.15	29.95	36.51	-36.97	-32.74	-10.35
G740	Cross-Stage	Audience	X	dB	-106.80	61.62	25.05	-20.56	4.90	37.21	34.72	-25.90	-39.44	-7.13
G740	Cross-Stage	SideWallsL	X	dB	-96.98	56.95	34.66	-16.05	6.51	27.34	37.09	-34.78	-39.75	2.07
G740	Cross-Stage	SideWallsR	X	dB	-107.52	72.48	26.56	-13.32	9.45	37.03	40.02	-45.73	-39.06	-9.12
G740	Cross-Stage	Top/Bottom		dB	-1.63	-2.80	6.09	-0.20	2.89	3.83	1.34	-8.66	-1.29	-0.70
G740	Cross-Stage	Front/Rear		dB	-0.87	0.02	1.33	-10.23	7.52	-3.77	-5.82	8.99	1.32	-0.67
G740	Cross-Stage	Left/Right		dB	9.46	-13.23	5.38	0.41	-8.68	-0.34	2.87	8.76	-0.19	9.16
G740	Cross-Stage	Front/Sides		dB	-37.77	18.07	2.74	-12.14	-4.84	18.27	7.98	9.23	-10.12	-9.91
G740	Cross-Stage	Top/Sides		dB	-19.77	11.94	6.75	-7.36	-7.79	12.61	7.01	-0.78	-2.04	-9.65
G740	Cross-Stage	Top/Rear		dB	2.63	1.71	5.02	-10.01	3.60	-1.79	1.12	-4.80	4.74	0.17
G740	Cross-Stage	FrontTop/ RearBottom		dB	-2.50	-2.78	7.42	-10.43	10.41	0.05	-4.48	0.33	0.03	-1.37
G740	UpDown-Stage	Top		dB	46.66	-6.54	-7.47	-1.12	9.65	-12.06	-5.90	-15.77	15.80	6.10
G740	UpDown-Stage	Bottom		dB	48.28	-17.06	-11.56	-10.10	20.63	-28.33	-6.75	-25.09	19.47	7.90
G740	UpDown-Stage	Front		dB	43.15	-3.32	-6.31	0.25	8.55	-11.82	-14.83	-10.54	16.15	5.92
G740	UpDown-Stage	Rear		dB	44.02	0.62	11.72	2.91	19.90	-9.10	-8.05	-15.41	22.26	19.84
G740	UpDown-Stage	Left		dB	49.14	-15.67	-11.49	-6.22	12.22	-12.38	-7.72	0.86	14.59	6.95
G740	UpDown-Stage	Right		dB	39.68	-4.44	1.91	0.75	21.42	-9.76	-9.23	-15.48	28.41	18.70
G740	UpDown-Stage	Audience		dB	28.66	-0.26	-7.56	-9.46	12.00	-3.61	-7.08	-6.49	13.09	5.88
G740	UpDown-Stage	SideWallsL		dB	38.48	-11.21	-5.25	3.21	5.03	-11.41	-5.70	0.68	9.28	4.43
G740	UpDown-Stage	SideWallsR		dB	27.95	-4.67	2.86	-8.84	17.70	-4.48	-3.83	-11.57	21.75	8.81
G740	UpDown-Stage	Top	X	dB	-88.81	16.67	4.13	5.64	-36.54	29.66	20.34	24.94	-42.54	-26.61
G740	UpDown-Stage	Bottom	X	dB	-87.18	6.15	0.04	-3.34	-25.56	13.40	19.49	15.62	-38.87	-24.81
G740	UpDown-Stage	Front	X	dB	-92.32	19.89	5.29	7.01	-37.63	29.91	11.41	30.17	-42.19	-26.79
G740	UpDown-Stage	Rear	X	dB	-91.44	23.83	23.32	9.67	-26.28	32.63	18.19	25.30	-36.08	-12.87
G740	UpDown-Stage	Left	X	dB	-86.32	7.54	0.11	0.55	-33.96	29.35	18.52	41.57	-43.74	-25.75
G740	UpDown-Stage	Right	X	dB	-95.78	18.77	13.51	7.51	-24.77	31.96	17.01	25.23	-29.93	-14.01
G740	UpDown-Stage	Audience	X	dB	-106.80	22.95	4.04	-2.70	-34.18	38.12	19.16	34.22	-45.24	-26.83
G740	UpDown-Stage	SideWallsL	X	dB	-96.98	12.00	6.35	9.97	-41.15	30.32	20.54	41.39	-49.05	-28.27
G740	UpDown-Stage	SideWallsR	X	dB	-107.52	18.44	14.46	-2.08	-28.49	37.25	22.41	29.14	-36.59	-23.90
G740	UpDown-Stage	Top/Bottom		dB	-1.63	10.51	4.10	8.99	-10.98	16.27	0.85	9.32	-3.67	-1.80
G740	UpDown-Stage	Front/Rear		dB	-0.87	-3.94	-18.03	-2.66	-11.35	-2.72	-6.78	4.88	-6.11	-13.92
G740	UpDown-Stage	Left/Right		dB	9.46	-11.23	-13.40	-6.97	-9.20	-2.61	1.52	16.33	-13.82	-11.75
G740	UpDown-Stage	Front/Sides		dB	-37.77	15.62	-5.18	-3.83	-10.72	12.28	2.45	4.40	-17.94	-7.37
G740	UpDown-Stage	Top/Sides		dB	-19.77	9.34	-5.08	4.51	-13.08	3.83	3.64	-4.88	-15.23	-7.14
G740	UpDown-Stage	Top/Rear		dB	2.63	-7.16	-19.19	-4.02	-10.26	-2.97	2.15	-0.35	-6.46	-13.74
G740	UpDown-Stage	FrontTop/ RearBottom		dB	-2.50	6.57	-13.94	6.33	-22.34	13.54	-5.93	14.19	-9.78	-15.72
G40end	Cross-Stage	Top		dB	53.47	6.33	7.26	47.23	15.96	21.23	8.27	34.81	44.03	29.89
G40end	Cross-Stage	Bottom		dB	52.73	7.36	5.22	45.79	12.29	21.61	7.17	36.23	43.07	29.52
G40end	Cross-Stage	Front		dB	55.08	4.47	3.26	42.06	12.52	23.43	5.15	37.51	39.63	24.71
G40end	Cross-Stage	Rear		dB	48.70	3.20	9.04	48.67	12.91	22.80	6.51	34.17	39.29	25.98
G40end	Cross-Stage	Left		dB	49.49	12.79	1.50	42.64	14.89	22.08	11.87	38.76	43.36	29.99
G40end	Cross-Stage	Right		dB	55.79	10.57	7.34	44.09	18.47	20.76	13.75	33.93	42.94	24.00
G40end	Cross-Stage	Audience		dB	37.81	5.66	-0.69	27.06	11.79	19.33	5.15	28.02	30.69	18.19
G40end	Cross-Stage	SideWallsL		dB	37.70	8.04	0.63	31.03	8.40	12.74	5.66	26.82	29.08	21.02
G40end	Cross-Stage	SideWallsR		dB	41.81	5.74	5.62	33.39	12.62	13.54	6.12	21.63	30.29	16.19
G40end	Cross-Stage	Top	X	dB	-104.15	-16.03	-9.55	-88.01	-27.55	-44.72	-18.09	-72.90	-82.13	-52.15
G40end	Cross-Stage	Bottom	X	dB	-104.90	-15.00	-11.60	-89.45	-31.23	-44.34	-19.19	-71.47	-83.09	-52.53
G40end	Cross-Stage	Front	X	dB	-102.55	-17.89	-13.55	-93.18	-31.00	-42.52	-21.22	-70.20	-86.53	-57.34
G40end	Cross-Stage	Rear	X	dB	-108.93	-19.16	-7.77	-86.57	-30.61	-43.15	-19.85	-73.54	-86.88	-56.06
G40end	Cross-Stage	Left	X	dB	-108.14	-9.57	-15.32	-92.60	-28.62	-43.87	-14.49	-68.94	-82.80	-52.06
G40end	Cross-Stage	Right	X	dB	-101.83	-11.78	-9.47	-91.15	-25.05	-45.18	-12.62	-73.78	-83.22	-58.04
G40end	Cross-Stage	Audience	X	dB	-119.81	-16.69	-17.51	-108.17	-31.73	-46.62	-21.21	-79.69	-95.48	-63.86
G40end	Cross-Stage	SideWallsL	X	dB	-119.93	-14.31	-16.19	-104.21	-35.11	-53.21	-20.70	-80.88	-97.08	-61.03
G40end	Cross-Stage	SideWallsR	X	dB	-115.81	-16.62	-11.20	-101.85	-30.90	-52.41	-20.25	-86.07	-95.88	-65.86
G40end	Cross-Stage	Top/Bottom		dB	0.75	-1.03	2.05	1.44	3.67	-0.38	1.10	-1.42	0.96	0.38
G40end	Cross-Stage	Front/Rear		dB	6.38	1.27	-5.78	-6.61	-0.39	0.63	-1.37	3.34	0.35	-1.27
G40end	Cross-Stage	Left/Right		dB	-6.30	2.21	-5.84	-1.45	-3.57	1.31	-1.88	4.84	0.42	5.99
G40end	Cross-Stage	Front/Sides		dB	-41.69	-8.12	-6.94	-37.35	-9.23	-6.95	-6.62	-20.44	-28.68	-19.02
G40end	Cross-Stage	Top/Sides		dB	-26.03	-7.45	1.02	-17.18	-5.06	-5.05	-3.51	-13.65	-15.34	-7.32
G40end	Cross-Stage	Top/Rear		dB	4.78	3.13	-1.78	-1.44	3.05	-1.57	1.76	0.64	4.75	3.91
G40end	Cross-Stage	FrontTop/ RearBottom		dB	7.13	0.24	-3.73	-5.18	3.28	0.25	-0.27	1.92	1.30	-0.90
G40end	UpDown-Stage	Top		dB	53.47	22.57	8.92	21.46	39.19	-4.77	14.27	3.51	41.14	31.25
G40end	UpDown-Stage	Bottom		dB	52.73	21.30	8.11	20.29	41.28	-5.07	15.92	4.13	41.59	31.54
G40end	UpDown-Stage	Front		dB	55.08	26.83	6.73	19.85	36.31	-2.47	13.12	7.42	38.65	25.33
G40end	UpDown-Stage	Rear		dB	48.70	27.89	16.94	23.57	40.48	-3.81	14.80	3.02	41.71	29.75
G40end	UpDown-Stage	Left		dB	49.49	24.50	4.37	16.79	40.21	-4.05	13.78	10.28	43.46	31.44
G40end	UpDown-Stage	Right		dB	55.79	25.14	10.52	18.76	43.36	-5.59	16.05	3.39	39.23	28.49
G40end	UpDown-Stage	Audience		dB	37.81	20.93	1.98	7.55	29.87	-0.47	7.99	5.60	28.39	19.68
G40end	UpDown-Stage	SideWallsL		dB	37.70	18.55	3.23	17.24	25.89	-6.74	11.44	5.45	31.08	20.56
G40end	UpDown-Stage	SideWallsR		dB	41.81	17.76	9.26	9.40	31.07	-5.74	11.45	-0.05	27.31	17.17

PARAMETER					HALL									
Parameter	Location	Direction	Normalized	Units	Alb Recital	Alb Theatre	Bard	Buffalo	Eastman	EMPAC C	EMPAC Th	Skidmore	St. Rose	Vassar
G40end	UpDown-Stage	Top	X	dB	-104.15	-51.55	-18.88	-38.90	-81.23	8.11	-29.70	-12.36	-81.75	-57.64
G40end	UpDown-Stage	Bottom	X	dB	-104.90	-52.82	-19.68	-40.07	-79.13	7.81	-28.05	-11.74	-81.30	-57.36
G40end	UpDown-Stage	Front	X	dB	-102.55	-47.29	-21.07	-40.52	-84.11	10.41	-30.84	-8.45	-84.24	-63.57
G40end	UpDown-Stage	Rear	X	dB	-108.93	-46.23	-10.86	-36.79	-79.94	9.07	-29.17	-12.86	-81.18	-59.15
G40end	UpDown-Stage	Left	X	dB	-108.14	-49.62	-23.43	-43.57	-80.21	8.83	-30.18	-5.59	-79.43	-57.46
G40end	UpDown-Stage	Right	X	dB	-101.83	-48.98	-17.28	-41.61	-77.05	7.30	-27.92	-12.49	-83.66	-60.41
G40end	UpDown-Stage	Audience	X	dB	-119.81	-53.19	-25.82	-52.82	-90.55	12.41	-35.98	-10.27	-94.50	-69.22
G40end	UpDown-Stage	SideWallsL	X	dB	-119.93	-55.57	-24.57	-43.12	-94.52	6.14	-32.53	-10.42	-91.81	-68.34
G40end	UpDown-Stage	SideWallsR	X	dB	-115.81	-56.36	-18.54	-50.97	-89.35	7.14	-32.52	-15.92	-95.58	-71.73
G40end	UpDown-Stage	Top/Bottom		dB	0.75	1.27	0.80	1.17	-2.09	0.31	-1.65	-0.62	-0.45	-0.28
G40end	UpDown-Stage	Front/Rear		dB	6.38	-1.06	-10.21	-3.72	-4.17	1.34	-1.67	4.41	-3.06	-4.42
G40end	UpDown-Stage	Left/Right		dB	-6.30	-0.64	-6.15	-1.97	-3.15	1.53	-2.26	6.90	4.23	2.95
G40end	UpDown-Stage	Front/Sides		dB	-41.69	-15.38	-10.51	-19.09	-27.09	12.01	-14.90	0.19	-30.00	-18.05
G40end	UpDown-Stage	Top/Sides		dB	-26.03	-13.74	-3.57	-5.18	-17.77	7.72	-8.62	-1.90	-17.26	-6.48
G40end	UpDown-Stage	Top/Rear		dB	4.78	-5.32	-8.02	-2.11	-1.29	-0.95	-0.53	0.49	-0.58	1.50
G40end	UpDown-Stage	FrontTop/ RearBottom		dB	7.13	0.21	-9.41	-2.55	-6.26	1.65	-3.33	3.79	-3.52	-4.70
LQ740	Cross-Stage	Top		dB	-1.70	-9.18	-4.28	-10.51	-5.06	-8.78	-6.22	-6.33	-6.47	-6.73
LQ740	Cross-Stage	Bottom		dB	-1.11	-8.74	-5.29	-10.10	-4.86	-9.83	-6.28	-4.52	-5.91	-6.46
LQ740	Cross-Stage	Front		dB	-2.98	-9.14	-4.20	-9.28	-3.22	-9.82	-7.18	-3.56	-6.23	-5.65
LQ740	Cross-Stage	Rear		dB	-1.17	-8.83	-5.98	-8.37	-5.19	-8.72	-6.07	-4.97	-6.47	-5.80
LQ740	Cross-Stage	Left		dB	-0.09	-11.05	-2.66	-9.21	-3.91	-9.48	-5.71	-5.40	-6.70	-5.34
LQ740	Cross-Stage	Right		dB	-4.03	-7.19	-5.46	-9.67	-2.63	-9.06	-6.90	-6.38	-6.55	-6.13
LQ740	Cross-Stage	Audience		dB	-3.05	-9.98	-4.39	-8.89	-4.37	-9.18	-6.94	-2.84	-6.88	-5.16
LQ740	Cross-Stage	SideWallsL		dB	0.26	-12.32	-1.63	-8.71	-2.70	-10.28	-6.31	-5.41	-6.45	-3.04
LQ740	Cross-Stage	SideWallsR		dB	-4.62	-6.38	-5.99	-8.59	-3.13	-7.31	-5.49	-7.33	-6.62	-5.16
LQ740	Cross-Stage	Top	X	dB	0.14	-0.16	0.37	-0.99	-0.91	0.50	0.17	-1.14	-0.09	-0.71
LQ740	Cross-Stage	Bottom	X	dB	0.74	0.28	-0.65	-0.58	-0.72	-0.55	0.11	0.67	0.48	-0.45
LQ740	Cross-Stage	Front	X	dB	-1.14	-0.12	0.44	0.25	0.93	-0.54	-0.78	1.64	0.16	0.37
LQ740	Cross-Stage	Rear	X	dB	0.68	0.19	-1.33	1.15	-1.05	0.56	0.33	0.22	-0.08	0.22
LQ740	Cross-Stage	Left	X	dB	1.76	-2.03	1.99	0.32	0.24	-0.19	0.68	-0.20	-0.31	0.68
LQ740	Cross-Stage	Right	X	dB	-2.18	1.83	-0.82	-0.15	1.51	0.22	-0.51	-1.18	-0.16	-0.11
LQ740	Cross-Stage	Audience	X	dB	-1.20	-0.96	0.25	0.63	-0.22	0.10	-0.54	2.35	-0.49	0.86
LQ740	Cross-Stage	SideWallsL	X	dB	2.11	-3.30	3.02	0.82	1.44	-1.00	0.08	-0.21	-0.06	2.98
LQ740	Cross-Stage	SideWallsR	X	dB	-2.77	2.64	-1.34	0.94	1.02	1.97	0.90	-2.13	-0.23	0.86
LQ740	Cross-Stage	Top/Bottom		dB	-0.59	-0.44	1.01	-0.41	-0.19	1.05	0.06	-1.81	-0.56	-0.27
LQ740	Cross-Stage	Front/Rear		dB	-1.81	-0.31	1.78	-0.90	1.98	-1.10	-1.11	1.41	0.24	0.15
LQ740	Cross-Stage	Left/Right		dB	3.94	-3.86	2.80	0.46	-1.28	-0.41	1.19	0.98	-0.15	0.79
LQ740	Cross-Stage	Front/Sides		dB	-0.87	-0.62	-0.58	-0.24	-1.45	-0.39	-1.03	3.52	-0.35	-1.06
LQ740	Cross-Stage	Top/Sides		dB	0.48	0.17	-0.47	-1.87	-2.14	0.02	-0.32	0.03	0.06	-2.63
LQ740	Cross-Stage	Top/Rear		dB	-0.54	-0.36	1.70	-2.14	0.14	-0.06	-0.16	-1.36	0.00	-0.94
LQ740	Cross-Stage	FrontTop/ RearBottom		dB	-1.20	-0.38	1.39	-0.66	0.89	-0.03	-0.53	-0.20	-0.16	-0.06
LQ740	UpDown-Stage	Top		dB	-1.70	-7.28	-4.10	-5.64	-7.39	-1.82	-5.04	-4.82	-6.33	-6.29
LQ740	UpDown-Stage	Bottom		dB	-1.11	-9.59	-4.92	-7.60	-5.16	-5.81	-5.67	-7.30	-5.53	-5.91
LQ740	UpDown-Stage	Front		dB	-2.98	-7.54	-3.26	-4.90	-6.94	-2.34	-6.99	-4.49	-5.63	-4.85
LQ740	UpDown-Stage	Rear		dB	-1.17	-6.82	-1.31	-5.17	-5.14	-1.32	-5.71	-4.61	-4.86	-2.48
LQ740	UpDown-Stage	Left		dB	-0.09	-10.04	-3.97	-5.75	-7.00	-2.08	-5.38	-2.36	-7.22	-6.12
LQ740	UpDown-Stage	Right		dB	-4.03	-7.39	-2.15	-4.50	-5.49	-1.04	-6.32	-4.72	-2.71	-2.45
LQ740	UpDown-Stage	Audience		dB	-3.05	-7.06	-3.18	-5.67	-5.95	-1.04	-5.02	-4.03	-5.10	-4.60
LQ740	UpDown-Stage	SideWallsL		dB	0.26	-9.92	-2.83	-4.68	-6.95	-1.56	-5.71	-1.59	-7.27	-5.38
LQ740	UpDown-Stage	SideWallsR		dB	-4.62	-7.48	-2.13	-6.08	-4.46	0.42	-5.09	-3.84	-1.86	-2.79
LQ740	UpDown-Stage	Top	X	dB	0.14	0.83	-0.81	-0.05	-1.20	0.58	0.81	-0.10	-0.95	-1.61
LQ740	UpDown-Stage	Bottom	X	dB	0.74	-1.48	-1.64	-2.01	1.02	-3.41	0.18	-2.59	-0.15	-1.23
LQ740	UpDown-Stage	Front	X	dB	-1.14	0.57	0.02	0.69	-0.75	0.07	-1.14	0.23	-0.25	-0.17
LQ740	UpDown-Stage	Rear	X	dB	0.68	1.29	1.98	0.43	1.04	1.08	0.14	0.11	0.52	2.20
LQ740	UpDown-Stage	Left	X	dB	1.76	-1.93	-0.68	-0.16	-0.81	0.32	0.48	2.36	-1.84	-1.44
LQ740	UpDown-Stage	Right	X	dB	-2.18	0.72	1.13	1.09	0.70	1.36	-0.47	0.00	2.67	2.24
LQ740	UpDown-Stage	Audience	X	dB	-1.20	1.05	0.10	-0.08	0.23	1.36	0.83	0.69	0.28	0.08
LQ740	UpDown-Stage	SideWallsL	X	dB	2.11	-1.81	0.46	0.92	-0.77	0.85	0.14	3.12	-1.89	-0.69
LQ740	UpDown-Stage	SideWallsR	X	dB	-2.77	0.63	1.15	-0.48	1.73	2.82	0.76	0.88	3.52	1.90
LQ740	UpDown-Stage	Top/Bottom		dB	-0.59	2.31	0.82	1.95	-2.22	3.99	0.63	2.48	-0.80	-0.38
LQ740	UpDown-Stage	Front/Rear		dB	-1.81	-0.72	-1.96	0.27	-1.80	-1.02	-1.28	0.12	-0.76	-2.38
LQ740	UpDown-Stage	Left/Right		dB	3.94	-2.65	-1.81	-1.25	-1.51	-1.04	0.94	2.36	-4.51	-3.68
LQ740	UpDown-Stage	Front/Sides		dB	-0.87	1.63	-0.70	-0.29	-0.25	-0.48	0.38	-1.31	-0.54	-0.52
LQ740	UpDown-Stage	Top/Sides		dB	0.48	1.42	-1.62	-0.27	-1.68	-1.26	0.36	-2.10	-1.77	-2.21
LQ740	UpDown-Stage	Top/Rear		dB	-0.54	-0.46	-2.79	-0.48	-2.24	-0.50	0.67	-0.21	-1.47	-3.81
LQ740	UpDown-Stage	FrontTop/ RearBottom		dB	-1.20	0.80	-0.57	1.11	-2.01	1.49	-0.33	1.30	-0.78	-1.38
Glate	Cross-Stage	Top		dB	43.40	1.13	-2.09	36.21	8.51	15.82	-1.44	29.57	36.75	23.84
Glate	Cross-Stage	Bottom		dB	42.73	2.41	-3.78	34.34	5.30	16.20	-1.02	31.18	36.65	23.31
Glate	Cross-Stage	Front		dB	44.88	0.60	-4.17	33.94	6.52	18.33	-3.59	30.36	34.51	19.30
Glate	Cross-Stage	Rear		dB	37.55	-1.89	-0.01	37.67	5.40	17.24	-2.54	26.77	32.86	19.85
Glate	Cross-Stage	Left		dB	39.39	8.84	-6.33	31.46	7.73	17.26	3.43	32.72	37.70	23.74
Glate	Cross-Stage	Right		dB	48.71	5.41	-2.09	33.76	10.65	15.29	4.63	28.20	35.17	18.35
Glate	Cross-Stage	Audience		dB	30.49	2.09	-5.94	22.33	7.29	15.25	-1.01	22.85	26.43	14.03
Glate	Cross-Stage	SideWallsL		dB	29.77	5.39	-5.19	22.84	3.68	8.38	-0.86	22.05	25.25	16.35
Glate	Cross-Stage	SideWallsR		dB	37.03	0.91	-0.77	26.02	6.80	9.57	-0.45	17.68	23.40	12.04
Glate	Cross-Stage	Top	X	dB	-84.93	-7.12	7.15	-67.48	-13.54	-34.25	-1.17	-59.83	-70.07	-40.36
Glate	Cross-Stage	Bottom	X	dB	-85.60	-5.85	5.45	-69.35	-16.75	-33.87	-0.76	-58.22	-70.17	-40.89
Glate	Cross-Stage	Front	X	dB	-83.45	-7.65	5.06	-69.75	-15.53	-31.74	-3.33	-59.04	-72.30	-44.89

PARAMETER					HALL									
Parameter	Location	Direction	Normalized	Units	Alb Recital	Alb Theatre	Bard	Buffalo	Eastman	EMPAC C	EMPAC Th	Skidmore	St Rose	Vassar
Glate	Cross-Stage	Rear	X	dB	-90.78	-10.14	9.23	-66.02	-16.65	-32.83	-2.28	-62.63	-73.96	-44.35
Glate	Cross-Stage	Left	X	dB	-88.94	0.58	2.91	-72.23	-14.32	-32.81	3.69	-56.68	-69.12	-40.46
Glate	Cross-Stage	Right	X	dB	-79.61	-2.84	7.14	-69.94	-11.40	-34.77	4.90	-61.20	-71.65	-45.85
Glate	Cross-Stage	Audience	X	dB	-97.84	-6.16	3.30	-81.36	-14.76	-34.81	-0.75	-66.55	-80.39	-50.16
Glate	Cross-Stage	SideWallsL	X	dB	-98.56	-2.86	4.05	-80.86	-18.37	-41.69	-0.59	-67.35	-81.57	-47.85
Glate	Cross-Stage	SideWallsR	X	dB	-91.30	-7.34	8.46	-77.67	-15.25	-40.50	-0.18	-71.72	-83.42	-52.15
Glate	Cross-Stage	Top/Bottom		dB	0.67	-1.27	1.70	1.87	3.21	-0.39	-0.42	-1.61	0.10	0.53
Glate	Cross-Stage	Front/Rear		dB	7.33	2.49	-4.17	-3.73	1.12	1.09	-1.05	3.59	1.66	-0.55
Glate	Cross-Stage	Left/Right		dB	-9.33	3.42	-4.24	-2.30	-2.92	1.97	-1.21	4.52	2.53	5.39
Glate	Cross-Stage	Front/Sides		dB	-36.31	-4.21	0.02	-26.52	-3.20	-2.69	0.29	-16.87	-22.22	-14.36
Glate	Cross-Stage	Top/Sides		dB	-23.40	-5.17	3.87	-12.65	-1.98	-2.13	-0.13	-10.15	-11.90	-4.55
Glate	Cross-Stage	Top/Rear		dB	5.85	3.02	-2.08	-1.46	3.11	-1.42	1.10	2.80	3.89	3.99
Glate	Cross-Stage	FrontTop/ RearBottom		dB	8.00	1.21	-2.47	-1.86	4.33	0.70	-1.47	1.98	1.75	-0.02
Glate	UpDown-Stage	Top		dB	43.40	17.18	0.56	15.68	30.84	-7.38	7.77	-0.84	36.88	25.00
Glate	UpDown-Stage	Bottom		dB	42.73	16.82	-1.23	15.40	30.95	-7.56	9.70	0.16	36.94	24.62
Glate	UpDown-Stage	Front		dB	44.88	22.43	-0.77	13.75	28.55	-5.10	5.88	1.93	35.20	20.12
Glate	UpDown-Stage	Rear		dB	37.55	20.52	4.48	16.22	29.84	-6.70	6.90	-1.65	36.07	23.12
Glate	UpDown-Stage	Left		dB	39.39	20.06	-3.35	10.63	30.49	-6.41	6.14	4.81	38.41	25.73
Glate	UpDown-Stage	Right		dB	48.71	17.08	-0.15	12.49	33.39	-8.17	8.00	-1.66	34.61	22.41
Glate	UpDown-Stage	Audience		dB	30.49	17.14	-3.47	3.02	23.84	-2.30	3.47	1.77	25.44	15.21
Glate	UpDown-Stage	SideWallsL		dB	29.77	15.31	-3.53	12.65	19.42	-8.53	4.88	1.27	27.25	16.59
Glate	UpDown-Stage	SideWallsR		dB	37.03	11.09	1.70	4.62	23.51	-8.12	3.97	-3.71	23.67	12.84
Glate	UpDown-Stage	Top	X	dB	-84.93	-39.87	0.79	-26.41	-61.19	13.28	-14.43	-2.22	-72.17	-45.51
Glate	UpDown-Stage	Bottom	X	dB	-85.60	-40.23	-1.00	-26.69	-61.08	13.10	-12.49	-1.21	-72.12	-45.88
Glate	UpDown-Stage	Front	X	dB	-83.45	-34.62	-0.53	-28.33	-63.48	15.56	-16.31	0.55	-73.85	-50.38
Glate	UpDown-Stage	Rear	X	dB	-90.78	-36.52	4.72	-25.86	-62.19	13.96	-15.29	-3.02	-72.99	-47.38
Glate	UpDown-Stage	Left	X	dB	-88.94	-36.98	-3.12	-31.46	-61.54	14.25	-16.06	3.43	-70.64	-44.77
Glate	UpDown-Stage	Right	X	dB	-79.61	-39.96	0.08	-29.59	-58.64	12.50	-14.19	-3.03	-74.45	-48.09
Glate	UpDown-Stage	Audience	X	dB	-97.84	-39.91	-3.24	-39.06	-68.19	18.37	-18.73	0.40	-83.61	-55.29
Glate	UpDown-Stage	SideWallsL	X	dB	-98.56	-41.74	-3.29	-29.44	-72.61	12.13	-17.32	-0.10	-81.81	-53.91
Glate	UpDown-Stage	SideWallsR	X	dB	-91.30	-45.96	1.94	-37.46	-68.52	12.55	-18.22	-5.08	-85.38	-57.66
Glate	UpDown-Stage	Top/Bottom		dB	0.67	0.36	1.79	0.28	-0.11	0.18	-1.93	-1.00	-0.06	0.37
Glate	UpDown-Stage	Front/Rear		dB	7.33	1.91	-5.25	-2.47	-1.29	1.60	-1.02	3.57	-0.86	-3.00
Glate	UpDown-Stage	Left/Right		dB	-9.33	2.98	-3.20	-1.87	-2.89	1.75	-1.87	6.46	3.81	3.32
Glate	UpDown-Stage	Front/Sides		dB	-36.31	-9.26	-1.65	-14.24	-19.10	14.35	-5.38	4.21	-25.48	-14.23
Glate	UpDown-Stage	Top/Sides		dB	-23.40	-9.22	2.38	-1.59	-12.10	9.27	-1.08	1.59	-14.04	-4.44
Glate	UpDown-Stage	Top/Rear		dB	5.85	-3.35	-3.93	-0.54	0.99	-0.68	0.87	0.80	0.82	1.88
Glate	UpDown-Stage	FrontTop/ RearBottom		dB	8.00	2.26	-3.46	-2.19	-1.41	1.77	-2.95	2.57	-0.92	-2.62
RR160	Cross-Stage	Top		dB	-10.44	-5.14	-7.22	-6.19	-7.79	-3.96	-8.13	-4.35	-4.75	-5.06
RR160	Cross-Stage	Bottom		dB	-11.02	-4.99	-7.30	-5.78	-8.23	-3.66	-7.86	-4.67	-4.81	-5.43
RR160	Cross-Stage	Front		dB	-10.37	-5.19	-6.26	-4.06	-7.85	-2.89	-7.43	-6.02	-3.75	-4.91
RR160	Cross-Stage	Rear		dB	-11.24	-4.60	-6.66	-5.76	-8.18	-3.88	-8.13	-5.77	-4.44	-4.99
RR160	Cross-Stage	Left		dB	-12.03	-4.60	-7.42	-5.62	-8.89	-2.90	-7.92	-4.71	-3.80	-5.38
RR160	Cross-Stage	Right		dB	-8.90	-5.41	-7.11	-5.36	-9.86	-3.85	-7.86	-4.43	-4.66	-4.93
RR160	Cross-Stage	Audience		dB	-10.60	-5.10	-5.99	-3.29	-7.98	-3.32	-7.31	-6.20	-4.05	-5.17
RR160	Cross-Stage	SideWallsL		dB	-12.71	-4.49	-7.59	-5.56	-9.19	-3.23	-7.83	-4.69	-3.53	-6.12
RR160	Cross-Stage	SideWallsR		dB	-8.34	-5.63	-6.74	-5.19	-9.85	-3.94	-8.15	-3.87	-5.54	-4.99
RR160	Cross-Stage	Top	X	dB	0.22	-0.15	-0.22	-0.73	0.68	-0.44	-0.24	0.64	-0.38	0.06
RR160	Cross-Stage	Bottom	X	dB	-0.35	0.00	-0.31	-0.32	0.24	-0.13	0.03	0.32	-0.44	-0.32
RR160	Cross-Stage	Front	X	dB	0.29	-0.20	0.74	1.40	0.61	0.64	0.46	-1.03	0.62	0.21
RR160	Cross-Stage	Rear	X	dB	-0.57	0.39	0.34	-0.30	0.29	-0.36	-0.24	-0.77	-0.07	0.13
RR160	Cross-Stage	Left	X	dB	-1.36	0.39	-0.43	-0.16	-0.42	0.62	-0.04	0.28	0.57	-0.27
RR160	Cross-Stage	Right	X	dB	1.77	-0.42	-0.11	0.10	-1.39	-0.33	0.02	0.56	-0.29	0.19
RR160	Cross-Stage	Audience	X	dB	0.07	-0.11	1.01	2.17	0.49	0.20	0.58	-1.21	0.31	-0.06
RR160	Cross-Stage	SideWallsL	X	dB	-2.04	0.50	-0.60	-0.10	-0.72	0.29	0.05	0.30	0.83	-1.01
RR160	Cross-Stage	SideWallsR	X	dB	2.33	-0.64	0.25	0.28	-1.38	-0.41	-0.27	1.12	-1.17	0.13
RR160	Cross-Stage	Top/Bottom		dB	0.58	-0.15	0.08	-0.41	0.44	-0.31	-0.27	0.32	0.06	0.38
RR160	Cross-Stage	Front/Rear		dB	0.86	-0.59	0.40	1.69	0.32	1.00	0.70	-0.25	0.69	0.08
RR160	Cross-Stage	Left/Right		dB	-3.13	0.81	-0.32	-0.26	0.97	0.95	-0.06	-0.28	0.86	-0.46
RR160	Cross-Stage	Front/Sides		dB	-0.07	-0.04	1.18	2.09	1.54	0.27	0.69	-1.92	0.48	0.38
RR160	Cross-Stage	Top/Sides		dB	0.08	-0.08	-0.05	-0.81	1.73	-0.38	-0.14	-0.07	-0.21	0.50
RR160	Cross-Stage	Top/Rear		dB	0.79	-0.54	-0.56	-0.43	0.39	-0.08	0.00	1.42	-0.31	-0.07
RR160	Cross-Stage	FrontTop/ RearBottom		dB	0.72	-0.37	0.24	0.64	0.38	0.35	0.21	0.03	0.38	0.23
RR160	UpDown-Stage	Top		dB	-10.44	-4.34	-6.87	-3.84	-5.80	-6.68	-7.00	-4.88	-5.21	-5.37
RR160	UpDown-Stage	Bottom		dB	-11.02	-4.07	-6.37	-3.06	-7.93	-4.65	-7.37	-3.97	-5.68	-5.64
RR160	UpDown-Stage	Front		dB	-10.37	-4.60	-7.01	-4.45	-5.19	-6.20	-6.88	-5.80	-5.25	-4.90
RR160	UpDown-Stage	Rear		dB	-11.24	-5.85	-9.50	-4.68	-8.36	-7.29	-7.36	-4.74	-5.59	-6.90
RR160	UpDown-Stage	Left		dB	-12.03	-3.94	-6.41	-4.14	-6.86	-6.36	-7.96	-6.61	-4.86	-5.20
RR160	UpDown-Stage	Right		dB	-8.90	-5.78	-8.33	-4.34	-7.64	-7.30	-7.52	-4.74	-6.05	-6.72
RR160	UpDown-Stage	Audience		dB	-10.60	-4.73	-6.76	-4.06	-5.51	-6.97	-7.16	-5.88	-5.21	-5.28
RR160	UpDown-Stage	SideWallsL		dB	-12.71	-4.34	-7.10	-4.40	-6.68	-6.60	-8.31	-6.79	-4.86	-4.72
RR160	UpDown-Stage	SideWallsR		dB	-8.34	-5.93	-8.43	-3.80	-8.24	-7.93	-7.99	-5.07	-6.22	-6.54
RR160	UpDown-Stage	Top	X	dB	0.22	0.42	0.54	0.25	1.17	-0.27	0.35	0.24	0.23	0.41
RR160	UpDown-Stage	Bottom	X	dB	-0.35	0.70	1.04	1.02	-0.97	1.77	-0.02	1.15	-0.24	0.15
RR160	UpDown-Stage	Front	X	dB	0.29	0.16	0.41	-0.36	1.77	0.22	0.47	-0.68	0.19	0.89
RR160	UpDown-Stage	Rear	X	dB	-0.57	-1.09	-2.09	-0.59	-1.40	-0.88	-0.01	0.39	-0.15	-1.11
RR160	UpDown-Stage	Left	X	dB	-1.36	0.83	1.00	-0.06	0.11	0.06	-0.61	-1.48	0.58	0.59
RR160	UpDown-Stage	Right	X	dB	1.77	-1.02	-0.91	-0.25	-0.68	-0.89	-0.17	0.38	-0.61	-0.94

PARAMETER					HALL									
Parameter	Location	Direction	Normalized	Units	Alb Recital	Alb Theatre	Bard	Buffalo	Eastman	EMPAC C	EMPAC Th	Skidmore	St. Rose	Vassar
RR160	Up/Down-Stage	Audience	X	dB	0.07	0.03	0.65	0.03	1.45	-0.56	0.19	-0.76	0.23	0.51
RR160	Up/Down-Stage	SideWallsL	X	dB	-2.04	0.42	0.32	-0.32	0.28	-0.19	-0.96	-1.67	0.57	1.07
RR160	Up/Down-Stage	SideWallsR	X	dB	2.33	-1.17	-1.01	0.29	-1.28	-1.51	-0.63	0.06	-0.79	-0.76
RR160	Up/Down-Stage	Top/Bottom		dB	0.58	-0.27	-0.50	-0.78	2.13	-2.04	0.37	-0.91	0.47	0.26
RR160	Up/Down-Stage	Front/Rear		dB	0.86	1.25	2.50	0.23	3.17	1.10	0.48	-1.06	0.34	2.00
RR160	Up/Down-Stage	Left/Right		dB	-3.13	1.85	1.92	0.20	0.78	0.95	-0.44	-1.87	1.19	1.53
RR160	Up/Down-Stage	Front/Sides		dB	-0.07	0.40	1.00	0.05	1.94	0.29	0.98	0.04	0.33	0.35
RR160	Up/Down-Stage	Top/Sides		dB	0.08	0.80	0.89	0.26	1.66	0.58	1.15	1.05	0.33	0.26
RR160	Up/Down-Stage	Top/Rear		dB	0.79	1.51	2.63	0.84	2.57	0.61	0.36	-0.14	0.38	1.53
RR160	Up/Down-Stage	FrontTop/ RearBottom		dB	0.72	0.49	1.00	-0.27	2.65	-0.47	0.43	-0.98	0.40	1.13
MTF	Cross-Stage	Top		none (0-1)	1.01	0.55	0.69	0.95	0.72	0.09	0.50	0.79	1.00	0.87
MTF	Cross-Stage	Bottom		none (0-1)	1.00	0.51	0.67	0.92	0.72	0.06	0.46	0.85	0.99	0.86
MTF	Cross-Stage	Front		none (0-1)	0.97	0.52	0.62	0.84	0.78	0.06	0.44	0.92	0.95	0.87
MTF	Cross-Stage	Rear		none (0-1)	1.01	0.49	0.65	0.91	0.72	0.10	0.53	0.90	0.97	0.88
MTF	Cross-Stage	Left		none (0-1)	1.06	0.49	0.66	0.92	0.76	0.05	0.46	0.83	0.93	0.90
MTF	Cross-Stage	Right		none (0-1)	0.90	0.51	0.68	0.90	0.82	0.08	0.49	0.80	1.01	0.89
MTF	Cross-Stage	Audience		none (0-1)	0.97	0.50	0.59	0.76	0.74	0.08	0.44	0.94	0.94	0.89
MTF	Cross-Stage	SideWallsL		none (0-1)	1.06	0.55	0.68	0.90	0.82	0.07	0.47	0.84	0.92	0.98
MTF	Cross-Stage	SideWallsR		none (0-1)	0.87	0.52	0.63	0.89	0.83	0.09	0.53	0.75	1.04	0.91
MTF	Cross-Stage	Top	X	none (0-1)	0.01	0.04	0.03	0.04	-0.04	0.02	0.02	-0.06	0.02	0.00
MTF	Cross-Stage	Bottom	X	none (0-1)	0.01	0.00	0.01	0.02	-0.03	-0.01	-0.03	0.00	0.02	-0.02
MTF	Cross-Stage	Front	X	none (0-1)	-0.02	0.01	-0.04	-0.07	0.03	-0.01	-0.04	0.07	-0.02	-0.01
MTF	Cross-Stage	Rear	X	none (0-1)	0.02	-0.02	-0.01	0.01	-0.04	0.03	0.05	0.05	-0.01	0.00
MTF	Cross-Stage	Left	X	none (0-1)	0.07	-0.02	-0.01	0.01	0.01	-0.03	-0.02	-0.02	-0.05	0.02
MTF	Cross-Stage	Right	X	none (0-1)	-0.09	0.00	0.01	0.00	0.07	0.01	0.01	-0.05	0.03	0.01
MTF	Cross-Stage	Audience	X	none (0-1)	-0.02	-0.02	-0.07	-0.14	-0.01	0.00	-0.04	0.09	-0.04	0.01
MTF	Cross-Stage	SideWallsL	X	none (0-1)	0.07	0.03	0.02	0.00	0.06	-0.01	-0.01	-0.01	-0.05	0.10
MTF	Cross-Stage	SideWallsR	X	none (0-1)	-0.12	0.00	-0.03	-0.02	0.08	0.01	0.05	-0.09	0.07	0.03
MTF	Cross-Stage	Top/Bottom		none (0-1)	0.01	0.04	0.02	0.02	-0.01	0.03	0.05	-0.06	0.01	0.01
MTF	Cross-Stage	Front/Rear		none (0-1)	-0.04	0.03	-0.02	-0.07	0.07	-0.04	-0.09	0.02	-0.01	-0.01
MTF	Cross-Stage	Left/Right		none (0-1)	0.16	-0.02	-0.02	0.02	-0.06	-0.03	-0.03	0.03	-0.08	0.01
MTF	Cross-Stage	Front/Sides		none (0-1)	0.00	-0.04	-0.06	-0.13	-0.08	0.00	-0.06	0.14	-0.05	-0.06
MTF	Cross-Stage	Top/Sides		none (0-1)	0.04	0.02	0.04	0.05	-0.11	0.02	0.00	-0.01	0.01	-0.07
MTF	Cross-Stage	Top/Rear		none (0-1)	-0.01	0.06	0.05	0.03	0.00	-0.01	-0.03	-0.11	0.03	-0.01
MTF	Cross-Stage	FrontTop/ RearBottom		none (0-1)	-0.02	0.03	0.00	-0.03	0.03	0.00	-0.02	-0.02	0.00	0.00
MTF	Up/Down-Stage	Top		none (0-1)	1.01	0.85	0.26	0.45	0.78	1.01	0.56	0.59	0.80	0.88
MTF	Up/Down-Stage	Bottom		none (0-1)	1.00	0.78	0.25	0.40	0.86	0.82	0.53	0.51	0.81	0.91
MTF	Up/Down-Stage	Front		none (0-1)	0.97	0.82	0.26	0.47	0.77	0.97	0.54	0.66	0.81	0.90
MTF	Up/Down-Stage	Rear		none (0-1)	1.01	0.91	0.37	0.51	0.85	1.03	0.62	0.62	0.83	1.01
MTF	Up/Down-Stage	Left		none (0-1)	1.06	0.79	0.22	0.46	0.84	0.99	0.60	0.71	0.77	0.90
MTF	Up/Down-Stage	Right		none (0-1)	0.90	0.91	0.34	0.48	0.88	1.03	0.61	0.60	0.92	1.03
MTF	Up/Down-Stage	Audience		none (0-1)	0.97	0.84	0.24	0.46	0.80	1.04	0.53	0.64	0.81	0.92
MTF	Up/Down-Stage	SideWallsL		none (0-1)	1.06	0.78	0.27	0.47	0.83	1.00	0.64	0.75	0.77	0.86
MTF	Up/Down-Stage	SideWallsR		none (0-1)	0.87	0.97	0.31	0.48	0.92	1.11	0.65	0.64	0.98	1.00
MTF	Up/Down-Stage	Top	X	none (0-1)	0.01	0.00	-0.02	-0.01	-0.05	0.03	-0.01	-0.02	-0.02	-0.06
MTF	Up/Down-Stage	Bottom	X	none (0-1)	0.01	-0.06	-0.04	-0.06	0.03	-0.16	-0.05	-0.11	-0.01	-0.03
MTF	Up/Down-Stage	Front	X	none (0-1)	-0.02	-0.02	-0.02	0.01	-0.06	0.00	-0.04	0.04	-0.01	-0.03
MTF	Up/Down-Stage	Rear	X	none (0-1)	0.02	0.06	0.08	0.05	0.02	0.05	0.04	0.01	0.00	0.08
MTF	Up/Down-Stage	Left	X	none (0-1)	0.07	-0.05	-0.06	0.00	0.01	0.01	0.02	0.10	-0.05	-0.04
MTF	Up/Down-Stage	Right	X	none (0-1)	-0.09	0.07	0.06	0.02	0.05	0.06	0.03	-0.02	0.10	0.09
MTF	Up/Down-Stage	Audience	X	none (0-1)	-0.02	-0.01	-0.04	0.00	-0.03	0.07	-0.04	0.02	-0.02	-0.02
MTF	Up/Down-Stage	SideWallsL	X	none (0-1)	0.07	-0.06	-0.02	0.01	0.01	0.03	0.07	0.14	-0.06	-0.07
MTF	Up/Down-Stage	SideWallsR	X	none (0-1)	-0.12	0.12	0.03	0.02	0.09	0.13	0.08	0.03	0.15	0.06
MTF	Up/Down-Stage	Top/Bottom		none (0-1)	0.01	0.07	0.01	0.06	-0.08	0.19	0.03	0.09	-0.01	-0.03
MTF	Up/Down-Stage	Front/Rear		none (0-1)	-0.04	-0.09	-0.10	-0.04	-0.08	-0.05	-0.08	0.04	-0.02	-0.11
MTF	Up/Down-Stage	Left/Right		none (0-1)	0.16	-0.12	-0.12	-0.02	-0.04	-0.04	-0.01	0.11	-0.15	-0.13
MTF	Up/Down-Stage	Front/Sides		none (0-1)	0.00	-0.04	-0.05	-0.01	-0.07	-0.01	-0.12	-0.06	-0.07	-0.01
MTF	Up/Down-Stage	Top/Sides		none (0-1)	0.04	-0.03	-0.03	-0.02	-0.10	-0.05	-0.09	-0.10	-0.07	-0.05
MTF	Up/Down-Stage	Top/Rear		none (0-1)	-0.01	-0.06	-0.11	-0.05	-0.07	-0.02	-0.05	-0.03	-0.03	-0.14
MTF	Up/Down-Stage	FrontTop/ RearBottom		none (0-1)	-0.02	-0.01	-0.04	0.01	-0.08	0.07	-0.02	0.06	-0.02	-0.07
EDT	Cross-Stage	Top		s	0.88	1.43	1.56	1.47	1.58	2.12	0.98	2.08	1.55	1.58
EDT	Cross-Stage	Bottom		s	0.85	1.49	1.64	1.52	1.61	2.08	1.02	1.94	1.51	1.59
EDT	Cross-Stage	Front		s	0.92	1.44	1.67	1.69	1.69	2.12	1.05	1.82	1.62	1.64
EDT	Cross-Stage	Rear		s	0.89	1.46	1.60	1.58	1.55	2.10	0.98	1.92	1.60	1.60
EDT	Cross-Stage	Left		s	0.84	1.52	1.66	1.55	1.63	2.13	1.01	2.02	1.66	1.61
EDT	Cross-Stage	Right		s	0.99	1.46	1.57	1.58	1.40	2.04	1.02	2.12	1.58	1.64
EDT	Cross-Stage	Audience		s	0.93	1.51	1.72	1.88	1.68	2.05	1.05	1.78	1.63	1.62
EDT	Cross-Stage	SideWallsL		s	0.80	1.55	1.69	1.58	1.70	2.16	1.01	1.99	1.68	1.61
EDT	Cross-Stage	SideWallsR		s	1.05	1.43	1.67	1.65	1.28	2.03	0.97	2.13	1.57	1.65
EDT	Cross-Stage	Top	X	s	-0.01	-0.04	-0.06	-0.10	0.00	0.02	-0.03	0.10	-0.04	-0.03
EDT	Cross-Stage	Bottom	X	s	-0.05	0.02	0.02	-0.04	0.03	-0.02	0.01	-0.04	-0.07	-0.02
EDT	Cross-Stage	Front	X	s	0.03	-0.02	0.05	0.13	0.11	0.02	0.04	-0.17	0.03	0.03
EDT	Cross-Stage	Rear	X	s	0.00	0.00	-0.02	0.02	-0.02	0.00	-0.03	-0.07	0.01	-0.01
EDT	Cross-Stage	Left	X	s	-0.06	0.05	0.05	-0.01	0.05	0.03	0.00	0.04	0.07	0.00
EDT	Cross-Stage	Right	X	s	0.10	-0.01	-0.04	0.01	-0.17	-0.05	0.01	0.14	-0.01	0.03
EDT	Cross-Stage	Audience	X	s	0.03	0.04	0.10	0.32	0.10	-0.05	0.04	-0.20	0.05	0.01
EDT	Cross-Stage	SideWallsL	X	s	-0.10	0.09	0.07	0.02	0.12	0.07	0.00	0.01	0.10	0.00
EDT	Cross-Stage	SideWallsR	X	s	0.16	-0.04	0.05	0.08	-0.30	-0.06	-0.04	0.15	-0.02	0.04

PARAMETER					HALL									
Parameter	Location	Direction	Normalized	Units	Alb Recital	Alb Theatre	Bard	Buffalo	Eastman	EMPAC C	EMPAC Th	Skidmore	St. Rose	Vassar
EDT	Cross-Stage	Top/Bottom		s	0.04	-0.06	-0.08	-0.06	-0.04	0.04	-0.04	0.14	0.03	-0.01
EDT	Cross-Stage	Front/Rear		s	0.03	-0.02	0.07	0.11	0.14	0.02	0.07	-0.10	0.02	0.04
EDT	Cross-Stage	Left/Right		s	-0.15	0.06	0.09	-0.03	0.23	0.08	-0.01	-0.10	0.08	-0.04
EDT	Cross-Stage	Front/Sides		s	0.01	0.02	0.04	0.26	0.19	-0.05	0.06	-0.28	0.01	-0.01
EDT	Cross-Stage	Top/Sides		s	-0.04	-0.06	-0.12	-0.15	0.09	0.02	-0.01	0.02	-0.08	-0.05
EDT	Cross-Stage	Top/Rear		s	-0.01	-0.04	-0.04	-0.11	0.02	0.03	0.00	0.16	-0.05	-0.02
EDT	Cross-Stage	FrontTop/ RearBottom		s	0.03	-0.04	0.00	0.03	0.05	0.03	0.01	0.02	0.03	0.01
EDT	UpDown-Stage	Top		s	0.88	1.46	1.52	1.97	1.73	2.20	1.14	2.25	1.67	1.54
EDT	UpDown-Stage	Bottom		s	0.85	1.54	1.50	2.00	1.52	2.24	1.10	2.29	1.64	1.48
EDT	UpDown-Stage	Front		s	0.92	1.47	1.52	1.87	1.81	2.25	1.16	2.18	1.65	1.61
EDT	UpDown-Stage	Rear		s	0.89	1.39	1.23	1.83	1.52	2.23	1.06	2.15	1.66	1.48
EDT	UpDown-Stage	Left		s	0.84	1.57	1.60	1.93	1.65	2.26	1.04	2.16	1.65	1.52
EDT	UpDown-Stage	Right		s	0.99	1.38	1.43	1.93	1.57	2.22	1.06	2.26	1.61	1.56
EDT	UpDown-Stage	Audience		s	0.93	1.45	1.53	1.90	1.75	2.21	1.15	2.14	1.63	1.58
EDT	UpDown-Stage	SideWallsL		s	0.80	1.52	1.58	1.89	1.73	2.25	0.99	2.13	1.68	1.59
EDT	UpDown-Stage	SideWallsR		s	1.05	1.37	1.38	1.94	1.48	2.19	1.02	2.19	1.62	1.59
EDT	UpDown-Stage	Top	X	s	-0.01	-0.01	0.05	0.05	0.10	-0.03	0.05	0.03	0.02	0.00
EDT	UpDown-Stage	Bottom	X	s	-0.05	0.07	0.03	0.08	-0.11	0.01	0.01	-0.08	-0.01	-0.06
EDT	UpDown-Stage	Front	X	s	0.03	0.00	0.06	-0.05	0.17	0.02	0.07	-0.03	0.00	0.08
EDT	UpDown-Stage	Rear	X	s	0.00	-0.08	-0.24	-0.09	-0.12	-0.01	-0.03	-0.06	0.01	-0.05
EDT	UpDown-Stage	Left	X	s	-0.06	0.10	0.14	0.01	0.02	0.03	-0.05	-0.06	0.01	-0.01
EDT	UpDown-Stage	Right	X	s	0.10	-0.09	-0.03	0.01	-0.06	-0.01	-0.04	0.04	-0.04	0.03
EDT	UpDown-Stage	Audience	X	s	0.03	-0.02	0.06	-0.02	0.12	-0.03	0.06	-0.07	-0.02	0.05
EDT	UpDown-Stage	SideWallsL	X	s	-0.10	0.05	0.12	-0.03	0.10	0.02	-0.11	-0.09	0.03	0.06
EDT	UpDown-Stage	SideWallsR	X	s	0.16	-0.10	-0.09	0.02	-0.15	-0.05	-0.07	-0.03	-0.02	0.06
EDT	UpDown-Stage	Top/Bottom		s	0.04	-0.08	0.02	-0.03	0.21	-0.04	0.04	-0.05	0.03	0.06
EDT	UpDown-Stage	Front/Rear		s	0.03	0.08	0.29	0.04	0.29	0.02	0.10	0.03	-0.01	0.13
EDT	UpDown-Stage	Left/Right		s	-0.15	0.19	0.17	0.00	0.08	0.04	-0.02	-0.10	0.05	-0.04
EDT	UpDown-Stage	Front/Sides		s	0.01	0.01	0.04	-0.02	0.14	-0.01	0.15	-0.01	-0.03	-0.01
EDT	UpDown-Stage	Top/Sides		s	-0.04	0.02	0.03	0.05	0.12	-0.02	0.14	0.09	0.02	-0.06
EDT	UpDown-Stage	Top/Rear		s	-0.01	0.07	0.29	0.14	0.21	-0.03	0.08	0.09	0.01	0.06
EDT	UpDown-Stage	FrontTop/ RearBottom		s	0.03	0.00	0.15	0.01	0.25	-0.01	0.07	-0.01	0.01	0.10
EDTR	Cross-Stage	Top		none	0.77	0.55	0.95	0.78	0.67	0.91	0.96	0.94	1.02	1.11
EDTR	Cross-Stage	Bottom		none	0.74	0.58	0.99	0.81	0.69	0.90	1.01	0.88	0.99	1.12
EDTR	Cross-Stage	Front		none	0.81	0.56	1.01	0.90	0.72	0.91	1.03	0.82	1.06	1.15
EDTR	Cross-Stage	Rear		none	0.78	0.57	0.97	0.84	0.66	0.90	0.96	0.87	1.05	1.13
EDTR	Cross-Stage	Left		none	0.74	0.59	1.01	0.82	0.70	0.92	0.99	0.91	1.09	1.13
EDTR	Cross-Stage	Right		none	0.87	0.56	0.96	0.84	0.60	0.88	1.00	0.96	1.04	1.16
EDTR	Cross-Stage	Audience		none	0.82	0.58	1.04	1.00	0.72	0.88	1.03	0.80	1.07	1.14
EDTR	Cross-Stage	SideWallsL		none	0.70	0.60	1.02	0.84	0.73	0.93	0.99	0.90	1.11	1.14
EDTR	Cross-Stage	SideWallsR		none	0.92	0.55	1.01	0.88	0.55	0.88	0.96	0.96	1.03	1.16
EDTR	Cross-Stage	Top	X	none	-0.01	-0.02	-0.03	-0.05	0.00	0.01	-0.03	0.04	-0.02	-0.02
EDTR	Cross-Stage	Bottom	X	none	-0.04	0.01	0.01	-0.02	0.01	-0.01	0.01	-0.02	-0.05	-0.01
EDTR	Cross-Stage	Front	X	none	0.02	-0.01	0.03	0.07	0.05	0.01	0.04	-0.08	0.02	0.02
EDTR	Cross-Stage	Rear	X	none	0.00	0.00	-0.01	0.01	-0.01	0.00	-0.03	-0.03	0.01	-0.01
EDTR	Cross-Stage	Left	X	none	-0.05	0.02	0.03	-0.01	0.02	0.01	0.00	0.02	0.05	0.00
EDTR	Cross-Stage	Right	X	none	0.09	0.00	-0.03	0.01	-0.07	-0.02	0.01	0.06	-0.01	0.02
EDTR	Cross-Stage	Audience	X	none	0.03	0.02	0.06	0.17	0.04	-0.02	0.04	-0.09	0.03	0.01
EDTR	Cross-Stage	SideWallsL	X	none	-0.09	0.03	0.04	0.01	0.05	0.03	0.00	0.00	0.07	0.00
EDTR	Cross-Stage	SideWallsR	X	none	0.14	-0.01	0.03	0.04	-0.13	-0.03	-0.04	0.07	-0.01	0.03
EDTR	UpDown-Stage	Top		none	0.00	0.57	0.92	1.04	0.74	0.95	1.12	1.01	1.10	1.08
EDTR	UpDown-Stage	Bottom		none	0.15	0.60	0.91	1.06	0.65	0.97	1.08	1.03	1.08	1.04
EDTR	UpDown-Stage	Front		none	0.00	0.57	0.92	0.99	0.77	0.97	1.14	0.99	1.09	1.14
EDTR	UpDown-Stage	Rear		none	0.00	0.54	0.75	0.97	0.65	0.96	1.05	0.97	1.09	1.04
EDTR	UpDown-Stage	Left		none	0.15	0.61	0.97	1.02	0.71	0.97	1.02	0.97	1.09	1.07
EDTR	UpDown-Stage	Right		none	0.00	0.53	0.87	1.02	0.67	0.96	1.04	1.02	1.06	1.10
EDTR	UpDown-Stage	Audience		none	0.00	0.56	0.93	1.01	0.75	0.95	1.13	0.97	1.07	1.12
EDTR	UpDown-Stage	SideWallsL		none	0.00	0.59	0.96	1.00	0.74	0.97	0.97	0.96	1.10	1.12
EDTR	UpDown-Stage	SideWallsR		none	0.00	0.53	0.84	1.03	0.64	0.94	1.01	0.99	1.07	1.12
EDTR	UpDown-Stage	Top	X	none	-0.05	0.00	0.03	0.03	0.04	-0.01	0.05	0.01	0.02	0.00
EDTR	UpDown-Stage	Bottom	X	none	0.10	0.03	0.02	0.04	-0.05	0.00	0.01	0.03	0.00	-0.04
EDTR	UpDown-Stage	Front	X	none	-0.05	0.00	0.03	-0.03	0.07	0.01	0.06	-0.02	0.00	0.06
EDTR	UpDown-Stage	Rear	X	none	-0.05	-0.03	-0.14	-0.05	-0.05	0.00	-0.03	-0.03	0.01	-0.04
EDTR	UpDown-Stage	Left	X	none	0.10	0.04	0.08	0.01	0.01	0.01	-0.05	-0.03	0.00	-0.01
EDTR	UpDown-Stage	Right	X	none	-0.05	-0.03	-0.02	0.00	-0.03	-0.01	-0.04	0.02	-0.03	0.02
EDTR	UpDown-Stage	Audience	X	none	-0.05	-0.01	0.04	-0.01	0.05	-0.01	0.06	-0.03	-0.01	0.04
EDTR	UpDown-Stage	SideWallsL	X	none	-0.05	0.02	0.07	-0.02	0.04	0.01	-0.11	-0.04	0.02	0.04
EDTR	UpDown-Stage	SideWallsR	X	none	-0.05	-0.04	-0.05	0.01	-0.06	-0.02	-0.07	-0.01	-0.02	0.04
DD (0-30 ms)	Cross-Stage			%	70.18	1.60	19.10	12.41	0.40	34.09	24.59	32.13	16.52	3.18
DD (0-30 ms)	UpDown-Stage			%	70.18	41.05	50.52	60.07	24.10	16.39	7.08	15.26	31.74	27.10
MTF	Cross-Stage	Omni		none (0-1)	1.03	0.80	0.67	0.86	0.93	0.34	0.63	0.84	1.12	1.03
MTF	UpDown-Stage	Omni		none (0-1)	1.03	0.30	0.52	1.00	0.89	1.03	0.58	1.08	1.26	1.14
Gtotal	Cross-Stage	Omni		dB	17.65	14.50	13.79	15.78	16.22	9.21	12.77	14.72	16.90	18.25
Gtotal	UpDown-Stage	Omni		dB	17.65	9.16	11.59	16.95	16.90	14.16	12.57	15.19	17.81	18.86
Gearly	Cross-Stage	Omni		dB	16.46	12.85	12.00	13.72	14.89	7.29	11.64	12.01	15.16	16.08
Gearly	UpDown-Stage	Omni		dB	16.46	7.68	9.77	15.00	15.37	13.45	11.25	13.75	16.35	17.09
Glate	Cross-Stage	Omni		dB	11.44	9.49	9.10	11.57	10.44	4.73	6.37	11.39	12.09	14.20
Glate	UpDown-Stage	Omni		dB	11.44	3.75	6.92	12.54	11.60	5.94	6.76	9.67	12.38	14.10
Gsupport	Cross-Stage	Omni		dB	13.96	8.74	9.80	11.96	11.90	3.98	7.94	11.25	12.64	13.86

PARAMETER					HALL									
Parameter	Location	Direction	Normalized	Units	Alb Recital	Alb Theatre	Bard	Buffalo	Eastman	EMPAC C	EMPAC Th	Skidmore	St. Rose	Vassar
Gsupport	UpDown-Stage	Omni		dB	13.96	4.42	9.12	12.51	13.71	5.24	9.09	8.99	12.15	14.47
G740	Cross-Stage	Omni		dB	13.06	6.29	8.64	9.16	11.04	1.88	4.73	8.99	11.81	12.19
G740	UpDown-Stage	Omni		dB	13.06	2.51	7.07	10.93	11.68	7.58	7.21	8.25	11.94	14.07
G40end	Cross-Stage	Omni		dB	14.34	11.27	11.26	13.97	12.64	6.00	9.17	12.88	13.87	15.80
G40end	UpDown-Stage	Omni		dB	14.34	5.74	9.17	14.44	14.22	7.01	8.83	11.16	13.94	15.73
LQ740	Cross-Stage	Omni		dB	-1.28	-4.98	-2.62	-4.81	-1.60	-4.12	-4.44	-3.90	-2.07	-3.61
LQ740	UpDown-Stage	Omni		dB	-1.28	-3.24	-2.10	-3.52	-2.54	0.57	-1.62	-2.90	-2.00	-1.66
RR160	Cross-Stage	Omni		dB	-14.93	-11.24	-10.88	-9.04	-13.80	-9.46	-14.20	-8.30	-11.08	-10.54
RR160	UpDown-Stage	Omni		dB	-14.93	-11.72	-10.82	-9.77	-12.00	-14.74	-13.09	-11.14	-11.38	-11.00
ST1	Average	Omni		dB	-14.30	-18.70	-17.70	-13.00	-12.70	-16.30	-14.30	-15.00	-10.70	-10.30
ST2	Average	Omni		dB	-19.30	-18.30	-16.70	-12.30	-15.00	-14.70	-16.00	-14.30	-10.30	-9.70
ST3	Average	Omni		dB	-13.00	-15.00	-14.30	-9.70	-10.70	-12.30	-12.00	-11.30	-7.00	-7.00
C80	Average	Omni		dB	3.20	0.37	1.93	1.33	1.40	4.57	2.40	2.73	2.10	1.33
D50	Average	Omni		%	53.67	39.67	48.67	47.67	42.33	68.67	50.00	53.33	52.00	49.00
Tc	Average	Omni		ms	63.67	101.67	95.67	100.00	102.00	60.67	67.00	85.67	82.33	85.67
EDT	Average	Omni		s	0.90	1.49	1.47	1.96	1.71	2.15	1.11	2.24	1.60	1.52
T30	Average	Omni		s	0.97	1.53	1.78	2.05	2.01	2.25	1.07	2.18	1.64	1.56
BR	Average	Omni		none	1.31	1.18	0.91	0.98	1.15	1.19	1.39	1.03	1.22	0.93
EDTStageAvg	Average	Omni		s	0.93	1.40	1.47	1.75	1.54	2.03	1.08	2.02	1.49	1.41
EDTAudAvg	Average	Omni		s	1.14	2.58	1.65	1.89	2.34	2.32	1.02	2.22	1.52	1.42
EDTR	Average	Omni		none	0.82	0.54	0.89	0.93	0.66	0.87	1.06	0.91	0.98	0.99

APPENDIX C

IMAGES

C.1 Measurement



Figure C.1: Sound Source (Mid and High-Frequency Dodecahedron Loudspeakers and Subwoofer) and Spherical Microphone Array on Stand

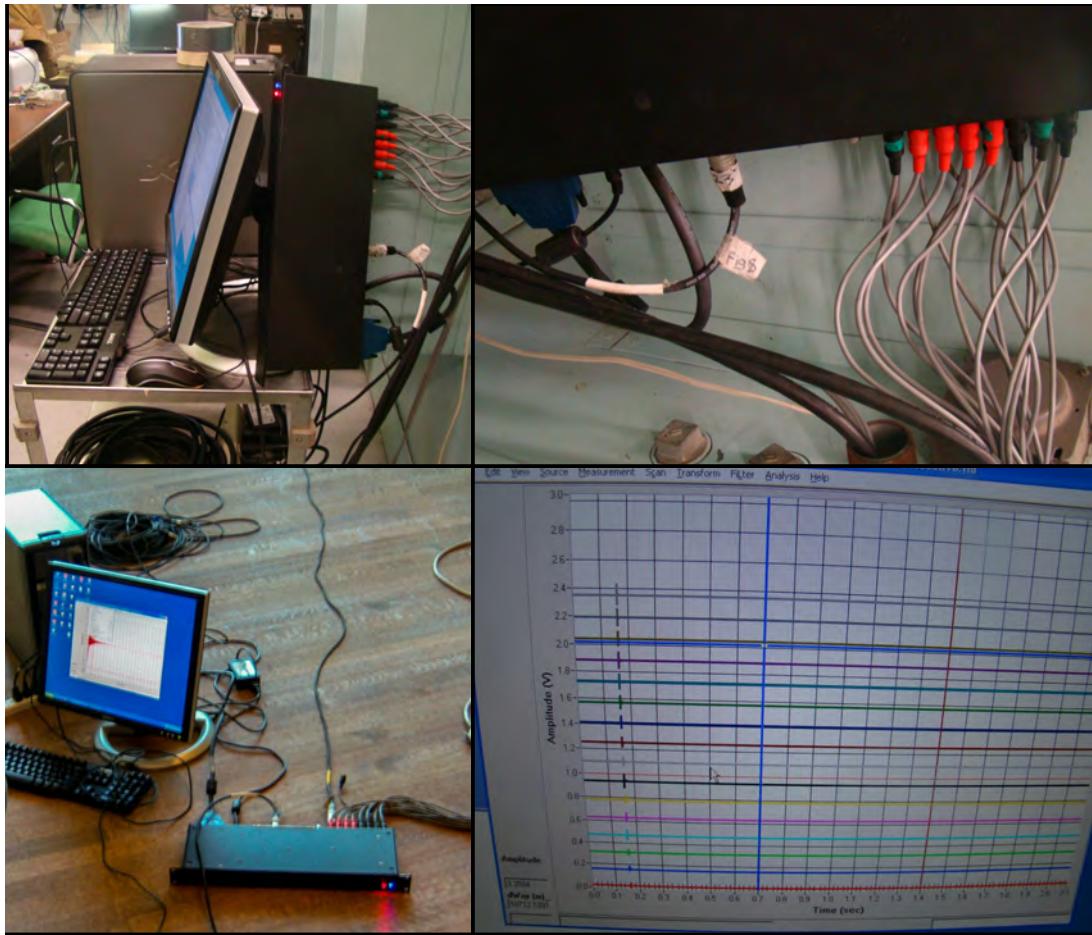


Figure C.2: Spherical Array Interface and Processor with MaxSens Software

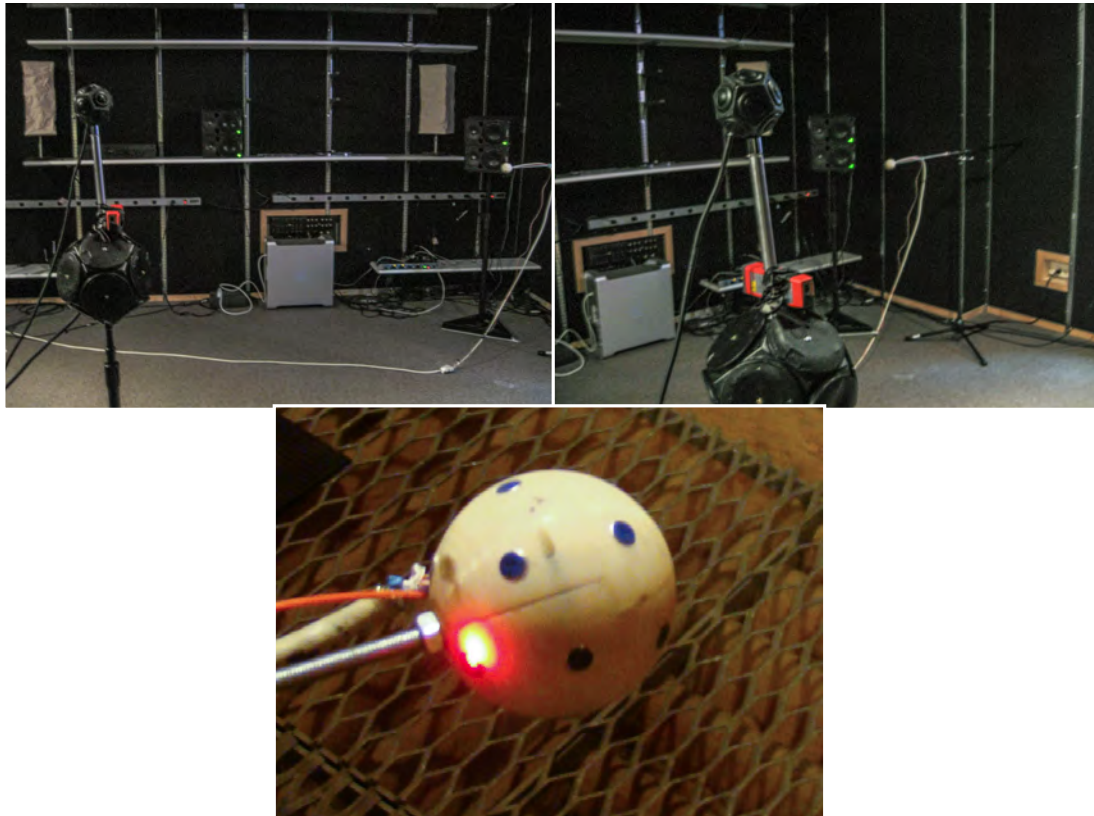


Figure C.3: Individual Capsule Calibration at NYSTAR Acoustics and Telepresence Lab



Figure C.4: Test Setup for Spherical Microphone Array

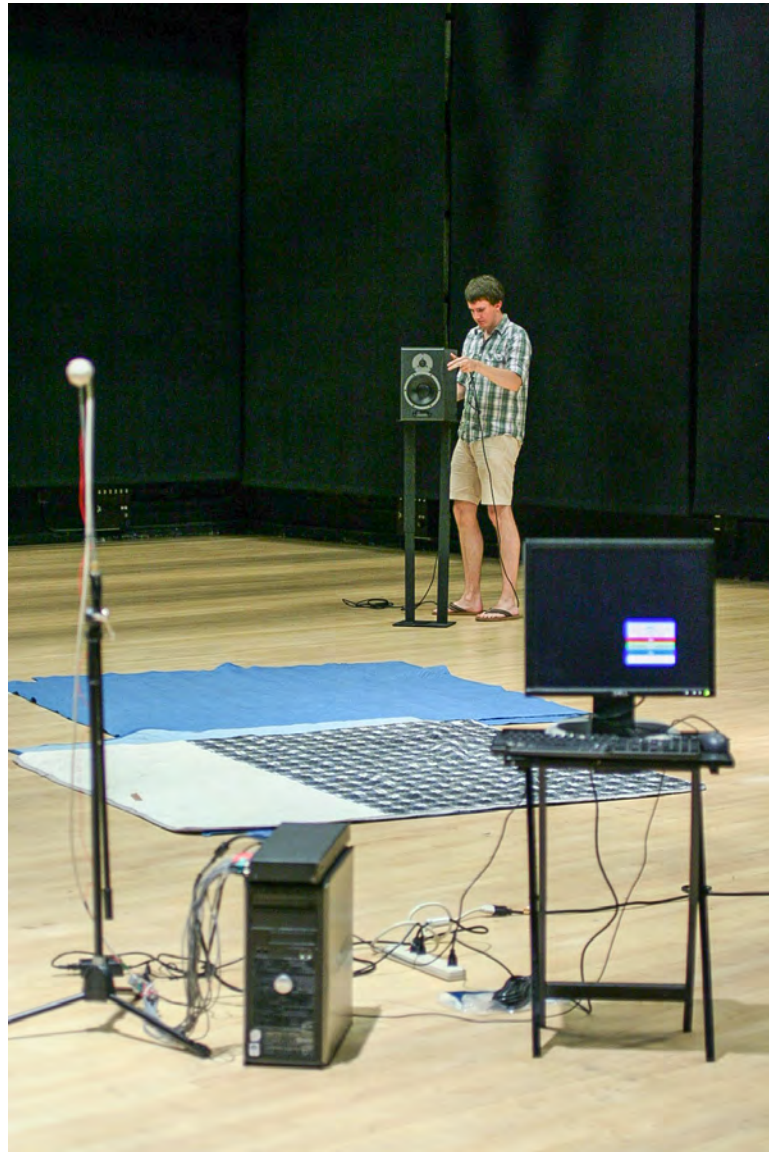


Figure C.5: Free Field Measurements at EMPAC, Studio 2



Figure C.6: Concert Hall Measurement Setup

C.2 Spatial Analysis

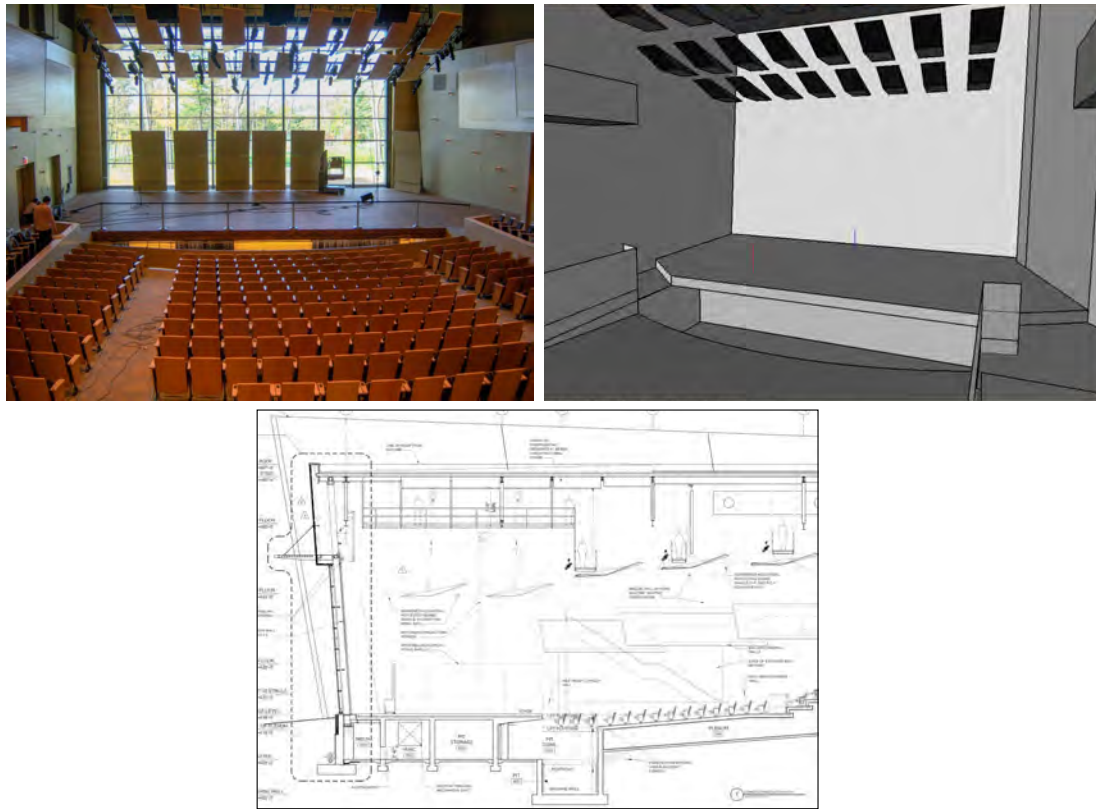


Figure C.7: Skidmore 3D Model and References (Figure Used with Permission of Skidmore College)

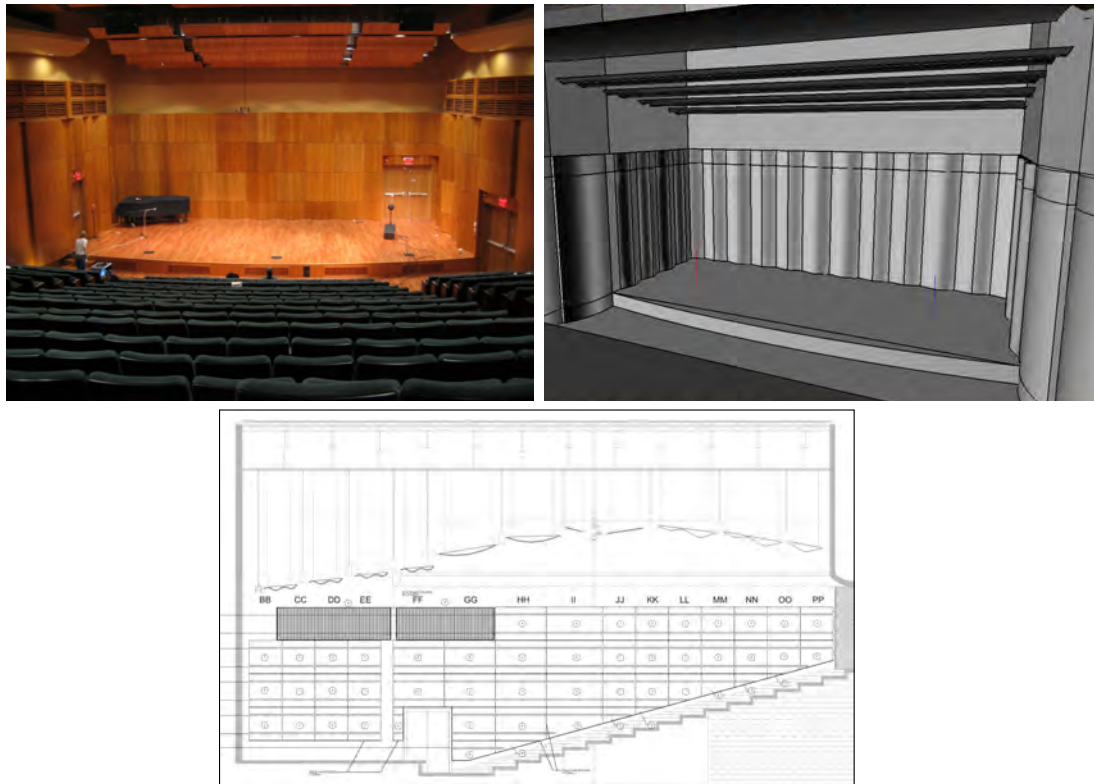


Figure C.8: St. Rose 3D Model and References (Figure Used with Permission of College of St. Rose)

C.3 Subjective Testing



Figure C.9: Solo Violin Recording in an Anechoic Chamber



Figure C.10: Arup SoundLab NY: IR Measurements



Figure C.11: Arup SoundLab NY: RTA IR Measurements



Figure C.12: Arup SoundLab LA: RTA System Testing (with Temporary MDF Platform)



Figure C.13: Musician Platform in NY SoundLab



Figure C.14: Musician Platform in NY SoundLab with Surrounding “Stage Floor”

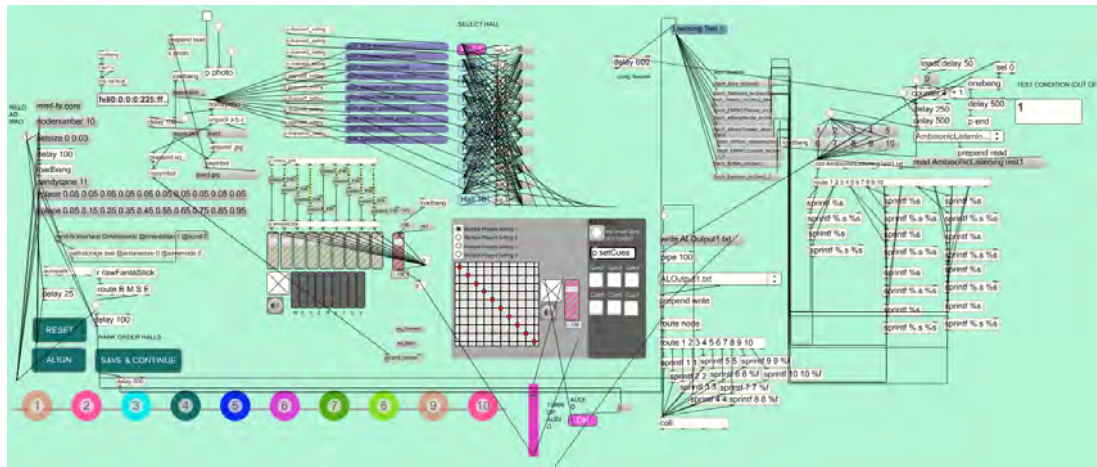


Figure C.15: Max/MSP Patch for Test 1 (Listening)

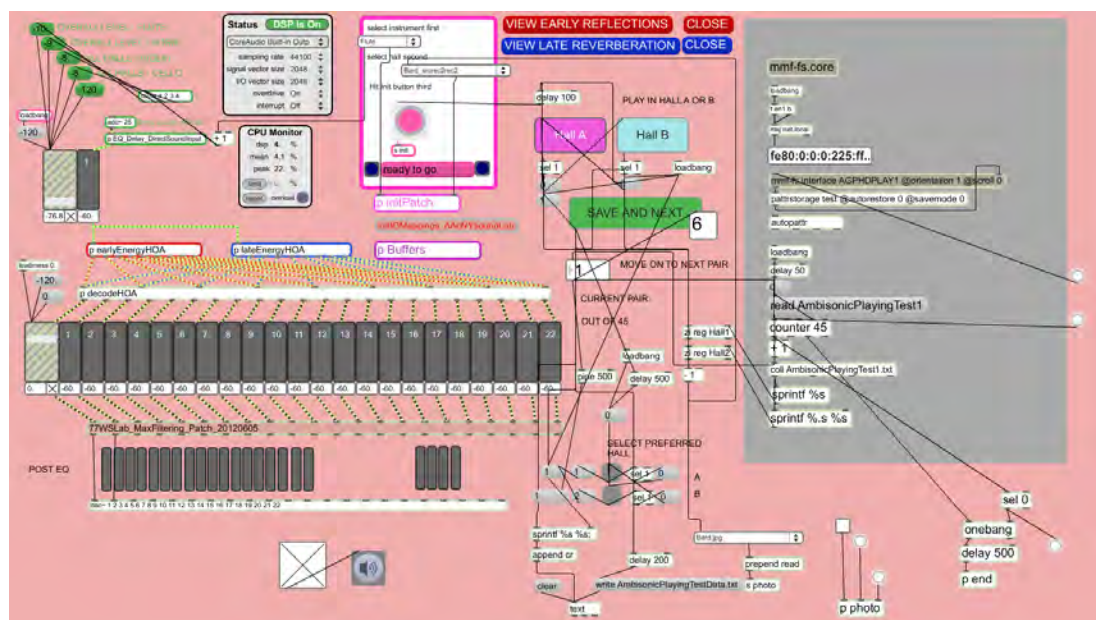


Figure C.16: Max/MSP Patch for Test 2 (Solo Playing)

Figure C.17: iPad Interface for Test 3 (Ensemble Playing)

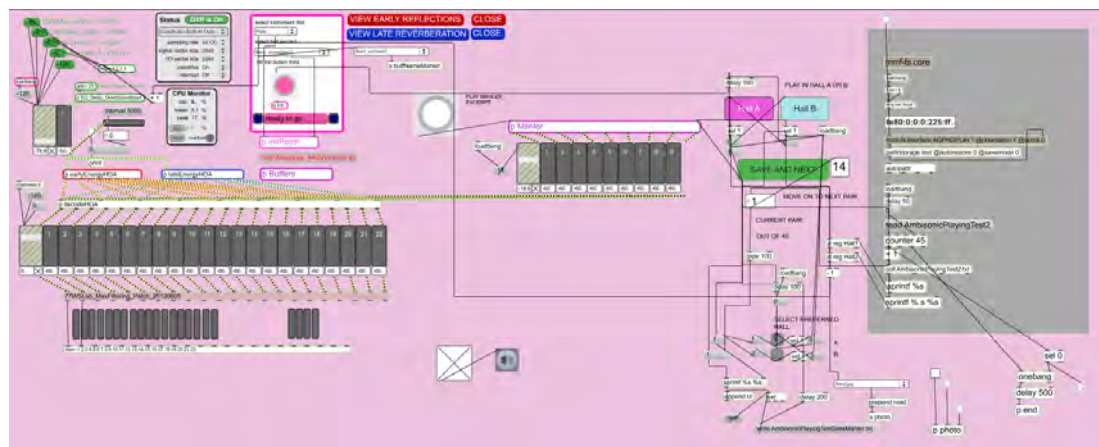
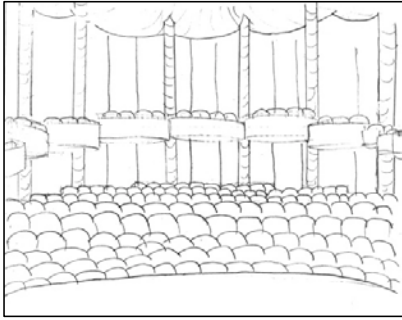
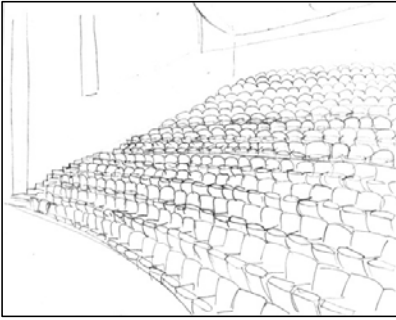


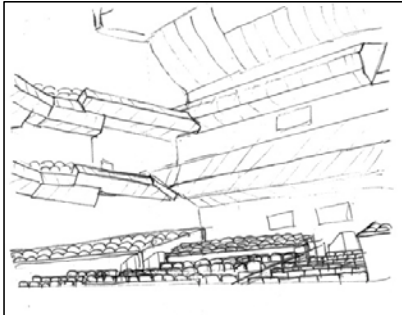
Figure C.18: Max/MSP Patch for Test 3 (Ensemble Playing)



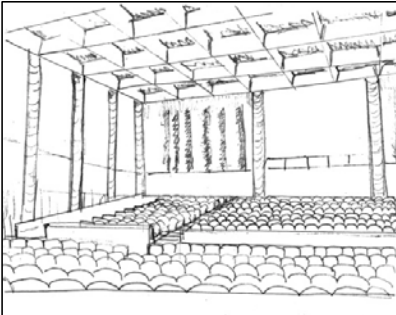
Recital Hall,
SUNY Albany



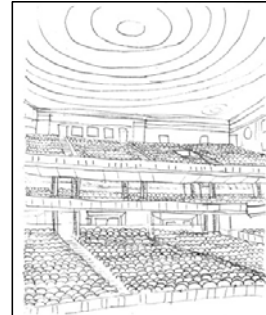
Theater,
SUNY Albany



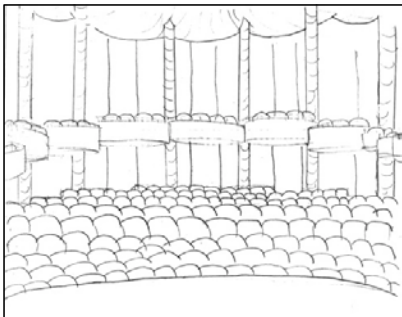
Fisher Center,
Bard



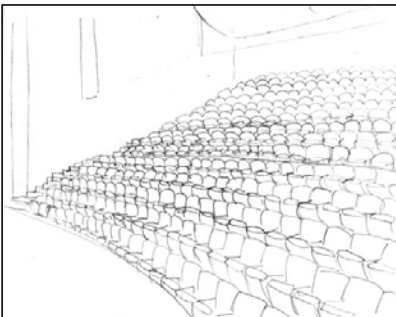
Lippes Concert Hall,
SUNY Buffalo



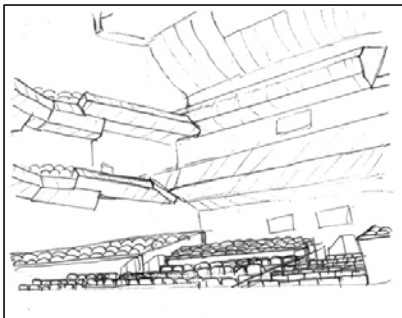
Kodak Hall,
Eastman



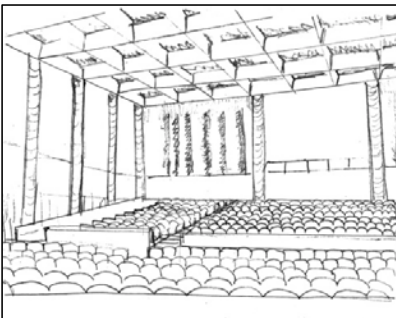
Recital Hall,
SUNY Albany



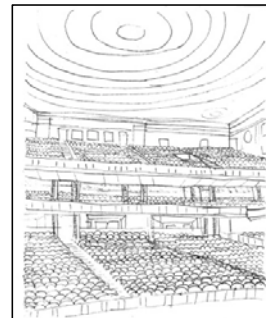
Theater,
SUNY Albany



Fisher Center,
Bard



Lippes Concert Hall,
SUNY Buffalo



Kodak Hall,
Eastman

Figure C.19: Projected Hall Drawings Used in Subjective Tests